Geometric combinatorics of paths and deformations of convex polytopes

Germain Poullot

École Doctorale Sciences Mathématiques de Paris Centre

Sorbonne Université
Insitut Mathématiques de Jussieu-Paris Rive Gauche

Thèse de doctorat

Discipline : Mathématiques

présentée par

Germain Poullot

Geometric combinatorics of paths and deformations of convex polytopes

---

réalisée sous la direction de

Arnau Padrol
IMJ-PRG, Sorbonne Université
DMI, Universitat de Barcelona

Vincent Pilaud
CNRS
LIX, École polytechnique

Président du jury	Frédéric MEUNIER	École Nationale des Ponts et Chaussées
Rapportrice	Fu LIU	University of California at Davis
Rapporteur	Lionel POURNIN	LIPN - Université Paris 13
Examinateur	Jesús DE LOERA	University of California at Davis
Examinatrice	Martina JUHNKE-KUBITZKE	Universität Osnabrück
Examinateur	Vic REINER	University of Minnesota

Contents

List of Figures

Remerciements - Acknowledgments

Comment remercier en si peu de mots autant de gens ?

Ma thèse, c'est avant tout 3 années de vie, à la fois trop longues et bien trop courtes, peuplées d'une myriade de rencontres, où le travail s'entremêle directement avec la vie privée. C'est pourquoi il n'y aura pas d'ordre dans ces remerciements, et pas véritablement d'organisation non plus. En outre, chacun sait à peu près ce pourquoi je tiens à le remercier : derrière chaque petite phrase se cache une longue histoire, de beaux souvenirs.

Tout d'abord, et il me semble essentiels de commencer par eux car sans eux rien n'aurait eu lieu, un gigantesque merci à mes deux directeurs de thèse, Arnau et Vincent. Merci de m'avoir fait découvrir le meilleur domaine des mathématiques qu'il soit : la combinatoire des polytopes. Merci de m'avoir encadré en thèse durant 3 ans, dans tout ce que cela implique professionnellement et personnellement. Merci pour la pédagogie dont vous avez fait preuve : j'ai grandement apprécié votre patience et votre capacité à répéter, reformuler jusqu'à ce que je comprenne. Merci pour les réussites que vous m'avez permis d'atteindre, peu de choses se seraient faites sans vous deux.

Merci à Guillaume S. pour toutes les excellentes discussions que nous avons eues, sur des centaines de sujets, et les heures de gameplay endiablées. Merci aussi à Léa H. pour son accueil toujours chaleureux.

Merci à Amaury B. et Julie A. et à leur amour invétéré des peluches. Je me souviens avec plaisir de notre voyage (enrhumé) en Alsace.

Merci à Christophe L. pour m'avoir apporté des éléments... instructifs sur les choses de la vie (dont l'administration allemande). Merci de même à Nicolas d'avoir accepté de nous accompagner à Cologne pour un sympathique séjour.

Merci à Arnaud E. de m'avoir offert son bureau et (le commencement du début de l'introduction de) ses connaissances en théorie des catégories. Merci pour tous les sous-entendus et toutes les découvertes, excellentes comme inattendues. Et merci à Grégoire et à Bojo pour l'accueil à Mareil jusque tard dans la nuit.

Merci à toute la bande : François-Marie, Nour, Sophia, Morgane, Sarah et Arthur. Nos restaurants, nos longues conversations sur nos souvenirs de prépa, nos franches tranches de rire devant les déboires des uns et des autres, nos échanges de BDs, etc. En particulier, merci à Morgane de m'avoir accueilli à Grenoble, et à François-Marie non seulement pour avoir récupéré de nombreux ouvrages, mais aussi pour tout ce qu'il m'a apporté durant ces années en prépa comme à l'X.

Merci à Thomas LM. pour m'avoir supporté en tant que colocataire pendant 2 ans. Bien peu nombreux sont ceux qui auraient été à même de le faire, surtout vu le nombre de parties de Smash et de vaisselle que cela t'a demandé !

Merci aux habitants du 93 route des Gardes, pour leur joie de vivre, leur organisation, leur aide (notamment face à une certaine porte récalcitrante), etc.

Merci à Gabriel P. de nous avoir prêté les ZomeTools indispensable (car complètement contingent) à la réalisation de magnifiques polytopes dans notre bureau.

Merci à Mathieu R. pour ses yeux plein d'étoiles.

Merci à Gabin M. pour le soutien et l'amitié qu'il m'a témoigné sans forcément s'en rendre compte.

Merci à MCV pour le savoir qu'elle m'a transmis et l'occasion qu'elle m'a offerte de me lancer dans la formidable aventure des khôlles de l'autre côté du miroir. Merci pour nos passionnants échanges de mails, des tranches de vie toujours bienvenues. Merci à Éric CV. pour son le conseil avisé qui m'a conforté dans le choix de mes directeurs.

Merci Anthony R. pour la visite du laboratoire de Chimie, et la stimulante question de géométrie plane qu'il m'a posée.

Merci à Clément R. pour sa surprenante question : non, il n'y a toujours pas de zoologie bien organisée des polyèdres.

Merci à François Ch., ce sera toujours un plaisir de jouer au frisbee avec toi ou d'admirer ta carte des courants océaniques.

Merci à Roni K. d'avoir repris l'origami et d'avoir entretenu la vitrine après mon passage.

Merci à toute ma famille. Mes parents pour m'avoir supporté (dans tous les sens du terme) durant de nombreuses années, et d'avoir accepté les changements houleux qui ont suivi mes multiples prises de consciences. Ma sœur, pour être toujours un source de grandes surprises, que ce soit dans les cadeaux que tu fais que dans les décisions que tu prends. Mes grands-parents pour avoir aidé durant les épreuves de ma jeunesse, pour m'avoir toujours accueilli en vacances et m'avoir prêté votre appartement alors que ma deuxième année commençait. Ma mamie de m'avoir transmis l'amour des mathématiques et de l'enseignement, et pour toujours accepter de discuter le fond des choses. Janine pour l'accueil à Bordeaux et l'ouverture d'esprit dont tu fais preuve. Mes cousins pour tous ces Noëls, ces anniversaires, ces vacances, ces jeux vidéos (en particulier V), ces repas, ces joyeux moments... et bravo à tous ! Merci à mes oncles et tantes de me permettre de contempler de multiples choix de vie, certain qui me donne envie et d'autres qui me confortent dans ma volonté de ne pas les reproduire.

Merci à ma confraternité des thésards combinatoriciens, autrement appelé "Doctorants en Géométrie Combinatoire". Doriann, Daniel, Noémie, Balthazar, Chiara, Loïc, j'ai pris grand plaisir à co-organiser le DGeCo avec vous, et si c'était à refaire, je referais ce chemin (comme disait Aragon) ! On s'est bien amusé, on a bien progressé et j'ai hâte de vivre avec vous la fin de cette grande aventure (qui n'est que le début des suivantes). J'ai gardé Eva à part, car rien ne remplace une telle co-bureau, une telle consœur ! On a partagé bien plus qu'un directeur, quelques livres, des déboires administratifs, des notions de maths et de (longs) voyages en train : tu m'as grandement motivé au sortir du Covid pour venir au bureau, et un florilège de bonnes décisions en a découlé. Merci Eva.

Merci à Viviane P. pour ses conseils, son aide et son sens de l'organisation. Merci pour ton regard pertinent sur les questions humaines : cela m'a fait beaucoup réfléchir.

Merci à toute l'équipe du LIX : outre un passionnant séminaire aux exposés toujours compréhensibles, je me souviendrai longtemps du trépidant *escape game* que nous avons résolu ensemble.

Merci Corentin de m'avoir donné dès mes début la motivation de revenir, encore et encore. Ce fut très très important pour moi.

Merci à Jimmy L. d'avoir été un chef d'équipe plein de ressources. J'ignore comment tu fais pour jongler avec autant de missions, mais tu as toujours su apporter des solutions pertinentes à mes problèmes, avec une indéfectible bonne humeur ! Et merci d'avoir accepté de diriger mon comité de suivi de thèse alors que je ne connaissais encore personne.

Merci aux gens compétents de l'administration de l'IMJ et de Sorbonne Université : Sitti M., Évariste C., Ayano T., Émilie J., vous avez été d'un recours indispensable pour l'organisation de ma thèse à de nombreux égards.

Merci aux étudiants à qui j'ai eu la chance de donner cours pour leur L1 et leur L2. Même si ma mémoire ne me permet pas de retenir vos noms, je me souviens des challenges, des épiphanies, les vôtres comme les miennes.

Merci à eux avec qui j'ai eu l'occasion de faire du frisbee. Que ce soit les sympathiques rencontres dominicales à Cité U, ou les anciens de la section, chercheurs aux SageDays, les gens de passage chez moi : j'aime toujours autant le frisbee malgré les rares opportunités que j'ai de le pratiquer.

Merci à Raphaël P. pour sa bonne humeur, son sempiternel sourire, ses discussions passionnantes et l'aide efficace qu'il distribue toujours avec gentillesse.

Merci à Jacques A. et Xenia de régulièrement avoir essayé de me sortir de ma zone de confort, avec un bilan positif.

Merci à mes co-bureaux, Thomas G., Francisco M., Pierre G., et tous ceux qui y sont passés temporairement. J'y ai toujours trouvé une ambiance à la fois chaleureuse (surtout l'été) et propice au travail. Bien des fois, j'aurais aimé que quelqu'un rentre par hasard dans notre bureau et contemple les écritures hétéroclites et ésotériques qui couvrent inlassablement le tableau.

Merci à tous ceux qui sont passés dans le couloir des doctorants à l'IMJ. Camille, Lucas, Étienne, Thomas (tous les Thomas), Mahya, Perla, Adrien, Adrien, Mattias, Christina, Mathieu, Haowen, Nastaran, Tristan, les pauses du midi n'auraient certes pas été si longues sans vous, mais

mon thé aurait surtout grandement manqué de saveur ! Gracias a los hispanohablantes, Anna, Juan Felipe, Joachin, me hubiera gustado practicar más mi español con vosotros, pero ya estoy encantado de haberos conocido. Obrigado a toda comunidade brasileira, Nelson, Thiago, João, Pietro, Odylo, mesmo que você sempre chegasse barulhento, os sorrisos que os acompanhavam eram um prazer de ver. (Je suis sûr que j'ai oublié quelqu'un...)

Merci à Lionel Pournin d'avoir accepté de rapporter ma thèse : ta relecture attentive m'a beaucoup aidé à en parfaire les détails jusque-là incertains. Merci pour les questions que nous avons discutées ces dernières années, et j'espère que tu auras apprécié les améliorations survenues depuis ma soutenance de M2.

Merci à Frédéric Meunier d'avoir accepté de faire partie de mon jury de soutenance, et de mon comité de suivi de thèse. Merci aussi grandement de m'avoir conseillé la lecture très enrichissante de Matoušek, et d'avoir participé au DGeCo avec des questions toujours pertinentes (et difficiles).

Thanks to Fu Liu to have accepted to review my thesis. Thanks to Vic Reiner, Jesús De Loera and Martina Juhnke for being part of the jury of my defense. Your articles and presentations were a great source of inspiration and understanding, thus it is an honor for me to show you my modest contribution.

Thank a lot to all the mathematicians that I have met during my Ph.D. You taught me a lot about mathematics, life, people, presentations, and thinking in general. I will not list every one, as I don't want to double the length of my thesis, but I want to address special thanks to Ziegler, Sturmfels, Matoušek, Diestel, Santos for their beautiful books; to Williams, Postnikov, Hampe, Ardilla & Aguiar for their instructive articles, and all the people I have met at Kleinwalsertal, Bielefeld, PAGCAP, PolyTopics, Polytopes in Paris, and many more events.

Thank a lot to the whole Sage community : your well writen functions (and tutorials) helped me understand both maths and computer science. Especially, thank to all the team of SageDays 117 that got me involved in the project and allowed me to improve drastically me coding skills.

Vielen Dank an Raman und Aenne für das großartige Projekt, das wir gemeinsam durchgeführt haben. Dadurch konnte ich erstmals in der riesigen Welt der Optimierung von Polytopen Fuß fassen. Ich habe meinen Aufenthalt in Frankfurt, seine Atmosphäre, seine Architektur und seine Mathematiker sehr genossen.

Vielen Dank an das Osnabrücker Team, das mich als Postdoktorand willkommen heißt. Justus, ich habe mich gefreut, dich in Österreich kennenzulernen! Martina, ich hoffe, dass dich unsere zukünftige Zusammenarbeit dich genauso begeistert wie mich.

Vielen Dank an die Verwaltung der Universität Osnabrück, Frau Mallek und Frau Wolterink, die mir die Anreise erheblich erleichtert haben.

感林岳教我中文... 取得了一定的成功！恭喜您完成文，我很快就遇到其他令人的言。

また折りをやりたいと思わせてくれた早苗さんに感します。アパトをったり、友への完璧なり物を作ったりするだけでなく、折りは折るときにいつもしみの源です。

Introduction

That the powerful play goes on, and you may contribute a verse.
– Walt Whitman, "Oh Me! Oh Life!" in *Leaves of Grass*

Mathematicians study geometry for more than 2 500 years. Even though they may not be the first to have explored such concepts, Greek scholars are renown for having introduced both the art of the proof and the formalization of abstract geometry. In particular, polygons and polyhedra seem to have held a very special place in their representation of the world.

Polygons, for instance, were at the heart of a burning controversy about the essence of Nature. At first, integers were thought to be the *natural numbers*. Furthermore, as ratios of integers, the *rational numbers* were also thought as perfect: a fraction is no more than two commensurable (integer) lengths, that is two lengths that can be drawn as integer lengths in a well-chosen scaling. Greek philosophers thought for a time that perfect objects can only involve such numbers, but regular polygons seem to be perfect as well: nevertheless, the length of the diagonal of a square with unit-length side is not a rational number, and more and more irrational numbers appear when considering all regular polygons. This cataclysmic discovery led the majority of Greek mathematicians and philosophers to accept *constructible numbers* as (somewhat) perfect, and to state the famous three problems of Ancient history: trisecting the angle, doubling the cube, and squaring the circle.

Besides, 3-dimensional studies were not outdone. Pythagoras, and his school after him, discovered the tetrahedron, the hexahedron (*a.k.a.* the cube), and the dodecahedron. Later on, Theaetetus constructed the two last of the five *Platonic solids*, namely the octahedron and the icosahedron. Plato, in the *Timaeus*, associated each of these five polyhedra with an element: Fire (tetrahedron), Earth (cube), Air (octahedron), Water (icosahedron), and the element "the demiurge used for arranging the constellations on the whole heaven" (dodecahedron).

The Greek history of geometry is synthesized by Euclid. Books IV and XIII of his famous *Elements* ($\Sigma\tau o\iota\chi\varepsilon\iota\alpha$) are devoted to regular polygons and regular polyhedra, respectively. He proved numerous and numerical relations between these objects, gave explicit constructions, stated and solved problems and puzzles. In his honor, the name *Euclidean geometry* has ever since designated the usual geometry (which was the only existing one before the Euclid's fifth postulate was put into question, and Gauss defined non-Euclidean geometries).

Researches around polygons and polyhedra have never stopped since, and it is hard to find a great mathematician that has spoken no word about them. On top of that, polyhedra are among the very few abstract mathematical objects to make repeated appearances in Arts and Letters. To begin with, not only did Plato give his solids a central role in his cosmogony, but Johannes Kepler, in his *Mysterium Cosmographicum*, also thought that the distances between the planets in the solar system were explained by the possibility to circumscribe Platonic solids around each of their orbits. He soon abandoned this idea when realizing planet's orbits were not circular. Architecture obviously benefited from the study of plane and spacial geometry, while making contributions to it. Especially, it is worth mentioning the *Grande Arche de La Défense*, designed by Johan Otto von Spreckelsen as a gigantic 3-dimensional embodiment of a 4-dimensional cube. Painting as well, above all during the Renaissance period, was largely inspired by plane geometry and the symmetry regular polygons and polyhedra exhibit. Albrecht Dürer famously portrayed an eponymous polyhedron in *Melancolia I*, and Platonc solids appear in the *Portrait of Luca Pacioli* from Jacopo de' Barbari. Even music is imbued with geometry: the *Timaeus* is a dialogue on music, and the recent piece *Polytopes* from Iannis Xenakis is constructed thanks to polytopal ideas.

By dint of all these cultural occurrences, polyhedra are well known to the public. It is then quite remarkable that the research on polygons, polyhedra, and polytopes, is still greatly flourishing: after thousands of years and thousands of contributors, some questions are still open, and new exciting ones keep being thought of.

Such a keen interest for polyhedra may be explained by their duality. Indeed, polyhedra are both simple to define, and rich in the behaviors they can express; they are sitting on the fence between concrete numerical geometry and purely abstract topology; they are drawn and visualized

by everyone but elementary properties can be hard to prove; they seem alighting from the realm of ideas, although they can be directly encountered in nature (from capsids of viruses to furnishing). If this has participated in draping polyhedra with a mystical allure, it has also exerted a prolific fascination on numerous mathematicians. In particular, the help of modern computers have greatly improved our capacity to construct polyhedra and play with them, leading to numerous conjectures and open problems. In return, the discrete nature of computer science's problems has paved the way for a large panel of new challenges and applications of polyhedral geometry.

The main objects of the present manuscript are polytopes: a polytope is defined as the convex hull of finitely many points in the Euclidean space $\mathbb{R}^d$. As such, polytopes are the generalization of polygons and polyhedra to higher dimensions. In this thesis, I will try to unveil some links between the geometric aspects of polytopes and their combinatorial behaviors. We give hereafter a precise description of the context each chapter contributes to, and the new results proven. Two concepts will be at the center of this polytopal journey: *generalized permutahedra* and *linear programs*.

The first notion arises from the systematic research of the combinatorial properties of polytopes, which have played a great role in the development of the field since their (re)popularization during the 20th century, see [Grü03, Zie98] for the history of the subject. Polytopes naturally come with various combinatorial properties: foremost, one can try to understand their faces (which are themselves polytopes), and how its faces are included one in another, leading to the definition of the *face lattice* of a polytope. If exploring the face lattice of a polytope is already fascinating, the reverse question turns out to be even more fecund: given a combinatorial structure, how to construct a polytope to embody it? An epitome of such quest is surely the construction of the *permutahedron*. Discovered by Schoute in 1911 [Sch11], the vertices of the permutahedron are in one-to-one correspondence with the permutations. Moreover, the faces of it can be labelled by the *ordered partitions*, while its (oriented) graph naturally describes the *Bruhat order* on permutations.

But this is only the tip of the iceberg: the permutahedron can be *deformed* (in a sense that will be made clear in Section 2) to create *generalized permutahedra*. Originally defined by Edmonds [Edm70] under the name *polymatroids*, their rediscovery by Postnikov in 2009 [Pos09] was the starting point of a myriad of researches. In particular, various combinatorial families can be encapsulated in the combinatorics of certain generalized permutahedra. A first example is the (hyper)cube whose vertices are in bijection with binary sequences, and help for instance to understand Hamming codes [Ham50]. Besides, the matroid polytopes also arises as generalized permutahedra [ABD10, Ard21], and play an important role in the search for Minkowski indecomposable generalized permutahedron. But the one and foremost example of generalized permutahedra is probably the *associahedron*: known as the "mythical polytope" [Hai84] and introduced by Tamari [Tam51] and Stasheff [Sta63], its first realizations were given by Milnor (unpublished), Haiman [Hai84], Lee [Lee89], and then Loday [Lod04, PSZ23]. Its combinatorics encapsulate the one of *Catalan families*, that is to say triangulations of a polygon, binary search trees, subpartitions of the staircase partition, non-crossing arborescences, etc. The realization of the associahedron as a generalized permutahedron allows for numerous links between the combinatorics of permutations and Catalan families, this is nowadays the subject of an abundant literature ranging from mathematical physics [AHBHY18] to cluster algebra [FZ02] and moduli space [Sta63, Kel01].

On top of that, the set of generalized permutahedra is not only a list of relevant examples, it is also endowed with its own structure: it forms a cone, called the *submodular cone*. This cone is the type cone of the permutahedron, in the sense of McMullen [McM73], and as such have been studied from a wide variety of perspectives: for instance, the name *submodular cone* comes from the notion of diminishing returns in economy [JKS22], while in the domain of toric varieties, it is known as the *numerically effective cone* [CLS11]. Furthermore, it is the natural (and universal) setting for the construction of a Hopf monoid of polytopes [AA17]; it appears in the study of the Grassmannian, especially in positive geometry [AHBL17, LP20], and the amplituahedron program (with links to mathematical physics) [AHT14, AHBC+16].

On the other side, linear programming delves into the geometrical aspects of polytopes. Optimization is known for being a supremely useful but notably difficult theory, and linear optimization

encompasses the optimization problems in which both the constraints and the quantity to optimize are linear in the involved variables. This kind of problems originally appeared for logistic grounds: Dantzig [Dan63] was working for the U.S. Air Force in 1947 when he introduced the general concept, and Kantorovich already thought about some specific cases in 1939 for the timber industry of U.S.S.R. However, the field grew only slowly at first, until two crucial breakthroughs: Kantorovich and Koopmans earned the Nobel Prize of Economy in 1975 for their work on resource allocation, and computers became a growing part of the organization of our civilizations throughout the end of the century.

There are several methods to solve a linear problem, among which some are known to be of polynomial complexity (see [MG07, Chapter 7] and [RTV05, DNT08]), but the original method, which is still of prime importance, is the simplex method, whose complexity class is not fully understood for now [KM72, DS14]. The *simplex method* can be thought of as the counterpart of the Gaussian elimination, but when dealing with linear inequalities (and a linear functional to optimize). In broad, the key idea is to consider the set of solutions of your system of inequalities as a polytope (or an unbounded polyhedra), and to jump from one vertex onto one of its neighbors, increasing the value of the linear functional at each step. This method will end at a point maximizing the linear functional, thanks to the convexity of the polytope. Nevertheless, one needs to set up a rule on how to choose the neighbor to jump onto: this is the *pivot rule*. Pivot rules and how to elect the right one have been written about extensively (see [MG07, APR14, DS14, FS14] among many other), and we certainly do not intend to fully answer this question here.

Instead of taking a computer science approach, the point of view we would like to develop on the simplex method centers around its combinatorial behavior: given a polytope and a direction, what can be said about the structure of the set of (edge) paths on the polytope that are increasing for this direction? There are several ways to understand (and to tackle) this question. When focusing on the worst case scenario, it is natural to explore monotone paths [AER00, BLL20], and even monotone path polytopes [BS92, ALRS00, MSS20, BL21], while new works focus on the whole decision tree that a (memory-less) pivot rule gives rise to, and construct several pivot rule polytopes [BDLLS22, BDLLSon]. Among the pivot rule polytopes, the *max-slope pivot rule polytope* is a generalization of the monotone path polytope, moreover, the latter is a deformation of the first.

In addition, the pivot rules that max-slope pivot rule polytopes and monotone path polytopes casts about, namely the *max-slope pivot rules* (a generalisation of *shadow vertex rules*), echo more algebraic researches. More precisely, *fiber polytopes* were defined by Billera and Sturmfels [BS92] to understand both projections and subdivisions of polytopes. While pivot rules address edge paths on polytopes, fiber polytopes aim at encompassing triangulations which can be thought of as their higher-dimensional counterpart. This construction opened the door to new ways of thinking about classical polytopes: for instance, the permutahedron is the monotone path polytope of the cube [BS92], and the fiber polytope for the projection from a simplex is deeply linked to the triangulations of points configuration through the secondary polytope of Gelfand, Kapranov and Zelevinski [GKZ90, GKZ91]. Furthermore, it led to fruitful developments in a wide variety of research areas such as convex geometry [Est08, Mer22], type B Coxeter associahedron [Rei02], and even power series [McD95].

In this manuscript, we study on the one hand generalized permutahedra and the submodular cone, and on the other hand max-slope pivot rule polytopes and fiber polytopes. Although the domains undeniably interact all along the present thesis, ideas coming from one side being steadily applied to the other, the pre-eminent result creating a neat bridge between these two realms is Section 3.3: we state that the combinatorial behavior of the class of max-slope pivot rules can be handled more easily by embedding the question inside the realm of generalized permutahedra. We hope that such a new insight may open the way to a better understanding of (memory-less) pivot rules.

The rest of this introduction details the content of the present thesis, especially the contexts and results of each following section.

Section 1 is dedicated to a short introduction to the basic notions we will need on polytopes, order theory and linear programming. The three main chapters (Sections 2 to 4) begin by their own preliminaries, before presenting two new results. For each result, we have implemented the key objects thanks to the open source software Sage. We end each sub-section by discussing these implementations and putting some light on possible mathematical perspectives.

After the preliminary Section 1, each chapter can be read independently, even though they are thought to be read in order. Likewise, inside each section, the first sub-section shall be read first, but the two others can be read independently. Note however that Section 4.3 deeply relies on Section 3.2.

Section 1: Preliminaries. The reader probably already knows what is presented in this introductory chapter. The crucial definitions are highlighted so he or she can swiftly consult them and look at the figures. Yet, we may emphasize some key elements:

- Partially ordered sets: The notion of pre-orders is probably the less known among the presented notions, while ordered partitions and permutations are the most important ones.
- Polytopes: The definition of polytopes, faces and lattices of faces are of prime importance, but the dual notion of fans and normal fans is more central in this thesis. The examples, especially the permutahedron and the associahedron, will be the key objects for the next chapters.
- Linear programming: As this thesis is not about linear programming itself, its presentation will be succinct and only aims at giving a different yet enlightening point of view on the geometry of polytopes.

Section 2: Deformations of polytopes. The first main section is devoted to the study of deformations of polytopes. A *deformation* of a polytope P can be equivalently described as (i) a polytope whose normal fan coarsens the normal fan of P [McM73], (ii) a Minkowski summand of a dilate of P [Mey74, She63], (iii) a polytope obtained from P by perturbing the vertices so that the directions of all edges are preserved [Pos09, PRW08], (iv) a polytope obtained from P by gliding its facets in the direction of their normal vectors without passing a vertex [Pos09, PRW08]. A sequence of deformations is illustrated in Figure 10. The deformations of P form a polyhedral cone under dilation and Minkowski addition, called the *deformation cone* of P [Pos09]. The interior of the deformation cone of P, called the *type cone* [McM73], contains those polytopes with the same normal fan as P. When P is a rational polytope, it has an associated toric variety [CLS11], and the type cone (also known as the *numerically effective cone* or *nef cone*) encodes its embeddings into projective space [CLS11, Sect. 6.3]. Among the different ways to parametrize and describe the deformation cone of a polytope P (see *e.g.* [PRW08, App. 15]), we use the parametrization by the *heights* corresponding to the facets of P and the description given by the *wall-crossing inequalities* corresponding to the edges of P [CFZ02]. While this inequality description is immediately derived from the linear dependencies among certain normal vectors of P, it is in general more difficult to extract the irredundant facet inequality description of the deformation cone.

Fundamental examples of deformations of polytopes are the *deformed permutahedra* (*a.k.a.* generalized permutahedra or polymatroids) studied in [Edm70, Pos09, PRW08], which are classically parametrized by *submodular functions*. The set of deformed permutahedra is the set of deformations of the standard permutahedron. As such, it forms a cone, namely the *submodular cone*. In the present thesis, we give the facet-description of some faces of the submodular cone. The key idea lies in the following fact: if Q is a deformation of P, then the deformation cone of Q is a face of the deformation cone of P, see Section 2.1. As numerous deformations of the standard permutahedron are already well studied, this fact grants us access to faces of the submodular cone. We present two new results in this domain: the facet-description of the deformation cone of graphical zonotopes in Section 2.2, and the facet-description of the deformation cone of nestohedra in Section 2.3. Moreover, we characterize which graphical zonotopes and which nestohedra have a simplicial type cone.

Section 2.2 is directly adapted from our paper [PPP22b] (accepted for publication), while Section 2.3 is adapted from our published paper [PPP23].

Section 3: Max-slope pivot rule polytopes. The second main section is dedicated to max-slope pivot rule polytopes. For solving linear programs, the *simplex method* has been used since its introduction by Dantzig [Dan63]. This algorithm was not only used for numerical computing, it also brought new understanding to the combinatorial and geometrical problems, such as finding a flow in a graph or the largest circle in a polygon [MG07]. The simplex method requires a *pivot rule* to guide the consecutive choices that are to be made. Understanding pivot rules is crucial to discuss the complexity of the simplex method [KM72, APR14, DS14, FS14]. An important class of pivot rules are the *max-slope pivot rules*, introduced in [BDLLS22] to generalize the *shadow vertex rule*. A given max-slope pivot rule is encoded by the *arborescence* (directed tree) it induces on the graph of the feasibility domain. Remarkably, when the feasibility domain is a polytope P, the combinatorial behavior of the max-slope pivot rules can be captured by the face lattice of a polytope, called the *max-slope pivot rule polytope* of P.

These polytopes are not yet well understood. The case of the standard cube has been detailed in the original article [BDLLS22], and the simplex will be dealt with in the upcoming [BDLLSon]. In the present thesis, we explore in Section 3.2 the max-slope pivot rule polytope of the cyclic polytopes, that we call *cyclic associahedra*, helped by ideas developed in [ALRS00] for fiber polytopes between cyclic polytopes. They generalize the standard associahedron Asso_n defined in Section 1.2.4, and their genesis prompts a natural complexity parameter on Catalan families (parenthesizations, binary search trees, triangulations of polygons...).

Moreover, generalized permutahedra will step again into play in Section 3.3, and prove themselves a powerful framework to analyze max-slope pivot rule polytopes. The key idea of this part is to realize that comparing slopes of line segments between points amounts ultimately to comparing real numbers, and consequently to wander inside the *braid fan* (the normal fan of the permutahedron). This shed a new light on max-slope pivot rule polytopes, linking them with generalized permutahedra, and help us understand their behavior with respect to products of polytopes. We conclude this part by constructing the max-slope pivot rule polytopes of products of simplices. Thanks to the work of Chapoton and Pilaud [CP22] on *shuffle products* of generalized permutahedra, we show that the max-slope pivot rule polytope of the product of simplices is the shuffle product of the max-slope pivot polytope of each involved simplex. Furthermore, we explicit a piece-wise linear transformation from the max-slope pivot rule polytope of a simplex to the standard associahedron of Loday [Lod04], and point out that several basic examples of products of simplices gives rise to known polytopes, *e.g.* multiplihedra and constrainahedra.

Section 4: Fiber polytopes. The third main section focuses on fiber polytopes. In their seminal paper, Billera and Sturmfels [BS92] introduced and studied *fiber polytopes*, which have since proven to be a powerful tool to understand both projections and subdivisions of polytopes. It has also found applications in algebraic geometry [McD95], and theoretical physics as part of the *amplituhedron program* [GPW19, AHHST22]. In particular, numerous famous polytopes can be realized as fiber polytopes, prominently permutahedra, associahedra, and some other generalized permutahedra naturally appear [BS92, ALRS00, Rei02, LRS10], and new constructions come to enrich the subject, such as fiber bodies [Est08, Mer22], or (partial) sweep polytopes [PP22].

However, fiber polytopes are hard to compute in general. In their original paper [BS92], the authors link the fiber polytopes to *secondary polytopes* defined by Gelfand, Kapranov and Zelevinsky in [GKZ90, GKZ91], the vertices of which are in bijection with triangulations of a point configuration. On top of that, when one projects a polytope P onto a segment of direction $\boldsymbol{c}$, the associated fiber polytope is the *monotone path polytope* of P in direction $\boldsymbol{c}$: its vertices are in bijection with the monotone paths that the shadow vertex rules follow to go from the minimal vertex to the optimal one (*i.e.* from $\boldsymbol{v} \in \mathsf{P}$ that minimizes $\langle \boldsymbol{v}, \boldsymbol{c} \rangle$ to $\boldsymbol{v} \in \mathsf{P}$ maximizing it). Billera and Sturmfels constructed the monotone path polytopes of simplices and cubes, while recent articles solved the cases of cyclic polytopes [ALRS00], and cross-polytopes [BL21] and more. Section 4.2 centers on the monotone path polytopes of hypersimplices. We connect monotone paths on an hypersimplex with the realm of lattice paths, and conclude by giving some arguments in favor of log-concavity of the number of (coherent) monotone paths sorted by length, which was

conjectured by Jesús de Loera (for all polytopes).

Numerous works on fiber polytopes either deal with projections onto a segment (*i.e.* monotone path polytopes), or examine the general case. In Section 4.3, thanks to the ideas elaborated in Section 3.2 and [ALRS00], we tackle the fiber polytope for the projection of the cyclic polytope of dimension d onto the cyclic polytope of dimension 2.

1 Preliminaries

All things are difficult before they are easy.
– Thomas Fuller

1.1 Partially ordered sets

This thesis is not on partially ordered sets, but some basic knowledge of order theory is necessary to understand combinatorial polytope theory, and especially the combinatorics of the permutahedron, see Section 1.2.3. For this reason, we will define in this section the notions of partially ordered sets, lattices, pre-orders and ordered partitions. These notions are presented for the sake of completeness and self-containment, and the reader, surely well aware of them, shall focus on pre-orders and ordered partitions.

We denote $[n] := \{1, \dots, n\} \subset \mathbb{N}$ for $n \geq 1$, and $[i, j] := \{i, \dots, j\} \subset \mathbb{N}$ for integers $i < j$.

Definition 1.1. A *binary relation* on a set E is a subset $\mathcal{E}$ of $E \times E$, and we denote $\mathcal{R}(x, y)$ instead of $(x, y) \in \mathcal{E}$. A binary relation is *total* when $\big(\mathcal{R}(x, y)$ or $\mathcal{R}(y, x)\big)$ for all $x, y \in E$, and we emphasize its possible non-totality by calling it *partial* in the general case. A binary relation is

1. *reflexive* when, for all $x \in E$, $\mathcal{R}(x, x)$.
2. *symmetric* when for all $x, y \in E$, if $\mathcal{R}(x, y)$ then $\mathcal{R}(y, x)$.
3. *anti-symmetric* when for all $x, y \in E$, if $\mathcal{R}(x, y)$ and $\mathcal{R}(y, x)$ then $x = y$.
4. *transitive* when for all $x, y, z \in E$, if $\mathcal{R}(x, y)$ and $\mathcal{R}(y, z)$ then $\mathcal{R}(x, z)$.

A binary relation is called:

(a) a *pre-order relation* when it is reflexive and transitive.
(b) an *equivalence relation* when it is reflexive, symmetric, and transitive.
(c) an *order relation* when it is reflexive, anti-symmetric and transitive.

A *partially ordered set* or *poset* is a couple $(E, \mathcal{R})$ where $\mathcal{R}$ is a (partial) order relation on E.

To a pre-order $\mathcal{R}$, we associate an equivalence relation $\mathcal{S}$ with $\mathcal{S}(x, y) = \big(\mathcal{R}(x, y)$ and $\mathcal{R}(y, x)\big)$. This creates a partition of E into *equivalence classes* $\mathrm{cl}(x) := \{y \in E \ ; \ \mathcal{S}(x, y)\}$. On the set of equivalence classes, $\mathcal{R}$ induces a pre-order $\overline{\mathcal{R}}$ defined by $\overline{\mathcal{R}}\big(\mathrm{cl}(x), \mathrm{cl}(y)\big) = \mathcal{R}(x, y)$. With this definition, $\overline{\mathcal{R}}$ is not only reflexive and transitive, but also *anti-symmetric*. When denoting a pre-order by the infix notation $\preccurlyeq$, we will denote its equivalence relation by $\simeq$ and introduce $x \prec y := \big(x \preccurlyeq y$ and not $x \simeq y\big)$. We will also slightly abuse notations by denoting again $\preccurlyeq$ the partial order associated on the set of its equivalence classes.

In a poset $(E, \preccurlyeq)$, an element y *covers* an element x when $x \prec y$ and there exists no $z \in E$ with $x \prec z \prec y$. A poset is *graded* when it can be endowed with a *rank function* $r : E \to \mathbb{N}$ such that $r(y) = r(x) + 1$ when y covers x.

We say that a pre-order $\trianglelefteq$ *extends* a pre-order $\preccurlyeq$ when if $x \preccurlyeq y$, then $x \trianglelefteq y$. This extension shall be thought of as adding an order relation between some pairs (x, y) that are not already ordered by $\preccurlyeq$.

The *dual* of a poset $(E, \preccurlyeq)$ is the poset $(E, \succcurlyeq)$ where $x \succcurlyeq y$ if and only if $y \preccurlyeq x$.

Definition 1.2. In a poset $(E, \preccurlyeq)$, the *meet* of two elements $x, y \in E$ is, when it exists, the unique maximum $x \wedge y$ of the elements that are less than both x and y: $x \wedge y = \max\{z \in E \ ; \ z \preccurlyeq x, \ z \preccurlyeq y\}$.

The *join* of two elements $x, y \in E$ is, when it exists, the unique minimum $x \vee y$ of the elements that are greater than both x and y: $x \vee y = \min\{z \in E \ ; \ x \preccurlyeq z, \ y \preccurlyeq z\}$.

A poset is a *lattice* when every pairs of elements have a meet and a join.

A lattice $(\mathscr{L}, \preccurlyeq)$ always has a minimum element called 0 by convention, and a maximal element called 1 by convention. An *atom* is an element that covers 0, and the lattice is *atomic*[1] when all its elements can be written as a join of atoms. A *co-atom* is an element that is covered by 1, and the lattice is *co-atomic*[1] when all its elements can be written as a meet of co-atoms.

The dual of $(\mathscr{L}, \preccurlyeq)$ is the poset $(\mathscr{L}, \succcurlyeq)$. It is a lattice called its *dual lattice*.

[1] Some authors prefer the term *(co-)atomistic*, saving the word *(co-)atomic* for another property.

Definition 1.3. An *ordered partition* is an ordered collection of sets $I_1 \prec \cdots \prec I_k$ that partition $[n]$, *i.e.* $I_i \cap I_j = \varnothing$ for all $i \neq j$ and $\bigcup_i I_i = [n]$. Dually to ordered partitions, we define an *(integer) surjection* as a map $\sigma : [n] \to [k]$ with $k \leq n$ such that for all $a \in [k]$, $\sigma^{-1}(a) \neq \varnothing$. The collection $I_a := \sigma^{-1}(a)$ for $a \in [k]$ form an ordered partition where $I_a \preccurlyeq I_b$ when $a \leq b$. When $k = n$, the surjection is a bijection, and the ordered partition is the corresponding permutation.

A surjection σ naturally induces a total pre-order on $[n]$ by $i \preccurlyeq j$ when $\sigma(i) \leq \sigma(j)$.

1.2 Polytopes

Polytopes are beautiful objects, they are going to be at the heart of the present thesis. The aim of this section is to introduce the basic definitions and properties of polytopes that will be used all along this thesis. For a complete presentation on polytopes, the reader is invited to look at the wonderful *Lectures on Polytopes* of Ziegler [Zie98]. As what we state here are known theorems, we will mainly refer to the literature for proofs.

Polytopes come, foremost, as objects embedded in the Euclidean space $\mathbb{R}^d$. Vectors of $\mathbb{R}^d$ will usually be denoted in bold font like $\boldsymbol{x} \in \mathbb{R}^d$, and their coordinates are the real numbers $x_1, \dots, x_d$. We denote the standard basis of $\mathbb{R}^d$ by $(\boldsymbol{e}_1, \dots, \boldsymbol{e}_d)$, and for $\boldsymbol{x}, \boldsymbol{y} \in \mathbb{R}^d$, the standard scalar product is $\langle \boldsymbol{x}, \boldsymbol{y} \rangle := \sum_{i=1}^d x_i y_i$.

Definition 1.4. A *polytope* P is the convex hull of a finite number of points in $\mathbb{R}^d$:

$$\mathsf{P} = \operatorname{conv}\{\boldsymbol{v}_1, \dots, \boldsymbol{v}_n\} = \left\{ \boldsymbol{x} \in \mathbb{R}^d \ ; \ \begin{array}{l} \boldsymbol{x} = \sum_{i=1}^n \lambda_i \boldsymbol{v}_i \\ \forall i, \lambda_i \geq 0 \text{ and } \sum_{i=1}^n \lambda_i = 1 \end{array} \right\}$$

This endows polytopes with a first manifestation of duality, coming from the duality of $\mathbb{R}^d$ as a Euclidean space: sharing a linear dependency is equivalent to being orthogonal to a vector.

Definition 1.5. For a vector $\boldsymbol{a} \in \mathbb{R}^d \smallsetminus \{\boldsymbol{0}\}$ and a constant $b \in \mathbb{R}$, the *affine hyperplane* $H_{(\boldsymbol{a},b)}$ associated is $H := \{\boldsymbol{x} \ ; \ \langle \boldsymbol{x}, \boldsymbol{a} \rangle = b\}$. An *open half-space* is the open component of $\mathbb{R}^d \smallsetminus H$ where H is an affine hyperplane of $\mathbb{R}_d$. A *closed half-space* is a closure of the latter. We denote $H^+_{(\boldsymbol{a},b)} := \{\boldsymbol{x} \ ; \ \langle \boldsymbol{x}, \boldsymbol{a} \rangle \geq b\}$ and $H^-_{(\boldsymbol{a},b)} := \{\boldsymbol{x} \ ; \ \langle \boldsymbol{x}, \boldsymbol{a} \rangle \leq b\}$ the two possible closed half-spaces.

Theorem 1.6. (Minkowski–Weyl, see [Zie98, Theorem 1.1]). *A polytope is a bounded intersection of closed half-spaces: There exist $\boldsymbol{v}_1, \dots, \boldsymbol{v}_n \in \mathbb{R}^d$ such that $\mathsf{P} = \operatorname{conv}\{\boldsymbol{v}_1, \dots, \boldsymbol{v}_n\}$ if and only if there exist $\boldsymbol{a}_1, \dots, \boldsymbol{a}_m \in (\mathbb{R}^d)^m$ and $b_1, \dots, b_m \in \mathbb{R}^m$ such that P is bounded and:*

$$\mathsf{P} = \bigcap_{j=1}^m H^-_{(\boldsymbol{a}_j, b_j)} = \left\{ \boldsymbol{x} \in \mathbb{R}^d \ ; \ \forall i, \ \langle \boldsymbol{x}, \boldsymbol{a}_j \rangle \leq b_j \right\}$$

Figure 1 illustrates this ambivalence. In the upcoming concept of duality, the notion of dimension and faces will play a role.

Definition 1.7. The *dimension* of P is the dimension of its affine hull, denoted $\dim(\mathsf{P})$.

Note that the dimension of a polytope is not necessary the dimension of the Euclidean space it is embedded in. Indeed, it often comes in handy to embed a polytope in an affine subspace (often a hyperplane) of $\mathbb{R}^d$, see for instance Section 1.2.3.

Definition 1.8. A *face* of a polytope P is a subset of P with, for some $\boldsymbol{c} \in \mathbb{R}^d$, the form: $\mathsf{P}^{\boldsymbol{c}} = \{\boldsymbol{x} \in \mathsf{P} \ ; \ \langle \boldsymbol{x}, \boldsymbol{c} \rangle = \max_{\boldsymbol{y} \in \mathsf{P}} \langle \boldsymbol{y}, \boldsymbol{c} \rangle\}$. The polytope P itself is a face of P (with $\boldsymbol{c} = \boldsymbol{0}$), and by convention $\varnothing$ is a face of P.

For a given direction $\boldsymbol{c} \in \mathbb{R}^d$, as P is compact (it is convex and bounded), the maximum δ of $\boldsymbol{y} \mapsto \langle \boldsymbol{y}, \boldsymbol{c} \rangle$ is attained on P, so the above is well-defined and non-empty. Moreover, the face $\mathsf{P}^{\boldsymbol{c}}$ trivially satisfies $\mathsf{P}^{\boldsymbol{c}} = H_{(\boldsymbol{c},\delta)} \cap \mathsf{P} = H^+_{(\boldsymbol{c},\delta)} \cap H^-_{(\boldsymbol{c},\delta)} \cap \mathsf{P}$. The Minkoswki–Weyl theorem then ensures:

Proposition 1.9. *Every face of P is a polytope.*

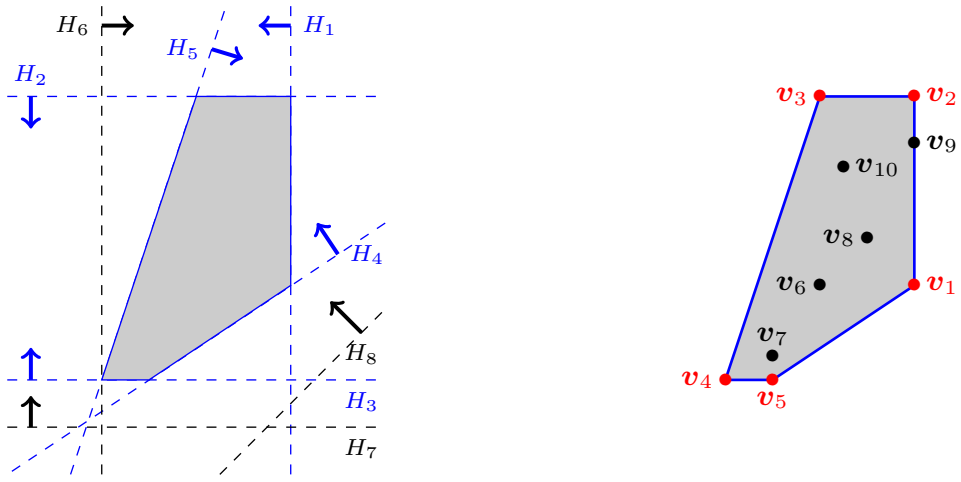

Figure 1: (Left) A polytope defined as a (bounded) intersection of half-spaces, the facet-defining ones being in blue, while black inequalities are redundant; (Right) the same polytope as the convex hull of a finite set of points, vertices are in red and edges in blue, while black points are redundant.

A hyperplane H such that $H \cap \mathsf{P}$ is a face of P will be called a *valid hyperplane*. Nevertheless, such a hyperplane does not necessarily appear in the description of P as a bounded intersection of half-spaces: a valid hyperplane sometimes shares with P a lower dimensional intersection. The dimension of a face F of P is the dimension of F as a polytope (*i.e.* the dimension of its affine hull). By convention, the empty face $\varnothing$ has dimension -1.

This naturally leads to ordering the set of faces of P by inclusion.

Theorem 1.10. ([Zie98, Theorem 2.7]). *The face lattice $\mathscr{L}(\mathsf{P})$ of P is the set of faces of P ordered by inclusion. It is a graded, atomic, co-atomic lattice with rank function $\mathsf{F} \mapsto \dim(\mathsf{F}) + 1$. The meet of two faces F and G is $\mathsf{F} \cap \mathsf{G}$ (while the join has no straightforward description).*

The faces of dimension 0, (*i.e.* the atoms of $\mathscr{L}(\mathsf{P})$) are the *vertices* of P, while the faces of co-dimension 1 (*i.e.* co-atoms of $\mathscr{L}(\mathsf{P})$) are the *facets* of P. The faces of dimension 1 are called *edges* of P, and the graph G_{P} whose vertices are the vertices of P and whose edges are the edges of P is the *graph of* P.

The set of vertices of P, denoted $V(\mathsf{P})$, is the unique set of extremal elements of P as a convex set, hence $\mathsf{P} = \operatorname{conv}\big(V(P)\big)$. The latter is called the *vertex-description* of P. In a dual fashion, the set of facets $\mathcal{H}(\mathsf{P})$ gives the unique minimal description of P as a bounded intersection of half-spaces. Such description is called the *facet-description* of P.

On that account, the description of a polytope comes across two mathematical challenges that can be solved on the algorithmic level but remain hard in high dimensions. On the one side, when a polytope is handled as a convex hull of points or as a set of linear inequalities, then extracting an extremal set from it is often arduous. On the other side, computing the vertex-description from a facet-description or the reverse can turn out to be convoluted (see the Fourier–Motzkin elimination of [Zie98, Chapter 1]).

The second notion of duality arises from a subtle embodiment of the above duality into the realm of lattices. Recall that the dual of a lattice is the lattice defined on the same set by reversing the order relation.

Theorem 1.11. ([Zie98, Section 2.3]). *The dual lattice of $\mathscr{L}(\mathsf{P})$ is (isomorphic to) the lattice of a polytope. Especially, for $\mathsf{P}^{\triangle} := \{\boldsymbol{c} \in \mathbb{R}^d \ ; \ \langle \boldsymbol{c}, \boldsymbol{x} \rangle \leq 1 \text{ for all } \boldsymbol{x} \in \mathsf{P}\}$, the lattice $\mathscr{L}(\mathsf{P}^{\triangle})$ is anti-isomorphic to $\mathscr{L}(\mathsf{P})$.*

Though prodigious, this fact will not be at the center of the current thesis, but it invites us to introduce the following.

Definition 1.12. A *polyhedral cone*[2] C is the positive span of finitely many vectors, meaning there exists $\boldsymbol{v}_1, \dots, \boldsymbol{v}_m \in \mathbb{R}^d$ such that:

$$\mathsf{C} = \left\{ \sum_{i=1}^{m} \lambda_i \boldsymbol{v}_i \ ; \ \forall i, \ \lambda_i \geq 0 \right\}$$

One can define the notion of faces for cones the same way as for polytopes.

A polyhedral cone is *simplicial* when $\boldsymbol{v}_1, \dots, \boldsymbol{v}_m$ are linearly independent. It is then a cone over a simplex (see Section 1.2.1), and all its faces are simplicial polyhedral cones.

Definition 1.13. A *fan* $\mathcal{F}$ in $\mathbb{R}^d$ is a collection of polyhedral cones of $\mathbb{R}^d$ such that if $\mathsf{C} \in \mathcal{F}$ then all faces of C belong to $\mathcal{F}$, and the intersection $\mathsf{C} \cap \mathsf{C}'$ is a face of both C and C' when $\mathsf{C}, \mathsf{C}' \in \mathcal{F}$.A fan is:

- *complete* when it covers $\mathbb{R}^d$, that is $\bigcup_{\mathsf{C} \in \mathcal{F}} \mathsf{C} = \mathbb{R}^d$.
- *essential* when none of its cones contains a line, that is $\{\mathbf{0}\} \in \mathcal{F}$.
- *simplicial* when all of its cones are simplicial.
- *polytopal* when it is the normal fan of a polytope.

The face lattice of a fan is the set of its cones, ordered by inclusion. For a polytope P, the poset of faces of its normal fan $\mathcal{N}_\mathsf{P}$ is anti-isomorphic[3] to its own face lattice $\mathscr{L}(\mathsf{P})$.

A fan $\mathcal{G}$ *coarsens* a fan $\mathcal{F}$ when the cones of $\mathcal{G}$ are unions of cones of $\mathcal{F}$. Conversely, in this setting, $\mathcal{F}$ *refines* $\mathcal{G}$.

Definition 1.14. For a face F of a polytope P, its *normal cone* is $\mathcal{N}(\mathsf{F}) = \{\boldsymbol{c} \in \mathbb{R}^d \ ; \ \mathsf{P}^{\boldsymbol{c}} = \mathsf{F}\}$. The *normal fan* of the polytope P is the collection $\mathcal{N}_\mathsf{P} = \big(\mathcal{N}(\mathsf{F}) \ ; \ \mathsf{F} \text{ face of } \mathsf{P}\big)$.

Fans and normal fans, among other appearances, will be at the heart of Sections 2 and 3.3. Given a graded, atomic and co-atomic lattice, it is NP-hard to decide whether it is the lattice of a polytope. Notwithstanding, deciding if a fan is polytopal amounts to finding a solution to a set of linear inequalities, which is far easier. The notion of normal fan is more precise than the one of face lattice: two polytopes can share the same face lattice without sharing their normal fan. This gives a first hint of what it can mean for two polytopes to be "the same":

Definition 1.15. Two polytopes P and Q are said to be:

- *combinatorially isomorphic* or *combinatorially equivalent* when $\mathscr{L}(\mathsf{P}) \simeq \mathscr{L}(\mathsf{Q})$.
- *normally equivalent* when $\mathcal{N}_\mathsf{P} = \mathcal{N}_\mathsf{Q}$.
- *affinely equivalent* when there exists an affine transformation L such that $\mathsf{Q} = L(\mathsf{P})$.

Obviously, affine equivalence implies combinatorial equivalence, and normal equivalence also implies combinatorial equivalence. But the converse does not hold, and affine equivalence does not imply normal one (rotations are not allowed in normal equivalence, for instance).

An important operation on polytopes is the Minkowski sum. Although the construction is simple to describe in the setting of convex set, the faces are more easily accessed in the framework of normal fans. This gives rise to a simple but non-trivial behavior that allows us to encapsulate various combinatorics, see Sections 1.2.3 and 2 and Figures 28 and 58 for instance.

Definition 1.16. The *Minkowski sum* of two polytopes $\mathsf{P} \subset \mathbb{R}^p$ and $\mathsf{Q} \subset \mathbb{R}^q$ is the polytope:

$$\mathsf{P} + \mathsf{Q} := \{\boldsymbol{p} + \boldsymbol{q} \ ; \ \boldsymbol{p} \in \mathsf{P}, \ \boldsymbol{q} \in \mathsf{Q}\}$$

A *zonotope* is a Minkowski sum of segments.

[2] All the cones in the present thesis will be polyhedral, except if specified else way.

[3] The face lattice of $\mathcal{N}_\mathsf{P}$ needs to be completed by a top element for this anti-isomorphism to hold.

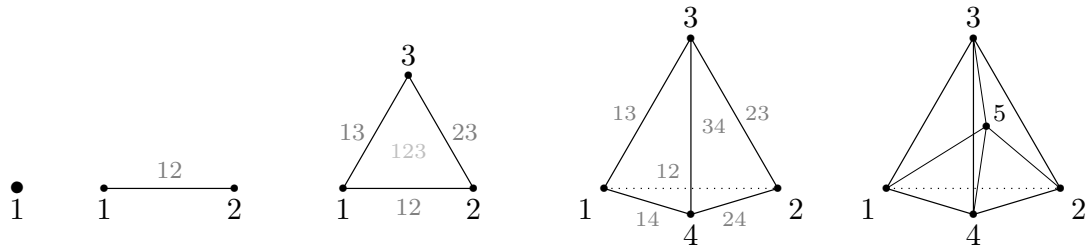

Figure 2: The standard simplices for dimension $d = 0$, 1, 2, 3 and 4 (from Left to Right). Each face is labelled by the corresponding subset of $[d]$. The 4-dimensional standard simplex (Right) is depicted thanks to its Schlegel projection.

It is immediate to see that the vertices of $\mathsf{P} + \mathsf{Q}$ are among the possible sums $\boldsymbol{v} + \boldsymbol{w}$ for $\boldsymbol{v}$ a vertex of P and $\boldsymbol{w}$ a vertex of Q (the reversed inclusion is false in general), that is:

$$V(\mathsf{P} + \mathsf{Q}) \subseteq \{\boldsymbol{v} + \boldsymbol{w} \ ; \ \boldsymbol{v} \in V(\mathsf{P}), \ \boldsymbol{w} \in V(\mathsf{Q})\}$$

The normal fan $\mathcal{N}_{\mathsf{P}+\mathsf{Q}}$ of $\mathsf{P} + \mathsf{Q}$ is the *common refinement* of $\mathcal{N}_{\mathsf{P}}$ and $\mathcal{N}_{\mathsf{Q}}$, meaning that:

$$\mathcal{N}_{\mathsf{P}+\mathsf{Q}} = \{\mathsf{C} \cap \mathsf{C}' \ ; \ \mathsf{C} \in \mathcal{N}_{\mathsf{P}}, \ \mathsf{C}' \in \mathcal{N}_{\mathsf{Q}}\}$$

The rest of this section will be devoted to presenting some special yet universal polytopes.

1.2.1 Simplex

A *d-simplex* is the convex hull of $d + 1$ affinely independent points. A d-simplex is d-dimensional, has $d + 1$ vertices, $d + 1$ facets, and $\binom{d+1}{k}$ faces of dimension k. Each face of dimension k is itself a k-simplex. The face lattice of a simplex is (isomorphic to) the lattice of subsets of $[d + 1]$, called the *boolean lattice*, see Figure 2. Hence, it is a self dual lattice.

The *standard simplex* of $\mathbb{R}^{d+1}$ is $\Delta_d := \text{conv}\{\boldsymbol{e}_1, \dots, \boldsymbol{e}_{d+1}\}$ where $(\boldsymbol{e}_1, \dots, \boldsymbol{e}_{d+1})$ is the canonical basis of $\mathbb{R}^{d+1}$. Note that the Δ_d has dimension d even if it lives in dimension $d + 1$.

1.2.2 Cube

The *standard cube* of $\mathbb{R}^d$ is the convex hull $\square_d := \text{conv}\{\sum_{i\in I} \boldsymbol{e}_i \ ; \ I \subseteq [d]\}$ where $[d] = \{1, \dots, d\}$. It is d-dimensional, has 2^d vertices and $2d$ facets. Its facet-description is given by the $2d$ inequalities $\square_d = \bigcap_{i=1}^{d} \{\boldsymbol{x} \in \mathbb{R}^d \ ; \ 0 \le \langle \boldsymbol{x}, \boldsymbol{e}_i \rangle \le 1\}$. Each k-dimensional face of a standard cube is (normally equivalent to) a standard cube, see Figure 3. A d-dimensional *cube* is a polytope combinatorially equivalent to the standard cube.

The standard cube is a zonotope as $\square_d = \sum_{i=1}^{d} [\boldsymbol{0}, \boldsymbol{e}_i]$. Moreover, any Minkowski sum of d linearly independent segments is a d-dimensional cube. Note also that all zonotopes arise as projections of the standard cube, see [Zie98, Section 7.3].

1.2.3 Permutahedron

The permutahedron Π_n is defined as the convex hull $\Pi_n = \text{conv}\left\{ \begin{pmatrix} \sigma(1) \\ \vdots \\ \sigma(n) \end{pmatrix} \ ; \ \sigma \in \mathcal{S}_n \right\} \subset \mathbb{R}^n$ where $\mathcal{S}_n$ is the set of all permutations of $\{1, \dots, n\}$. The permutahedron is a zonotope as it is the translation of $\sum_{i<j} \frac{1}{2}[\boldsymbol{e}_i - \boldsymbol{e}_j, \ \boldsymbol{e}_j - \boldsymbol{e}_i]$ by the vector $\frac{n+1}{2}(1, \dots, 1)$, see [Zie98, Example 7.15].

The vertices $\boldsymbol{v}$ of the permutahedron Π_n are naturally in bijection with permutations of $\{1, \dots, n\}$ by $\sigma \mapsto \sum_i \sigma(i)\boldsymbol{e}_i$. Two vertices are adjacent when the corresponding permutations

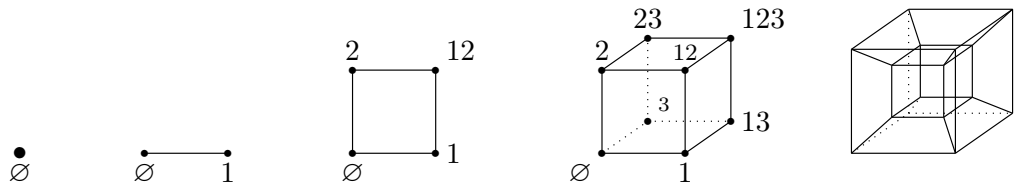

Figure 3: The standard cubes for dimension $d = 0$, 1, 2, 3 and 4 (from Left to Right). Each vertex is labelled by the corresponding subset of $[d]$. The 4-dimensional standard cube (Right) is depicted thanks to its Schlegel projection.

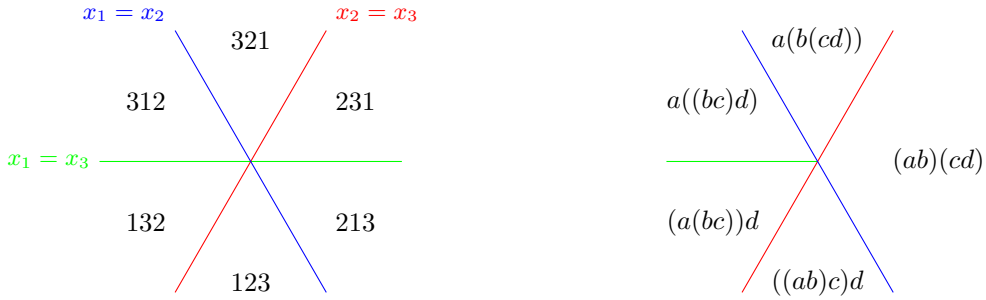

Figure 4: (Left) The braid fan of dimension 2, each maximal cone being labelled by the according permutation, (Right) the sylvester fan of dimension 2, each maximal cone being labelled by the according maximal parenthesization. These fans are the normal fans of the polytopes drawn in Figure 5(Middle Top) and Figure 7(Bottom).

σ and τ differ by an elementary transposition: $\sigma = (i \quad i+1) \circ \tau$. Consequently, the possible directions of edges of the permutahedron Π_n are $\boldsymbol{e}_j - \boldsymbol{e}_i$ for $i, j \in [n]$ with $i \neq j$, see Figure 5.

The facet-description of the permutahedron is:

$$\Pi_n = \left\{ \boldsymbol{x} \in \mathbb{R}^n \ ; \ \begin{array}{ll} \sum_{i=1}^n x_i = \binom{n+1}{2} & \\ \sum_{i \in I} x_i \geq \binom{|I|+1}{2} & \text{for all } \varnothing \subsetneq I \subsetneq [n] \end{array} \right\}$$

The face lattice of the permutahedron Π_n is (isomorphic to) the lattice of ordered partitions (or surjections) of $\{1, \dots, n\}$. Especially, it has $n!$ vertices, $2^n - 2$ facets, and dimension $n - 1$. Instead of describing this face lattice more thoroughly, we focus on its normal fan. The normal fan of the permutahedron Π_n is called the *braid fan* $\mathcal{B}_n$, see Figure 4(Left). It is the fan defined by the arrangement of hyperplanes, called the *braid arrangement*, composed by all hyperplanes $\{\boldsymbol{x} \in \mathbb{R}^n \ ; \ x_i = x_j\}$ for $i, j \in [n]$ with $i \neq j$. The cones of the braid fan are in bijection with the surjections on $[n]$: to a surjection σ, one associates the cone

$$\mathsf{C}_\sigma := \left\{ \boldsymbol{x} \in \mathbb{R}^n \ ; \ \begin{array}{lll} x_i < x_j & \text{if} & \sigma(i) < \sigma(j) \\ x_i = x_j & \text{if} & \sigma(i) = \sigma(j) \end{array} \right\}$$

The braid fan, as defined here, is not essential: each cone of $\mathcal{B}_n$ contains the line in direction $(1, \dots, 1)$. This fact will be problematic for the use we want to make of it. We will solve this issue in three different ways: in Section 3.3 we will keep the non-essential braid fan as defined above; in Section 2.2 we will divide each maximal cone of the braid fan in two simplicial cones (one containing a ray in direction $(1, \dots, 1)$ and one containing a ray in direction $(-1, \dots, -1)$); in Section 2.3 we will project orthogonally the braid fan onto the hyperplane $\{\boldsymbol{x} \in \mathbb{R}^n \ ; \ \sum_i x_i = 0\}$.

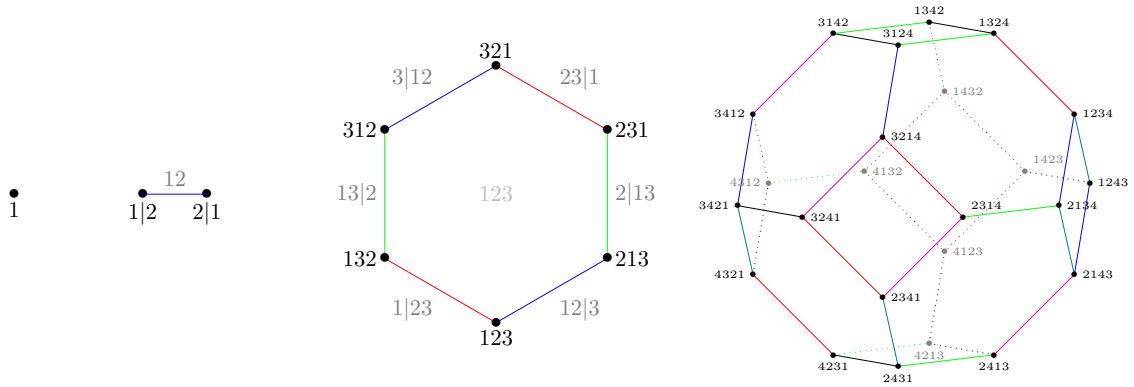

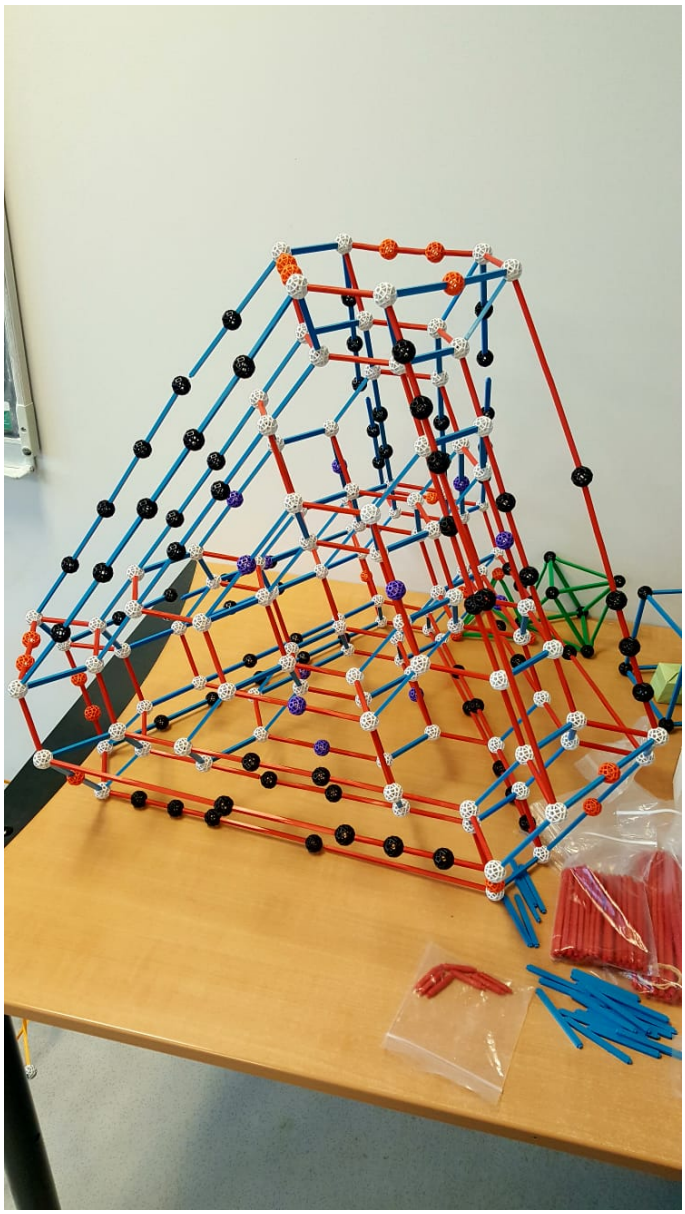

Figure 5: The permutahedra for dimensions $d = 0$, 1, 2, 3 and 4. Up to dimension 3, the vertices are labelled by the permutations, and each edge is colored according to its class of parallelism (for example, going through a blue edge amounts to exchanging the values 1 and 2). The 4-dimensional permutahedron have been made with Zometool, the vertices correspond to the white nodes.

1.2.4 Associahedron

The associahedron is the polytopal embedding of Catalan families. We will first give a quick but not-so-short overview of Catalan families and then define the associahedron as a combinatorial polytope (*i.e.* we will describe its face lattice). We will end by discussing Loday's realization of the associahedron and its link with the permutahedron.

Catalan families A Catalan family is, in first place, a family of objects counted by Catalan numbers. Neil Sloane, the founder of the (*Online*) *Encyclopedia of Integer Sequences*, claims that "the Catalan numbers are certainly the most common sequence that people don't know about" [Slo23]. A straightforward definition of the Catalan numbers C_n is their explicit formula:

$$C_n = \frac{1}{n+1}\binom{2n}{n}$$

We also mention their recursive formula:

$$C_0 = 1 \qquad \text{and} \qquad C_{n+1} = \sum_{i=0}^{n} C_i C_{n-i}$$

Note that Catalan numbers grow quite rapidly, as: $C_n \sim \frac{1}{\sqrt{\pi}} \frac{4^n}{n^{3/2}}$.

As said, a Catalan family is a family of combinatorial objects such that there are C_n objects of size n. For example, parenthesizations on $n+1$ letters, triangulations of a $(n+2)$-gon, non-crossing arborescences on $n+1$ nodes, binary search trees with n elements... The reader is invited to consult [Sta15] for a presentation of 214 Catalan families and bijections between them, we give here a shorthand on the 4 aforementioned families.

Each family is endowed with a very important notion of *flip*: they shall be thought of as a graph whose C_n vertices are the objects, and where two vertices share an edge when the corresponding objects differ by a flip. It is sometimes convenient to direct the flip, giving rise to a directed graph. Directed this way, this graph is a poset: the Tamari lattice. We will not present this lattice in details but only give a glimpse on it, see [Tam51, PSZ23]. Instead, we will be interested in the face lattice of the associahedron, which corresponds to super-Catalan families (and are counted by Schröder–Hipparchus numbers).

Before constructing the associahedron, we briefly review the four aforementioned Catalan families. The aim is not to give an extensive nor self-contained introduction, but rather a dictionary that will allow the reader to perceive the underlying general framework behind each specific lexicon (see the table of correspondences below). Therefore, we detail a bit the case of parenthesizations, as we find it easy to handle and insightful. We then give some explanations on binary search trees because it will be needed for Section 3.3.1, and we refer the reader to the indicated sections of the present thesis for non-crossing arborescences and triangulations.

	Max. parenthesization	Non-crossing arbo.	Triangulation	BST
Objects	parenthesis	arcs	triangles	(not defined here)
Compatibility	nested or disjoint	non-crossing	non-intersecting	(not defined here)
Flips	remove & re-add	remove & re-add	remove & re-add	rotations
Super-Catalan	parenthesizations	multi-arborescences	subdivisions	Schröder trees
See	here above	Sections 3.1 and 3.2	Section 4.3.1	Section 3.3

Parenthesizations Fix a n letter words $a_1 a_2 \dots a_n$ where a_i are just symbols. One can *parenthesize* this word by adding pairs of opening and closing parentheses $(\dots)$ where the opening one precedes the closing one: $a_1 \dots a_{i-1}(a_i \dots a_j)a_{j+1} \dots a_n$. Such a pair of parentheses can be identified by the pair (i, j) with $1 \leq i < j \leq n$. A pair of parentheses is valid when $(i, j) \neq (1, n)$. Two pairs of parentheses are *compatible* when the part they separate are either disjoint or included one in the other. A *maximal parenthesization* is a maximal family of pair-wise compatible pairs of parentheses.

There are C_{n-1} maximal parenthesizations for a word of n letters, each containing exactly $n-2$ pairs of parentheses.

The *flip* between two maximal parenthesizations consists in removing a pair of parentheses and adding the only other possible pair of parentheses. Such a flip is *forward* if the leftmost parenthesis moves from left to right, and *backward* else way.

In this context, the super-Catalan family is the family of all parenthesizations (not necessarily maximal ones). This family has a natural ordering: a parenthesization *refines* another one when it can be obtained by adding (compatible) pairs of parentheses to the first.

Binary search trees A *binary search tree* (BST) is a planar rooted binary tree whose nodes are labelled from 1 to n respecting that for each node i, all labels in its left sub-tree are smaller than i, and all labels in its right sub-tree are greater than i. Note that a binary search tree is fully defined by its skeleton, thus they are in bijection with binary trees and form a Catalan family.

Binary search trees are a powerful data structure for sorting the numbers from 1 to n. The key operations on this structure are insertion of a number and deletion of the root. Thanks to these operations, one can sort a list L in $O(n \log n)$ (time-)complexity by inserting all the numbers from L in order of appearance, and then extracting them. The binary search tree corresponding to L depends on which order does the numbers from 1 to n appear in L, *i.e.* its permutation. Consequently, to each permutation $\sigma \in \mathcal{S}_n$ one associates a binary search tree $T(\sigma)$ thanks to the following recursive algorithm:

- Inserting $\sigma(i)$ to an empty tree gives rise to a tree on one node $\sigma(i)$ (hence T initializes at the tree on one node labelled $\sigma(1)$);
- After having inserted $\sigma(1), \dots, \sigma(i-1)$ in T, one adds $\sigma(i)$: if $\sigma(i)$ is smaller than the root of T, then $\sigma(i)$ is recursively added to the left sub-tree of T; if $\sigma(i)$ is greater than the root of T, then $\sigma(i)$ is recursively added to the right sub-tree of T;
- Once inserted all values $\sigma(1), \dots, \sigma(n)$ (*i.e.* all numbers from 1 to n), the resulting tree is $T(\sigma)$.

A flip between binary search trees is a rotation of the tree, and the super-Catalan family is the family of Schröder trees.

We will encounter binary search trees again in Section 3.3.1.

Construction of the associahedron The associahedron was first defined by Tamari [Tam51] and later Stasheff [Sta63] as a combinatorial polytope, and then realized by Milnor (unpublished), Haiman [Hai84], Lee [Lee89] and Loday [Lod04, PSZ23]. They give a description of a super-Catalan family as defined above, and proved that this poset is the face lattice of a polytope. Hence, any polytope whose face lattice if isomorphic to the super-Catalan poset can to be called an associahedron. To this extent, several different realizations of the associahedron will appear in the present thesis, see Example 2.22 and Sections 3.2, 3.3.1 and 4.3. Nevertheless, we will emphasize a specific realization of the associahedron that, as far as we believe, would deserve to be called *standard*, namely Loday's realization of the associahedron [Lod04, PSZ23].

A straightforward way to define it and to emphasize its link with the permutahedron Π_n is thanks to its facet-description:

$$\mathsf{Asso}_n = \left\{ \boldsymbol{x} \in \mathbb{R}^n \ ; \ \begin{array}{ll} \sum_{i=1}^n x_i = \binom{n+1}{2} & \\ \sum_{i \in I} x_i \geq \binom{|I|+1}{2} & \text{for all } \varnothing \subsetneq I = [a,b] \subsetneq [n] \end{array} \right\}$$

Instead of the $2^n - 2$ facets of the permutahedron Π_n that correspond to the non-trivial subsets of $[n]$, the associahedron Asso_n is supported by the $\binom{n}{2} - 1$ facets that correspond to non-trivial sub-intervals of $[n]$. Consequently, the associahedron Asso_n is a removahedron for the permutahedron Π_n, meaning that is can be obtained by removing some inequalities in its facets-description[4], see Figure 6. A 3-dimensional model of a permutahedron inside the Loday associahedron can also be found on Viviane Pons' website [Pon18]. This will be relevant for Section 2.

[4]The standard cube $\square_n$ is linearly isomorphic to the removahedron obtained by keeping only the inequalities corresponding to I of the form $[1,i]$ or $[i,n]$ for $i \in [n]$. The latter is also a removahedron for the associahedron Asso_n.

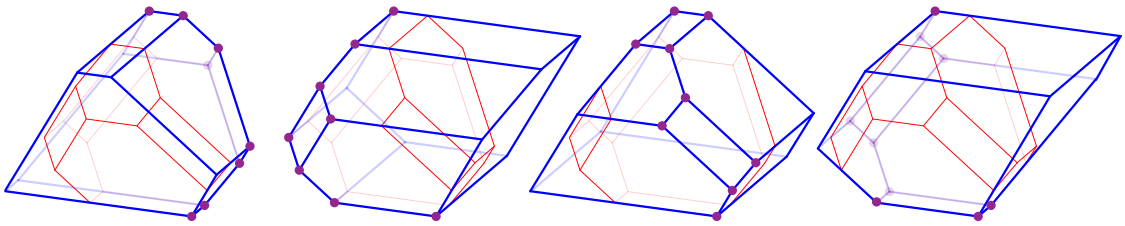

Figure 6: Four realizations of the 3-dimensional permutahedron Π_3 sitting inside an associahedron. The left-most associahedron is the Loday's associahedron Asso_3. Illustration from [PSZ23, Figure 7(Top)].

The associahedron Asso_n has C_n vertices, $\binom{n}{2} - 1$ facets, dimension $n-1$ (although being embedded in $\mathbb{R}^n$), and its face lattice is the super-Catalan poset, thus its edges correspond to the flips between Catalan objects, see Figure 7. Note that there exists an orientation of the ambient space $\mathbb{R}^n$ such that the induced orientation on the graph G_{Asso_n} is precisely the Tamari orientation of flips.

We will not provide here a (coordinate) vertex description of the associahedron Asso_n and refer to the abounding literature [Lod04, Pos09, PSZ23]. Instead, we briefly describe the normal fan of the associahedron Asso_n, called the *sylvester fan*. The maximal cones of the sylvester fan (*i.e.* the normal cones of the vertices of Asso_n) can be described easily thanks to binary search trees, see Figure 4(Right). With the definition of C_σ given above for the permutahedron, for a binary search tree T, the associated normal cone is $\mathsf{C}_T = \bigcup_{\sigma \ ; \ T(\sigma)=T} \mathsf{C}_\sigma$.

1.3 Linear programming

Linear programming has proven to be a powerful tool to tackle theoretical and applied problems. The aim is to optimize a linear functional subject to linear constraints. For example, imagine I want to breed goats and cows. My barn has 15 boxes, a goat takes 1 box and a cow 3 boxes. Milking a goat gives 4L, while a cow gives 3L, and my storage allows at most 24L. I want to maximize the number of animals I have. Denote by g the number of goats and c the number of cows, then this toy example amounts to maximize $g + c$ under the conditions:

$$g \geq 0 \qquad c \geq 0 \qquad g + 3c \leq 15 \qquad 4g + 3c \leq 24$$

Even though this optimization problem seems simple (and the numbers chosen are quite unrealistic), it encapsulates a wide variety of problems, from its prototypical purpose of optimizing a diet from a nutritional point of view [Dan63], to constructing the best line to fit data, or finding the largest disk in a polygon, see [MG07].

A linear problem can be thought of as the problem of finding the vertex (or face) of a convex polyhedron that is maximal for the scalar product with a certain direction $\boldsymbol{c}$. The polyhedron is called its *feasibility domain* while the direction $\boldsymbol{c}$ is its *objective function*. In the present thesis, the feasibility domain will be bounded (*i.e.* it will be a polytope), and the objective function will be generic (*i.e.* it will not be orthogonal to any edge of the feasibility domain, so the optimum will be attained at a vertex). Precisely, for our toy example, the four inequalities define a quadrilateral in the plane, and we want to find its furthest point in direction $\binom{1}{1}$, see Figure 8. Here, the optimal solution is 3 goats and 4 cows.

Note that we conveniently created a toy example where the optimal solution is a couple of integers. Notwithstanding, the optimal solution of a linear problem is not integral in general: the added requirement of finding the optimal integral point for a linear program is the focus of integer programming [MG07, Chapter 3], which is far more difficult than linear programming. Furthermore, a plethora of natural questions and generalizations can be asked from our toy example, that we will not address in this light introduction.

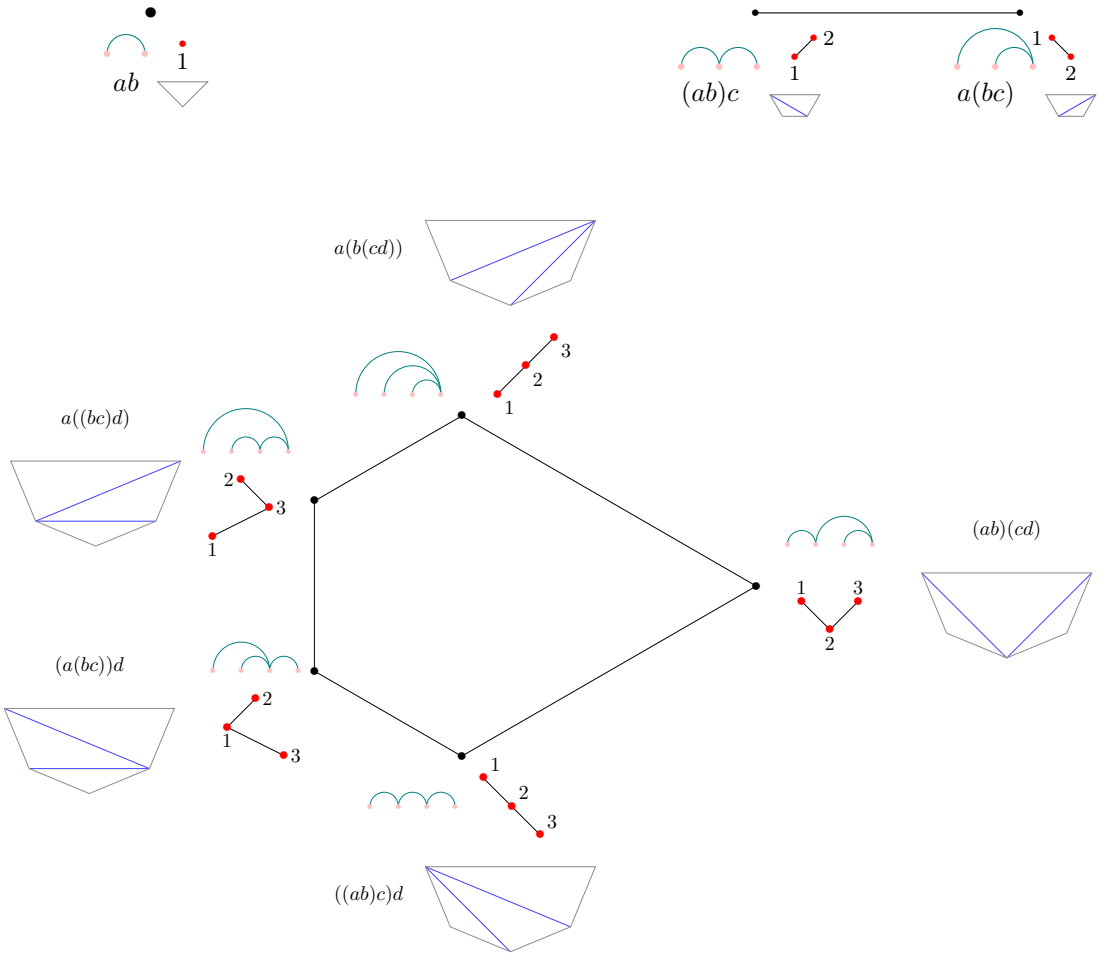

Figure 7: (Bottom) The 2-dimensional Loday's associahedron with each vertex labelled by the corresponding maximal parenthesization (on 4 letters), triangulation (of a pentagon), binary search tree (on [3], rooted at their bottoms) and non-crossing arborescence (on 4 nodes). Note that the permutations 213 and 231 both yield the same binary search tree, namely the rightmost one, thus the normal cone of the rightmost vertex is the union of the normal cone of the two right vertices of the 2-dimensional permutahedron in Figures 4 and 5. (Top) The 0 and 1-dimensional counterparts. The interested reader shall refer to page 12 of [Lod04] for the 3-dimensional picture.

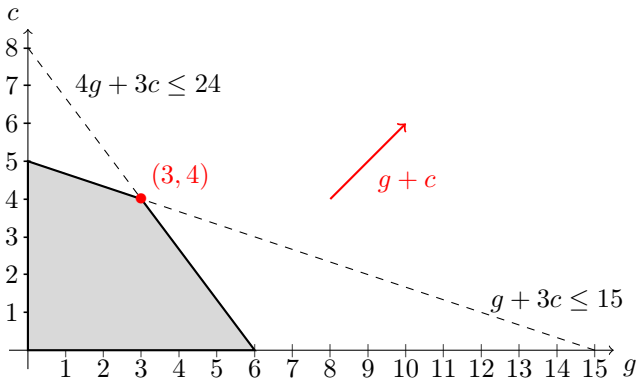

Figure 8: Feasibility domain, objective function and optimal vertex of the toy example.

A widely used method for solving linear problems is the simplex algorithm [Dan63]. Suppose known a vertex $\boldsymbol{v}$ of the feasibility domain, then it is algorithmically not difficult to find the neighbors of $\boldsymbol{v}$ that increase the scalar product $\langle \boldsymbol{v}, \boldsymbol{c} \rangle$. Choose one of these improving neighbors and pursue the algorithm from there. By convexity, this algorithm ends at a vertex $\boldsymbol{v}_{\text{opt}}$ maximizing $\langle \boldsymbol{x}, \boldsymbol{c} \rangle$ for $\boldsymbol{x}$ in the feasibility domain. The path followed by the simplex method depends on the *pivot rule* used to choose the improving neighbor.

It has been proven that, given a linear problem, it is possible to solve it in polynomial time (with respect to the size of its entries) using interior-point methods [RTV05, DNT08]. Nevertheless, the polynomiality of the simplex method is still open [KM72, DS14]. The core of the simplex method is thus the choice of the pivot rule, see [MG07, Section 5.7] for a short review of the main ones, and [BDLLS22, Section 2] for a polytopal discussion on the subject. Here, we will only recall the useful definitions and detail the ideas behind the pivot rules called the shadow vertex rules and the max-slope pivot rules.

In this thesis, a *linear program* is a couple $(\mathsf{P}, \boldsymbol{c})$ where $\mathsf{P} \subset \mathbb{R}^d$ is a bounded feasibility domain (*i.e.* a polytope), and $\boldsymbol{c} \in \mathbb{R}^d$ is a generic objective function (*i.e.* a vector such that $\langle \boldsymbol{u}, \boldsymbol{c} \rangle \neq \langle \boldsymbol{v}, \boldsymbol{c} \rangle$ for $\boldsymbol{u}, \boldsymbol{v} \in V(\mathsf{P})$ with $\boldsymbol{u} \neq \boldsymbol{v}$). The vertex of P that maximizes the scalar product with respect to $\boldsymbol{c}$ is called the *optimal vertex* of the linear program. The generic objective function orients the graph G_{P} of P by orienting each edge from $\boldsymbol{u}$ to $\boldsymbol{v}$ such that $\langle \boldsymbol{u}, \boldsymbol{c} \rangle < \langle \boldsymbol{v}, \boldsymbol{c} \rangle$. This orientation is acyclic. The out-neighbors of a vertex $\boldsymbol{v} \in V(\mathsf{P})$ are called its *improving neighbors*. A directed path in this oriented graph is called a *$\boldsymbol{c}$-monotone path on P*, or simply a *monotone path* when $(\mathsf{P}, \boldsymbol{c})$ is clear from the context.

The reader shall think of a pivot rule as an oracle that, if you give it a linear program $(\mathsf{P}, \boldsymbol{c})$ and a starting vertex $\boldsymbol{v}_{\text{init}}$ (not necessarily the vertex that minimizes the scalar product against $\boldsymbol{c}$), will return a monotone path that starts at $\boldsymbol{v}_{\text{init}}$ and ends at $\boldsymbol{v}_{\text{opt}}$. Pivot rules are hard to describe in general, see [APR14, DS14, FS14] for a study of their complexity. However, we can restrict ourselves to an easy-to-describe subclass of pivot rules, the ones that are defined by their local behavior.

Definition 1.17. A *memoryless pivot rule* R is a pivot rule that associates each non-optimal vertex $\boldsymbol{v}$ of each linear program $(\mathsf{P}, \boldsymbol{c})$ to one of its improving neighbors $R_{(\mathsf{P},\boldsymbol{c})}(\boldsymbol{v})$.

For a linear program $(\mathsf{P}, \boldsymbol{c})$ and a starting vertex $\boldsymbol{v}_{\text{init}}$, its monotone path is formed by the successive images of $\boldsymbol{v}_{\text{init}}$ under $R_{(\mathsf{P},\boldsymbol{c})}$, namely $\big(\boldsymbol{v}_{\text{init}},\ R_{(\mathsf{P},\boldsymbol{c})}(\boldsymbol{v}_{\text{init}}),\ R_{(\mathsf{P},\boldsymbol{c})}(R_{(\mathsf{P},\boldsymbol{c})}(\boldsymbol{v}_{\text{init}})), \dots, \boldsymbol{v}_{\text{opt}}\big)$.

For a fixed linear program $(\mathsf{P}, \boldsymbol{c})$, a memoryless pivot rule induces an arborescence A on the graph G_{P}, formed by the edges $\boldsymbol{uv}$ such that $\boldsymbol{v} = R_{(\mathsf{P},\boldsymbol{c})}(\boldsymbol{u})$. Memoryless pivot rules are fully defined by the arborescences they induce on each linear program, as all monotone paths can be retrieved from the knowledge of this arborescence. The study of possible arborescences is at the heart of pivot rule polytopes, see [BDLLS22] and Section 3.1.

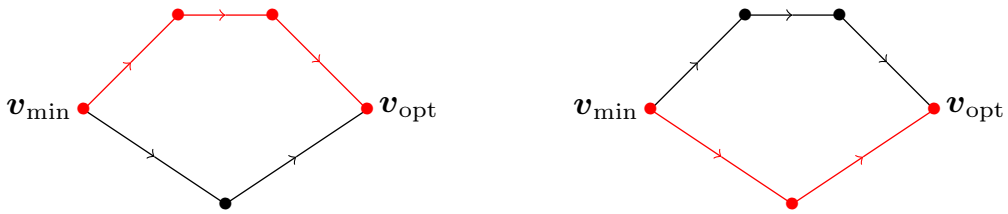

Figure 9: The two possible monotone paths starting at the minimal vertex for a 2-dimensional polytope (the objective function is from left to right).

When P is 2-dimensional, pivot rules are very simple, see Figure 9. The only vertex where a choice shall be made is the vertex $\boldsymbol{v}_{\min}$ that minimizes the scalar product against $\boldsymbol{c}$. This vertex has two possible monotone paths to choose from.

When P is higher dimensional, the situation becomes far more convoluted. An efficient idea is to simplify the problem by making it 2-dimensional again. By choosing a vector $\boldsymbol{\omega} \in \mathbb{R}^d$ linearly independent from $\boldsymbol{c} \in \mathbb{R}^d$, one can project the polytope P onto the 2-dimensional plane of basis $(\boldsymbol{c}, \boldsymbol{\omega})$, and perform the simplex algorithm on this projection. This method will find the optimal vertex $\tilde{\boldsymbol{v}}_{\text{opt}}$ in the plane $(\boldsymbol{c}, \boldsymbol{\omega})$. As $\boldsymbol{c}$ is generic, $\boldsymbol{v}_{\text{opt}}$ is the only vertex of P that projects onto $\tilde{\boldsymbol{v}}_{\text{opt}}$, solving the higher dimensional linear problem, see Figure 25(Left). Consequently, one can define a family of memoryless pivot rules as follows:

Definition 1.18. A memoryless pivot rule R is a *max-slope pivot rule* when for every linear program $(\mathsf{P}, \boldsymbol{c})$, there exists $\boldsymbol{\omega}$ linearly independent from $\boldsymbol{c}$ such that the arborescence $A^{\boldsymbol{\omega}}$ induced by R on $(\mathsf{P}, \boldsymbol{c})$ is defined by its edges between $\boldsymbol{u} \in V(\mathsf{P}) \setminus \{\boldsymbol{v}_{\text{opt}}\}$ and

$$A^{\boldsymbol{\omega}}(\boldsymbol{u}) := \operatorname{argmax} \left\{ \frac{\langle \boldsymbol{\omega}, \boldsymbol{v} - \boldsymbol{u} \rangle}{\langle \boldsymbol{c}, \boldsymbol{v} - \boldsymbol{u} \rangle} \ ; \ \boldsymbol{v} \text{ improving neighbor of } \boldsymbol{u} \right\}$$

The study of max-slope pivot rules is of prime importance, as it links the world of linear optimization with the one of fiber polytopes. Presenting some aspects of this nexus is the focal point of Sections 3 and 4: especially, we will fix a linear program $(\mathsf{P}, \boldsymbol{c})$ and study all the possible arborescences that arise when varying the parameter $\boldsymbol{\omega}$ of the max-slope pivot rules.

It is worth noting that max-slope pivot rules are the memoryless version of *shadow vertex rules*, which may be more familiar to the reader. A pivot rule is a shadow vertex rule when, for every linear program $(\mathsf{P}, \boldsymbol{c})$ and every vertex $\boldsymbol{v}_{\text{init}} \in V(\mathsf{P})$, there exists $\boldsymbol{\omega}$ linearly independent from $\boldsymbol{c}$ such that the $\boldsymbol{c}$-monotone path from $\boldsymbol{v}_{\text{init}}$ to $\boldsymbol{v}_{\text{opt}}$ is the upper part of the 2-dimensional projection of P onto the plane of basis $(\boldsymbol{c}, \boldsymbol{\omega})$. Although very similar, these definitions are different: in a max-slope pivot rule, one chooses a fix $\boldsymbol{\omega}$ for all the vertices of P; whereas the choice of $\boldsymbol{\omega}$ is subordinated to the vertex $\boldsymbol{v}_{\text{init}}$ at stake for a shadow vertex rule, see [BDLLS22, Section 6.1].

2 Deformations of polytopes and generalized permutahedra

"Surely," said I, "surely that is something at my window lattice;
Let me see, then, what thereat is, and this mystery explore
Let my heart be still a moment and this mystery explore;"
– Edgar Allan Poe, *The Raven*

2.1 Deformations of polytopes

In Section 1.2.4, we have seen that a realization of the associahedron, Loday's associahedron, can be retrieved from the standard permutahedron by removing facets. In this construction, edge directions are preserved, and only the normal fan is coarsened. This process embodies the combinatorics of flips of Catalan families inside the graph of the weak order on permutations. This section is devoted to the presentation of the general concept of "gliding facets", and the vast family of polytopes one can obtain from the permutahedron by this construction.

Definition 2.1. A *deformation* (or *weak Minkowski summand*) of a polytope P is a polytope Q whose normal fan $\mathcal{N}_\mathsf{Q}$ coarsens the normal fan of P. The set of deformations of P is called its *deformation cone*:

$$\mathbb{DC}(\mathsf{P}) = \left\{\mathsf{Q} \subset \mathbb{R}^d \ ; \ \mathcal{N}_\mathsf{Q} \trianglelefteq \mathcal{N}_\mathsf{P}\right\}$$

The name *deformation* comes from the pictorial illustration of gliding facets along their normal vectors, see Figure 10. To justify the appellation *cone*, note the following: For Q and R two polytopes, then $\mathcal{N}_{\lambda\mathsf{Q}} = \mathcal{N}_\mathsf{Q}$ for all $\lambda > 0$, and $\mathcal{N}_{\mathsf{Q}+\mathsf{R}}$ is the common refinement of $\mathcal{N}_\mathsf{Q}$ and $\mathcal{N}_\mathsf{R}$. Consequently, $\mathcal{N}_{\lambda\mathsf{Q}}$ and $\mathcal{N}_{\mathsf{Q}+\mathsf{R}}$ coarsen $\mathcal{N}_\mathsf{P}$ when $\mathcal{N}_\mathsf{Q}$ and $\mathcal{N}_\mathsf{R}$ do, which means $\mathbb{DC}(\mathsf{P})$ is closed by dilation and Minkowski sums.

Howbeit, it is hard to understand the deformation cone as a cone of polytopes, one would prefer to parameterize it by a cone in the Euclidean space $\mathbb{R}^N$ for some N. There are several ways to do so, this thesis will focus on the so-called *height deformation cone*, and briefly present the other realizations.

Let $\mathsf{P} \subset \mathbb{R}^d$ be a polytope with normal fan $\mathcal{F}$ supported on the vector set $\boldsymbol{S}$. Let $\boldsymbol{G}$ be the $N \times d$-matrix whose rows are the vectors in $\boldsymbol{S}$. For any height vector $\boldsymbol{h} \in \mathbb{R}^N$, we define the polytope $\mathsf{P}_{\boldsymbol{h}} := \left\{\boldsymbol{x} \in \mathbb{R}^d \ ; \ \boldsymbol{G}\boldsymbol{x} \leq \boldsymbol{h}\right\}$. It is not hard to see that any weak Minkowski summand of P is of the form $\mathsf{P}_{\boldsymbol{h}}$ for some $\boldsymbol{h} \in \mathbb{R}^N$.

Moreover, for deformations $\mathsf{P}_{\boldsymbol{h}}$ and $\mathsf{P}_{\boldsymbol{h}'}$ of P, we have $\mathsf{P}_{\boldsymbol{h}} + \mathsf{P}_{\boldsymbol{h}'} = \mathsf{P}_{\boldsymbol{h}+\boldsymbol{h}'}$ and $\lambda\mathsf{P}_{\boldsymbol{h}} = \mathsf{P}_{\lambda\boldsymbol{h}}$ for any $\lambda > 0$. Hence, the deformation cone is parameterized by the *height deformation cone*:

$$\mathbb{DC}(\mathsf{P}) \simeq \mathbb{DC}_\mathrm{h}(\mathsf{P}) := \left\{\boldsymbol{h} \in \mathbb{R}^N \ ; \ \mathcal{N}_{\mathsf{P}_{\boldsymbol{h}}} \trianglelefteq \mathcal{N}_\mathsf{P}\right\}.$$

Other descriptions of the deformation cones are of theoretical importance. As we will not use them in this thesis, we restrain ourselves to a succinct glimpse of their definitions.

For a polytope P, let $E(\mathsf{P})$ be the set of its edges. To P, one can associate the vector $\boldsymbol{\ell} \in \mathbb{R}^{E(\mathsf{P})}$ of its edge-lengths, where ℓ_e is simply the length of $e \in E(\mathsf{P})$. Conversely, a vector in $\mathbb{R}_+^{E(\mathsf{P})}$ gives rise to a polytope $\mathsf{Q}_{\boldsymbol{\ell}}$: for $e \in E(\mathsf{P})$, choose a direction and denote $\boldsymbol{u}_e$ the unitary vector in this direction, then $\mathsf{Q}_{\boldsymbol{\ell}} = \operatorname{conv}\left\{\sum_{e\in\mathcal{P}} \varepsilon_e^{\mathcal{P}} \ell_e \boldsymbol{u}_e \ ; \ \mathcal{P} \text{ directed edge-path in } G_\mathsf{P}\right\}$ where $\varepsilon_e^{\mathcal{P}} = 1$ if the direction of $e \in \mathcal{P}$ is the same as in $\boldsymbol{u}_e$, and $\varepsilon_e^{\mathcal{P}} = -1$ else way. The deformation cone is isomorphic to the *edge deformation cone* $\left\{\boldsymbol{\ell} \in \mathbb{R}_+^{E(\mathsf{P})} \ ; \ \mathsf{Q}_{\boldsymbol{\ell}} \trianglelefteq \mathcal{N}_\mathsf{P}\right\}$, see [PRW08, Appendix 15] for instance.

On top of that, a deformation of P can also be described as a polytope whose support functional is a convex piece-wise linear continuous function supported on the face fan of P [CLS11, Section 6.1] and [DRS10, Section 9.5]. The deformation cone is isomorphic to the cone of such linear functionals.

From now on, we will slightly abuse notations by using ambiguously the word *deformation cone* to designate the cone of the deformations of a polytope or the height deformation cone. Besides, although we define the deformation cone for a polytope, it only depends on the normal equivalence class of the latter, *i.e.* of its normal fan. Consequently, we will sometimes prefer to talk about the

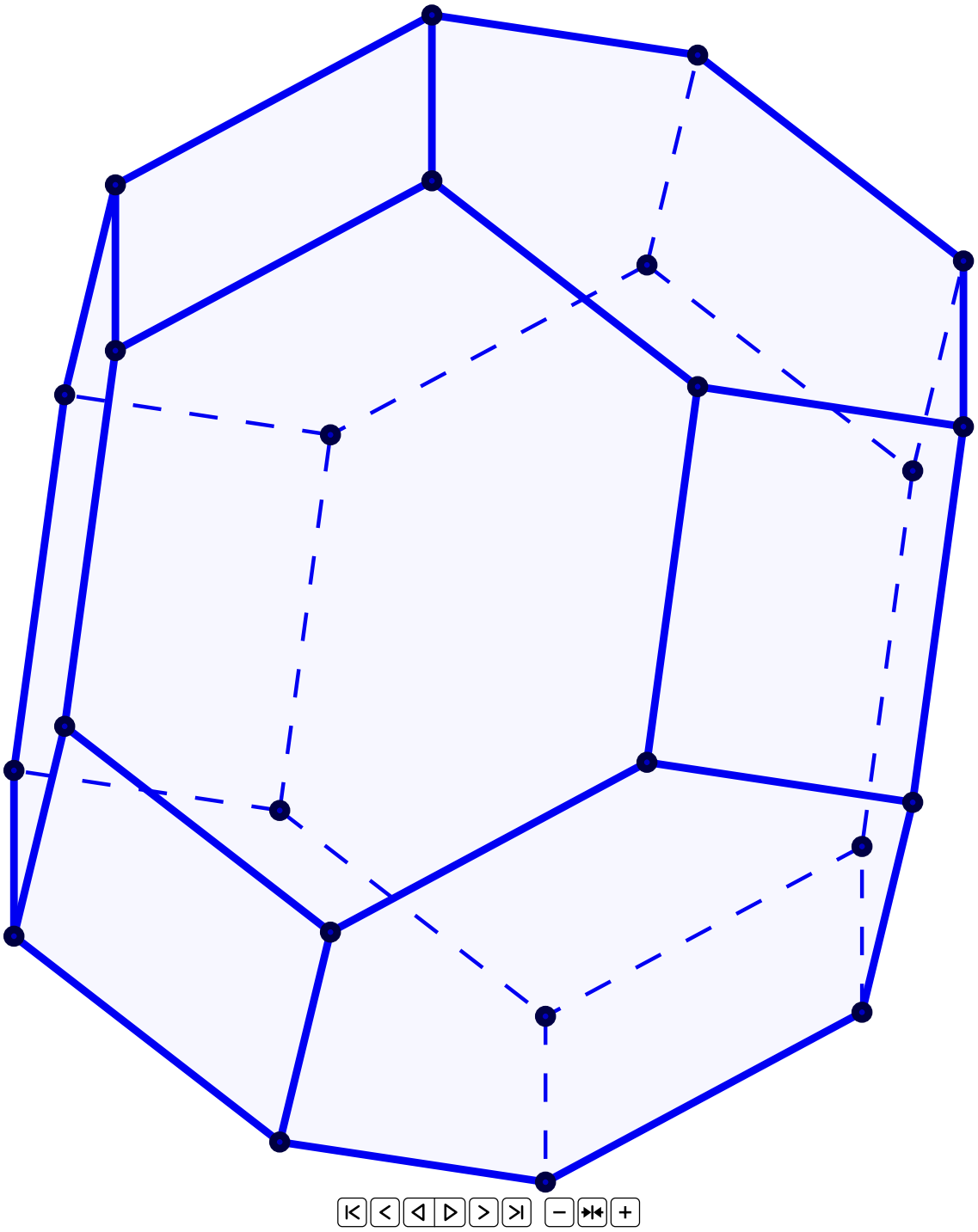

Figure 10: Animated sequence of deformations. The first polyhedron is the permutahedron Π_4 (First frame). One by one, we remove inequalities from its facet-description (by augmenting the constant b in $\langle \boldsymbol{x}, \boldsymbol{a} \rangle \leq b$) to obtain the associahedron Asso_4 (Middle pause), and then pursue the process to obtain a cube linearly isomorphic to $\square_3$ (Final frame). See also Figure 6. *(Animated figures obviously do not display on paper, and some PDF readers do not support the format: it is advised to use Adobe Acrobat Reader. If no solution is suitable, the animation can be found on my website or asked by email.)*

deformation cone of a fan (especially in Section 2.3): when the fan $\mathcal{F}$ is polytopal, then $\mathbb{DC}(\mathcal{F})$ would be the deformation cone $\mathbb{DC}(\mathsf{P})$ of any polytope P with $\mathcal{N}_{\mathsf{P}} = \mathcal{F}$; and $\mathbb{DC}(\mathcal{F}) = \varnothing$ when $\mathcal{F}$ is not polytopal.

The height deformation cone is a polyhedral cone, and the two following propositions give an inequality description of it. The first one is devoted to simple polytopes and will be used for describing the deformation cones of nestohedra in Section 2.3, while the second one deals with general polytopes exploiting a triangulation of their normal fan, allowing a description of the deformation cones of graphical zonotopes in Section 2.2. Note that, in general, these propositions give an inequality description far from being a facet-description: namely, many inequalities are actually redundant.

Proposition 2.2 ([CFZ02, GKZ08])**.** *Let $\mathsf{P} \subset \mathbb{R}^d$ be a simple polytope with simplicial normal fan $\mathcal{F}$ supported on the rays $\boldsymbol{S}$. Then the deformation cone $\mathbb{DC}(\mathsf{P})$ is the set of polytopes $\mathsf{P}_{\boldsymbol{h}}$ for all $\boldsymbol{h}$ in the cone of $\mathbb{R}^{\boldsymbol{S}}$ defined by the inequalities*

$$\sum_{\boldsymbol{s} \in \boldsymbol{R} \cup \boldsymbol{R}'} \alpha_{\boldsymbol{R},\boldsymbol{R}'}(\boldsymbol{s})\, \boldsymbol{h}_{\boldsymbol{s}} \geq 0$$

for all adjacent maximal cones $\mathbb{R}_{\geq 0}\boldsymbol{R}$ and $\mathbb{R}_{\geq 0}\boldsymbol{R}'$ of $\mathcal{F}$ with $\boldsymbol{R} \smallsetminus \{\boldsymbol{r}\} = \boldsymbol{R}' \smallsetminus \{\boldsymbol{r}'\}$, where $\alpha_{\boldsymbol{R},\boldsymbol{R}'}(\boldsymbol{s})$ denote the coefficients in the unique linear dependence[5]

$$\sum_{\boldsymbol{s} \in \boldsymbol{R} \cup \boldsymbol{R}'} \alpha_{\boldsymbol{R},\boldsymbol{R}'}(\boldsymbol{s})\, \boldsymbol{s} = \boldsymbol{0}$$

among the rays of $\boldsymbol{R} \cup \boldsymbol{R}'$ such that $\alpha_{\boldsymbol{R},\boldsymbol{R}'}(\boldsymbol{r}) + \alpha_{\boldsymbol{R},\boldsymbol{R}'}(\boldsymbol{r}') = 2$.

The edge deformation cone also enjoys an inequality description. Indeed, an edge vector $\boldsymbol{\ell} \in \mathbb{R}_+^E$ corresponds to a deformation of a simple polytope P when it satisfies the *polygonal face equations*: for each 2-dimensional face F of P, $\sum_{e \in E(\mathsf{F})} \ell_e \boldsymbol{u}_e = \boldsymbol{0}$ where the sum is on the edges of F. The edge deformation cone of a simple polytope P is the intersection of $\mathbb{R}_+^{E(\mathsf{P})}$ with the kernel of polygonal face equations [PRW08, Pos09].

Similarly, the cone of convex piece-wise linear continuous functions on the face fan of a simple polytope has an inequality description.

The characterization of the height deformation cone can be extended to general (not necessarily simple) polytopes. One straightforward way to do so is via a simplicial refinement of the normal fan. If such a simplicial refinement contains additional rays, then the type cone will be embedded in a higher dimensional space, but projecting out these additional coordinates gives a linear isomorphism with the standard presentation. See [PS19, Prop. 3] and [PPPP19, Prop. 1.7].

Proposition 2.3. *Let $\mathsf{P} \subset \mathbb{R}^d$ be a polytope whose normal fan $\mathcal{F}$ is refined by the simplicial fan $\mathcal{G}$ supported on the rays $\boldsymbol{S}$. Then the deformation cone $\mathbb{DC}(\mathsf{P})$ is the set of polytopes $\mathsf{P}_{\boldsymbol{h}}$ for all $\boldsymbol{h}$ in the cone of $\mathbb{R}^{\boldsymbol{S}}$ defined by*

- *the equalities $\sum_{\boldsymbol{s} \in \boldsymbol{R} \cup \boldsymbol{R}'} \alpha_{\boldsymbol{R},\boldsymbol{R}'}(\boldsymbol{s})\, \boldsymbol{h}_{\boldsymbol{s}} = 0$ for any adjacent maximal cones $\mathbb{R}_{\geq 0}\boldsymbol{R}$ and $\mathbb{R}_{\geq 0}\boldsymbol{R}'$ of $\mathcal{G}$ belonging to **the same** maximal cone of $\mathcal{F}$,*
- *the inequalities $\sum_{\boldsymbol{s} \in \boldsymbol{R} \cup \boldsymbol{R}'} \alpha_{\boldsymbol{R},\boldsymbol{R}'}(\boldsymbol{s})\, \boldsymbol{h}_{\boldsymbol{s}} \geq 0$ for any adjacent maximal cones $\mathbb{R}_{\geq 0}\boldsymbol{R}$ and $\mathbb{R}_{\geq 0}\boldsymbol{R}'$ of $\mathcal{G}$ belonging to **distinct** maximal cones of $\mathcal{F}$,*

where $\sum_{\boldsymbol{s} \in \boldsymbol{R} \cup \boldsymbol{R}'} \alpha_{\boldsymbol{R},\boldsymbol{R}'}(\boldsymbol{s})\, \boldsymbol{s} = \boldsymbol{0}$ is the unique linear dependence with $\alpha_{\boldsymbol{R},\boldsymbol{R}'}(\boldsymbol{r}) + \alpha_{\boldsymbol{R},\boldsymbol{R}'}(\boldsymbol{r}') = 2$ among the rays of two adjacent maximal cones $\mathbb{R}_{\geq 0}\boldsymbol{R}$ and $\mathbb{R}_{\geq 0}\boldsymbol{R}'$ of $\mathcal{G}$ with $\boldsymbol{R} \smallsetminus \{\boldsymbol{r}\} = \boldsymbol{R}' \smallsetminus \{\boldsymbol{r}'\}$.

[5] The linear dependence is unique up to rescaling, and we fix this arbitrary positive rescaling for convenience in the exposition.

As a polyhedral cone, the height deformation cone possesses a face lattice. In particular, if $\boldsymbol{h} \in \mathbb{DC}_{\mathrm{h}}(\mathsf{P})$ is in the interior of the deformation cone, then $\mathsf{P}_{\boldsymbol{h}}$ has the same normal fan as P, *i.e.* is normally equivalent to P. The interior of the deformation cone is sometimes called the *type cone* in the literature, while the word *deformations* can refer to non-(normally)-equivalent deformations of P. Consequently, (the interior of) each face of $\mathbb{DC}_{\mathrm{h}}(\mathsf{P})$ is associated to a class of normally equivalent polytopes, and the face lattice of $\mathbb{DC}_{\mathrm{h}}(\mathsf{P})$ gives rise to a lattice of (classes of normally equivalent) deformations of P. The following proposition grants us access to the faces of the deformation cone.

Proposition 2.4. *If* Q *is a deformation of* P*, then* $\mathbb{DC}(\mathsf{Q})$ *is a face of* $\mathbb{DC}(\mathsf{P})$*.*

Though simple, this proposition is of great importance. As a first application, suppose we want to study the deformation cone of P and we know one of its deformations, Q, then studying the deformation cone of Q is a simpler problem (because Q is of lower dimension than P) which describes a face of $\mathbb{DC}(\mathsf{P})$. A second purpose of this proposition is to measure how deformed is Q with respect to P. For example, the associahedron is a deformation of the permutahedron, and we will see in Proposition 2.33 that the respective dimensions of $\mathbb{DC}\big(\mathsf{\Pi}_n\big)$ and $\mathbb{DC}(\mathsf{Asso}_n)$ are 2^n-n-1 and $\binom{n}{2}$: in high dimension, the associahedron is very low in the lattice of deformations of $\mathsf{\Pi}_n$.

Deformations of the standard permutahedron $\mathsf{\Pi}_n$ are called *generalized permutahedra*. Originally introduced by Edmonds in 1970 under the name of *polymatroids* as a polyhedral generalization of matroids in the context of linear optimization [Edm70], the generalized permutahedra were rediscovered by Postnikov in 2009 [Pos09], who initiated the investigation of their rich combinatorial structure. They have since become a widely studied family of polytopes that appears naturally in several areas of mathematics, such as algebraic combinatorics [AA17, ABD10, PRW08], optimization [Fuj05], game theory [DK00], statistics [MPS+09, MUWY18], and economic theory [JKS22]. The set of deformed permutahedra can be parametrized by the cone of *submodular functions* [Edm70, Pos09].

The search for irredundant facet descriptions of deformation cones of particular families of combinatorial polytopes has received considerable attention recently [ACEP20, BMDM+18, CDG+20, CL20, PPPP19, APR21]. One of the motivations sparking this interest arises from the *amplituhedron program* to study scattering amplitudes in mathematical physics [AHT14]. As described in [PPPP19, Sec. 1.4], the deformation cone provides canonical realizations of a polytope (seen as a *positive geometry* [AHBL17]) in the positive region of the kinematic space, akin to those of the associahedron in [AHBHY18].

Contributing to this domain, Sections 2.2 and 2.3 set forth and prove the facet-descriptions of deformation cones of two families of generalized permutahedra: graphical zonotopes and nestohedra respectively.

2.2 Deformation cones of graphical zonotopes

This section is joint work with Arnau Padrol and Vincent Pilaud. It comes from our paper [PPP22b] (accepted for publication), enriched with some additional details and figures.

The *graphical zonotope* of a graph G is a convex polytope Z_G whose geometry encodes several combinatorial properties of G. For example, its vertices are in bijection with the acyclic orientations of G [Sta07, Prop. 2.5] and its volume is the number of spanning trees of G [Sta12, Ex. 4.64]. When G is the complete graph K_n, the graphical zonotope is a translation of the classical n-dimensional permutahedron, see Section 1.2.3.

The main result of this section (Theorem 2.12) presents complete irredundant descriptions of the deformation cones of graphical zonotopes. Note that, since graphical zonotopes are deformed permutahedra, their type cones appear as particular faces of the submodular cone. Faces of the submodular cone are far from being well understood. For example, determining its rays remains an open problem since the 1970s, when it was first asked by Edmonds [Edm70].

It is worth noting that most of the existing approaches to compute deformation cones only focus on simple polytopes with simplicial normal fans [CFZ02, PRW08]. Nevertheless, most graphical zonotopes are not simple. They are simple only for chordful graphs (those where every cycle induces a clique), see [PRW08, Prop. 5.2], [Kim08, Rmk. 6.2], or [Pil21, Prop. 52]. In this section, we thus use an alternative approach to describe the deformation cone of a non-simple polytope based on a simplicial refinement of its normal cone.

This section is organized as follows. We first recall in Section 2.2.1 the necessary material concerning graphical zonotopes. We then describe the deformation cone of any graphical zonotope, providing first a possibly redundant description (Section 2.2.2), then irredundant descriptions of its linear span (Section 2.2.2) and of its facet-defining inequalities (Section 2.2.3), and finally a characterization of graphical zonotopes with simplicial type cones (Section 2.2.4).

2.2.1 Graphical zonotopes

Let $G = (V, E)$ be a graph with vertex set V and edge set E. The *graphical arrangement* $\mathcal{A}_G$ is the arrangement of the hyperplanes $\{\boldsymbol{x} \in \mathbb{R}^V \;:\; \boldsymbol{x}_u = \boldsymbol{x}_v\}$ for all edges $\{u, v\} \in E$. It induces the *graphical fan* $\mathcal{F}_G$ whose cones are all possible intersections of one of the sets $\{\boldsymbol{x} \in \mathbb{R}^V \;:\; \boldsymbol{x}_u = \boldsymbol{x}_v\}$, $\{\boldsymbol{x} \in \mathbb{R}^V \;:\; \boldsymbol{x}_u \geq \boldsymbol{x}_v\}$, or $\{\boldsymbol{x} \in \mathbb{R}^V \;:\; \boldsymbol{x}_u \leq \boldsymbol{x}_v\}$ for each edge $\{u, v\} \in E$. The lineality of $\mathcal{F}_G$ is the subspace $\mathbb{K}_G$ of $\mathbb{R}^V$ spanned by the characteristic vectors of the connected components of G.

The *graphical zonotope* Z_G is the Minkowski sum of the line segments $[\boldsymbol{e}_u, \boldsymbol{e}_v]$ in $\mathbb{R}^V$ for all edges $\{u, v\} \in E$. Here, $(\boldsymbol{e}_v)_{v \in V}$ denotes the canonical basis of $\mathbb{R}^V$. Note that Z_G lies in a subspace orthogonal to $\mathbb{K}_G$. The graphical fan $\mathcal{F}_G$ is the normal fan of the graphical zonotope Z_G.

The following result is well-known. For example, it can be easily deduced from [Sta07, Proposition 2.5] or [BLS+99] (for the latter, see that the graphical matroid from Section 1.1 is realized by the graphical arrangement, and use the description of the cells of the arrangement in terms of covectors from Section 1.2(c)).

An *ordered partition* (μ, ω) of G consists of a partition μ of V where each part induces a connected subgraph of G, together with an acyclic orientation ω of the quotient graph G/μ. We say that (μ, ω) refines (μ', ω') if each part of μ is contained in a part of μ' and the orientations are compatible; that is, for all $u, v \in V$ if there is a directed path in ω between the parts of μ respectively containing u and v, then there is a directed path in ω' between the parts of μ' respectively containing u and v.

Proposition 2.5. *The face lattice of $\mathcal{F}_G$ is antiisomorphic to the lattice of ordered partitions of G ordered by refinement. Explicitly, the antiisomorphism is given by the map that associates the ordered partition (μ, ω) to the cone $\mathsf{C}_{\mu,\omega}$ defined by the inequalities $\boldsymbol{x}_u \leq \boldsymbol{x}_v$ for all $u, v \in V$ such that there is a directed path in ω from the part containing u to the part containing v (in particular, $\boldsymbol{x}_u = \boldsymbol{x}_v$ if u, v are in the same part of μ).*

Some easy consequences of Proposition 2.5 are:

- The maximal cones of $\mathcal{F}_G$ are in bijection with the acyclic orientations of G. We denote by C_ω the maximal cone of $\mathcal{F}_G$ associated to the acyclic orientation ω.
- The minimal cones of $\mathcal{F}_G$, that is the rays of $\mathcal{F}_G/\mathbb{K}_G$, are in bijection with the *biconnected subsets* of G, *i.e.* non-empty subsets S of V such that there is a disjoint non-empty subset T of V such that $S \cup T$ is a connected component of G and the induced subgraphs $G[S]$ and $G[T]$ are connected.
- The rays of $\mathcal{F}_G/\mathbb{K}_G$ that belong to the maximal cone associated to an acyclic orientation are the biconnected subsets which form an upper set of the acyclic orientation (hence, they are in bijection with the minimal directed cuts of the acyclic orientation).
- Similarly, the rays of $\mathcal{F}_G/\mathbb{K}_G$ that belong to the cone associated to an ordered partition (μ, ω) are the biconnected sets that contracted by μ give rise to an upper set of ω.

Note that the natural embedding of a graphical fan $\mathcal{F}_G$ is not essential, as it has a lineality given by its connected components. This is why we cannot directly talk about the rays of the fan in the enumeration above. The usual solution to avoid this is to consider the quotient by the subspace $\mathbb{K}_G$. However, this subspace depends on the graph, and with such a quotient we would lose the capacity of uniformly treating all the graphs with a fixed vertex set. We will instead work with the natural non-essential embedding, together with a collection of vectors supporting simultaneously all graphical fans.

Example 2.6. As seen in Section 1.2.3, when G is the complete graph K_n, the graphical zonotope is the *permutahedron*. The graphical fan is the *braid fan* $\mathcal{B}_n$, induced by the *braid arrangement* consisting of the hyperplanes $\{\boldsymbol{x} \in \mathbb{R}^n \ ; \ \boldsymbol{x}_i = \boldsymbol{x}_j\}$ for all $1 \leq i < j \leq n$. Its lineality is spanned by the all-ones vector $\mathbb{1}_n := (1, \dots, 1)$. Since all the proper subsets of $[n]$ are biconnected in K_n, the face lattice of $\mathcal{B}_n$ is isomorphic to the lattice of ordered partitions of $[n]$. The rays of $\mathcal{B}_n/\mathbb{1}_n$ correspond to proper subsets of $[n]$, and its maximal cells are in bijection with permutations of $[n]$. Each maximal cell is the positive hull of the $n-1$ rays corresponding to the proper upper sets of the order given by the permutation. In particular, $\mathcal{B}_n/\mathbb{1}_n$ is a simplicial fan.

2.2.2 Graphical deformation cones

Our main result is an irredundant facet description of the deformation cone of Z_G for every graph $G = (V, E)$. Our starting point is Proposition 2.10, which gives a (possibly redundant) description derived from Proposition 2.3. It is strongly based on the fact that the braid fan simultaneously refines all the graphical fans. Note however that the braid fan is not simplicial (due to its lineality). The classical approach to overcome this issue is to quotient the braid fan by its lineality space. However, we prefer to triangulate the braid fan, since it simplifies the presentation of the proof.

A first polyhedral description Associate to each subset $S \subseteq V$ the vector

$$\boldsymbol{\iota}_S := \sum_{v \in S} \boldsymbol{e}_v - \sum_{v \notin S} \boldsymbol{e}_v.$$

This is essentially the characteristic vector of S, but it has the advantage that $\boldsymbol{\iota}_V = \mathbb{1}_V$ and $\boldsymbol{\iota}_\varnothing = -\mathbb{1}_V$ positively span the line $\mathbb{1}_V\mathbb{R}$, which is the lineality $\mathbb{K}_{K_V}$ of the braid fan.

Lemma 2.7. *For any ordered partition (μ, ω) of a graph $G = (V, E)$, we have*

$$\mathsf{C}_{\mu,\omega} = \operatorname{cone}\{\boldsymbol{\iota}_S \ ; \ S \subseteq V \text{ upper set of } \omega\}.$$

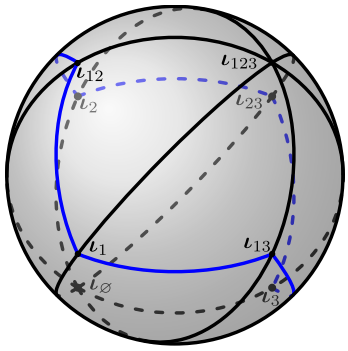

Figure 11: The fan $\widehat{\mathcal{B}}_{123}$ intersected with the unit sphere. (For brevity, here and in the labels we write 123 to denote the set $\{1,2,3\}$, and so on.) The braid fan $\mathcal{B}_{123}$ is the Cartesian product of a regular hexagonal fan with a line. To obtain $\widehat{\mathcal{B}}_{123}$, each maximal cell is divided into two simplicial cells, one containing $\boldsymbol{\iota}_\varnothing$ and one containing $\boldsymbol{\iota}_{123}$.

Here, we mean that S is an upper set of ω when contracted by μ. Note that $\varnothing$ and V are always upper sets, which is consistent with the fact that the lineality of $\mathcal{F}_G$ always contains the line spanned by $\mathbb{1}_V$.

We will work with a refined version $\widehat{\mathcal{B}}_V$ of the braid fan whose maximal cells are

$$\mathsf{C}_\sigma^\varnothing := \operatorname{cone}\{\boldsymbol{\iota}_S \ ; \ S \subsetneq V \text{ upper set of } \sigma\} \quad \text{and} \quad \mathsf{C}_\sigma^V := \operatorname{cone}\{\boldsymbol{\iota}_S \ ; \ \varnothing \neq S \subseteq V \text{ upper set of } \sigma\}$$

for every acyclic orientation of the complete graph K_V, which we identify with a permutation σ of V. An example is depicted in Figure 11. The following two immediate statements are left to the reader.

Lemma 2.8. *For any finite set V:*

(i) The fan $\widehat{\mathcal{B}}_V$ is an essential complete simplicial fan in $\mathbb{R}^V$ supported on the $2^{|V|}$ vectors $\boldsymbol{\iota}_S$ for $S \subseteq V$.

(ii) For any permutation σ, the maximal cones $\mathsf{C}_\sigma^\varnothing$ and C_σ^V are adjacent, and the unique linear relation supported on the rays of $\mathsf{C}_\sigma^\varnothing \cup \mathsf{C}_\sigma^V$ is $\boldsymbol{\iota}_\varnothing + \boldsymbol{\iota}_V = \mathbf{0}$.

(iii) The other pairs of adjacent maximal cells are of the form C_σ^X and $\mathsf{C}_{\sigma'}^X$, where $X \in \{\varnothing, V\}$ and $\sigma = PuvS$ and $\sigma' = PvuS$ are permutations that differ in the inversion of two consecutive elements. The two rays that are not shared by C_σ^X and $\mathsf{C}_{\sigma'}^X$ are $\boldsymbol{\iota}_{S\cup\{u\}}$ and $\boldsymbol{\iota}_{S\cup\{v\}}$, and the unique linear relation supported on the rays of $\mathsf{C}_\sigma^X \cup \mathsf{C}_{\sigma'}^X$ is given by

$$\boldsymbol{\iota}_{S\cup\{u\}} + \boldsymbol{\iota}_{S\cup\{v\}} = \boldsymbol{\iota}_S + \boldsymbol{\iota}_{S\cup\{u,v\}}.$$

Lemma 2.9. *For any graph $G = (V, E)$:*

(i) The fan $\widehat{\mathcal{B}}_V$ is a simplicial refinement of the graphical fan $\mathcal{F}_G$.

(ii) For an acyclic orientation ω of G and $S \subseteq V$, we have $\boldsymbol{\iota}_S \in \mathsf{C}_\omega$ if and only if S is an upper set of ω.

(iii) For an acyclic orientation σ of K_V and $X \in \{\varnothing, V\}$ we have $\mathsf{C}_\sigma^X \subseteq \mathsf{C}_\omega$ if and only if σ is a linear extension of ω.

We are now ready to describe the deformation cone of the graphical zonotope Z_G. For any $\boldsymbol{h} \in \mathbb{R}^{2^V}$, let $\mathsf{D}_{\boldsymbol{h}}$ be the polytope given by

$$\mathsf{D}_{\boldsymbol{h}} := \Big\{ \boldsymbol{x} \in \mathbb{R}^V \ ; \ \sum_{v\in S} \boldsymbol{x}_v - \sum_{v\notin S} \boldsymbol{x}_v \leq \boldsymbol{h}_S \text{ for all } S \subseteq V \Big\}.$$

Proposition 2.10. *For any graph $G = (V, E)$, the deformation cone $\mathbb{DC}(\mathsf{Z}_G)$ of the graphical zonotope Z_G is the set of polytopes $\mathsf{D}_{\boldsymbol{h}}$ for all $\boldsymbol{h}$ in the cone of $\mathbb{R}^{2^V}$ defined by the following (possibly redundant) description:*

- $\boldsymbol{h}_\varnothing = -\boldsymbol{h}_V$,
- $\boldsymbol{h}_{S\cup\{u\}} + \boldsymbol{h}_{S\cup\{v\}} = \boldsymbol{h}_S + \boldsymbol{h}_{S\cup\{u,v\}}$ *for each* $\{u, v\} \in \binom{V}{2} \smallsetminus E$ *and* $S \subseteq V \smallsetminus \{u, v\}$, *and*
- $\boldsymbol{h}_{S\cup\{u\}} + \boldsymbol{h}_{S\cup\{v\}} \geq \boldsymbol{h}_S + \boldsymbol{h}_{S\cup\{u,v\}}$ *for each* $\{u, v\} \in E$ *and* $S \subseteq V \smallsetminus \{u, v\}$.

Proof. Observe first that, as stated in Lemma 2.9, $\widehat{\mathcal{B}}_V$ provides a simplicial refinement of $\mathcal{F}_G$. Following Proposition 2.3, we need to consider all pairs of adjacent maximal cones of $\widehat{\mathcal{B}}_V$, and to study which ones lie in the same cone of $\mathcal{F}_G$.

Adjacent maximal cones of $\widehat{\mathcal{B}}_V$ are described in Lemma 2.8, and the containment relations of the cones of $\widehat{\mathcal{B}}_V$ in the cones of $\mathcal{F}_G$ are described in Lemma 2.9.

For any σ, the cones $\mathsf{C}^{\varnothing}_{\sigma}$ and C^{V}_{σ} belong to the same cell of $\mathcal{F}_G$. Hence, by Proposition 2.3, the following equation holds in the deformation cone:

$$\boldsymbol{h}_\varnothing = -\boldsymbol{h}_V.$$

The remaining pairs of adjacent maximal cones of $\widehat{\mathcal{B}}_V$ correspond to pairs of acyclic orientations of K_V differing in a single edge; or equivalently, to pairs of permutations of V of the form $\sigma = PuvS$ and $\sigma' = PvuS$. The unique linear relation supported on the rays of $\mathsf{C}^X_\sigma \cup \mathsf{C}^X_{\sigma'}$ for $X \in \{\varnothing, V\}$ is then

$$\boldsymbol{\iota}_{S\cup\{u\}} + \boldsymbol{\iota}_{S\cup\{v\}} = \boldsymbol{\iota}_S + \boldsymbol{\iota}_{S\cup\{u,v\}}.$$

We consider first the case when $\{u, v\} \notin E$. Observe that both σ and σ' induce the same acyclic orientation of G, which we call ω. We have then $\mathsf{C}^X_\sigma \cup \mathsf{C}^X_{\sigma'} \subseteq \mathsf{C}_\omega$ by Lemma 2.9. Therefore, by Proposition 2.3 and Lemma 2.8, we have

$$\boldsymbol{h}_{S\cup\{u\}} + \boldsymbol{h}_{S\cup\{v\}} = \boldsymbol{h}_S + \boldsymbol{h}_{S\cup\{u,v\}}$$

for any $\boldsymbol{h}$ in $\mathbb{DC}(\mathsf{Z}_G)$. Note that, for any $\{u, v\} \notin E$ and $S \subset V \smallsetminus \{u, v\}$, we can construct such permutations σ and σ'. This gives the claimed description of the linear span of $\mathbb{DC}(\mathsf{Z}_G)$.

In contrast, if $\{u, v\} \in E$, then σ and σ' induce different orientations of G, and hence they belong to different adjacent cones of $\mathcal{F}_G$ by Lemma 2.9. Therefore, by Proposition 2.3 and Lemma 2.8, we have

$$\boldsymbol{h}_{S\cup\{u\}} + \boldsymbol{h}_{S\cup\{v\}} \geq \boldsymbol{h}_S + \boldsymbol{h}_{S\cup\{u,v\}}$$

for any $\boldsymbol{h}$ in $\mathbb{DC}(\mathsf{Z}_G)$. As before, for any $\{u, v\} \in E$ and $S \subset V \smallsetminus \{u, v\}$, we can construct such permutations σ and σ'. This gives the claimed inequalities describing $\mathbb{DC}(\mathsf{Z}_G)$. □

The linear span of graphical deformation cones The description of the deformation cone of Proposition 2.10 is highly redundant, both in the equations describing its linear span and in the inequalities describing its facets. We will give a non-redundant description in Theorem 2.12. The first step will be to give linearly independent equations describing the linear span. As an important by-product, we will obtain the dimension and a linear basis of (the vector space generated by) the deformation cone $\mathbb{DC}(\mathsf{Z}_G)$.

It is sometimes convenient to consider the set of deformations of P embedded inside the real vector space of *virtual d-dimensional polytopes* $\mathbb{V}^d$ [PK92]. This is the set of formal differences of polytopes $\mathsf{P} - \mathsf{Q}$ under the equivalence relation $(\mathsf{P}_1 - \mathsf{Q}_1) = (\mathsf{P}_2 - \mathsf{Q}_2)$ whenever $\mathsf{P}_1 + \mathsf{P}_2 = \mathsf{Q}_1 + \mathsf{Q}_2$. Endowed with Minkowski addition, it is the Grothendieck group of the semigroup of polytopes, which are embedded into $\mathbb{V}^d$ via the map $\mathsf{P} \mapsto \mathsf{P} - \{\mathbf{0}\}$. It extends to a real vector space via dilation: for $\mathsf{P} - \mathsf{Q} \in \mathbb{V}^d$ and $\lambda \in \mathbb{R}$, we set $\lambda(\mathsf{P} - \mathsf{Q}) := \lambda\mathsf{P} - \lambda\mathsf{Q}$ when $\lambda \geq 0$, and $\lambda(\mathsf{P} - \mathsf{Q}) := ((-\lambda)\mathsf{Q}) - ((-\lambda)\mathsf{P})$ when $\lambda < 0$. Here, $\lambda\mathsf{P} := \{\lambda\boldsymbol{p} \ ; \ \boldsymbol{p} \in \mathsf{P}\}$ denotes the dilation[6] of P by $\lambda \geq 0$.

[6] Note in particular that $-\mathsf{P}$ does not represent the reflection of P, but its group inverse.

For a polytope $\mathsf{P} \subset \mathbb{R}^d$, we define the space $\mathbb{VD}(\mathsf{P}) \subset \mathbb{V}^d$ of *virtual deformations* of P as the vector sub-space of virtual polytopes generated by the deformations of P. Equivalently, $\mathbb{VD}(\mathsf{P})$ is the linear span of the deformation cone $\mathbb{DC}(\mathsf{P})$. Every virtual polytope in $\mathbb{VD}(\mathsf{P})$ is of the form $\mathsf{P}_{\boldsymbol{h}} - \mathsf{P}_{\boldsymbol{h'}}$ for deformations $\mathsf{P}_{\boldsymbol{h}}, \mathsf{P}_{\boldsymbol{h'}} \in \mathbb{DC}(P)$. Note that the vector $\boldsymbol{h} - \boldsymbol{h'}$ uniquely describes the equivalence class of this virtual polytope, and we will use the notation $\mathsf{P}_{\boldsymbol{h}-\boldsymbol{h'}}$ to denote it.

Denote by $\Delta_U := \operatorname{conv}\{\boldsymbol{e}_u \ ; \ u \in U\} \subset \mathbb{R}^V$ the face of the standard simplex Δ_V corresponding to a subset $U \subseteq V$. These polytopes are particularly important deformed permutahedra as they form a linear basis of the deformation space of the permutahedron [DK00] (see also [ABD10, Prop. 2.4]). Namely, any (virtual) deformed permutahedron can be uniquely written as a signed Minkowski sum of dilates of Δ_I. Our first result states that this linear basis is adapted to graphical zonotopes.

Theorem 2.11. *For any graph $G = (V, E)$:*

(i) The dimension of $\mathbb{VD}(\mathsf{Z}_G)$ is the number of non-empty induced cliques in G (the vertices of G count for the dimension as they correspond to the lineality space).

(ii) The faces Δ_K of the standard simplex Δ_V corresponding to the non-empty induced cliques K of G form a linear basis of $\mathbb{VD}(\mathsf{Z}_G)$.

(iii) $\mathbb{VD}(\mathsf{Z}_G)$ is the set of virtual polytopes $\mathsf{D}_{\boldsymbol{h}}$ for all $\boldsymbol{h} \in \mathbb{R}^{2^V}$ fulfilling the following linearly independent equations:

- *$\boldsymbol{h}_\varnothing = -\boldsymbol{h}_V$ and*
- *$\boldsymbol{h}_{S\smallsetminus\{u\}} + \boldsymbol{h}_{S\smallsetminus\{v\}} = \boldsymbol{h}_S + \boldsymbol{h}_{S\smallsetminus\{u,v\}}$ for each $S \subseteq V$ with $|S| \geq 2$ not inducing a clique of G and any $\{u, v\} \in \binom{S}{2} \smallsetminus E$ (here, we only choose one missing edge for each subset S, for example, the lexicographically smallest).*

Proof. Observe first that the faces Δ_I of the standard simplex Δ_V corresponding to the induced cliques I of G are all in the deformation cone $\mathbb{DC}(\mathsf{Z}_G)$. Indeed, faces of the standard simplex Δ_I belong to the deformation cone of the complete graph K_I by [Pos09, Prop. 6.3]. The graphical zonotope $\mathsf{Z}_{G'}$ is a Minkowski summand of Z_G for any subgraph G' of G, and hence summands of $\mathsf{Z}_{G'}$ are also summands of Z_G.

Moreover, all faces Δ_I for $\varnothing \neq I \subsetneq V$ are Minkowski independent by [ABD10, Prop. 2.4]. This shows that the dimension of $\mathbb{VD}(\mathsf{Z}_G)$ is at least the number of non-empty induced cliques of G.

Let $(\boldsymbol{f}_X)_{X\subseteq V}$ be the canonical basis of $\left(\mathbb{R}^{2^V}\right)^*$. The vectors

$$\boldsymbol{o}^S := \boldsymbol{f}_S - \boldsymbol{f}_{S\smallsetminus\{u\}} - \boldsymbol{f}_{S\smallsetminus\{v\}} + \boldsymbol{f}_{S\smallsetminus\{u,v\}},$$

for all subsets $\varnothing \neq S \subseteq V$ not inducing a clique of G and one selected missing edge $\{u, v\}$ for each S, are clearly linearly independent. Indeed, if the $\boldsymbol{f}_X$ are ordered according to any linear extension of the inclusion order on the indices X, and the $\boldsymbol{o}^S$ are ordered analogously in terms of the indices S, then the equations are already in echelon form, as $\boldsymbol{f}_S$ is the greatest non-zero coordinate of $\boldsymbol{o}^S$. Finally, the vector $\boldsymbol{v} \in 2^V$ with $\boldsymbol{v}_X = |X|$ for $X \in 2^V$ is orthogonal to any $\boldsymbol{o}^S$ with $|S| \geq 2$ but not to $\boldsymbol{o}^\varnothing := \boldsymbol{f}_\varnothing + \boldsymbol{f}_V$, showing that the latter is linearly independent to the former. This proves that the dimension of $\mathbb{VD}(\mathsf{Z}_G)$ is at most the number of non-empty induced cliques of G.

We conclude that $\left\{\Delta_K \ ; \ \varnothing \neq K \subseteq V \text{ inducing a clique of } G\right\}$ is a linear basis of the deformation cone, and that $\left\{\boldsymbol{o}^S \ ; \ S = \varnothing \text{ or } S \subseteq V \text{ not inducing a clique of } G\right\}$ is a basis of its orthogonal complement (we slightly abuse notation here as $\boldsymbol{o}^S$ was defined in $\left(\mathbb{R}^{2^V}\right)^*$ instead of in $(\mathbb{V}^d)^*$, but note that each $\boldsymbol{f}_X$ can be considered as a linear functional in $(\mathbb{V}^d)^*$ if seen as a support function). □

Note that the dimension of the deformation space of graphical zonotopes has been independently computed by Raman Sanyal and Josephine Yu (personal communication), who computed the space of Minkowski 1-weights of graphical zonotopes in the sense of McMullen [McM96]. Their proof also uses the basis from Theorem 2.11 (ii), but with an alternative argument to show that they are a generating family.

2.2.3 The facets of graphical deformation cones

To conclude, it remains to compute the facets of the deformation cones, *i.e.* a non-redundant inequality description.

We define the *neighborhood* of a vertex v in a graph $G = (V, E)$ as $N(v) := \{u \in V \ ; \ \{u, v\} \in E\}$.

Theorem 2.12. *For any graph $G = (V, E)$, the deformation cone $\mathbb{DC}(\mathsf{Z}_G)$ of the graphical zonotope Z_G is the set of polytopes $\mathsf{D}_{\boldsymbol{h}}$ for all $\boldsymbol{h}$ in the cone of $\mathbb{R}^{2^V}$ defined by the following irredundant facet description:*

- $\boldsymbol{h}_\varnothing = -\boldsymbol{h}_V$,
- $\boldsymbol{h}_{S\smallsetminus\{u\}} + \boldsymbol{h}_{S\smallsetminus\{v\}} = \boldsymbol{h}_S + \boldsymbol{h}_{S\smallsetminus\{u,v\}}$ *for each* $\varnothing \neq S \subseteq V$ *and any* $\{u, v\} \in \binom{S}{2} \smallsetminus E$,
- $\boldsymbol{h}_{S\cup\{u\}} + \boldsymbol{h}_{S\cup\{v\}} \geq \boldsymbol{h}_S + \boldsymbol{h}_{S\cup\{u,v\}}$ *for each* $\{u, v\} \in E$ *and* $S \subseteq N(v) \cap N(v)$.

Note that this description is given as a face of the submodular cone, embedded into $\mathbb{R}^{2^V}$. One gets easily an intrinsic presentation by restricting to the space spanned by the biconnected subsets of V. However, that presentation loses its symmetry, and the explicit equations depend on the biconnected sets of G.

Proof of Theorem 2.12. We know by Proposition 2.10 that $\mathbb{DC}(\mathsf{Z}_G)$ is the intersection of the cone

$$\boldsymbol{h}_{S\cup\{u\}} + \boldsymbol{h}_{S\cup\{v\}} \geq \boldsymbol{h}_S + \boldsymbol{h}_{S\cup\{u,v\}} \tag{1}$$

for $\{u, v\} \in E$ and $S \subseteq V \smallsetminus \{u, v\}$ with the linear space given by the equations $\boldsymbol{h}_\varnothing = -\boldsymbol{h}_V$ and

$$\boldsymbol{h}_{S\cup\{u\}} + \boldsymbol{h}_{S\cup\{v\}} = \boldsymbol{h}_S + \boldsymbol{h}_{S\cup\{u,v\}} \tag{2}$$

for $\{u, v\} \in \binom{V}{2} \smallsetminus E$ and $S \subseteq V \smallsetminus \{u, v\}$.

We have already determined the equations describing the linear span in Theorem 2.11, so it only remains to provide non-redundant inequalities describing the deformation cone.

We will prove first that the inequalities from (1) indexed by $\{u, v\} \in E$ and $S \subseteq N(v) \cap N(v)$ suffice to describe $\mathbb{DC}(\mathsf{Z}_G)$. To this end, consider an inequality from (1) for which $S \nsubseteq N(v) \cap N(v)$. Without loss of generality, assume that there is some $x \in S$ such that $\{x, v\} \notin E$. We will show that this inequality is induced (in the sense that the half-spaces they define coincide on the linear span of $\mathbb{DC}(\mathsf{Z}_G)$) by the inequality

$$\boldsymbol{h}_{S'\cup\{u\}} + \boldsymbol{h}_{S'\cup\{v\}} \geq \boldsymbol{h}_{S'} + \boldsymbol{h}_{S'\cup\{u,v\}} \tag{3}$$

where $S' = S \smallsetminus \{x\}$. Our claim will then follow from this by induction on the elements of $S \smallsetminus (N(v) \cap N(v))$.

Indeed, if $\{x, v\} \notin E$, we know by (2) that the following two equations hold in the linear span of $\mathbb{DC}(\mathsf{Z}_G)$ by considering the non-edge $\{x, v\}$ with the subsets S' and $S' \cup \{u\}$, respectively:

$$\boldsymbol{h}_{S\cup\{u\}} + \boldsymbol{h}_{S'\cup\{u,v\}} = \boldsymbol{h}_{S'\cup\{u\}} + \boldsymbol{h}_{S\cup\{u,v\}}, \tag{4}$$

$$\boldsymbol{h}_S + \boldsymbol{h}_{S'\cup\{v\}} = \boldsymbol{h}_{S'} + \boldsymbol{h}_{S\cup\{v\}}, \tag{5}$$

where we used that $(S' \cup \{u\}) \cup \{x\} = S \cup \{u\}$ and $(S' \cup \{u\}) \cup \{x, v\} = S \cup \{u, v\}$ in the first equation, and that $S' \cup \{x\} = S$ and $S' \cup \{x, v\} = S \cup \{v\}$ in the second equation. To conclude, note that (1) is precisely the linear combination (3) + (4) − (5).

We know therefore that the descriptions in Proposition 2.10 and Theorem 2.12 give rise to the same cone. It remains to show that the latter is irredundant. That is, that each of the inequalities gives rise to a unique facet of $\mathbb{DC}(\mathsf{Z}_G)$.

Let $(\boldsymbol{f}_X)_{X\subseteq V}$ be the canonical basis of $\left(\mathbb{R}^{2^V}\right)^*$. For $u, v \in V$ and $S \subseteq V \smallsetminus \{u, v\}$, let

$$\boldsymbol{n}(u, v, S) := \boldsymbol{f}_{S\cup\{u\}} + \boldsymbol{f}_{S\cup\{v\}} - \boldsymbol{f}_S - \boldsymbol{f}_{S\cup\{u,v\}}.$$

Note that, if $\{u,v\} \notin E$, then $\boldsymbol{n}(u,v,S)$ is orthogonal to $\mathbb{DC}(\mathsf{Z}_G)$, whereas if $\{u,v\} \in E$, then $\boldsymbol{n}(u,v,S)$ is an inner normal vector to $\mathbb{DC}(\mathsf{Z}_G)$.

Fix $\{u,v\} \in E$ and $S \subseteq N(v) \cap N(v)$. To prove that the half-space with normal $\boldsymbol{n}(u,v,S)$ is not redundant, we will exhibit a vector $\boldsymbol{w} \in \mathbb{R}^{2^V}$ in the linear span of $\mathbb{DC}(\mathsf{Z}_G)$ that belongs to the interior of all the half-spaces describing $\mathbb{DC}(\mathsf{Z}_G)$ except for this one. That is, we will construct a vector $\boldsymbol{w} \in \mathbb{R}^{2^V}$ respecting the system:

$$\begin{cases} \langle \boldsymbol{w},\ \boldsymbol{n}(u,v,S)\rangle \leq 0, & \\ \langle \boldsymbol{w},\ \boldsymbol{n}(u,v,X)\rangle > 0 & \text{for } S \neq X \subseteq N(u) \cap N(v), \\ \langle \boldsymbol{w},\ \boldsymbol{n}(a,b,X)\rangle > 0 & \text{for } \{a,b\} \in E \smallsetminus \{u,v\} \text{ and } X \subseteq N(a) \cap N(b), \text{ and} \\ \langle \boldsymbol{w},\ \boldsymbol{n}(a,b,X)\rangle = 0 & \text{for } \{a,b\} \in \binom{V}{2} \smallsetminus E \text{ and } X \subseteq V \smallsetminus \{a,b\}. \end{cases} \tag{6}$$

Denote by $T := N(u) \cap N(v) \smallsetminus S$. We will construct $\boldsymbol{w}$ as the sum $\boldsymbol{w} := \boldsymbol{t}^S - \boldsymbol{t}^T + \boldsymbol{c}$ for some vectors $\boldsymbol{t}^S$, $\boldsymbol{t}^T$, and $\boldsymbol{c} \in \mathbb{R}^{2^V}$ defined below, whose scalar products with $\boldsymbol{n}(a,b,X)$ for $\{a,b\} \in \binom{V}{2}$ and $X \subseteq V \smallsetminus \{a,b\}$ fulfill:

	$\langle \boldsymbol{t}^S,\ \boldsymbol{n}(a,b,X)\rangle$	$\langle -\boldsymbol{t}^T,\ \boldsymbol{n}(a,b,X)\rangle$	$\langle \boldsymbol{c},\ \boldsymbol{n}(a,b,X)\rangle$
if $\{a,b\} = \{u,v\}$ and $X = S$	$-\lvert S\rvert$	0	$\lvert S\rvert$
if $\{a,b\} = \{u,v\}$ and $S \neq X \subseteq N(u) \cap N(v)$	$-\lvert S \cap X\rvert$	$\lvert T \cap X\rvert$	$\lvert S\rvert$
if $\{a,b\} \in E \smallsetminus \{u,v\}$ and $X \subseteq N(a) \cap N(b)$	≥ -1	≥ 0	2
if $\{a,b\} \notin E$	0	0	0

It immediately follows from this table that the vector $\boldsymbol{w}$ will fulfill the desired properties from (6). For the second one, note that if $S \neq X \subseteq S \sqcup T$, then either $\lvert S \cap X\rvert < \lvert S\rvert$ or $\lvert T \cap X\rvert > 0$.

To define these vectors, first, for $\{x,y,z\} \in \binom{V}{3}$, let $\boldsymbol{t}^{xyz} \in \mathbb{R}^{2^V}$ be the vector such that $\boldsymbol{t}^{xyz}_X = 1$ if $\{x,y,z\} \subseteq X$ and $\boldsymbol{t}^{xyz}_X = 0$ otherwise. Note that, for any $a,b \in \binom{V}{2}$ and $X \subseteq V \smallsetminus \{a,b\}$, we have

$$\langle \boldsymbol{t}^{xyz},\ \boldsymbol{n}(a,b,X)\rangle = \begin{cases} -1 & \text{if } \{x,y,z\} = \{a,b,t\} \text{ for some } t \in X, \text{ and} \\ 0 & \text{otherwise.} \end{cases} \tag{7}$$

We define

$$\boldsymbol{t}^S := \sum_{s \in S} \boldsymbol{t}^{uvs} \qquad \text{and} \qquad \boldsymbol{t}^T := \sum_{t \in T} \boldsymbol{t}^{uvt}.$$

It is straightforward to derive the identities in the table from (7). For the inequalities, notice that if $\langle \boldsymbol{t}^{uvx},\ \boldsymbol{n}(a,b,X)\rangle = -1$ but $\{a,b\} \neq \{u,v\}$, then either $\{a,b\} = \{u,x\}$ or $\{a,b\} = \{v,x\}$, and in both cases $\langle \boldsymbol{t}^{uvy},\ \boldsymbol{n}(a,b,X)\rangle = 0$ for any $y \neq x$.

Now, for $\{x,y\} \in \binom{V}{2}$, let $\boldsymbol{c}^{xy} \in \mathbb{R}^{2^V}$ be the vector such that $\boldsymbol{c}^{xy}_X = 1$ if $\lvert\{x,y\} \cap X\rvert = 1$ (that is, if $\{x,y\}$ belongs to the cut defined by X), and $\boldsymbol{c}^{xy}_X = 0$ otherwise. Note that, for any $a,b \in \binom{V}{2}$ and $X \subseteq V \smallsetminus \{a,b\}$, we have

$$\langle \boldsymbol{c}^{xy},\ \boldsymbol{n}(a,b,X)\rangle = \begin{cases} 2 & \text{if } \{a,b\} = \{x,y\}, \text{ and} \\ 0 & \text{otherwise.} \end{cases} \tag{8}$$

We set

$$\boldsymbol{c} := \frac{\lvert S\rvert}{2} \boldsymbol{c}^{uv} + \sum_{\{a,b\} \in E \smallsetminus \{u,v\}} \boldsymbol{c}^{ab}.$$

The identities in the table are straightforward to derive from (8). □

Corollary 2.13. *For any graph $G = (V,E)$, the dimension of $\mathbb{DC}(\mathsf{Z}_G)$ is the number of induced cliques in G, the dimension of the lineality space of $\mathbb{DC}(\mathsf{Z}_G)$ is $\lvert V\rvert$, and the number of facets of $\mathbb{DC}(\mathsf{Z}_G)$ is the number of triplets (u,v,S) with $\{u,v\} \in E$ and $S \subseteq N(u) \cap N(v)$.*

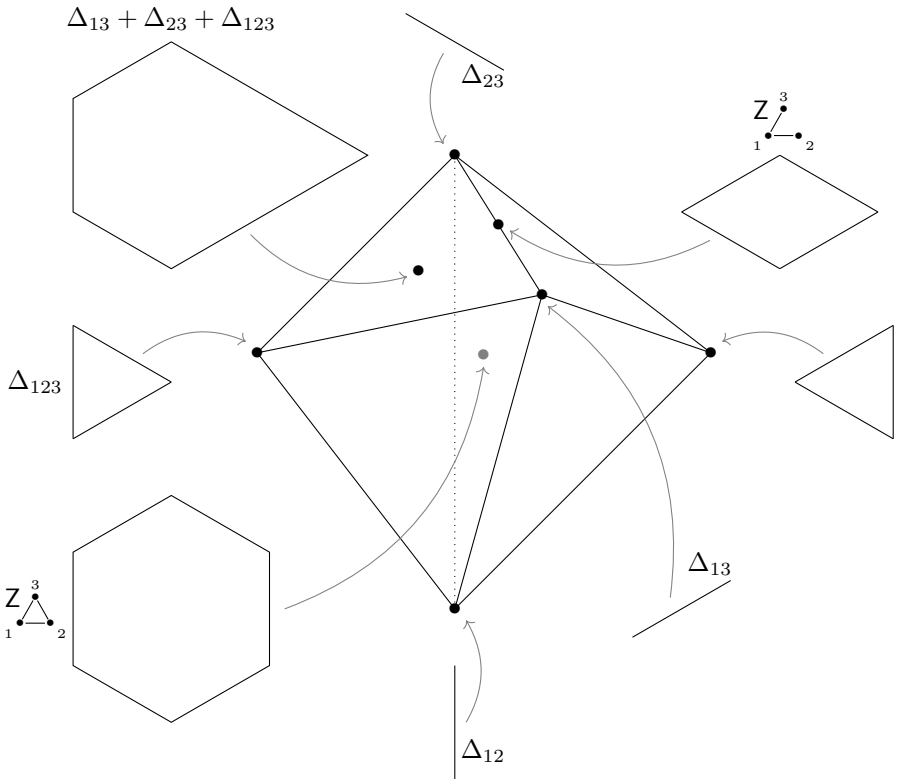

Figure 12: A 3-dimensional affine section of the deformation cone $\mathbb{DC}(\mathsf{Z}_{K_3})$ for the triangle K_3. The deformations of Z_{K_3} corresponding to some of the points of $\mathbb{DC}(\mathsf{Z}_{K_3})$ are depicted. Especially, all points in the interior correspond to polytopes normally equivalent to Π_3, while the above left polytope is the Loday associahedron Asso_3.

Example 2.14. For the complete graph K_V, the graphical zonotope Z_{K_V} is a permutahedron and the deformation cone $\mathbb{DC}(\mathsf{Z}_{K_V})$ is the submodular cone given by the irredundant inequalities $\boldsymbol{h}_{S\cup\{u\}} + \boldsymbol{h}_{S\cup\{v\}} \geq \boldsymbol{h}_S + \boldsymbol{h}_{S\cup\{u,v\}}$ for each $\{u,v\} \subseteq V$ and $S \subseteq V \smallsetminus \{u,v\}$. (The usual presentation imposes $\boldsymbol{h}_\varnothing = 0$, but both presentations are clearly equivalent up to translation). It has dimension $2^{|V|}-1$ and $\binom{|V|}{2}2^{|V|-2}$ facets. The lineality space is $|V|$-dimensional, given by the space of translations in $\mathbb{R}^{|V|}$.

For instance, for the triangle K_3, the graphical zonotope $\mathsf{Z}_{K_3} = \Pi_3$ is the regular hexagon depicted in the bottom left of Figure 12, which arises as the Minkowski sum of 3 coplanar vectors in $\mathbb{R}^3$. Its deformation cone $\mathbb{DC}(\mathsf{Z}_{K_3})$ lives in the 8-dimensional space $\mathbb{R}^{2^{[3]}}$, has dimension 7, a lineality space of dimension 3, and 6 facets. It admits as irredundant description the equation $\boldsymbol{h}_\varnothing = -\boldsymbol{h}_{123}$ and the following 6 inequalities:

$$\begin{array}{ccc} \boldsymbol{h}_1 + \boldsymbol{h}_2 \geq \boldsymbol{h}_\varnothing + \boldsymbol{h}_{12} & \boldsymbol{h}_1 + \boldsymbol{h}_3 \geq \boldsymbol{h}_\varnothing + \boldsymbol{h}_{13} & \boldsymbol{h}_2 + \boldsymbol{h}_3 \geq \boldsymbol{h}_\varnothing + \boldsymbol{h}_{23} \\ \boldsymbol{h}_{12} + \boldsymbol{h}_{13} \geq \boldsymbol{h}_1 + \boldsymbol{h}_{123} & \boldsymbol{h}_{12} + \boldsymbol{h}_{23} \geq \boldsymbol{h}_2 + \boldsymbol{h}_{123} & \boldsymbol{h}_{13} + \boldsymbol{h}_{23} \geq \boldsymbol{h}_3 + \boldsymbol{h}_{123}. \end{array}$$

After quotienting the lineality and intersecting with an affine hyperplane, we get the bipyramid over a triangle (living in dimension $7-3-1=3$) illustrated in Figure 12. Note that the four rays of $\mathbb{DC}(\mathsf{Z}_{K_3})$ (*i.e.* vertices of the bipyramid) of the form Δ_K for an induced clique K of K_3 provide a linear basis of $\mathbb{DC}(\mathsf{Z}_{K_3})$ (*i.e.* an affine basis of the bipyramid). Nevertheless, the last ray can not be written as a positive Minkowski sum of Δ_K and remain thus unlabeled.

Example 2.15. For a triangle-free graph $G = (V, E)$, the deformation cone $\mathbb{DC}(\mathsf{Z}_G)$ has dimension $|V| + |E|$ and $|E|$ facets. As before, the lineality is $|V|$-dimensional, given by the space of

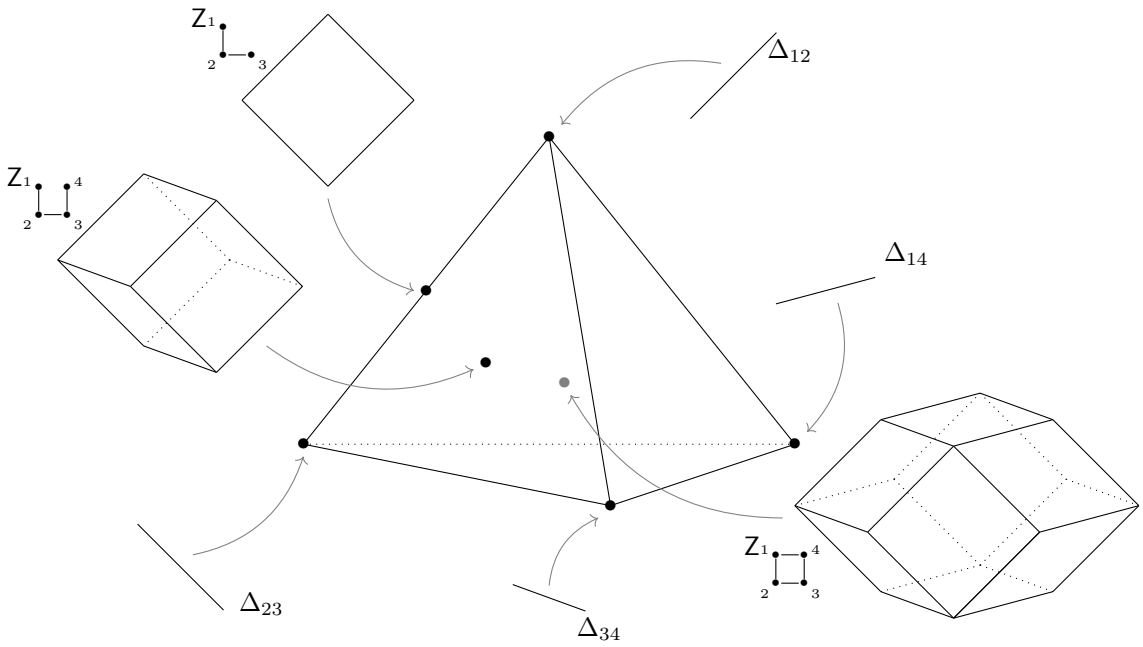

Figure 13: A 3-dimensional affine section of the deformation cone $\mathbb{DC}(\mathsf{Z}_{C_4})$ for the 4-cycle C_4. The deformations of Z_{C_4} corresponding to some of the points of $\mathbb{DC}(\mathsf{Z}_{C_4})$ are depicted. Especially, interior all points correspond to polytopes normally equivalent to Z_{C_4}. Note that as the rays of $\mathbb{DC}(\mathsf{Z}_{C_4})$ correspond to segments, all deformations of Z_{C_4} are zonotopes (which is not the case for the deformations of Π_n).

translations in $\mathbb{R}^{|V|}$. Thus $\mathbb{DC}(\mathsf{Z}_G)$ is simplicial.

For instance, for the 4-cycle C_4, the graphical zonotope Z_{C_4} is the 3-dimensional zonotope depicted in the bottom right of Figure 13 (a rhombic dodecahedron), which arises as the Minkowski sum of 4 vectors in a hyperplane of $\mathbb{R}^4$. Its deformation cone $\mathbb{DC}(\mathsf{Z}_{C_4})$ lives in the 16-dimensional space $\mathbb{R}^{2^{[4]}}$, has dimension 8, a lineality space of dimension 4, and 4 facets. It admits as irredundant description the following 8 equations and 4 inequalities:

$$\begin{array}{ccc}
\boldsymbol{h}_\varnothing = -\boldsymbol{h}_{1234} & \boldsymbol{h}_{12} + \boldsymbol{h}_{14} = \boldsymbol{h}_{124} + \boldsymbol{h}_1 & \boldsymbol{h}_1 + \boldsymbol{h}_2 \geq \boldsymbol{h}_{12} + \boldsymbol{h}_\varnothing \\
\boldsymbol{h}_1 + \boldsymbol{h}_3 = \boldsymbol{h}_{13} + \boldsymbol{h}_\varnothing & \boldsymbol{h}_{12} + \boldsymbol{h}_{23} = \boldsymbol{h}_{123} + \boldsymbol{h}_2 & \boldsymbol{h}_2 + \boldsymbol{h}_3 \geq \boldsymbol{h}_{23} + \boldsymbol{h}_\varnothing \\
\boldsymbol{h}_2 + \boldsymbol{h}_4 = \boldsymbol{h}_{24} + \boldsymbol{h}_\varnothing & \boldsymbol{h}_{23} + \boldsymbol{h}_{34} = \boldsymbol{h}_{234} + \boldsymbol{h}_3 & \boldsymbol{h}_3 + \boldsymbol{h}_4 \geq \boldsymbol{h}_{34} + \boldsymbol{h}_\varnothing \\
\boldsymbol{h}_{123} + \boldsymbol{h}_{134} = \boldsymbol{h}_{1234} + \boldsymbol{h}_{13} & \boldsymbol{h}_{14} + \boldsymbol{h}_{34} = \boldsymbol{h}_{134} + \boldsymbol{h}_4 & \boldsymbol{h}_1 + \boldsymbol{h}_4 \geq \boldsymbol{h}_{14} + \boldsymbol{h}_\varnothing .
\end{array}$$

After quotienting the lineality and intersecting with an affine hyperplane, we get the 3-simplex (*i.e.* tetrahedron) illustrated in Figure 13.

2.2.4 Simplicial graphical deformation cones

As an immediate corollary, we obtain a characterization of those graphical zonotopes whose deformation cone is simplicial.

Corollary 2.16. *The deformation cone $\mathbb{DC}(\mathsf{Z}_G)$ is simplicial (modulo its lineality) if and only if G is triangle-free.*

Proof. If G is triangle-free, the deformation cone $\mathbb{DC}(\mathsf{Z}_G)$ has dimension $|V| + |E|$, lineality space of dimension $|V|$, and $|E|$ facets, and hence it is simplicial. If G is not triangle-free, then we claim that the number of induced cliques K of G with $|K| \geq 2$ is strictly less than the number

of triples (u, v, S) with $\{u, v\} \in E$ and $S \subseteq N(u) \cap N(v)$. Indeed, each induced clique K of G with $|K| \geq 2$ already produces $\binom{|K|}{2}$ triples of the form $(u, v, K \smallsetminus \{u, v\})$ which satisfy $\{u, v\} \in E$ and $K \smallsetminus \{u, v\} \subseteq N(u) \cap N(v)$ and are all distinct. Since $\binom{|K|}{2} > |K|$ as soon as $|K| \geq 3$, by Corollary 2.13, this shows that the deformation cone $\mathbb{DC}(\mathsf{Z}_G)$ is not simplicial. □

Corollary 2.17. *If G is triangle-free, then every deformation of Z_G is a zonotope, which is the graphical zonotope of a subgraph of G up to rescaling of the generators.*

Proof. For any induced clique K of G of size at least 2, Δ_K is a Minkowski indecomposable $(|K| - 1)$-dimensional polytope in the deformation cone $\mathbb{DC}(\mathsf{Z}_G)$ (see for example [Grü03, 15.1.3] for a certificate of indecomposability). It spans therefore a ray of $\mathbb{DC}(\mathsf{Z}_G)$. When G is triangle-free, the deformation cone modulo its lineality is of dimension $|E|$, and the polytopes Δ_e for $e \in E$ account for the $|E|$ rays of the simplicial deformation cone $\mathbb{DC}(\mathsf{Z}_G)$.

Therefore, each polytope $P \in \mathbb{DC}(\mathsf{Z}_G)$ can be uniquely[7] expressed as a Minkowski sum

$$P = \sum_{e \in E} \lambda_e \Delta_e$$

with non-negative coefficients λ_e. Since each Δ_e is a segment, P is a zonotope, normally equivalent to the graphical zonotope of the subgraph $G' = (V, E')$ with $E' = \{e \in E \ ; \ \lambda_e \neq 0\}$. □

Remark 2.18. Note that if G is not triangle-free, its deforamation cone is not simplicial and hence has a ray that do not correspond to a face of the standard simplex, *i.e.* not all the deformations of Z_G are graphical zonotopes.

2.2.5 Perspectives and open questions

Computational remarks The computation of deformation cones of graphical zonotopes has been implemented with Sage, allowing us to conjecture Corollary 2.13 before proving it. Thanks to this code, one can input a graph G and compute the deformation cone of its graphical zonotope as the cone of heights in $\mathbb{R}^{2^n}$, illustrating Theorem 2.12. Although very symmetric and well suited for mathematical purposes, this first implementation has the inconvenient to live in a highly dimensional space. For this reason, I have also implemented a second version that computes the deformation cone in $\mathbb{R}^{BS(G)}$ where $BS(G)$ is the collection of biconnected subsets of G (which are in bijection with the rays of $\mathcal{F}(G)$). Some technical choices have to be made to speed up this computation, in particular by efficiently using the dual graph of $\mathcal{F}(G)$ in order to get rid of some redundant equalities.

Assets and limits of the current approach, open questions The question of the dimension space of the deformation is of prime importance for a larger subject. In [McM93, McM96], McMullen constructed several algebras associated to a polytope P: in particular, its polytope algebra and its weight algebra. This construction was used to provide an alternative proof of the famous g-theorem of Billera–Lee and Stanley [Sta80]. Both algebras are graded. When P is simple, these two algebras are isomorphic, but in general there is only an embedding of the polytope algebra in the weight algebra. For example, the permutahedron Π_n is simple and the dimension of the k-th graded piece of its polytope algebra is the Eulerian number $A(n, k)$, see [Ham17].

The first graded piece of the polytope algebra of P is the linear span of $\mathbb{DC}(\mathsf{P})$ (*i.e.* the space of virtual deformations discussed above Theorem 2.11). This means that in the present section, we have computed the dimension of the first graded piece of the polytope algebra of graphical zonotopes (and of nestohedra in the next section). On top of that, our result gives a basis of this first graded piece, and the polytope algebra is generated in degree 1.

With Arnau Padrol, we considered the second graded piece of the polytope algebra of graphical zonotopes and managed to find an explicit basis of it. We are currently attempting to extend these results to higher graded pieces. Furthermore, graphical zonotopes are (in general) non-simple polytopes: therefore, we hope to describe the gap between both algebras for graphical zonotopes.

[7] Uniqueness comes from the simpliciality of $\mathbb{DC}(\mathsf{Z}_G)$.

2.3 Deformation cones of nestohedra

This section is a joint work with Arnau Padrol and Vincent Pilaud. It comes from the article [PPP23] (where the majority of the figures come from), enriched with some additional details and figures.

This section focuses on some specific deformed permutahedra generalizing the associahedra, namely the graph associahedra and nestohedra. Graph associahedra were defined by M. Carr and S. Devadoss [CD06] in connection to C. De Concini and C. Procesi's wonderful compactification [DCP95]. For a given graph G, the *G-associahedron* $\mathsf{Asso}(G)$ is a simple polytope whose combinatorial structure encodes the connected induced subgraphs of G and their nested structure. More precisely, the G-associahedron is a polytopal realization of the *nested complex* of G, defined as the simplicial complex of all collections of *tubes* (connected induced subgraphs) of G which are pairwise *compatible* (either nested, or disjoint and non-adjacent). As illustrated in Figure 14, the graph associahedra of certain special families of graphs coincide with well-known families of polytopes: complete graph associahedra are permutahedra, path associahedra are classical associahedra, cycle associahedra are cyclohedra, and star associahedra are stellohedra. Graph associahedra were extended to *nestohedra*, which are simple polytopes realizing the nested complex of arbitrary *building sets* [FS05, Pos09]. Graph associahedra and nestohedra have been constructed in different ways: by successive truncations of faces of the standard simplex [CD06], as Minkowski sums of faces of the standard simplex [FS05, Pos09], or from their normal fans by exhibiting explicit inequality descriptions [Zel06, Dev09]. For a given building set, the resulting polytopes all have the same normal fan, called *nested fan*, whose rays are given by the characteristic vectors of the building blocks, and whose cones are given by the nested sets. As all nested fans coarsen the braid fan, all graph associahedra and nestohedra are deformed permutahedra, and hence they can be obtained by gliding facets of the permutahedron. However, in contrast to the classical associahedron [SS93, Lod04, HL07], note that some graph associahedra and nestohedra cannot be obtained by deleting inequalities in the facet description of the permutahedron [Pil17].

In this section, we describe all realizations of the nested fans by studying the deformation cone of the G-associahedron for any graph G (Section 2.3.1) and of the $\mathcal{B}$-nestohedron of any building set $\mathcal{B}$ (Section 2.3.2). Our main contribution is an irredundant facet description of these deformation cones, characterizing which of the wall-crossing inequalities are irreplaceable (Theorems 2.28 and 2.62). Even though the graphical case is a specialization of the general case, we present it first separately, since it admits a much simpler description that serves as an introduction for the general case. This simplification relies on two pleasant properties (Proposition 2.23): first, the classical simple characterization of the pairs of exchangeable tubes, and second, the fact that the wall-crossing inequalities only depend on their exchanged tubes.

The non-graphical case is much more involved. First, we need a characterization of the pairs of exchangeable blocks (Proposition 2.49), which was surprisingly missing for arbitrary building sets (Remark 2.56). Second, the wall-crossing inequalities do not any more correspond to the pairs of exchangeable blocks. Namely, the wall-crossing inequalities do not only depend on the exchanged blocks, but also on an additional structure that we call the *frame* of the exchange. Moreover, some distinct exchange frames actually yield the same wall-crossing inequalities.

These irredundant inequality descriptions enable us to count the facets of these deformation cones and thus to determine when these deformation cones are simplicial. It turns out that the deformation cone of the G-associahedron is simplicial if and only if G is a disjoint union of paths (*i.e.* the G-associahedron is a Cartesian product of classical associahedra). In contrast, there is much more freedom for nestohedra of arbitrary building sets, and we show that the deformation cone of the nestohedron is always simplicial for an *interval building set*, that is a building set whose blocks are some intervals of $[n]$ (Proposition 2.69). As advocated in [PPPP19], the simpliciality of the deformation cone leads to an elegant description of all deformations of the polytope in the so-called kinematic space [AHBHY18]. Generalizing the kinematic associahedra of [AHBHY18], we thus define the *kinematic nestohedra* of arbitrary interval building sets (Proposition 2.73).

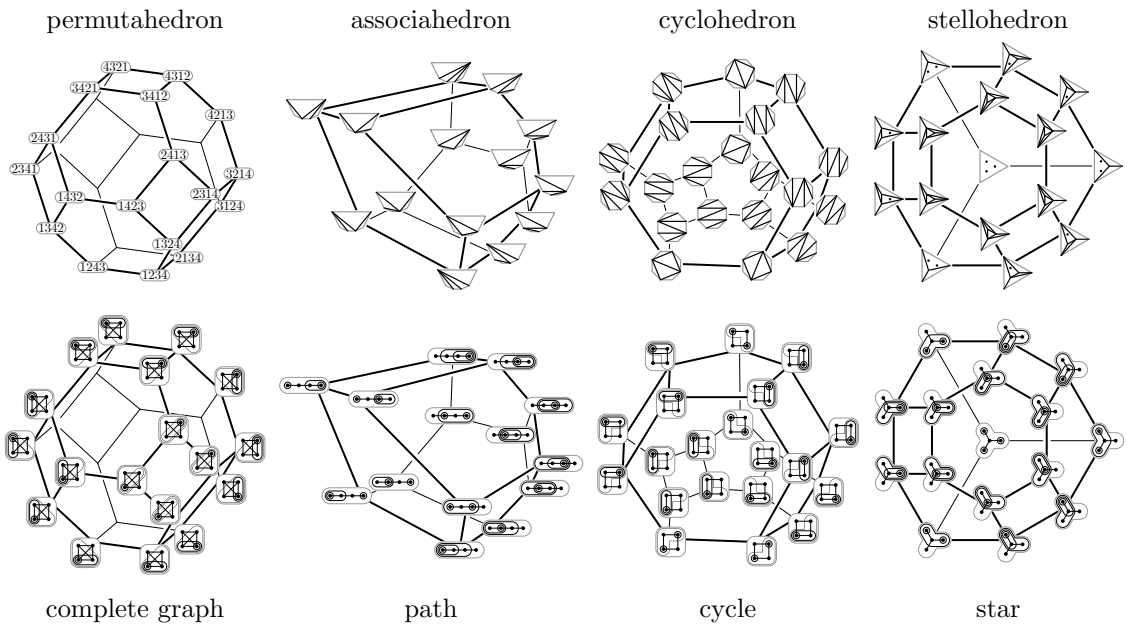

Figure 14: Some classical families of polytopes as graph associahedra. Illustration from [MP17].

2.3.1 Deformation cones of graphical nested fans

In this section, we study graphical nested fans, postponing the study of arbitrary nested fans to Section 2.3.2. While the graphical case is significantly simpler than the general case, some proof ideas presented here will be transported to Section 2.3.2. This section is thus useful both to the readers only interested in the graphical case and as a prototype for the general case.

Graphical nested complex, graphical nested fan, and graph associahedron We start with the definitions and properties of the nested complex of a graph, using material from [FS05, CD06, Zel06, Pos09, MP17].

Graphical nested complex Let G be a graph with vertex set V. A *tube* of G is a non-empty subset of vertices of G whose induced subgraph is connected. The set of tubes of G is denoted by $\mathcal{B}G$. The (inclusion) maximal tubes of G are its *connected components* $\kappa(G)$. Two tubes t, t' of G are *compatible* if they are either nested (*i.e.* $\mathsf{t} \subseteq \mathsf{t}'$ or $\mathsf{t}' \subseteq \mathsf{t}$), or disjoint and non-adjacent (*i.e.* $\mathsf{t} \cup \mathsf{t}' \notin \mathcal{B}G$). Note that any connected component of G is compatible with any other tube of G. A *tubing* on G is a set T of pairwise compatible tubes of G containing all connected components $\kappa(G)$. Examples are illustrated in Figure 15. The *nested complex* of G is the simplicial complex $\mathcal{N}(G)$ whose faces are $\mathsf{T} \setminus \kappa(G)$ for all tubings T on G. If $\mathsf{T} \setminus \{\mathsf{t}\} = \mathsf{T}' \setminus \{\mathsf{t}'\}$ for two maximal tubings T and T' and two tubes t and t', we say that T and T' are *adjacent* and that t and t' are *exchangeable*.

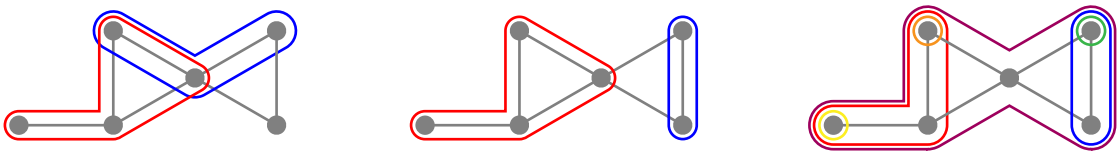

Figure 15: Some incompatible tubes (Left and Middle), and a maximal tubing (Right).

Graphical nested fan Let $(\boldsymbol{e}_v)_{v\in V}$ be the canonical basis of $\mathbb{R}^V$. We consider the subspace $\mathbb{H} := \{\boldsymbol{x} \in \mathbb{R}^V \ ; \ \sum_{v\in K} x_v = 0 \text{ for all } K \in \kappa(G)\}$ and let $\pi : \mathbb{R}^V \to \mathbb{H}$ denote the orthogonal projection onto $\mathbb{H}$. The *$\boldsymbol{g}$-vector* of a tube t of G is the projection $\boldsymbol{g}(\mathsf{t}) := \pi\big(\sum_{v\in\mathsf{t}} \boldsymbol{e}_v\big)$ of the characteristic vector of t. We set $\boldsymbol{g}(\mathsf{T}) := \{\boldsymbol{g}(\mathsf{t}) \ ; \ \mathsf{t} \in \mathsf{T}\}$ for a tubing T on G. Note that by definition, $\boldsymbol{g}(\varnothing) = \mathbf{0}$ and $\boldsymbol{g}(K) = \mathbf{0}$ for all connected components $K \in \kappa(G)$. The vectors $\boldsymbol{g}(\mathsf{t})$ with $\mathsf{t} \in \mathcal{B}G$ support a complete simplicial fan realization of the nested complex, see Figure 16.

Theorem 2.19 ([FS05, CD06, Zel06, Pos09]). *For any graph G, the set of cones*

$$\mathcal{F}(G) := \{\mathbb{R}_{\geq 0}\, \boldsymbol{g}(\mathsf{T}) \ ; \ \mathsf{T} \text{ tubing on } G\}$$

is a complete simplicial fan of $\mathbb{H}$, called the nested fan of G, realizing the nested complex $\mathcal{N}(G)$.

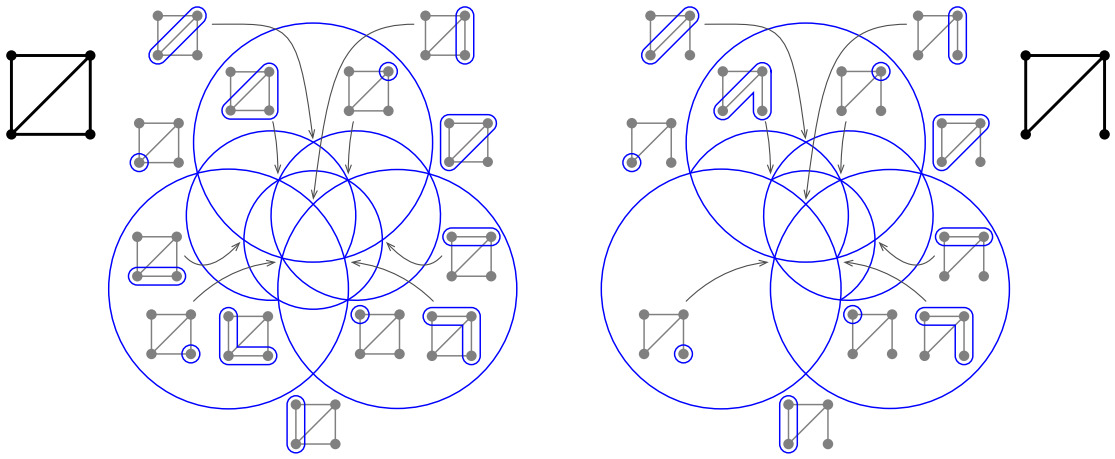

Figure 16: Two graphical nested fans. The rays are labeled by the corresponding tubes. As the fans are 3-dimensional, we intersect them with the sphere and stereographically project them from the direction $(-1,-1,-1)$.

Graph associahedron The following statement is proved in [FS05, Zel06, CD06, Dev09, Pos09]. As before, for a subset $U \subseteq V$, denote by $\Delta_U := \operatorname{conv}\{\boldsymbol{e}_u \ ; \ u \in U\}$ the face of the standard simplex Δ_V corresponding to U.

Theorem 2.20 ([FS05, Zel06, CD06, Dev09, Pos09]). *For any graph G, the nested fan $\mathcal{F}(G)$ is the normal fan of a polytope. For instance, $\mathcal{F}(G)$ is the normal fan of*

(i) the intersection of $\mathbb{H}$ with the half-spaces $\langle \boldsymbol{g}(\mathsf{t}),\ \boldsymbol{x}\rangle \leq -3^{|\mathsf{t}|}$ for all tubes $\mathsf{t} \in \mathcal{B}G$ [Dev09]

(ii) the Minkowski sum $\sum_{\mathsf{t}\in\mathcal{B}G} \Delta_{\mathsf{t}}$ of the faces of the standard simplex given by all $\mathsf{t} \in \mathcal{B}G$ [Pos09]

Definition 2.21. Any polytope whose normal fan is the nested fan $\mathcal{F}(G)$ is called *graph associahedron* and denoted by $\mathsf{Asso}(G)$.

For example, Figure 17 represents the graph associahedra realizing the graphical nested fans of Figure 16 and obtained using the construction (ii) of Theorem 2.20.

Example 2.22. For instance,

(i) for the complete graph K_n, the tubes are all non-empty subsets of $[n]$, the tubings correspond to ordered partitions of $[n]$, the maximal tubings correspond to permutations of $[n]$, the graphical nested fan $\mathcal{F}(K_n)$ is the intersection of the classical *braid fan* with $\mathbb{H} = \{\boldsymbol{x} \in \mathbb{R}^n \ ; \ \sum_i x_i = 0\}$, and the graph associahedron $\mathsf{Asso}(K_n)$ is the classical *permutahedron* embedded in $\mathbb{H}$ (see *e.g.* [Zie98, Hoh12] or Section 1.2.3), this gives a slightly different point of view on Example 2.14;

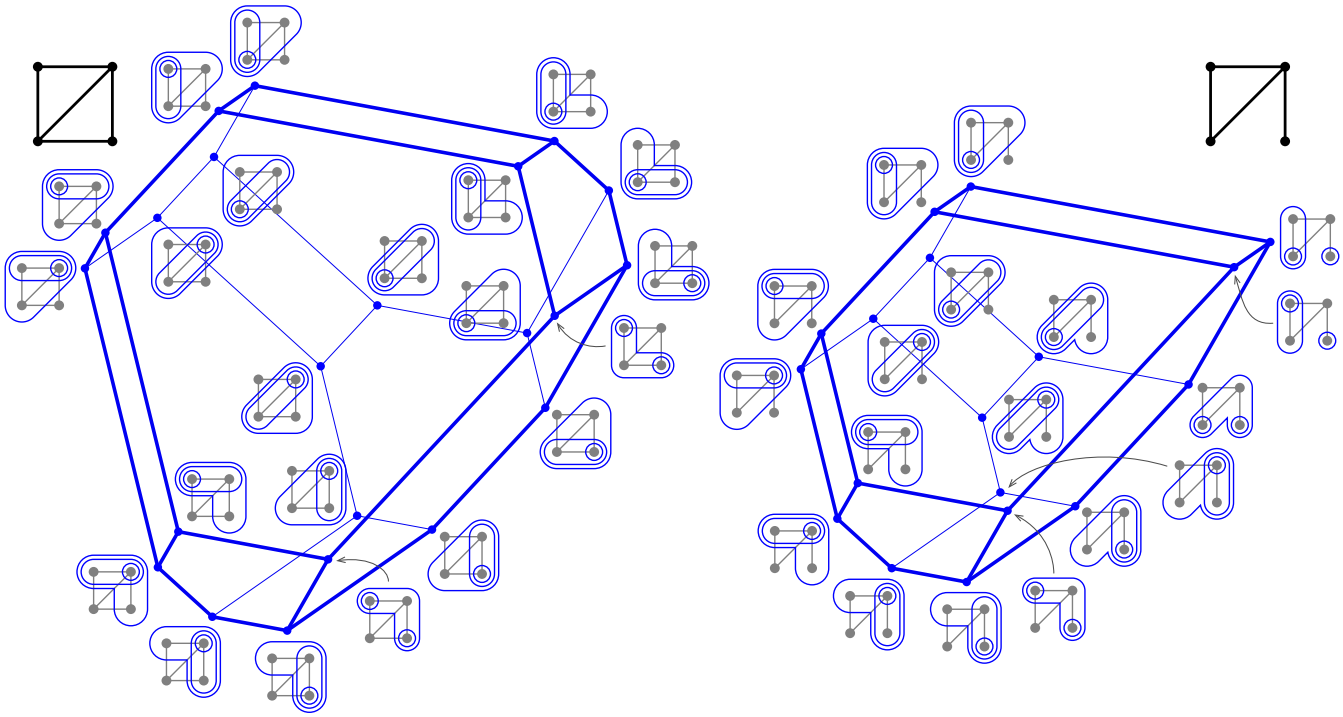

Figure 17: Two graph associahedra, realizing the graphical nested fans of Figure 16. The vertices are labeled by the corresponding maximal tubings.

(ii) for the path P_n, the tubes are all non-empty intervals of $[n]$, the tubings correspond to Schröder trees with $n+1$ leaves, the maximal tubings correspond to binary trees with $n+1$ leaves, the graphical nested fan $\mathcal{F}(P_n)$ is the classical *sylvester fan*, and the graph associahedron $\mathsf{Asso}(P_n)$ is the classical *associahedron* (see [SS93, Lod04, PSZ23] or Section 1.2.4).

Exchangeable tubes and g-vector dependencies The next statement follows from [Zel06, MP17].

Proposition 2.23. *Let t, t' be two tubes of G. Then*

(i) The tubes t and t' are exchangeable in $\mathcal{F}(G)$ if and only if t' has a unique neighbor v in $\mathsf{t} \smallsetminus \mathsf{t}'$ and t has a unique neighbor v' in $\mathsf{t}' \smallsetminus \mathsf{t}$.

(ii) For any adjacent maximal tubings T, T' on G with $\mathsf{T} \smallsetminus \{\mathsf{t}\} = \mathsf{T}' \smallsetminus \{\mathsf{t}'\}$, both T and T' contain the tube $\mathsf{t} \cup \mathsf{t}'$ and the connected components of $\mathsf{t} \cap \mathsf{t}'$.

(iii) The linear dependence between the $\boldsymbol{g}$-vectors of $\mathsf{T} \cup \mathsf{T}'$ is given by

$$\boldsymbol{g}(\mathsf{t}) + \boldsymbol{g}(\mathsf{t}') = \boldsymbol{g}(\mathsf{t} \cup \mathsf{t}') + \sum_{\mathsf{s} \in \kappa(\mathsf{t} \cap \mathsf{t}')} \boldsymbol{g}(\mathsf{s}).$$

In particular, it only depends on the exchanged tubes t and t', not on the tubings T and T'.

Proof. Points (i) and (ii) were proved in [MP17]. Point (iii) follows from the fact that

$$\sum_{v \in \mathsf{t}} \boldsymbol{e}_v + \sum_{v \in \mathsf{t}'} \boldsymbol{e}_v = \sum_{v \in \mathsf{t} \cup \mathsf{t}'} \boldsymbol{e}_v + \sum_{v \in \mathsf{t} \cap \mathsf{t}'} \boldsymbol{e}_v = \sum_{v \in \mathsf{t} \cup \mathsf{t}'} \boldsymbol{e}_v + \sum_{\mathsf{s} \in \kappa(\mathsf{t} \cap \mathsf{t}')} \sum_{v \in \mathsf{s}} \boldsymbol{e}_v. \qquad \square$$

For instance, the two tubes on the left of Figure 15 are exchangeable, while the two tubes in the middle of Figure 15 are not.

Deformation cones of graphical nested fans As a direct consequence of Proposition 2.2 and Proposition 2.23, we obtain the following (possibly redundant) description of the deformation cone of the graphical nested fan $\mathcal{F}(G)$. Note that as $\mathcal{F}(G)$ is simplicial, there are (almost) no equalities to deal with, contrarily to the case of graphical zonotopes of Section 2.2. This simplifies sorely the computation of the dimension of $\mathbb{DC}(\mathcal{F}(G))$.

Corollary 2.24. *For any graph G, the deformation cone of the nested fan $\mathcal{F}(G)$ is given by*

$$\mathbb{DC}(\mathcal{F}(G)) = \left\{ \boldsymbol{h} \in \mathbb{R}^{\mathcal{B}G} \;;\; \begin{array}{l} \boldsymbol{h}_K = 0 \text{ for any connected component } K \in \kappa(G) \text{ and} \\ \boldsymbol{h}_{\mathsf{t}} + \boldsymbol{h}_{\mathsf{t}'} \geq \boldsymbol{h}_{\mathsf{t}\cup\mathsf{t}'} + \sum_{\mathsf{s}\in\kappa(\mathsf{t}\cap\mathsf{t}')} \boldsymbol{h}_{\mathsf{s}} \text{ for any exchangeable tubes } \mathsf{t},\mathsf{t}' \end{array} \right\}.$$

We denote by $\boldsymbol{f}_{\mathsf{t}}$ for $\mathsf{t} \in \mathcal{B}G$ the canonical basis of $\mathbb{R}^{\mathcal{B}G}$ and by

$$\boldsymbol{n}(\mathsf{t},\mathsf{t}') := \boldsymbol{f}_{\mathsf{t}} + \boldsymbol{f}_{\mathsf{t}'} - \boldsymbol{f}_{\mathsf{t}\cup\mathsf{t}'} - \sum_{\mathsf{s}\in\kappa(\mathsf{t}\cap\mathsf{t}')} \boldsymbol{f}_{\mathsf{s}}$$

the inner normal vector of the inequality of the deformation cone $\mathbb{DC}(\mathcal{F}(G))$ corresponding to an exchangeable pair $\{\mathsf{t},\mathsf{t}'\}$ of tubes of G. Thus $\boldsymbol{h} \in \mathbb{DC}(\mathcal{F}(G))$ if and only if $\langle \boldsymbol{n}(\mathsf{t},\mathsf{t}'),\ \boldsymbol{h}\rangle \geq 0$ for all exchangeable tubes $\mathsf{t},\mathsf{t}' \in \mathcal{B}G$.

Remark 2.25. For instance,

(i) for the complete graph K_n, the deformation cone $\mathbb{DC}(\mathcal{F}(K_n))$ is formed by all submodular functions, *i.e.* functions $\boldsymbol{h} : 2^{[n]} \to \mathbb{R}$ such that $\boldsymbol{h}_\varnothing = 0 = \boldsymbol{h}_{[n]}$ and $\boldsymbol{h}_A + \boldsymbol{h}_B \geq \boldsymbol{h}_{A\cap B} + \boldsymbol{h}_{A\cup B}$ for any $A, B \subseteq [n]$. The inequalities $\boldsymbol{h}_{U\smallsetminus\{v\}} + \boldsymbol{h}_{U\smallsetminus\{v'\}} \geq \boldsymbol{h}_U + \boldsymbol{h}_{U\smallsetminus\{v,v'\}}$ for $v, v' \in V$ and $\{v, v'\} \subseteq U \subseteq V$ clearly imply all submodular inequalities. This was already studied with the framework of graphical zonotopes in Example 2.14 as well as in [Pos09].

(ii) for the path P_n, the deformation cone $\mathbb{DC}(\mathcal{F}(P_n))$ is formed by the functions $\boldsymbol{h} : \{[i,j]\ ;\ 1 \leq i \leq j \leq n\} \mapsto \mathbb{R}$ such that $\boldsymbol{h}_{[1,n]} = 0 = \boldsymbol{h}_{\{i\}}$ for all $i \in [n]$ and $\boldsymbol{h}_{[i,j]} + \boldsymbol{h}_{[k,\ell]} \geq \boldsymbol{h}_{[i,\ell]} + \boldsymbol{h}_{[k,j]}$ for all $1 \leq i \leq j \leq n$ and $1 \leq k \leq \ell \leq n$ such that $i < k$, $j < \ell$ and $k \leq j+1$ (where $\boldsymbol{h}_{[k,j]} = 0$ if $k = j+1$). This was already studied in the context of mathematical physics [AHBHY18] whose results bring back deformation cones to the fore.

Example 2.26. Consider the graphical nested fans illustrated in Figure 16. The deformation cone of the left fan lives in $\mathbb{R}^{13}$, has a lineality space of dimension 3 and 19 facet-defining inequalities (given below). In particular, it is not simplicial. Note that, as in Figure 16, we express the $\boldsymbol{g}$-vectors in the basis given by the maximal tubing containing the first three tubes below.

tubes	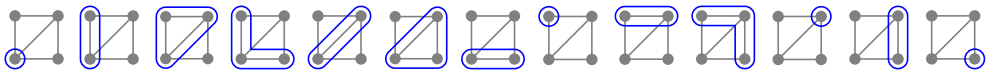												
$\boldsymbol{g}$-vectors	$\begin{bmatrix}1\\0\\0\end{bmatrix}$	$\begin{bmatrix}0\\1\\0\end{bmatrix}$	$\begin{bmatrix}0\\0\\1\end{bmatrix}$	$\begin{bmatrix}0\\1\\-1\end{bmatrix}$	$\begin{bmatrix}1\\-1\\1\end{bmatrix}$	$\begin{bmatrix}1\\-1\\0\end{bmatrix}$	$\begin{bmatrix}1\\0\\-1\end{bmatrix}$	$\begin{bmatrix}-1\\1\\0\end{bmatrix}$	$\begin{bmatrix}-1\\0\\1\end{bmatrix}$	$\begin{bmatrix}-1\\0\\0\end{bmatrix}$	$\begin{bmatrix}0\\-1\\1\end{bmatrix}$	$\begin{bmatrix}0\\-1\\0\end{bmatrix}$	$\begin{bmatrix}0\\0\\-1\end{bmatrix}$
facet	0	0	0	0	0	0	0	0	0	0	1	−1	1
defining	0	0	0	0	0	1	0	0	0	1	0	−1	0
inequalities	−1	1	0	−1	0	0	1	0	0	0	0	0	0
	0	0	0	0	0	0	0	0	1	−1	−1	1	0
	0	0	0	0	0	−1	1	0	0	0	0	1	−1
	−1	1	−1	0	1	0	0	0	0	0	0	0	0
	−1	0	0	0	1	−1	1	0	0	0	0	0	0
	0	1	−1	0	0	0	0	−1	1	0	0	0	0
	0	0	−1	0	1	0	0	0	1	0	−1	0	0
	0	0	0	0	1	−1	0	0	0	0	−1	1	0
	0	0	1	0	0	0	0	0	−1	1	0	0	0
	0	0	1	0	−1	1	0	0	0	0	0	0	0
	0	0	0	0	0	0	0	1	−1	0	1	0	0
	1	0	0	0	0	0	−1	0	0	0	0	0	1
	1	0	0	0	−1	0	0	0	0	0	1	0	0
	1	−1	0	0	0	0	0	1	0	0	0	0	0
	0	0	0	1	0	0	0	−1	0	1	0	0	−1
	0	0	0	1	0	1	−1	0	0	0	0	0	0
	0	−1	1	1	0	0	0	0	0	0	0	0	0

The deformation cone of the right fan lives in $\mathbb{R}^{11}$, has a lineality space of dimension 3 and 12 facet-defining inequalities (given below). In particular, it is not simplicial. Note that, as in Figure 16, we express the $\boldsymbol{g}$-vectors in the basis given by the maximal tubing containing the first three tubes below.

tubes	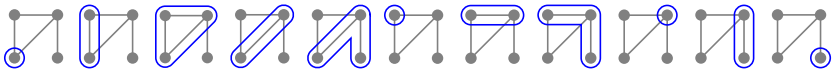										
$\boldsymbol{g}$-vectors	$\begin{bmatrix}1\\0\\0\end{bmatrix}$	$\begin{bmatrix}0\\1\\0\end{bmatrix}$	$\begin{bmatrix}0\\0\\1\end{bmatrix}$	$\begin{bmatrix}1\\-1\\1\end{bmatrix}$	$\begin{bmatrix}1\\-1\\0\end{bmatrix}$	$\begin{bmatrix}-1\\1\\0\end{bmatrix}$	$\begin{bmatrix}-1\\0\\1\end{bmatrix}$	$\begin{bmatrix}-1\\0\\0\end{bmatrix}$	$\begin{bmatrix}0\\-1\\1\end{bmatrix}$	$\begin{bmatrix}0\\-1\\0\end{bmatrix}$	$\begin{bmatrix}0\\0\\-1\end{bmatrix}$
facet	−1	1	−1	1	0	0	0	0	0	0	0
defining	1	−1	0	0	0	1	0	0	0	0	0
inequalities	0	1	−1	0	0	−1	1	0	0	0	0
	1	0	0	−1	0	0	0	0	1	0	0
	0	0	−1	1	0	0	1	0	−1	0	0
	0	0	0	1	−1	0	0	0	−1	1	0
	0	0	0	0	0	1	−1	0	1	0	0
	0	0	0	0	0	0	1	−1	−1	1	0
	0	0	0	0	0	0	0	0	1	−1	1
	0	0	0	0	1	0	0	1	0	−1	0
	0	0	1	0	0	0	−1	1	0	0	0
	0	0	1	−1	1	0	0	0	0	0	0

Example 2.27. We can exploit Corollary 2.24 to show that certain height functions belong to (the interior of) the deformation cone of $\mathcal{F}(G)$ and recover some classical constructions of the graph associahedron.

(i) Consider the height function $\boldsymbol{h} \in \mathbb{R}^{\mathcal{B}G}$ given by $\boldsymbol{h}_{\mathsf{t}} := -3^{|\mathsf{t}|}$. Then for any exchangeable tubes t and t', we have

$$\langle \boldsymbol{n}(\mathsf{t},\mathsf{t}'),\ \boldsymbol{h}\rangle = -3^{|\mathsf{t}|} - 3^{|\mathsf{t}'|} + 3^{|\mathsf{t}\cup\mathsf{t}'|} + \sum_{\mathsf{s}\in\kappa(\mathsf{t}\cap\mathsf{t}')} 3^{|\mathsf{s}|} \geq -2\cdot 3^{|\mathsf{t}\cup\mathsf{t}'|-1} + 3^{|\mathsf{t}\cup\mathsf{t}'|} > 0.$$

Therefore, the height function $\boldsymbol{h}$ belongs to the interior of the deformation cone $\mathbb{DC}(\mathcal{F}(G))$. The corresponding polytope $P_{\boldsymbol{h}} := \big\{\boldsymbol{x} \in \mathbb{R}^V \ ;\ \langle \boldsymbol{g}(\mathsf{t}),\ \boldsymbol{x}\rangle \leq \boldsymbol{h}_{\mathsf{t}} \text{ for } \mathsf{t} \in \mathcal{B}G\big\}$ is the graph associahedron constructed by S. Devadoss's in [Dev09].

(ii) Consider the height function $\boldsymbol{h} \in \mathbb{R}^{\mathcal{B}G}$ given by $\boldsymbol{h}_{\mathsf{t}} := -\big|\big\{\mathsf{s} \in \mathcal{B}G \ ;\ \mathsf{s} \subseteq \mathsf{t}\big\}\big|$. Then for any exchangeable tubes t and t', we have

$$\langle \boldsymbol{n}(\mathsf{t},\mathsf{t}'),\ \boldsymbol{h}\rangle = \big|\big\{\mathsf{s} \in \mathcal{B}G \ ;\ \mathsf{s} \not\subseteq \mathsf{t} \text{ and } \mathsf{s} \not\subseteq \mathsf{t}' \text{ but } \mathsf{s} \subseteq \mathsf{t}\cup\mathsf{t}'\big\}\big| > 0$$

since $\mathsf{t}\cup\mathsf{t}'$ fulfills the conditions on s. Thus, the height function $\boldsymbol{h}$ belongs to the interior of the deformation cone $\mathbb{DC}(\mathcal{F}(G))$. The polytope $P_{\boldsymbol{h}} := \big\{\boldsymbol{x} \in \mathbb{R}^V \ ;\ \langle \boldsymbol{g}(\mathsf{t}),\ \boldsymbol{x}\rangle \leq \boldsymbol{h}_{\mathsf{t}} \text{ for } \mathsf{t} \in \mathcal{B}G\big\}$ is the graph associahedron constructed by A. Postnikov's in [Pos09].

Note that many inequalities of Corollary 2.24 are redundant. In the remaining of this section, we describe the facet-defining inequalities of the deformation cone of the graphical nested fans. We say that an exchangeable pair $\{\mathsf{t},\mathsf{t}'\}$ of tubes of G is

- *extremal* if its corresponding inequality in Corollary 2.24 defines a facet of $\mathbb{DC}(\mathcal{F}(G))$,
- *maximal* if $\mathsf{t} \smallsetminus \{v\} = \mathsf{t}' \smallsetminus \{v'\}$ for some neighbor v of t' and some neighbor v' of t.

We can now state our main result on graphical nested complexes.

Theorem 2.28. *An exchangeable pair is extremal if and only if it is maximal.*

Proof. We treat separately the two implications:

Extremal ⇒ maximal. Consider an exchangeable pair $\{\mathsf{t},\mathsf{t}'\}$ of tubes of G. By Proposition 2.23, t' has a unique neighbor v in $\mathsf{t} \smallsetminus \mathsf{t}'$ and t has a unique neighbor v' in $\mathsf{t}' \smallsetminus \mathsf{t}$. Therefore, $\mathsf{t} \smallsetminus \mathsf{t}'$ and $\mathsf{t}' \smallsetminus \mathsf{t}$ are both connected. Assume that $\{\mathsf{t},\mathsf{t}'\}$ is not maximal, for instance that $\mathsf{t} \smallsetminus \mathsf{t}' \neq \{v\}$, and let $w \neq v$ be a non-disconnecting node of $\mathsf{t} \smallsetminus \mathsf{t}'$. By Proposition 2.23, $\tilde{\mathsf{t}} := \mathsf{t} \smallsetminus \{w\}$ and t' are exchangeable, and $\tilde{\mathsf{t}}' := (\mathsf{t}\cup\mathsf{t}') \smallsetminus \{w\}$ and t are exchangeable as well. Moreover, we have

$$\begin{aligned}\boldsymbol{n}(\tilde{\mathsf{t}},\mathsf{t}') + \boldsymbol{n}(\mathsf{t},\tilde{\mathsf{t}}') &= \Big(\boldsymbol{f}_{\tilde{\mathsf{t}}} + \boldsymbol{f}_{\mathsf{t}'} - \boldsymbol{f}_{\tilde{\mathsf{t}}\cup\mathsf{t}'} - \sum_{\mathsf{s}\in\kappa(\tilde{\mathsf{t}}\cap\mathsf{t}')} \boldsymbol{f}_{\mathsf{s}}\Big) + \Big(\boldsymbol{f}_{\mathsf{t}} + \boldsymbol{f}_{\tilde{\mathsf{t}}'} - \boldsymbol{f}_{\mathsf{t}\cup\tilde{\mathsf{t}}'} - \sum_{\mathsf{s}\in\kappa(\mathsf{t}\cap\tilde{\mathsf{t}}')} \boldsymbol{f}_{\mathsf{s}}\Big)\\ &= \boldsymbol{f}_{\mathsf{t}} + \boldsymbol{f}_{\mathsf{t}'} - \boldsymbol{f}_{\mathsf{t}\cup\mathsf{t}'} - \sum_{\mathsf{s}\in\kappa(\mathsf{t}\cap\mathsf{t}')} \boldsymbol{f}_{\mathsf{s}} = \boldsymbol{n}(\mathsf{t},\mathsf{t}'),\end{aligned}$$

as $\tilde{\mathsf{t}}\cup\mathsf{t}' = \tilde{\mathsf{t}}'$, $\tilde{\mathsf{t}}\cap\mathsf{t}' = \mathsf{t}\cap\mathsf{t}'$, $\mathsf{t}\cup\tilde{\mathsf{t}}' = \mathsf{t}\cup\mathsf{t}'$ and $\kappa(\mathsf{t}\cap\tilde{\mathsf{t}}') = \kappa(\tilde{\mathsf{t}}) = \tilde{\mathsf{t}}$. Therefore $\boldsymbol{n}(\mathsf{t},\mathsf{t}')$ defines a redundant inequality and $\{\mathsf{t},\mathsf{t}'\}$ is not an extremal exchangeable pair. The proof is symmetric if $\mathsf{t}' \smallsetminus \mathsf{t} \neq \{v'\}$.

Maximal ⇒ extremal. Let $\{\mathsf{t},\mathsf{t}'\}$ be a maximal exchangeable pair. To prove that $\{\mathsf{t},\mathsf{t}'\}$ is extremal, we will construct a vector $\boldsymbol{w} \in \mathbb{R}^{\mathcal{B}G}$ such that $\langle \boldsymbol{n}(\mathsf{t},\mathsf{t}'),\ \boldsymbol{w}\rangle < 0$, but $\langle \boldsymbol{n}(\tilde{\mathsf{t}},\tilde{\mathsf{t}}'),\ \boldsymbol{w}\rangle > 0$ for any other maximal exchangeable pair $\{\tilde{\mathsf{t}},\tilde{\mathsf{t}}'\}$. This will show that the inequality induced by $\{\mathsf{t},\mathsf{t}'\}$ is not redundant.

Define $\alpha(\mathsf{t},\mathsf{t}') := \{\mathsf{s} \in \mathcal{B}G \ ; \ \mathsf{s} \not\subseteq \mathsf{t} \text{ and } \mathsf{s} \not\subseteq \mathsf{t}' \text{ but } \mathsf{s} \subseteq \mathsf{t} \cup \mathsf{t}'\}$. Note that $\alpha(\mathsf{t},\mathsf{t}')$ is non-empty since it contains $\mathsf{t} \cup \mathsf{t}'$. Define three vectors $\boldsymbol{x}, \boldsymbol{y}, \boldsymbol{z} \in \mathbb{R}^{\mathcal{B}G}$ by, for each tube $\mathsf{s} \in \mathcal{B}G$:

$$\begin{aligned}
\boldsymbol{x}_\mathsf{s} &:= -|\{\mathsf{r} \in \mathcal{B}G \smallsetminus \alpha(\mathsf{t},\mathsf{t}') \ ; \ \mathsf{r} \subseteq \mathsf{s}\}|,\\
\boldsymbol{y}_\mathsf{s} &:= -|\{\mathsf{r} \in \alpha(\mathsf{t},\mathsf{t}') \ ; \ \mathsf{r} \subseteq \mathsf{s}\}|,\\
\boldsymbol{z}_\mathsf{s} &:= \begin{cases} -1 & \text{if } \mathsf{t} \subseteq \mathsf{s} \text{ or } \mathsf{t}' \subseteq \mathsf{s},\\ 0 & \text{otherwise,}\end{cases}
\end{aligned}$$

We will prove below that their scalar products with $\boldsymbol{n}(\tilde{\mathsf{t}},\tilde{\mathsf{t}}')$ for any maximal exchangeable pair $\{\tilde{\mathsf{t}},\tilde{\mathsf{t}}'\}$ satisfy the following inequalities

	$\langle \boldsymbol{n}(\tilde{\mathsf{t}},\tilde{\mathsf{t}}'),\ \boldsymbol{x}\rangle$	$\langle \boldsymbol{n}(\tilde{\mathsf{t}},\tilde{\mathsf{t}}'),\ \boldsymbol{y}\rangle$	$\langle \boldsymbol{n}(\tilde{\mathsf{t}},\tilde{\mathsf{t}}'),\ \boldsymbol{z}\rangle$
if $\{\mathsf{t},\mathsf{t}'\} = \{\tilde{\mathsf{t}},\tilde{\mathsf{t}}'\}$	$= 0$	$= \lvert\alpha(\mathsf{t},\mathsf{t}')\rvert$	$= -1$
if $\alpha(\tilde{\mathsf{t}},\tilde{\mathsf{t}}') \not\subseteq \alpha(\mathsf{t},\mathsf{t}')$	≥ 1	≥ 0	≥ -1
otherwise	$= 0$	≥ 1	≥ 0

It immediately follows from this table that the vector $\boldsymbol{w} := \boldsymbol{x} + \delta\boldsymbol{y} + \varepsilon\boldsymbol{z}$ fulfills the desired properties for any δ, ε such that $0 < \delta \cdot |\alpha(\mathsf{t},\mathsf{t}')| < \varepsilon < 1$.

To prove the inequalities of the table, observe that for any maximal exchangeable pair $\{\tilde{\mathsf{t}},\tilde{\mathsf{t}}'\}$,

- $\langle \boldsymbol{n}(\tilde{\mathsf{t}},\tilde{\mathsf{t}}'),\ \boldsymbol{x}\rangle = |\alpha(\tilde{\mathsf{t}},\tilde{\mathsf{t}}') \smallsetminus \alpha(\mathsf{t},\mathsf{t}')|$,
- $\langle \boldsymbol{n}(\tilde{\mathsf{t}},\tilde{\mathsf{t}}'),\ \boldsymbol{y}\rangle = |\alpha(\tilde{\mathsf{t}},\tilde{\mathsf{t}}') \cap \alpha(\mathsf{t},\mathsf{t}')|$,
- $\langle \boldsymbol{n}(\tilde{\mathsf{t}},\tilde{\mathsf{t}}'),\ \boldsymbol{z}\rangle \geq -1$ since $\boldsymbol{z}_{\tilde{\mathsf{t}}} = -1$ or $\boldsymbol{z}_{\tilde{\mathsf{t}}'} = -1$ implies $\boldsymbol{z}_{\tilde{\mathsf{t}}\cup\tilde{\mathsf{t}}'} = -1$,
- $\langle \boldsymbol{n}(\tilde{\mathsf{t}},\tilde{\mathsf{t}}'),\ \boldsymbol{z}\rangle \geq 0$ when $\{\mathsf{t},\mathsf{t}'\} \neq \{\tilde{\mathsf{t}},\tilde{\mathsf{t}}'\}$ but $\alpha(\tilde{\mathsf{t}},\tilde{\mathsf{t}}') \subseteq \alpha(\mathsf{t},\mathsf{t}')$. Indeed $\alpha(\tilde{\mathsf{t}},\tilde{\mathsf{t}}') \subseteq \alpha(\mathsf{t},\mathsf{t}')$ implies $\tilde{\mathsf{t}} \cup \tilde{\mathsf{t}}' \subseteq \mathsf{t} \cup \mathsf{t}'$. If $\mathsf{t} \subseteq \tilde{\mathsf{t}}$, then $\mathsf{t} \subseteq \tilde{\mathsf{t}} \subsetneq \tilde{\mathsf{t}} \cup \tilde{\mathsf{t}}' \subseteq \mathsf{t} \cup \mathsf{t}'$, which implies that $\mathsf{t} = \tilde{\mathsf{t}}$ by maximality of t in $\mathsf{t} \cup \mathsf{t}'$. Similarly, $\mathsf{t}' \subseteq \tilde{\mathsf{t}}$ implies $\mathsf{t}' = \tilde{\mathsf{t}}$. Hence, if $\boldsymbol{z}_{\tilde{\mathsf{t}}} = -1$, then by definition $\mathsf{t} \subseteq \tilde{\mathsf{t}}$ or $\mathsf{t}' \subseteq \tilde{\mathsf{t}}$, which implies that $\tilde{\mathsf{t}} \in \{\mathsf{t},\mathsf{t}'\}$. Similarly, $\boldsymbol{z}_{\tilde{\mathsf{t}}'} = -1$ implies $\tilde{\mathsf{t}}' \in \{\mathsf{t},\mathsf{t}'\}$. Hence, $\boldsymbol{z}_{\tilde{\mathsf{t}}} = -1 = \boldsymbol{z}_{\tilde{\mathsf{t}}'}$ implies $\tilde{\mathsf{t}} = \tilde{\mathsf{t}}'$ (impossible since $\tilde{\mathsf{t}}$ and $\tilde{\mathsf{t}}'$ are exchangeable) or $\{\mathsf{t},\mathsf{t}'\} = \{\tilde{\mathsf{t}},\tilde{\mathsf{t}}'\}$ (contradicting our assumption). Therefore, at most one of $\boldsymbol{z}_{\tilde{\mathsf{t}}}$ and $\boldsymbol{z}_{\tilde{\mathsf{t}}'}$ equals to -1, and if exactly one does, then $\boldsymbol{z}_{\tilde{\mathsf{t}}\cup\tilde{\mathsf{t}}'} = -1$. We conclude that $\langle \boldsymbol{n}(\tilde{\mathsf{t}},\tilde{\mathsf{t}}'),\ \boldsymbol{z}\rangle \geq 0$. □

The following statement reformulates Theorem 2.28.

Corollary 2.29. *The extremal exchangeable pairs for the nested fan of G are precisely the pairs of tubes $\mathsf{s} \smallsetminus \{v'\}$ and $\mathsf{s} \smallsetminus \{v\}$ for any tube $\mathsf{s} \in \mathcal{B}G$ and distinct non-disconnecting vertices v, v' of s.*

We derive from Theorem 2.28 and Corollary 2.29 the irredundant facet description of the deformation cone $\mathbb{DC}(\mathcal{F}(G))$.

Corollary 2.30. *For any graph G, the deformation cone of the nested fan $\mathcal{F}(G)$ is given by the following irredundant facet description*

$$\mathbb{DC}(\mathcal{F}(G)) = \left\{ \boldsymbol{h} \in \mathbb{R}^{\mathcal{B}G} \ ; \ \begin{array}{l} \boldsymbol{h}_K = 0 \text{ for any connected component } K \in \kappa(G), \text{ and} \\ \boldsymbol{h}_{\mathsf{s}\smallsetminus\{v'\}} + \boldsymbol{h}_{\mathsf{s}\smallsetminus\{v\}} \geq \boldsymbol{h}_\mathsf{s} + \boldsymbol{h}_{\mathsf{s}\smallsetminus\{v,v'\}} \text{ for any tube } \mathsf{s} \in \mathcal{B}G \\ \text{and distinct non-disconnecting vertices } v, v' \in \mathsf{s} \end{array} \right\}.$$

Remark 2.31. For instance,

(i) for the complete graph K_n, all the inequalities $\boldsymbol{h}_{U\smallsetminus\{v\}} + \boldsymbol{h}_{U\smallsetminus\{v'\}} \geq \boldsymbol{h}_U + \boldsymbol{h}_{U\smallsetminus\{v,v'\}}$ for $v, v' \in V$ and $\{v, v'\} \subseteq U \subseteq V$ are facet defining inequalities of $\mathbb{DC}(\mathcal{F}(K_n))$ (fortunately, this result is coherent with Example 2.14).

(ii) for the path P_n, only the inequalities $\boldsymbol{h}_{[i,j-1]} + \boldsymbol{h}_{[i+1,j]} \geq \boldsymbol{h}_{[i,j]} + \boldsymbol{h}_{[i+1,j-1]}$ for $1 \leq i < j \leq n$ are facet defining inequalities of $\mathbb{DC}(\mathcal{F}(P_n))$ (where $\boldsymbol{h}_\varnothing = 0$ by convention).

We derive from Corollary 2.29 the number of facets of the deformation cone $\mathbb{DC}(\mathcal{F}(G))$. For a tube t of G, we denote by $\mathrm{nd}(\mathsf{t})$ the number of non-disconnecting vertices of t. In other words, $\mathrm{nd}(\mathsf{t})$ is the number of tubes covered by t in the inclusion poset of all tubes of G.

Corollary 2.32. *The deformation cone $\mathbb{DC}(\mathcal{F}(G))$ has $\sum_{\mathsf{s}\in\mathcal{B}G} \binom{\mathrm{nd}(\mathsf{s})}{2}$ facets. This cone has dimension $|\mathcal{B}G| - |\kappa(G)|$ and lineality $|V| - |\kappa(G)|$.*

We call *proper dimension* of $\mathbb{DC}(\mathcal{F}(G))$ the value $|\mathcal{B}G| - |V|$ (*i.e.* the number of tubes that not singletons) which is its dimension as a cone once quotiented out its lineality. The formula of Corollary 2.32 can be made more explicit for specific families of graph associahedra discussed in the introduction and illustrated in Figure 14.

Proposition 2.33. *The number of facets of the deformation cone $\mathbb{DC}(\mathcal{F}(G))$ is:*

- $2^{n-2}\binom{n}{2}$ *for the permutahedron (complete graph associahedron) in proper dimension 2^n-n-1;*
- $\binom{n}{2}$ *for the associahedron (path associahedron) in proper dimension $\binom{n}{2}$;*
- $3\binom{n}{2} - n$ *for the cyclohedron (cycle associahedron) in proper dimension $(n-1)^2$;*
- $n - 1 + 2^{n-3}\binom{n-1}{2}$ *for the stellohedron (star associahedron)in proper dimension $2^{n-1} - 1$.*

Proof. As the proper dimension is straightforward, we detail the computation of the number of facets. For the permutahedron, choose any two vertices v, v', and complete them into a tube by selecting any subset of the $n-2$ remaining vertices. For the associahedron, choose any two vertices v, v', and complete them into a tube by taking the path between them. For the cyclohedron, choose the two vertices v, v', and complete them into a tube by taking either all the cycle, or one of the two paths between v and v' (this gives three options in general, but only two when v, v' are neighbors). For the stellohedron, choose either v as the center of the star and v' as one of the $n-1$ leaves, or v and v' as leaves of the star and complete them into a tube by taking the center and any subset of the $n-3$ remaining leaves. □

Example 2.34. We would like to draw a figure similar to Figures 12 and 13. The proper dimension of such example shall be at most 4, so that we can intersect $\mathbb{DC}(\mathcal{F}(G))$ with a hyperplane and embed it in 3 dimensions. Unfortunately, the path P_4 already contains 6 tubes that are not singletons, and the star on 4 vertices contains 7 (non-singleton) tubes, so all connected graphs G with 4 vertices or more yield a deformation cone with proper dimension at least 6 and can not be drawn.

There are two connected graphs on 3 vertices: the complete graph K_3 and the path P_3. The deformation cone $\mathbb{DC}(\mathcal{F}(K_3))$ is depicted in Figure 12, and the deformation cone $\mathbb{DC}(\mathcal{F}(P_3))$ is the above left 2-dimensional face of the latter, as the associahedron can be written $\mathsf{Asso}_3 = \Delta_{13} + \Delta_{23} + \Delta_{123}$ in the setting of graphical zonotopes.

Simplicial deformation cone To conclude on graphical nested fans, we characterize the graphs G whose nested fan $\mathcal{F}(G)$ has a simplicial deformation cone.

Proposition 2.35. *The deformation cone $\mathbb{DC}(\mathcal{F}(G))$ is simplicial if and only if G is a disjoint union of paths.*

Proof. Observe first that the graphical nested fan $\mathcal{F}(G)$ has $N = |\mathcal{B}G| - |\kappa(G)|$ rays and dimension $n = |V| - |\kappa(G)|$. Moreover, any tube t with $|\mathsf{t}| \geq 2$ has two non-disconnecting vertices when it is a path, and at least three non-disconnecting vertices otherwise (the leaves of an arbitrary spanning tree of t, or any vertex if it is a cycle). Therefore, each tube of $\mathcal{B}G$ which is not a singleton contributes to at least one extremal exchangeable pair. We conclude that the number of extremal exchangeable pairs is at least

$$|\mathcal{B}G| - |V| = (|\mathcal{B}G| - |\kappa(G)|) - (|V| - |\kappa(G)|) = N - n,$$

with equality if and only if all tubes of G are paths, *i.e.* if and only if G is a collection of paths. Hence, $\mathbb{DC}(\mathcal{F}(G))$ is simplicial if and only if G is a disjoint union of paths. □

The motivation to study the simpliciality of the deformation cone $\mathbb{DC}(\mathcal{F}(G))$ stems from the *kinematic associahedra* of [AHBHY18, Sect. 3.2]. These polytopes are alternative realizations of the associahedron obtained as sections of the kinematic space (the positive orthant in $\mathbb{R}^{\binom{n}{2}}$) by a well-chosen affine subspace parametrized by positive vectors. While these polytopes are just affinely equivalent to the realizations in $\mathbb{R}^V$, they have the advantage of being more natural from the scattering amplitudes' perspective [AHBHY18]. As observed in [PPPP19], such realizations can be directly obtained from the facet description of the deformation cone, when the latter is simplicial. Hence, combining Proposition 2.35 and Corollary 2.30 produces kinematic realizations of all graph associahedra of disjoint union of paths (*i.e.* all Cartesian products of associahedra). Our next statement only recalls the construction of the kinematic associahedron as it serves as a prototype for Proposition 2.73 that will describe new families of kinematic nestohedra.

Proposition 2.36. *For any $\boldsymbol{p} \in \mathbb{R}_{>0}^{\binom{[n]}{2}}$, the polytope $R_{\boldsymbol{p}}(n)$ defined as the intersection of the positive orthant $\left\{\boldsymbol{z} \in \mathbb{R}^{\{[i,j]\ ;\ 1\le i\le j\le n\}}\ ;\ \boldsymbol{z} \ge 0\right\}$ with the hyperplanes*

- $\boldsymbol{z}_{[1,n]} = 0$ *and* $\boldsymbol{z}_{[i,i]} = 0$ *for* $i \in [n]$,
- $\boldsymbol{z}_{[i,j-1]} + \boldsymbol{z}_{[i+1,j]} - \boldsymbol{z}_{[i,j]} + \boldsymbol{z}_{[i+1,j-1]} = \boldsymbol{p}_{[i,j]}$ *for all* $1 \le i < j \le n$,

is an associahedron whose normal fan is $\mathcal{F}(P_n)$. Moreover, the polytopes $R_{\boldsymbol{p}}(n)$ for $\boldsymbol{p} \in \mathbb{R}_{>0}^{\binom{[n]}{2}}$ describe all polytopal realizations of $\mathcal{F}(P_n)$ (up to translations).

2.3.2 Deformation cones of arbitrary nested fans

We now extend our results from graph associahedra to nestohedra. In the general situation, the set of tubes is replaced by a building set $\mathcal{B}$, and the tubings are replaced by $\mathcal{B}$-nested sets (this generalization can equivalently be interpreted as replacing the graph by an arbitrary hypergraph). As in the graphical case, the nested sets define a nested complex and a nested fan, which is the normal fan of the nestohedron. In this section, we describe the deformation cones of arbitrary nested fans. We follow the same scheme as in the previous Section 2.3.1, even if the general situation is significantly more intricate (Remarks 2.50 and 2.55 highlight some of the complications of the general case).

Nested complex, nested fan, and nestohedron We first recall the definitions of arbitrary building sets, nested complexes, nested fans and nestohedra, following [FS05, Zel06, Pos09, Pil17].

Building sets A *building set* $\mathcal{B}$ on a ground set V is a set of non-empty subsets of V such that

- if $B, B' \in \mathcal{B}$ and $B \cap B' \neq \varnothing$, then $B \cup B' \in \mathcal{B}$, and
- $\mathcal{B}$ contains all singletons $\{v\}$ for $v \in V$.

We denote by $\kappa(\mathcal{B})$ the set of *connected components* of $\mathcal{B}$, defined as the (inclusion) maximal elements of $\mathcal{B}$. We denote by $\varepsilon(\mathcal{B})$ the set of *elementary blocks* of $\mathcal{B}$, defined as the blocks $B \in \mathcal{B}$ such that $|B| > 1$, and $B = B' \cup B''$ implies $B' \cap B'' = \varnothing$ for any $B', B'' \in \mathcal{B} \smallsetminus \{B\}$. For instance, consider the building set $\mathcal{B}_\circ$ on [9] defined by

$$\mathcal{B}_\circ := \{1, 2, 3, 4, 5, 6, 7, 8, 9, 14, 25, 123, 456, 789, 1234, 1235, 1456, 2456, 12345, 12456, 123456\}$$

(since all labels have a single digit, we abuse notation and write 123 for $\{1, 2, 3\}$). Its connected components are $\kappa(\mathcal{B}_\circ) = \{123456, 789\}$, and its elementary blocks are $\varepsilon(\mathcal{B}_\circ) = \{14, 25, 123, 456, 789\}$, which are represented in Figure 18 (left).

Remark 2.37. If $B \in \mathcal{B}$ is elementary, then the maximal blocks of $\mathcal{B}$ strictly contained in B are disjoint. Conversely, if there exist two disjoint maximal blocks $M, N \in \mathcal{B}$ strictly contained in $B \in \mathcal{B}$, then B is elementary. Otherwise, there would be $B', B'' \in \mathcal{B} \smallsetminus \{B\}$ such that $B = B' \cup B''$ and $B' \cap B'' \neq \varnothing$. By maximality, M and N are not strict subsets of B' and B'', hence M and N intersect both B' and B''. Since $M \cap B' \neq \varnothing$, we have $M \cup B' \in \mathcal{B}$. As $M \subseteq M \cup B' \subseteq B$, we obtain again by maximality of M that $M = M \cup B'$ or $M \cup B' = B$. In the former case, we have $\varnothing \neq B' \cap N \subseteq M \cap N$ contradicting our assumption on M and N. In the latter case, we have $N \subseteq B' \smallsetminus M$ contradicting the maximality of N.

Remark 2.38. For a graph G with vertex set V, the set $\mathcal{B}G$ of all tubes of G is a *graphical building set*. The blocks of $\kappa(\mathcal{B}G)$ are the vertex sets of the connected components $\kappa(G)$ of G, and the blocks of $\varepsilon(\mathcal{B}G)$ are the edges of G.

Remark 2.39. Note that not all building sets are graphical building sets. It was in fact proved in [Zel06, Prop. 7.3] that a building set is graphical if and only if for any $B \in \mathcal{B}$ and $\mathcal{C} \subset \mathcal{B}$, if $B \cup \bigcup \mathcal{C} \in \mathcal{B}$, then there is $C \in \mathcal{C}$ such that $B \cup C \in \mathcal{B}$. However, arbitrary building sets can be interpreted using hypergraphs [Ber89] instead of graphs. More precisely, a hypergraph H on V defines a building set $\mathcal{B}H$ on V given by all non-empty subsets of V which induce connected subhypergraphs of H (a path in H is a sequence of vertices where any two consecutive ones belong to a common hyperedge of H). Conversely, a building set $\mathcal{B}$ on V is the building set of various hypergraphs on V, all containing the hypergraph with hyperedge set $\varepsilon(\mathcal{B})$. See [DP11] for details.

Nested complex Given a building set $\mathcal{B}$, a *$\mathcal{B}$-nested set* $\mathcal{N}$ is a subset of $\mathcal{B}$ such that

- for any $B, B' \in \mathcal{N}$, either $B \subseteq B'$ or $B' \subseteq B$ or $B \cap B' = \varnothing$,
- for any $k \geq 2$ pairwise disjoint $B_1, \dots, B_k \in \mathcal{N}$, the union $B_1 \cup \dots \cup B_k$ is not in $\mathcal{B}$, and
- $\mathcal{N}$ contains $\kappa(\mathcal{B})$.

These are the original conditions that appeared for instance in [Pos09]. In this paper, we prefer to use the following convenient reformulation, similar to that of [Zel06]: $\mathcal{N} \subseteq \mathcal{B}$ is a $\mathcal{B}$-nested set if and only if $\kappa(\mathcal{B}) \subseteq \mathcal{N}$ and the union $\bigcup \mathcal{X}$ of any subset $\mathcal{X} \subseteq \mathcal{N}$ does not belong to $\mathcal{B} \smallsetminus \mathcal{X}$. It is known that all inclusion maximal nested sets have $|V|$ blocks. The *$\mathcal{B}$-nested complex* is the simplicial complex $\mathcal{N}(\mathcal{B})$ whose faces are $\mathcal{N} \smallsetminus \kappa(\mathcal{B})$ for all $\mathcal{B}$-nested sets $\mathcal{N}$. It is a simplicial sphere of dimension $|V| - |\kappa(\mathcal{B})|$. Note that it is convenient to include $\kappa(\mathcal{B})$ in all $\mathcal{B}$-nested sets as in [Pos09] for certain combinatorial manipulations, but to remove $\kappa(\mathcal{B})$ from all $\mathcal{B}$-nested sets as in [Zel06] when defining the $\mathcal{B}$-nested complex. If $\mathcal{N} \smallsetminus \{B\} = \mathcal{N}' \smallsetminus \{B'\}$ for two maximal $\mathcal{B}$-nested sets $\mathcal{N}$ and $\mathcal{N}'$ and two building blocks B and B', we say that $\mathcal{N}$ and $\mathcal{N}'$ are *adjacent* and that B and B' are *exchangeable*.

For instance, Figure 18(Middle) represents the two adjacent maximal $\mathcal{B}_\circ$-nested sets

$$\mathcal{N}_\circ := \{3, 4, 5, 7, 8, 14, 789, 12345, 123456\} \quad \text{and} \quad \mathcal{N}'_\circ := \{3, 4, 5, 7, 8, 25, 789, 12345, 123456\}.$$

Remark 2.40. For a graph G, a set of tubes of $\mathcal{B}G$ is nested if and only if its tubes are pairwise compatible in the sense of Section 2.3.1 (either nested or non-adjacent). The nested complex $\mathcal{N}(\mathcal{B}G)$ thus coincides with the graphical nested complex $\mathcal{N}(G)$ introduced in Section 2.3.1 (which justifies our notation there). Note that, in contrast to the graphical nested complexes, not all nested complexes are flag (*i.e.* clique complexes of their graphs).

For a $\mathcal{B}$-nested set $\mathcal{N}$ and $B \in \mathcal{N}$, we call *root* of B in $\mathcal{N}$ the set $\boldsymbol{r}(B, \mathcal{N}) := B \smallsetminus \bigcup_C C$ where the union runs over $C \in \mathcal{N}$ such that $C \subsetneq B$. The $\mathcal{B}$-nested set $\mathcal{N}$ is maximal if and only if all $\boldsymbol{r}(B, \mathcal{N})$ are singletons for $B \in \mathcal{N}$. In that case, we abuse notation writing $\boldsymbol{r}(B, \mathcal{N})$ for the only element of this singleton. For instance, in the maximal $\mathcal{B}_\circ$-nested sets $\mathcal{N}_\circ$ and $\mathcal{N}'_\circ$ represented in Figure 18 (middle), we have $\boldsymbol{r}(14, \mathcal{N}_\circ) = 1 = \boldsymbol{r}(12345, \mathcal{N}'_\circ)$ and $\boldsymbol{r}(12345, \mathcal{N}_\circ) = 2 = \boldsymbol{r}(25, \mathcal{N}'_\circ)$.

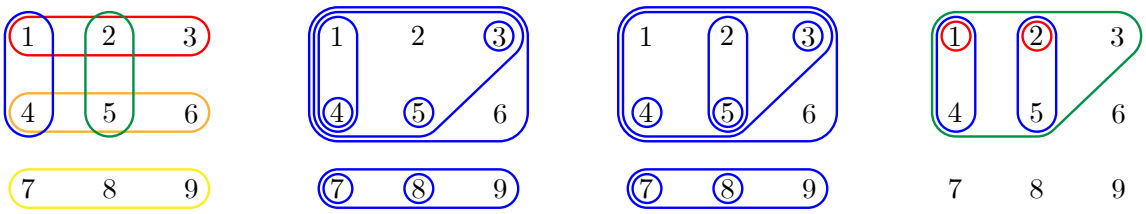

Figure 18: The elementary blocks of a building set $\mathcal{B}_\circ$ (Left), two adjacent maximal $\mathcal{B}_\circ$-nested sets (Middle), and the corresponding frame (Right).

Nested fan We still denote by $(\boldsymbol{e}_v)_{v\in V}$ the canonical basis of $\mathbb{R}^V$. We consider the subspace $\mathbb{H} := \{\boldsymbol{x} \in \mathbb{R}^V \ ; \ \sum_{v\in B} x_v = 0 \text{ for all } B \in \kappa(\mathcal{B})\}$ and let $\pi : \mathbb{R}^V \to \mathbb{H}$ denote the orthogonal projection onto $\mathbb{H}$. The ***g*-vector** of a building block B of $\mathcal{B}$ is the projection $\boldsymbol{g}(B) := \pi\big(\sum_{v\in B} \boldsymbol{e}_v\big)$ of the characteristic vector of B. We set $\boldsymbol{g}(\mathcal{N}) := \{\boldsymbol{g}(B) \ ; \ B \in \mathcal{N}\}$ for a $\mathcal{B}$-nested set $\mathcal{N}$. Note that by definition, $\boldsymbol{g}(K) = \mathbf{0}$ for all connected components $K \in \kappa(\mathcal{B})$. The vectors $\boldsymbol{g}(B)$ with $B \in \mathcal{B}$ support a complete simplicial fan realization of the nested complex. See Figure 19.

Theorem 2.41 ([FS05, Zel06, Pos09])**.** *For any building set $\mathcal{B}$, the set of cones*

$$\mathcal{F}(\mathcal{B}) := \{\mathbb{R}_{\geq 0}\, \boldsymbol{g}(\mathcal{N}) \ ; \ \mathcal{N} \text{ nested set of } \mathcal{B}\}$$

is a complete simplicial fan of $\mathbb{H}$, called the nested fan of $\mathcal{B}$, which realizes the nested complex $\mathcal{N}(\mathcal{B})$.

Remark 2.42. For a graph G, the nested fan $\mathcal{F}(\mathcal{B}G)$ coincides with the graphical nested fan $\mathcal{F}(G)$ introduced in Section 2.3.1 (which justifies our notation there).

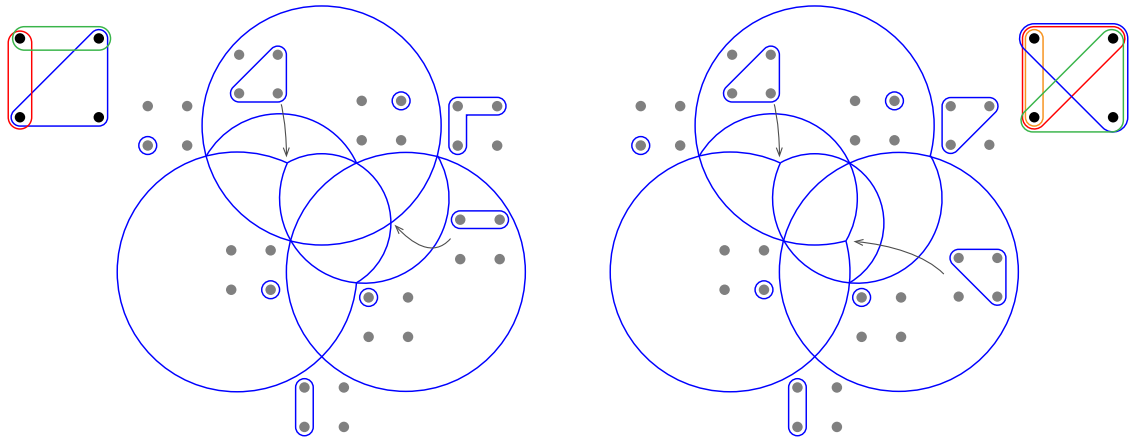

Figure 19: Two nested fans. The rays are labeled by the corresponding blocks. As the fans are 3-dimensional, we intersect them with the sphere and stereographically project them from the direction $(-1,-1,-1)$.

Nestohedron Again, the $\mathcal{B}$-nested fan is always the normal fan of a polytope, as shown in [FS05, Zel06, Pos09]. As usual, we still denote by $\Delta_U := \operatorname{conv}\{\boldsymbol{e}_u \ ; \ u \in U\}$ the face of the standard simplex Δ_V corresponding to a subset U of V.

Theorem 2.43 ([FS05, Zel06, Pos09])**.** *For any building set $\mathcal{B}$, the nested fan $\mathcal{F}(\mathcal{B})$ is the normal fan of a polytope. For instance, $\mathcal{F}(\mathcal{B})$ is the normal fan of*

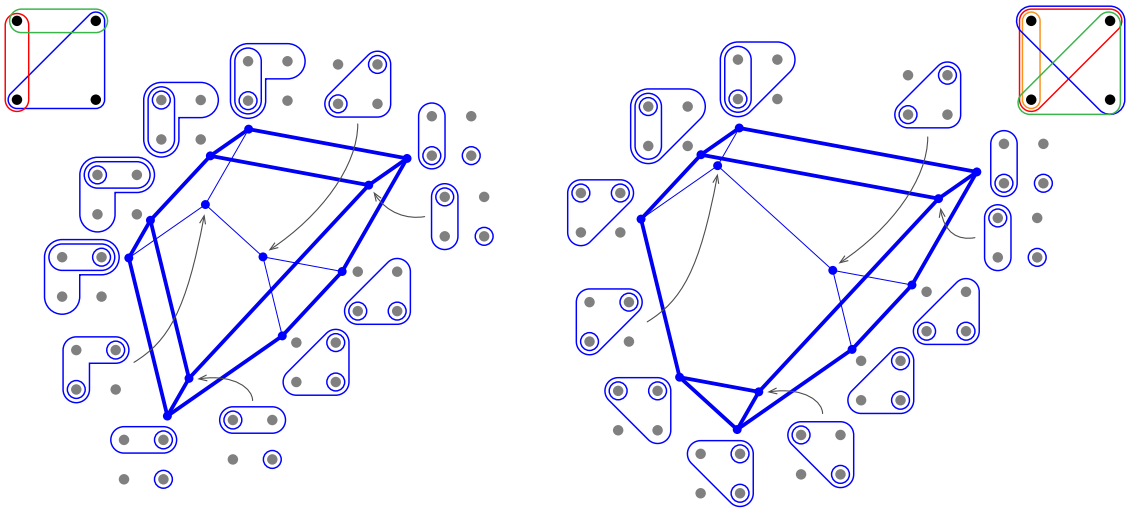

Figure 20: Two nestohedra, realizing the nested fans of Figure 19. The vertices are labeled by the corresponding maximal nested sets.

(i) the intersection of $\mathbb{H}$ *with the hyperplanes* $\langle \boldsymbol{g}(B),\ \boldsymbol{x}\rangle \leq -3^{|B|}$ *for all* $B \in \mathcal{B}$ *[Dev09, Pil17],*

(ii) the Minkowski sum $\sum_{B\in\mathcal{B}} \Delta_B$ *of faces of the standard simplex given by all* $B \in \mathcal{B}$ *[Pos09].*

Definition 2.44. Any polytope whose normal fan is the nested fan $\mathcal{F}(\mathcal{B})$ is called a *nestohedron* of $\mathcal{B}$ and denoted by $\mathsf{Nest}_{\mathcal{B}}$.

For instance, Figure 20 represents the nestohedra realizing the nested fans of Figure 19 and obtained using the construction (ii) of Theorem 2.43.

Remark 2.45. For a graph G, the nestohedra of $\mathcal{B}G$ are the graph associahedra of G.

Restrictions and contractions Following [Zel06], we describe a structural decomposition of links in nested complexes. For any $U \subseteq V$, define

- the *restriction* of $\mathcal{B}$ to U as the building set $\mathcal{B}_{|U} := \{B \in \mathcal{B}\ ;\ B \subseteq U\}$,
- the *contraction* of U in $\mathcal{B}$ as the building set $\mathcal{B}_{/U} := \{C \subseteq V \smallsetminus U\ ;\ C \in \mathcal{B} \text{ or } C \cup U \in \mathcal{B}\}$.

Proposition 2.46 ([Zel06, Prop. 3.2])**.** *For* $U \in \mathcal{B}\smallsetminus\kappa(\mathcal{B})$*, the link* $\{C \subseteq \mathcal{B} \smallsetminus \{U\}\ ;\ C \cup \{U\} \in \mathcal{N}(\mathcal{B})\}$ *is isomorphic to the Cartesian product* $\mathcal{N}(\mathcal{B}_{|U}) \times \mathcal{N}(\mathcal{B}_{/U})$.

In particular, two building blocks B and B' in U (resp. in $V \smallsetminus U$) are exchangeable in $\mathcal{N}(\mathcal{B})$ if and only if they are exchangeable in $\mathcal{N}(\mathcal{B}_{|U})$ (resp. in $\mathcal{N}(\mathcal{B}_{/U})$).

Slightly abusing notation when $\mathcal{B}$ is clear from the context, we define the *connected components* of U as $\kappa(U) := \kappa(\mathcal{B}_{|U})$. For instance, for the building set $\mathcal{B}_\circ$ whose elementary blocks are represented in Figure 18(Left) and $U = \{1, 2, 4, 5, 7, 8\}$, we have $\mathcal{B}_{\circ|U} = \{1, 2, 4, 5, 7, 8, 14, 25\}$ so that $\kappa(U) = \{14, 25, 7, 8\}$. Note that the definition of building sets implies that

- for any $U \subseteq V$, the connected components $\kappa(U)$ define a partition of U,
- for any $U, U' \subseteq V$ such that $U \cap U' = \varnothing$ and there is no $B \in \mathcal{B}$ with $B \subseteq U \sqcup U'$ and $U \cap B \neq \varnothing \neq U' \cap B$, we have $\kappa(U \sqcup U') = \kappa(U) \sqcup \kappa(U')$.

Exchangeable building blocks and exchange frames We now provide an analogue of Proposition 2.23 characterizing the exchangeable blocks for arbitrary building sets. The situation is however much more technical, as highlighted in Remarks 2.50 and 2.55. We start with two useful lemmas.

Lemma 2.47. *For any $\mathcal{B}$-nested set $\mathcal{N}$ and any block $B \in \mathcal{B} \smallsetminus \kappa(\mathcal{B})$, the set $\{C \in \mathcal{N} \ ; \ B \subsetneq C\}$ admits a unique (inclusion) minimal element M. Moreover, if $B \notin \mathcal{N}$, then M is also the unique (inclusion) maximal element of $\{C \in \mathcal{N} \ ; \ \boldsymbol{r}(C,\mathcal{N}) \cap B \neq \varnothing\}$.*

Proof. Let $\mathcal{X} := \{C \in \mathcal{N} \ ; \ B \subsetneq C\}$ and $\mathcal{Y} := \{C \in \mathcal{N} \ ; \ \boldsymbol{r}(C,\mathcal{N}) \cap B \neq \varnothing\}$. Note first that neither $\mathcal{X}$ nor $\mathcal{Y}$ are empty since $\varnothing \neq B \notin \kappa(\mathcal{B})$. Since all elements of $\mathcal{X}$ contain B and $\mathcal{N}$ is a $\mathcal{B}$-nested set, $\mathcal{X}$ forms a chain by inclusion, and thus admits a unique inclusion minimal element M. Moreover, any building block in $\mathcal{Y}$ intersects B so that $\bigcup \mathcal{Y} = B \cup \bigcup \mathcal{Y}$ is in $\mathcal{B}$. Hence, $\mathcal{Y}$ admits a unique maximal element $M' := \bigcup \mathcal{Y}$. By definition, $B \subseteq M'$. If $B \notin \mathcal{N}$, then $B \neq M'$ since $M' \in \mathcal{Y} \subseteq \mathcal{N}$. Hence, $M' \in \mathcal{X}$. Moreover, for any $C \in \mathcal{N}$ such that $C \subsetneq M'$, we have $C \cap \boldsymbol{r}(M',\mathcal{N}) = \varnothing$ so that $B \not\subseteq C$ and $C \notin \mathcal{X}$. We conclude that $M' = M$. □

Lemma 2.48. *If $\mathcal{N}$ and $\mathcal{N}'$ are two adjacent maximal $\mathcal{B}$-nested sets with $\mathcal{N} \smallsetminus \{B\} = \mathcal{N} \smallsetminus \{B'\}$, then $\{C \in \mathcal{N} \ ; \ B \subsetneq C\} = \{C' \in \mathcal{N}' \ ; \ B' \subsetneq C'\}$.*

Proof. Assume for instance that there is $C \in \mathcal{N} \cap \mathcal{N}'$ such that $B \subsetneq C$ but $B' \not\subseteq C$. We then claim that $\mathcal{N} \cup \mathcal{N}'$ would be a $\mathcal{B}$-nested set, contradicting the maximality of $\mathcal{N}$ and $\mathcal{N}'$. Consider a subset $\mathcal{X}$ of $\mathcal{N} \cup \mathcal{N}'$ whose union $\bigcup \mathcal{X}$ is in $\mathcal{B}$. If $B \notin \mathcal{X}$, then $\mathcal{X} \subseteq \mathcal{N}'$, hence $\bigcup \mathcal{X}$ is in $\mathcal{X}$ as $\mathcal{N}'$ is a $\mathcal{B}$-nested set. Similarly, if $B' \notin \mathcal{X}$, then $\bigcup \mathcal{X}$ is in $\mathcal{X}$. Assume now that both B and B' belong to $\mathcal{X}$. Define $\mathcal{Y} := \{C\} \cup \mathcal{X} \smallsetminus \{B\}$. Note that $\mathcal{Y} \subseteq \mathcal{N}'$ since $B \notin \mathcal{Y}$. Moreover, $\bigcup \mathcal{Y} = C \cup \bigcup \mathcal{X}$ belongs to $\mathcal{B}$ since C and $\bigcup \mathcal{X}$ both belong to $\mathcal{B}$ and intersect B. Hence, $\bigcup \mathcal{Y}$ is in $\mathcal{Y}$ since $\mathcal{N}'$ is a $\mathcal{B}$-nested set. Note that $\bigcup \mathcal{Y} \neq C$ since $B' \not\subseteq C$ and $B' \in \mathcal{Y}$. Therefore $\bigcup \mathcal{Y}$ is in $\mathcal{X}$, and thus $\bigcup \mathcal{X} = \bigcup \mathcal{Y}$ is in $\mathcal{X}$. □

For two adjacent maximal $\mathcal{B}$-nested sets $\mathcal{N}$ and $\mathcal{N}'$ with $\mathcal{N} \smallsetminus \{B\} = \mathcal{N} \smallsetminus \{B'\}$, we say that

- the unique minimal element P of $\{C \in \mathcal{N} \ ; \ B \subsetneq C\} = \{C' \in \mathcal{N}' \ ; \ B' \subsetneq C'\}$ is the *parent*,
- the vertices $v := \boldsymbol{r}(P,\mathcal{N}')$ and $v' := \boldsymbol{r}(P,\mathcal{N})$ are the *pivots*, and
- the triple (B, B', P) is the *frame*

of the exchange between $\mathcal{N}$ and $\mathcal{N}'$. Note that the parent is well-defined by Lemmas 2.47 and 2.48. We call an *exchange frame* a triple (B, B', P) which is the frame of an exchange between two adjacent maximal $\mathcal{B}$-nested sets. For instance, for the two adjacent maximal $\mathcal{B}_\circ$-nested sets $\mathcal{N}_\circ$ and $\mathcal{N}'_\circ$ represented in Figure 18(Middle), we have $B = 14$, $B' = 25$, $P = 12345$, $v = 1$ and $v' = 2$. The corresponding exchange frame is illustrated in Figure 18(Right).

We are now ready to characterize the pairs of exchangeable building blocks for arbitrary building sets. For three blocks $B, C, P \in \mathcal{B}$, we abbreviate the conditions $B \cap C \neq \varnothing$ and $C \subseteq P$ but $C \not\subseteq B$ into the short notation $B \vdash C \subseteq P$. The following statement generalizes Proposition 2.23 (i).

Proposition 2.49. *Two blocks $B, B' \in \mathcal{B}$ are exchangeable in $\mathcal{F}(\mathcal{B})$ if and only if there exist a block $P \in \mathcal{B}$, and some vertices $v \in B \smallsetminus B'$ and $v' \in B' \smallsetminus B$ such that*

- *$B \subsetneq P$ and $B' \subsetneq P$, and*
- *$v' \in C$ for any $B \vdash C \subseteq P$ while $v \in C'$ for any $B' \vdash C' \subseteq P$.*

Proof. Assume first that B and B' are exchangeable. Let $\mathcal{N}$ and $\mathcal{N}'$ be two adjacent maximal $\mathcal{B}$-nested sets such that $\mathcal{N} \smallsetminus \{B\} = \mathcal{N} \smallsetminus \{B'\}$. Let P be the parent and v, v' be the pivots of this exchange. Note that $v \in B$ (by Lemma 2.47) but $v \notin B'$ (by definition, since $B' \in \mathcal{N}'$ and $B' \subsetneq P$). Similarly, $v' \in B' \smallsetminus B$. Consider now a building block C such that $B \vdash C \subseteq P$. By definition,

$B \subsetneq B \cup C \subseteq P$ and $B \cup C \in \mathcal{B}$. If $B \cup C = P$, then $v' = \boldsymbol{r}(P, \mathcal{N})$ belongs to $B \cup C$ and thus to C. If $B \cup C \neq P$, then P is the inclusion minimal element of $\{D \in \mathcal{N} \ ; \ B \cup C \subsetneq D\}$. Since $B \cup C \notin \mathcal{N}$ by minimality of P in $\{D \in \mathcal{N} \ ; \ B \subsetneq D\}$, we obtain by Lemma 2.47 that $v' = \boldsymbol{r}(P, \mathcal{N})$ belongs to $B \cup C$ and thus to C. Similarly, $v \in C'$ for any $B' \vdash C' \subseteq P$.

Conversely, consider $B, B' \in \mathcal{B}$ so that there is $P \in \mathcal{B}$, $v \in B \smallsetminus B'$ and $v' \in B' \smallsetminus B$ satisfying the conditions of Proposition 2.49. Let $U := P \smallsetminus \{v, v'\}$, and $\mathcal{M}$ denote an arbitrary maximal $\mathcal{B}_{|U}$-nested set. Let $\mathcal{N} := \mathcal{M} \cup \{B\}$ and $\mathcal{N}' := \mathcal{M} \cup \{B'\}$. Consider a subset $\mathcal{X}$ of $\mathcal{N}$ whose union $\bigcup \mathcal{X}$ is in $\mathcal{B}$. If $B \notin \mathcal{X}$, then $\mathcal{X} \subseteq \mathcal{M}$, hence $\bigcup \mathcal{X}$ is in $\mathcal{X}$ since $\mathcal{M}$ is a $\mathcal{B}_{|U}$-nested set. If $B \in \mathcal{X}$, since $B \cap \bigcup \mathcal{X} \neq \varnothing$ and $\bigcup \mathcal{X} \subseteq P$ but $v' \notin \bigcup \mathcal{X}$, the conditions of Proposition 2.49 ensure that $\bigcup \mathcal{X} \subseteq B$, so that $\bigcup \mathcal{X} = B$ is in $\mathcal{X}$. Hence, $\mathcal{N}$ is a $\mathcal{B}_{|P}$-nested set. It is moreover maximal since $|\mathcal{N}| = |\mathcal{M} \cup \{B, P\}| = |\mathcal{M}| + 2 = |U| + 2 = |P|$. By symmetry, $\mathcal{N}'$ is a maximal $\mathcal{B}_{|P}$-nested set. Since $\mathcal{N} \smallsetminus \{B\} = \mathcal{N}' \smallsetminus \{B'\}$, we obtain that B and B' are exchangeable in $\mathcal{N}(\mathcal{B}_{|P})$, hence in $\mathcal{N}(\mathcal{B})$ by Proposition 2.46. The parent of this exchange is P and the pivots are v and v'. □

Remark 2.50. For the graphical nested fans, Proposition 2.23 (i) ensures that if B and B' are exchangeable, then $B \cup B'$ is always a block and is the only possible parent (note however that B and B' are not necessarily exchangeable when $B \cup B'$ is a block). In contrast to the graphical case, for a general building set,

- the same exchangeable blocks may admit several possible parents and pivots,
- the set of parents does not necessarily admit a unique (inclusion) minimal element,
- $B \cup B'$ is not always a block when B and B' are exchangeable. In other words, B and B' can be exchangeable even if $\{B, B'\} \cup \kappa(\mathcal{B})$ is a $\mathcal{B}$-nested set.

For instance, in the building set $\mathcal{B}_\circ$ of Figure 18(Left), the blocks $B = 14$ and $B' = 25$ are simultaneously compatible and exchangeable. They are exchangeable with parent 12345 and pivots $(1, 2)$ or with parent 12456 and pivots $(4, 5)$.

Remark 2.51. Observe also that it follows from the definitions that

- it suffices to check the condition of Proposition 2.49 for C and C' elementary blocks of $\mathcal{B}$,
- if B and B' are exchangeable, then $B \not\subseteq B'$ and $B' \not\subseteq B$,
- if (B, B', P) is an exchange frame and $B \cup B' \subseteq P' \subseteq P$, then (B, B', P') is also an exchange frame (using the same pivots),
- if B and B' are exchangeable and $B \cup B'$ is a block (in particular if $B \cap B' \neq \varnothing$), then $(B, B', B \cup B')$ is an exchange frame.

We now apply Proposition 2.49 to identify some exchange frames that will play an important role in the description of the deformation cone of the $\mathcal{B}$-nested fan.

Proposition 2.52. *If $B, B', P \in \mathcal{B}$ are such that B and B' are two distinct blocks of $\mathcal{B}$ strictly contained in P and inclusion maximal inside P, then (B, B', P) is an exchange frame.*

Proof. Consider $C \in \mathcal{B}$ such that $B \vdash C \subseteq P$. Since $B \cap C \neq \varnothing$, we have $B \cup C \in \mathcal{B}$. Since $C \subseteq P$ and $C \not\subseteq B$, we have $B \subsetneq B \cup C \subseteq P$. By maximality of B in P, we obtain that $B \cup C = P$. Hence, $B \vdash C \subseteq P$ implies $B' \smallsetminus B \subseteq C$ and similarly $B' \vdash C' \subseteq P$ implies $B \smallsetminus B' \subseteq C'$. Therefore, choosing any $v \in B \smallsetminus B'$ and $v' \in B' \smallsetminus B$, we obtain that B, B', P, v, v' satisfy the conditions of Proposition 2.49, and thus (B, B', P) is an exchange frame. □

We call *maximal exchange frames* the exchange frames defined by Proposition 2.52. For $P \in \mathcal{B}$, we will denote by $\mu(P)$ the maximal blocks of $\mathcal{B}$ strictly contained in P.

***g*-vector dependencies** We now describe the exchange relations in the $\mathcal{B}$-nested fan $\mathcal{F}(\mathcal{B})$. We first need to observe that certain building blocks are forced to belong to any two adjacent maximal nested sets with a given frame, generalizing Proposition 2.23 (ii).

Proposition 2.53. *For two adjacent maximal $\mathcal{B}$-nested sets $\mathcal{N}$ and $\mathcal{N}'$ with $\mathcal{N} \smallsetminus \{B\} = \mathcal{N}' \smallsetminus \{B'\}$ and parent P, all connected components of $\kappa(B \cap B')$ and of $\kappa\big(P \smallsetminus (B \cup B')\big)$ belong to $\mathcal{N} \cap \mathcal{N}'$.*

Proof. Even if we discuss separately the elements of $\kappa(B \cap B')$ from that of $\kappa(P \smallsetminus (B \cup B'))$, the reader will see a lot of similarities in the arguments below.

We first consider $K \in \kappa(B \cap B')$ and prove that $\mathcal{N} \cup \{K\}$ is a $\mathcal{B}$-nested set, which proves that $K \in \mathcal{N}$ by maximality of $\mathcal{N}$. Indeed, let us consider a subset $\mathcal{X}$ of $\mathcal{N} \cup \{K\}$ whose union $\bigcup \mathcal{X}$ is in $\mathcal{B}$, and prove that $\bigcup \mathcal{X}$ is in $\mathcal{X}$. We assume that $K \in \mathcal{X}$, since otherwise $\mathcal{X} \subseteq \mathcal{N}$ so that $\bigcup \mathcal{X}$ is in $\mathcal{X}$ as $\mathcal{N}$ is a $\mathcal{B}$-nested set. Assume now that $B \in \mathcal{X}$ and define $\mathcal{Y} := \mathcal{X} \smallsetminus \{K\}$. Since $K \subseteq B \in \mathcal{X}$, we have $\bigcup \mathcal{Y} = \bigcup \mathcal{X}$ in $\mathcal{B}$, thus in $\mathcal{Y} \subset \mathcal{X}$ since $\mathcal{Y} \subseteq \mathcal{N}$ and $\mathcal{N}$ is a $\mathcal{B}$-nested set. It remains to consider the case when $\mathcal{X} \subseteq (\mathcal{N} \cap \mathcal{N}') \cup \{K\}$. Assume now that $\bigcup \mathcal{X} \not\subseteq B$ and define $\mathcal{Y} := \{B\} \cup \mathcal{X} \smallsetminus \{K\}$. Since $K \subseteq B$, we have $\bigcup \mathcal{Y} = B \cup \bigcup \mathcal{X}$ which belongs to $\mathcal{B}$ since B and $\bigcup \mathcal{X}$ both belong to $\mathcal{B}$ and intersect K. Hence, $\bigcup \mathcal{Y}$ is in $\mathcal{Y}$ since $\mathcal{Y} \subseteq \mathcal{N}$ and $\mathcal{N}$ is a $\mathcal{B}$-nested set. Note that $\bigcup \mathcal{Y} \neq B$ by our assumption that $\bigcup \mathcal{X} \not\subseteq B$. Therefore, $\bigcup \mathcal{Y}$ is in $\mathcal{X}$, and thus $\bigcup \mathcal{X} = \bigcup \mathcal{Y}$ is in $\mathcal{X}$. By symmetry, we obtain that $\bigcup \mathcal{X}$ is in $\mathcal{X}$ if $\bigcup \mathcal{X} \not\subseteq B'$. Assume finally that $\bigcup \mathcal{X} \subseteq B \cap B'$. Then all the elements of $\mathcal{X}$ are in $B \cap B'$. Since $K \in \mathcal{X}$ is a connected component of $B \cap B'$ and $\bigcup \mathcal{X}$ is in $\mathcal{B}$, this implies that $\bigcup \mathcal{X} = K \in \mathcal{X}$.

We now consider $K \in \kappa(P \smallsetminus (B \cup B'))$ and prove that $\mathcal{N} \cup \{K\}$ is a $\mathcal{B}$-nested set, which proves that $K \in \mathcal{N}$ by maximality of $\mathcal{N}$. Indeed, let us consider a subset $\mathcal{X}$ of $\mathcal{N} \cup \{K\}$ whose union $\bigcup \mathcal{X}$ is in $\mathcal{B}$, and prove that $\bigcup \mathcal{X}$ is in $\mathcal{X}$. We assume that $K \in \mathcal{X}$, since otherwise $\mathcal{X} \subseteq \mathcal{N}$ so that $\bigcup \mathcal{X}$ is in $\mathcal{X}$ as $\mathcal{N}$ is a $\mathcal{B}$-nested set. Assume now that $\bigcup \mathcal{X} \not\subseteq P$ and define $\mathcal{Y} := \{P\} \cup \mathcal{X} \smallsetminus \{K\}$. Since $K \subseteq P$, we have $\bigcup \mathcal{Y} = P \cup \bigcup \mathcal{X}$ which belongs to $\mathcal{B}$ since P and $\bigcup \mathcal{X}$ both belong to $\mathcal{B}$ and intersect K. Hence, $\bigcup \mathcal{Y}$ is in $\mathcal{Y}$ since $\mathcal{Y} \subseteq \mathcal{N}$ and $\mathcal{N}$ is a $\mathcal{B}$-nested set. Note that $\bigcup \mathcal{Y} \neq P$ by our assumption that $\bigcup \mathcal{X} \not\subseteq P$. Therefore, $\bigcup \mathcal{Y}$ is in $\mathcal{X}$, and thus $\bigcup \mathcal{X} = \bigcup \mathcal{Y}$ is in $\mathcal{X}$. Assume now that $\bigcup \mathcal{X} \subseteq P \smallsetminus (B \cup B')$. Then all elements of $\mathcal{X}$ are in $P \smallsetminus (B \cap B')$. Since K is a connected component of $P \smallsetminus (B \cap B')$ and $\bigcup \mathcal{X}$ is in $\mathcal{B}$, this implies that $\bigcup \mathcal{X} = K \in \mathcal{X}$. Assume finally that $\bigcup \mathcal{X}$ is contained in P and intersects B or B'. If $B' \cap \bigcup \mathcal{X} \neq \varnothing$, then $B' \vdash \bigcup \mathcal{X} \subseteq P$, thus $v := \boldsymbol{r}(P, \mathcal{N}) \in \bigcup \mathcal{X}$ by Proposition 2.49. Hence, in both cases $B \cap \bigcup \mathcal{X} \neq \varnothing$, thus $B \vdash \bigcup \mathcal{X} \subseteq P$, and thus $v' := \boldsymbol{r}(P, \mathcal{N}) \in \bigcup \mathcal{X}$ by Proposition 2.49. Therefore, there is $C \in \mathcal{X} \smallsetminus \{K\} \subseteq \mathcal{N}$ containing v'. Since $v' = \boldsymbol{r}(P, \mathcal{N})$, we obtain that $P \subseteq C$, and hence $P = C$ because $C \subseteq \bigcup \mathcal{X} \subseteq P$. Thus $K \subseteq C$ and $\bigcup \mathcal{X} = \bigcup \mathcal{Y}$ where $\mathcal{Y} := \mathcal{X} \smallsetminus \{K\}$. Hence, $\bigcup \mathcal{Y}$ is in $\mathcal{Y}$ since $\mathcal{Y} \subseteq \mathcal{N}$ and $\mathcal{N}$ is a $\mathcal{B}$-nested set. We conclude that $\bigcup \mathcal{X} = \bigcup \mathcal{Y}$ is in $\mathcal{X}$.

We obtained that all blocks of $\kappa(B \cap B')$ and of $\kappa\big(P \smallsetminus (B \cup B')\big)$ belong to $\mathcal{N}$, and thus also to $\mathcal{N}'$ by symmetry. □

We are now ready to describe the exchange relations in the $\mathcal{B}$-nested fan. The main message here is that these relations only depend on the frames of the exchanges, generalizing Proposition 2.23 (iii).

Proposition 2.54. *For two adjacent maximal $\mathcal{B}$-nested sets $\mathcal{N}$ and $\mathcal{N}'$ with $\mathcal{N} \smallsetminus \{B\} = \mathcal{N}' \smallsetminus \{B'\}$ and parent P, the unique (up to rescaling) linear dependence between the $\boldsymbol{g}$-vectors of $\mathcal{N} \cup \mathcal{N}'$ is*

$$\boldsymbol{g}(B) + \boldsymbol{g}(B') + \sum_{K \in \kappa(P \smallsetminus (B \cup B'))} \boldsymbol{g}(K) = \boldsymbol{g}(P) + \sum_{K \in \kappa(B \cap B')} \boldsymbol{g}(K). \tag{9}$$

In particular, the $\boldsymbol{g}$-vector dependence only depends on the exchange frame (B, B', P).

Proof. Equation (9) is a valid linear dependence since it holds at the level of characteristic vectors, and $\boldsymbol{g}(C) := \pi\big(\sum_{v \in C} \boldsymbol{e}_v\big)$ where π is the orthogonal projection from $\mathbb{R}^V$ to $\mathbb{H}$. Since all building blocks involved in Equation (9) belong to $\mathcal{N} \cup \mathcal{N}'$ by Proposition 2.53, we conclude that Equation (9) is the unique (up to rescaling) linear dependence between the $\boldsymbol{g}$-vectors of $\mathcal{N} \cup \mathcal{N}'$. □

Remark 2.55. For the graphical nested fans studied in Section 2.3.1, the parent of the exchange of B and B' is always $B \cup B'$ and we recover the $\boldsymbol{g}$-vector relation of Proposition 2.23 (iii). In contrast to the graphical case, for an arbitrary building set,

- the sum on the left of Equation (9) is empty only when $P = B \cup B'$,
- Equation (9) depends on the exchange frame (B, B', P), not only on the exchangeable building blocks B and B'.

For instance, the $\boldsymbol{g}$-vector relation of the exchange between the two adjacent maximal $\mathcal{B}_\circ$-nested sets $\mathcal{N}_\circ$ and $\mathcal{N}'_\circ$ represented in Figure 18(Middle) is $\boldsymbol{g}_{14} + \boldsymbol{g}_{25} + \boldsymbol{g}_3 = \boldsymbol{g}_{12345}$. Another $\boldsymbol{g}$-vector relation for the same exchangeable blocks $B = 14$ and $B' = 25$ is $\boldsymbol{g}_{14} + \boldsymbol{g}_{25} + \boldsymbol{g}_6 = \boldsymbol{g}_{12456}$.

Remark 2.56. The $\boldsymbol{g}$-vector dependencies were already studied in [Zel06]. Namely, our Proposition 2.53 and Equation (9) are essentially Proposition 4.5 and Equation (6.6) of [Zel06]. Our versions are however more precise since we obtained in Proposition 2.49 a complete characterization of the exchangeable building blocks of $\mathcal{B}$, which was surprisingly missing in the literature.

Note that while the $\boldsymbol{g}$-vector dependence only depends on the exchange frame, different frames may lead to the same $\boldsymbol{g}$-vector dependence. In the next two statements, we describe which of the maximal exchange frames lead to the same $\boldsymbol{g}$-vector dependence. Remember that we denote by $\mu(P)$ the maximal blocks of $\mathcal{B}$ strictly contained in a block $P \in \mathcal{B}$.

Proposition 2.57. *For an elementary block $P \in \varepsilon(\mathcal{B})$, all exchange frames (B, B', P) for $B \neq B'$ in $\mu(P)$ lead to the same $\boldsymbol{g}$-vector dependence $\sum_{B \in \mu(P)} \boldsymbol{g}(B) = \boldsymbol{g}(P)$.*

Proof. Observe first that (B, B', P) is indeed an exchange frame by Proposition 2.52. We thus apply Proposition 2.54 to describe the corresponding $\boldsymbol{g}$-vector dependence. Observe first that the sum on the right of Equation (9) is empty because $B \cap B' = \varnothing$ by Remark 2.37 since P is elementary and $B, B' \in \mu(P)$. The result thus follows from the observation that $\kappa(P \smallsetminus (B \cup B')) = \mu(P) \smallsetminus \{B, B'\}$ which we prove next.

Let us consider $K \in \kappa(P \smallsetminus (B \cup B'))$ and prove that $K \in \mu(P) \smallsetminus \{B, B'\}$. Consider $L \in \mathcal{B}$ such that $K \subseteq L \subsetneq P$. If $L \cap B \neq \varnothing$, then $L \cup B \in \mathcal{B}$ and $B \subsetneq L \cup B \subseteq P$, so that $L \cup B = P$ by maximality of B, contradicting the elementarity of P. Hence, $L \subseteq P \smallsetminus (B \cup B')$, so that $K = L$ by maximality of K in $P \smallsetminus (B \cup B')$. We conclude that $K \in \mu(P) \smallsetminus \{B, B'\}$.

Conversely, let us consider $C \in \mu(P) \smallsetminus \{B, B'\}$ and prove that $C \in \kappa(P \smallsetminus (B \cup B'))$. Since P is elementary and $B, B', C \in \mu(P)$, the block C is disjoint from B and B' by Remark 2.37. Hence, $C \subseteq P \smallsetminus (B \cup B')$ and thus $C \in \kappa(P \smallsetminus (B \cup B'))$ by maximality of C. □

Proposition 2.58. *If (B_1, B'_1, P) and (B_2, B'_2, P) are two distinct maximal exchange frames with the same $\boldsymbol{g}$-vector dependence, then P is elementary.*

Proof. Since the exchange relations given by Equation (9) for the exchange frames (B_1, B'_1, P) and (B_2, B'_2, P) coincide, B_2 and B'_2 belong to $\{B_1, B'_1\} \cup \kappa(P \smallsetminus (B_1 \cup B'_1))$. Since (B_1, B'_1, P) and (B_2, B'_2, P) are distinct exchange frames, we can assume for instance that B_2 does not belong to $\{B_1, B'_1\}$. Hence, B_2 belongs to $\kappa(P \smallsetminus (B_1 \cup B'_1))$, thus $B_1 \cap B_2 = \varnothing$, and therefore P is elementary by Remark 2.37 since it contains two disjoint maximal blocks. □

Deformation cone of nested fans As a consequence of Proposition 2.54, we obtain the following redundant description of the deformation cone of the nested fan $\mathcal{F}(\mathcal{B})$.

Corollary 2.59. *For any building set $\mathcal{B}$, the deformation cone of the nested fan $\mathcal{F}(\mathcal{B})$ is given by*

$$\mathbb{DC}(\mathcal{F}(\mathcal{B})) = \left\{ \boldsymbol{h} \in \mathbb{R}^{\mathcal{B}G} \;;\; \begin{array}{l} \boldsymbol{h}_B = 0 \text{ for } B \in \kappa(\mathcal{B}) \text{ and for any exchange frame } (B, B', P) \\ \boldsymbol{h}_B + \boldsymbol{h}_{B'} + \sum_{K \in \kappa(P \smallsetminus (B \cup B'))} \boldsymbol{h}_K \geq \boldsymbol{h}_P + \sum_{K \in \kappa(B \cap B')} \boldsymbol{h}_K \end{array} \right\}.$$

We denote by $\boldsymbol{f}_B$ for $B \in \mathcal{B}$ the canonical basis of $\mathbb{R}^{\mathcal{B}}$ and by

$$\boldsymbol{n}(B, B', P) := \Big(\boldsymbol{f}_B + \boldsymbol{f}_{B'} + \sum_{K \in \kappa(P \smallsetminus (B \cup B'))} \boldsymbol{f}_K\Big) - \Big(\boldsymbol{f}_P + \sum_{K \in \kappa(B \cap B')} \boldsymbol{f}_K\Big)$$

the inner normal vector of the inequality of the deformation cone $\mathbb{DC}(\mathcal{F}(\mathcal{B}))$ corresponding to an exchange frame (B, B', P) of $\mathcal{B}$. Thus $\boldsymbol{h} \in \mathbb{DC}(\mathcal{F}(\mathcal{B}))$ if and only if $\langle \boldsymbol{n}(B, B', P),\ \boldsymbol{h}\rangle \geq 0$ for all exchange frames (B, B', P) of $\mathcal{B}$.

Example 2.60. Consider the nested fans illustrated in Figure 19. The deformation cone of the left fan lives in $\mathbb{R}^8$, has a lineality space of dimension 3 and 5 facet-defining inequalities (given below). In particular, it is simplicial. Note that, as in Figure 16, we express the $\boldsymbol{g}$-vectors in the basis given by the maximal tubing containing the first three tubes below.

blocks	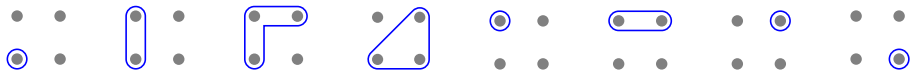							
$\boldsymbol{g}$-vectors	$\begin{bmatrix}1\\0\\0\end{bmatrix}$	$\begin{bmatrix}0\\1\\0\end{bmatrix}$	$\begin{bmatrix}0\\0\\1\end{bmatrix}$	$\begin{bmatrix}1\\-1\\0\end{bmatrix}$	$\begin{bmatrix}-1\\1\\0\end{bmatrix}$	$\begin{bmatrix}-1\\0\\1\end{bmatrix}$	$\begin{bmatrix}0\\-1\\1\end{bmatrix}$	$\begin{bmatrix}0\\0\\-1\end{bmatrix}$
facet	1	−1	0	0	1	0	0	0
defining	0	0	0	0	1	−1	1	0
inequalities	1	0	0	−1	0	0	1	1
	0	1	−1	0	−1	1	0	0
	−1	0	1	1	0	0	−1	0

The deformation cone of the right fan lives in $\mathbb{R}^8$, has a lineality space of dimension 3 and 7 facet-defining inequalities (given below). In particular, it is not simplicial.

blocks	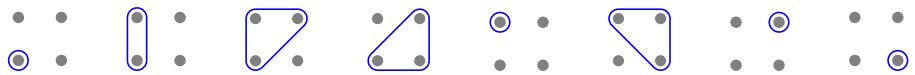							
$\boldsymbol{g}$-vectors	$\begin{bmatrix}1\\0\\0\end{bmatrix}$	$\begin{bmatrix}0\\1\\0\end{bmatrix}$	$\begin{bmatrix}0\\0\\1\end{bmatrix}$	$\begin{bmatrix}1\\-1\\0\end{bmatrix}$	$\begin{bmatrix}-1\\1\\0\end{bmatrix}$	$\begin{bmatrix}-1\\0\\0\end{bmatrix}$	$\begin{bmatrix}0\\-1\\1\end{bmatrix}$	$\begin{bmatrix}0\\0\\-1\end{bmatrix}$
facet	1	−1	0	0	1	0	0	0
defining	0	1	−1	0	0	0	1	0
inequalities	1	0	0	−1	0	0	1	1
	0	0	0	0	1	−1	1	1
	−1	0	1	1	0	0	−1	0
	0	0	1	0	−1	1	−1	0
	0	0	0	1	0	1	−1	−1

Example 2.61. We can exploit Corollary 2.59 to show that certain height functions belong to the (interior of the) deformation cone of $\mathcal{F}(\mathcal{B})$ and recover some classical constructions of the nestohedron, generalizing Example 2.27.

(i) Consider the height function $\boldsymbol{h} \in \mathbb{R}^{\mathcal{B}}$ given by $\boldsymbol{h}_B := -3^{|B|}$. Then for any exchange frame (B, B', P) of $\mathcal{B}$, we have

$$\begin{aligned}\langle \boldsymbol{n}(B, B'),\ \boldsymbol{h}\rangle &= -3^{|B|} - 3^{|B'|} - \sum_{K \in \kappa(P \smallsetminus (B \cup B'))} 3^{|K|} + 3^{|P|} + \sum_{K \in \kappa(B \cap B')} 3^{|K|} \\ &\geq -2 \cdot 3^{|B \cup B'|-1} - 3^{|P \smallsetminus (B \cup B'))|} + 3^{|P|} > 0.\end{aligned}$$

Therefore, the height function $\boldsymbol{h}$ belongs to the interior of the deformation cone $\mathbb{DC}(\mathcal{F}(\mathcal{B}))$. The corresponding polytope $P_{\boldsymbol{h}} := \{\boldsymbol{x} \in \mathbb{R}^V \ ; \ \langle \boldsymbol{g}(B), \ \boldsymbol{x}\rangle \leq \boldsymbol{h}_B \text{ for } B \in \mathcal{B}\}$ was constructed in [Pil17], generalizing the graph associahedra of [Dev09].

(ii) Consider the height function $\boldsymbol{h} \in \mathbb{R}^{\mathcal{B}}$ given by $\boldsymbol{h}_B := -|\{C \in \mathcal{B} \ ; \ C \subseteq B\}|$. Then for any exchange frame (B, B', P) of $\mathcal{B}$, we have

$$\langle \boldsymbol{n}(B, B', P), \ \boldsymbol{h}\rangle = |\{C \in \mathcal{B} \ ; \ C \not\subseteq B, \ C \not\subseteq B' \text{ and } C \not\subseteq P \smallsetminus (B \cup B') \text{ but } C \subseteq P\}| > 0$$

since P fulfills the conditions on C. Thus, the height function $\boldsymbol{h}$ belongs to the interior of the deformation cone $\mathbb{DC}(\mathcal{F}(\mathcal{B}))$. The polytope $P_{\boldsymbol{h}} := \{\boldsymbol{x} \in \mathbb{R}^V \ ; \ \langle \boldsymbol{g}(B), \ \boldsymbol{x}\rangle \leq \boldsymbol{h}_B \text{ for } B \in \mathcal{B}\}$ is the nestohedron constructed by A. Postnikov's in [Pos09].

Note that many inequalities of Corollary 2.59 are redundant. In the remaining of this section, we describe the facet-defining inequalities of $\mathbb{DC}(\mathcal{F}(\mathcal{B}))$. We say that an exchange frame (B, B', P) is

- *extremal* if its corresponding inequality in Corollary 2.59 defines a facet of $\mathbb{DC}(\mathcal{F}(\mathcal{B}))$,
- *maximal* if B and B' are both maximal building blocks in P as in Proposition 2.52.

We can now state our main result on nested complexes, generalizing Theorem 2.28.

Theorem 2.62. *An exchange frame is extremal if and only if it is maximal.*

Proof. We treat separately the two implications:

Extremal ⇒ maximal. Consider an exchange frame (B, B', P) of $\mathcal{B}$, and fix pivot vertices v, v' satisfying the conditions of Proposition 2.49. We assume that this frame is not maximal, and prove that it is not extremal by showing that the normal vector $\boldsymbol{n}(B, B', P)$ of the corresponding inequality of the deformation cone $\mathbb{DC}(\mathcal{F}(\mathcal{B}))$ is a positive linear combination of normal vectors of some other exchange frames. By symmetry, we can assume that there is $M \in \mathcal{B}$ such that $B \subsetneq M \subsetneq P$ and we can assume that M is maximal for this property. We decompose the proof into two cases, depending on whether $B' \subseteq M$ or $B' \not\subseteq M$.

Case 1: $B' \subseteq M$. Observe first that:

- (B, B', M) is an exchange frame, since (B, B', P) is an exchange frame and $B \cup B' \subseteq M \subseteq P$,
- (M, W, P) is an exchange frame for any connected component W of $P \smallsetminus (B \cup B')$ containing a vertex $w \in P \smallsetminus M$. Indeed, we just check the conditions of Proposition 2.49 for $v \in M \smallsetminus W$ and $w \in W \smallsetminus M$:
  - for any $M \vdash C \subseteq P$, we have $w \in P \smallsetminus M \subseteq C$ by maximality of M.
  - for any $W \vdash C' \subseteq P$, we have $C' \subseteq P$ and $C' \not\subseteq W$, hence $C' \cap (B \cup B') \neq \varnothing$ since W is a connected component of $P \smallsetminus (B \cup B')$. Assume for instance that $C' \cap B \neq \varnothing$ (the proof for $C' \cap B' \neq \varnothing$ is symmetric). Since $C' \cap W \neq \varnothing$, we obtain that $B \vdash C' \subseteq P$ and thus $v' \in C'$ by Proposition 2.49. We therefore obtain that $B' \vdash C' \subseteq P$ and thus $v \in C'$ by Proposition 2.49 again.

We claim that these two exchange frames enable us to write

$$\boldsymbol{n}(B, B', P) = \boldsymbol{n}(B, B', M) + \boldsymbol{n}(M, W, P).$$

Proving this identity amounts to check that

$$\kappa(P \smallsetminus (B \cup B')) \sqcup \kappa(M \cap W) = \kappa(M \smallsetminus (B \cup B')) \sqcup \kappa(P \smallsetminus (M \cup W)) \sqcup \{W\}. \tag{10}$$

For this, we distinguish two subcases, depending on whether or not M and W intersect.

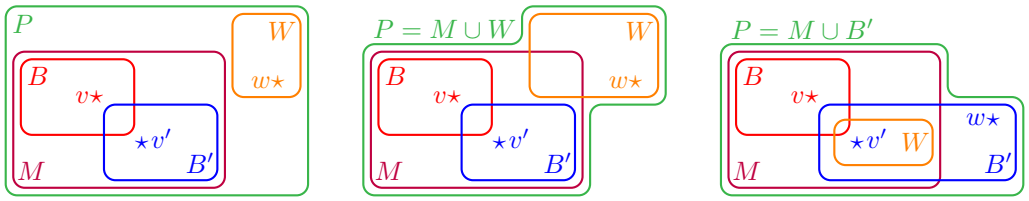

Case 1.1 Case 1.2 Case 2

Figure 21: Illustrations for the case analysis of the proof of Theorem 2.62.

Subcase 1.1: $M \cap W = \varnothing$. See Figure 21 (left). First, we claim that either $C \cap M = \varnothing$ or $C \subseteq M$ for any $C \in \mathcal{B}$ with $C \subseteq P \smallsetminus (B \cup B')$. Indeed, if $C \cap M \neq \varnothing$, then $C \cap W = \varnothing$ since $M \cap W = \varnothing$ and W is a connected component of $P \smallsetminus (B \cup B')$. Hence $C \cup M \in \mathcal{B}$ and $B \subsetneq C \cup M \subsetneq P$, and thus $C \subseteq M$ by maximality of M. We therefore obtain that

$$\kappa(P \smallsetminus (B \cup B')) = \kappa(M \smallsetminus (B \cup B')) \sqcup \kappa(P \smallsetminus (M \cup W)) \sqcup \{W\}.$$

This shows Equation (10) since $M \cap W = \varnothing$.

Subcase 1.2: $M \cap W \neq \varnothing$. See Figure 21 (middle). As $M \cup W \in \mathcal{B}$ and $B \subsetneq B \cup W \subseteq P$ and $W \not\subseteq M$, we have $P = M \cup W$ by maximality of M. Since $W \in \kappa(P \smallsetminus (B \cup B'))$, we have

$$\kappa(P \smallsetminus (B \cup B')) = \kappa(P \smallsetminus (B \cup B' \cup W)) \sqcup \{W\} = \kappa(M \smallsetminus (B \cup B' \cup W)) \sqcup \{W\}$$

Moreover, by maximality of W, we obtain that there is no block of $\mathcal{B}$ contained in $M \smallsetminus (B \cup B')$ and meeting both $M \cap W$ and $M \smallsetminus (B \cup B' \cup W)$. Hence

$$\kappa(M \cap W) \sqcup \kappa(M \smallsetminus (B \cup B' \cup W)) = \kappa(M \smallsetminus (B \cup B')).$$

Combining these two identities proves Equation (10) since $P = M \cup W$.

Case 2: $B' \not\subseteq M$. See Figure 21 (right). Observe that:

- (M, B', P) is an exchange frame. Indeed, we just check the conditions of Proposition 2.49 for $v \in M \smallsetminus B'$ and an arbitrary $w \in B' \smallsetminus M$:
  - for any $M \vdash C \subseteq P$, we have $w \in P \smallsetminus M \subseteq C$ by maximality of M.
  - for any $B' \vdash C' \subseteq P$, we have $v \in C'$ by Proposition 2.49.
- (B, W, M) is an exchange frame for the connected component W of $M \cap B'$ containing v'. Indeed, we just check the conditions of Proposition 2.49 for $v \in B \smallsetminus W$ and $v' \in W \smallsetminus B$:
  - for any $B \vdash C \subseteq M$, we have $B \vdash C \subseteq P$ and thus $v' \in C$ by Proposition 2.49.
  - for any $W \vdash C' \subseteq M$, we have $B' \vdash C' \subseteq P$ and thus $v \in C'$ by Proposition 2.49.

We claim that these two exchange frames enable to write

$$\boldsymbol{n}(B, B', P) = \boldsymbol{n}(M, B', P) + \boldsymbol{n}(B, W, M).$$

Proving this identity amounts to check that

$$\kappa(P \smallsetminus (B \cup B')) \sqcup \kappa(M \cap B') \sqcup \kappa(B \cap W) = \kappa(B \cap B') \sqcup \kappa(P \smallsetminus (M \cup B')) \sqcup \kappa(M \smallsetminus (B \cup W)) \sqcup \{W\}. \quad (11)$$

To prove this, we observe that:

- Since W contains v', Proposition 2.49 ensures that there is no block of $\mathcal{B}$ contained in $M \cap B'$ and meeting both B and $B' \smallsetminus (B \cup W)$. Since $W \in \kappa(M \cap B')$, we thus obtain

$$\kappa(M \cap B') = \kappa((M \cap B') \smallsetminus (B \cup W)) \sqcup \kappa(B \cap B' \smallsetminus W) \sqcup \{W\}.$$

- As $W \in \kappa(M \cap B')$, there is no block of $\mathcal{B}$ contained in $B \cap B'$ and meeting both $B \cap W$ and $B \cap B' \smallsetminus W$, hence

$$\kappa(B \cap W) \sqcup \kappa(B \cap B' \smallsetminus W) = \kappa(B \cap B').$$

- There is no block of $\mathcal{B}$ contained in $M \smallsetminus (B \cup W)$ and meeting both $M \smallsetminus (B \cup B')$ and $(M \cap B') \smallsetminus (B \cup W)$ (such a block C would satisfy $B' \vdash C \subseteq P$ and $v \notin C$, contradicting Proposition 2.49). Hence

$$\kappa(M \smallsetminus (B \cup B')) \sqcup \kappa((M \cap B') \smallsetminus (B \cup W)) = \kappa(M \smallsetminus (B \cup W)).$$

Combining these three identities proves (11) since $P = M \cup B'$ by maximality of M.

Maximal $\Rightarrow$ extremal. Let (B, B', P) be a maximal exchange frame. To prove that (B, B', P) is extremal, we will construct a vector $\boldsymbol{w} \in \mathbb{R}^{\mathcal{B}}$ such that $\langle \boldsymbol{n}(B, B', P),\ \boldsymbol{w}\rangle < 0$, but at the same time $\left\langle \boldsymbol{n}(\tilde{B}, \tilde{B}', \tilde{P}),\ \boldsymbol{w} \right\rangle > 0$ for any maximal exchange frame $(\tilde{B}, \tilde{B}', \tilde{P})$ with $\boldsymbol{n}(B, B', P) \neq \boldsymbol{n}(\tilde{B}, \tilde{B}', \tilde{P})$. This will show that the inequality induced by (B, B', P) is not redundant. Remember from Propositions 2.57 and 2.58 that, as (B, B', P) and $(\tilde{B}, \tilde{B}', \tilde{P})$ are maximal exchange frames, $\boldsymbol{n}(B, B', P) \neq \boldsymbol{n}(\tilde{B}, \tilde{B}', \tilde{P})$ if and only if $P \neq \tilde{P}$, or $P = \tilde{P}$ is not an elementary block.

Define $\alpha(B, B', P) := \{C \in \mathcal{B}\ ;\ C \not\subseteq B,\ C \not\subseteq B' \text{ and } C \not\subseteq P \smallsetminus (B \cup B') \text{ but } C \subseteq P\}$. Define three vectors $\boldsymbol{x}, \boldsymbol{y}, \boldsymbol{z} \in \mathbb{R}^{\mathcal{B}}$ by

$$\begin{aligned}
\boldsymbol{x}_C &:= -|\{D \in \mathcal{B} \smallsetminus \alpha(B, B', P)\ ;\ D \subseteq C\}|,\\
\boldsymbol{y}_C &:= -|\{D \in \alpha(B, B', P)\ ;\ D \subseteq C\}|,\\
\boldsymbol{z}_C &:= \begin{cases} -1 & \text{if } B \subseteq C \text{ or } B' \subseteq C,\\ 0 & \text{otherwise,}\end{cases}
\end{aligned}$$

for each bock $C \in \mathcal{B}$.

We will prove below that their scalar products with $\boldsymbol{n}(\tilde{B}, \tilde{B}', \tilde{P})$ for any maximal exchange frame $(\tilde{B}, \tilde{B}', \tilde{P})$ satisfy the following inequalities

	$\left\langle \boldsymbol{n}(\tilde{B}, \tilde{B}', \tilde{P}),\ \boldsymbol{x} \right\rangle$	$\left\langle \boldsymbol{n}(\tilde{B}, \tilde{B}', \tilde{P}),\ \boldsymbol{y} \right\rangle$	$\left\langle \boldsymbol{n}(\tilde{B}, \tilde{B}', \tilde{P}),\ \boldsymbol{z} \right\rangle$
if $\boldsymbol{n}(B, B', P) = \boldsymbol{n}(\tilde{B}, \tilde{B}', \tilde{P})$	$= 0$	$= \lvert\alpha(B, B', P)\rvert$	$= -1$
if $\alpha(\tilde{B}, \tilde{B}', \tilde{P}) \not\subseteq \alpha(B, B', P)$	≥ 1	≥ 0	≥ -1
otherwise	≥ 0	≥ 1	≥ 0

It immediately follows from this table that the vector $\boldsymbol{w} := \boldsymbol{x} + \delta\boldsymbol{y} + \varepsilon\boldsymbol{z}$ fulfills the desired properties for any δ, ε such that $0 < \delta \cdot |\alpha(B, B', P)| < \varepsilon < 1$.

The equalities of the table are immediate. To prove the inequalities, observe that for any maximal exchange frame $(\tilde{B}, \tilde{B}', \tilde{P})$,

- $\left\langle \boldsymbol{n}(\tilde{B}, \tilde{B}', \tilde{P}),\ \boldsymbol{x} \right\rangle \geq |\alpha(\tilde{B}, \tilde{B}', \tilde{P}) \smallsetminus \alpha(B, B', P)|$,
- $\left\langle \boldsymbol{n}(\tilde{B}, \tilde{B}', \tilde{P}),\ \boldsymbol{y} \right\rangle \geq |\alpha(\tilde{B}, \tilde{B}', \tilde{P}) \cap \alpha(B, B', P)|$,
- $\left\langle \boldsymbol{n}(\tilde{B}, \tilde{B}', \tilde{P}),\ \boldsymbol{z} \right\rangle \geq -1$. Indeed, observe that $\boldsymbol{z}_{\tilde{P}} = -1$ as soon as $\boldsymbol{z}_{\tilde{K}} = -1$ for some $\tilde{K} \in \{\tilde{B}, \tilde{B}'\} \sqcup \kappa(\tilde{P} \smallsetminus (\tilde{B} \cup \tilde{B}'))$. This already implies that $\left\langle \boldsymbol{n}(\tilde{B}, \tilde{B}', \tilde{P}),\ \boldsymbol{z} \right\rangle \geq -1$ except

if $\boldsymbol{z}_{\tilde{K}} = \boldsymbol{z}_{\tilde{K}'} = \boldsymbol{z}_{\tilde{K}''} = -1$ for three distinct $\tilde{K}, \tilde{K}', \tilde{K}'' \in \{\tilde{B}, \tilde{B}'\} \sqcup \kappa(\tilde{P} \smallsetminus (\tilde{B} \cup \tilde{B}'))$. But since $\tilde{B}$ and $\tilde{B}'$ are the only intersecting blocks among $\{\tilde{B}, \tilde{B}'\} \sqcup \kappa(\tilde{P} \smallsetminus (\tilde{B} \cup \tilde{B}'))$, the only option (up to permutation) is that $\tilde{K} = \tilde{B}$ and $\tilde{K}' = \tilde{B}'$ both contain B (resp. B'), K'' contains B' (resp. B), while none of the other blocks of $\{\tilde{B}, \tilde{B}'\} \sqcup \kappa(\tilde{P} \smallsetminus (\tilde{B} \cup \tilde{B}'))$ meets $B \cup B'$. This implies that $\boldsymbol{z}_{\tilde{P}} = -1 = \boldsymbol{z}_L$ for some $L \in \kappa(\tilde{B} \cap \tilde{B}')$, and thus $\left\langle \boldsymbol{n}(\tilde{B}, \tilde{B}', \tilde{P}),\ \boldsymbol{z} \right\rangle \geq -1$.

- $\left\langle \boldsymbol{n}(\tilde{B}, \tilde{B}', \tilde{P}),\ \boldsymbol{z} \right\rangle \geq 0$ when $\boldsymbol{n}(B, B', P) \neq \boldsymbol{n}(\tilde{B}, \tilde{B}', \tilde{P})$ but $\alpha(\tilde{B}, \tilde{B}', \tilde{P}) \subseteq \alpha(B, B', P)$. Indeed, $\alpha(\tilde{B}, \tilde{B}', \tilde{P}) \subseteq \alpha(B, B', P)$ implies that $\tilde{P} \subseteq P$. Let $\tilde{K} \in \{\tilde{B}, \tilde{B}'\} \sqcup \kappa(\tilde{P} \smallsetminus (\tilde{B} \cup \tilde{B}'))$. If $B \subseteq \tilde{K}$, then $B \subseteq \tilde{K} \subsetneq \tilde{P} \subseteq P$ which implies that $B = \tilde{K}$ and $P = \tilde{P}$ by maximality of B in P. Similarly, $B' \subseteq \tilde{K}$ implies $B' = \tilde{K}$ and $P = \tilde{P}$. Hence, if $\boldsymbol{z}_{\tilde{K}} = -1$, then by definition $B \subseteq \tilde{K}$ or $B' \subseteq \tilde{K}$, which implies that $\tilde{K} \in \{B, B'\}$. Hence, if $\tilde{K} \neq \tilde{K}'$ are two distinct blocks of $\{\tilde{B}, \tilde{B}'\} \sqcup \kappa(\tilde{P} \smallsetminus (\tilde{B} \cup \tilde{B}'))$ such that $\boldsymbol{z}_{\tilde{K}} = -1 = \boldsymbol{z}_{\tilde{K}'}$, then $(B, B', P) = (\tilde{K}, \tilde{K}', \tilde{P})$ and moreover either $\{B, B'\} = \{\tilde{K}, \tilde{K}'\}$, or $\tilde{K} \cap \tilde{K}' = \varnothing$, so that P is elementary by Remark 2.37 since it has two disjoint maximal blocks. In both cases, we obtain $\boldsymbol{n}(B, B', P) = \boldsymbol{n}(\tilde{B}, \tilde{B}', \tilde{P})$ by Proposition 2.58, contradicting our assumption. Therefore, at most one of $\boldsymbol{z}_{\tilde{K}}$ for $\tilde{K} \in \{\tilde{B}, \tilde{B}'\} \sqcup \kappa(\tilde{P} \smallsetminus (\tilde{B} \cup \tilde{B}'))$ equals to -1, and if exactly one does, then $\boldsymbol{z}_{\tilde{P}} = -1$. We conclude that $\left\langle \boldsymbol{n}(\tilde{B}, \tilde{B}', \tilde{P}),\ \boldsymbol{z} \right\rangle \geq 0$. □

We derive from Theorem 2.62 the facet description of the deformation cone $\mathbb{DC}(\mathcal{F}(\mathcal{B}))$. Remember that we denote by $\mu(P)$ the maximal blocks of $\mathcal{B}$ strictly contained in a block $P \in \mathcal{B}$.

Corollary 2.63. *The inequalities*

- $\sum_{B \in \mu(P)} \boldsymbol{h}_B \geq \boldsymbol{h}_P$ *for any elementary block* P *of* $\mathcal{B}$,
- $\boldsymbol{h}_B + \boldsymbol{h}_{B'} + \sum_{K \in \kappa(P \smallsetminus (B \cup B'))} \boldsymbol{h}_K \geq \boldsymbol{h}_P + \sum_{K \in \kappa(B \cap B')} \boldsymbol{h}_K$ *for any block* P *of* $\mathcal{B}$ *neither singleton nor elementary, and any two blocks* $B \neq B'$ *in* $\mu(P)$,

provide an irredundant facet description of the deformation cone $\mathbb{DC}(\mathcal{F}(\mathcal{B}))$.

Corollary 2.64. *The number of facets of the deformation cone* $\mathbb{DC}(\mathcal{F}(\mathcal{B}))$ *is*

$$|\varepsilon(\mathcal{B})| + \sum_P \binom{\mu(P)}{2}$$

where the sum runs over all blocks P *of* $\mathcal{B}$ *which are neither singletons nor elementary blocks. The dimension of* $\mathbb{DC}(\mathcal{F}(\mathcal{B}))$ *is* $|\mathcal{B}| - |\kappa(\mathcal{B})|$, *and its lineality* $|V| - |\kappa(\mathcal{B})|$.

Example 2.65. As for Examples 2.14 and 2.15, we can portray the deformation cone of a nestohedron. For the connected building set on 4 elements $\mathcal{B} = \{1, 2, 3, 4, 12, 123, 234, 1234\}$, the corresponding 3-dimensional nestohedron $\mathsf{Nest}_{\mathcal{B}}$ is depicted in Figure 22 as the Minkowski sum of faces of the standard simplex (faces corresponding to vertices of the standard simplex are omitted as they only account for translations in the Minkowski sum).

The deformation cone $\mathbb{DC}(\mathcal{F}(\mathcal{B}))$ has dimension $|\mathcal{B}| - |\kappa(\mathcal{B})| = 7$. Nonetheless, it has $|V| - |\kappa(\mathcal{B})| = 3$ dimensions of lineality. Thus, after intersecting it with a hyperplane, we can picture it in dimension 3 in Figure 23. By the above Corollary 2.64, it has 6 facets. Each vertex of the drawn bi-pyramid correspond to a ray of the deformation cone $\mathbb{DC}(\mathcal{F}(\mathcal{B}))$, *i.e.* to a Minkowski indecomposable polytope. Among them are the four simplices involved in the defining Minkowski sum $\mathsf{Nest}_{\mathcal{B}} = \Delta_{12} + \Delta_{134} + \Delta_{234} + \Delta_{1234}$. However, note that these polytopes do not have all the same dimension (even though they all live in $\mathbb{R}^3$ as deformations of $\mathsf{Nest}_{\mathcal{B}}$), and the last ray (rightmost polytope in Figure 23) do not correspond to a simplex. On the other side, the interior of $\mathbb{DC}(\mathcal{F}(\mathcal{B}))$ correspond to polytopes normally equivalent to $\mathsf{Nest}_{\mathcal{B}}$.

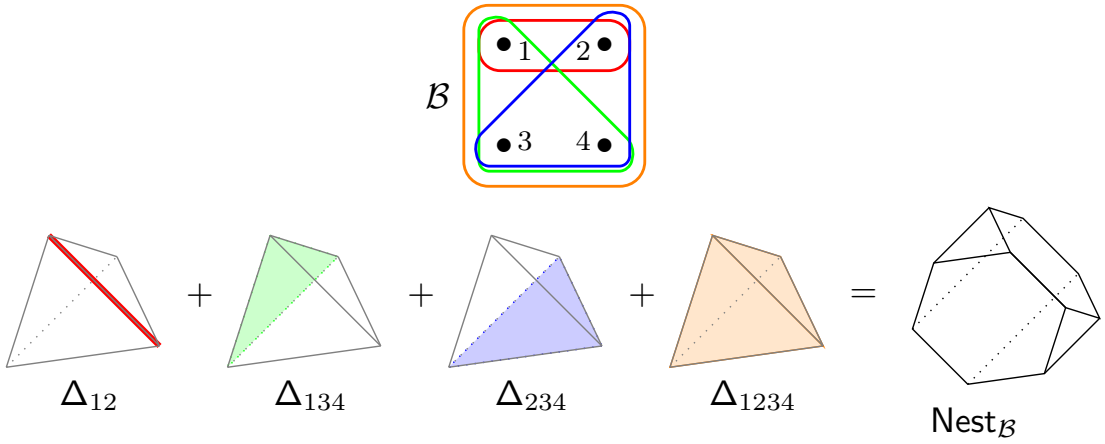

Figure 22: (Top) A building set $\mathcal{B}$ on 4 elements with 4 (no-singleton) blocks, (Bottom) the corresponding $\mathsf{Nest}_{\mathcal{B}}$ described as the Minkowski sum of faces of the standard simplex Δ_{1234}.

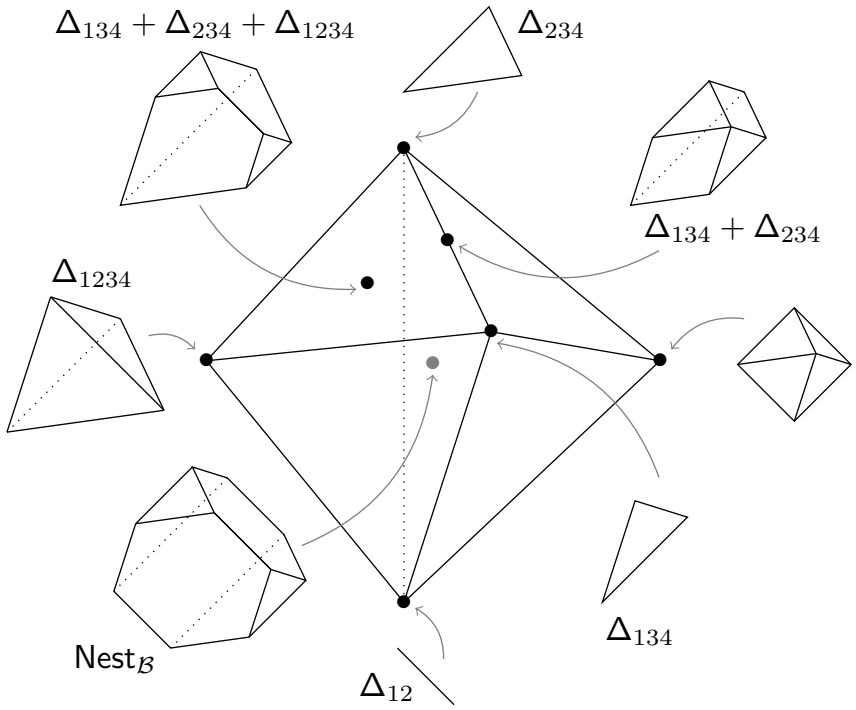

Figure 23: A 3-dimensional affine section of the deformation cone $\mathbb{DC}(\mathcal{F}(\mathcal{B}))$ for the building set of Example 2.65 and Figure 22. The deformations of $\mathsf{Nest}_{\mathcal{B}}$ corresponding to some of the points of $\mathbb{DC}(\mathcal{F}(\mathcal{B}))$ are depicted. Especially, all points in the interior correspond to polytopes normally equivalent to $\mathsf{Nest}_{\mathcal{B}}$, while the rightmost polytope is not a simplex. See also Figure 12 for the case of the complete graph on 3 vertices.

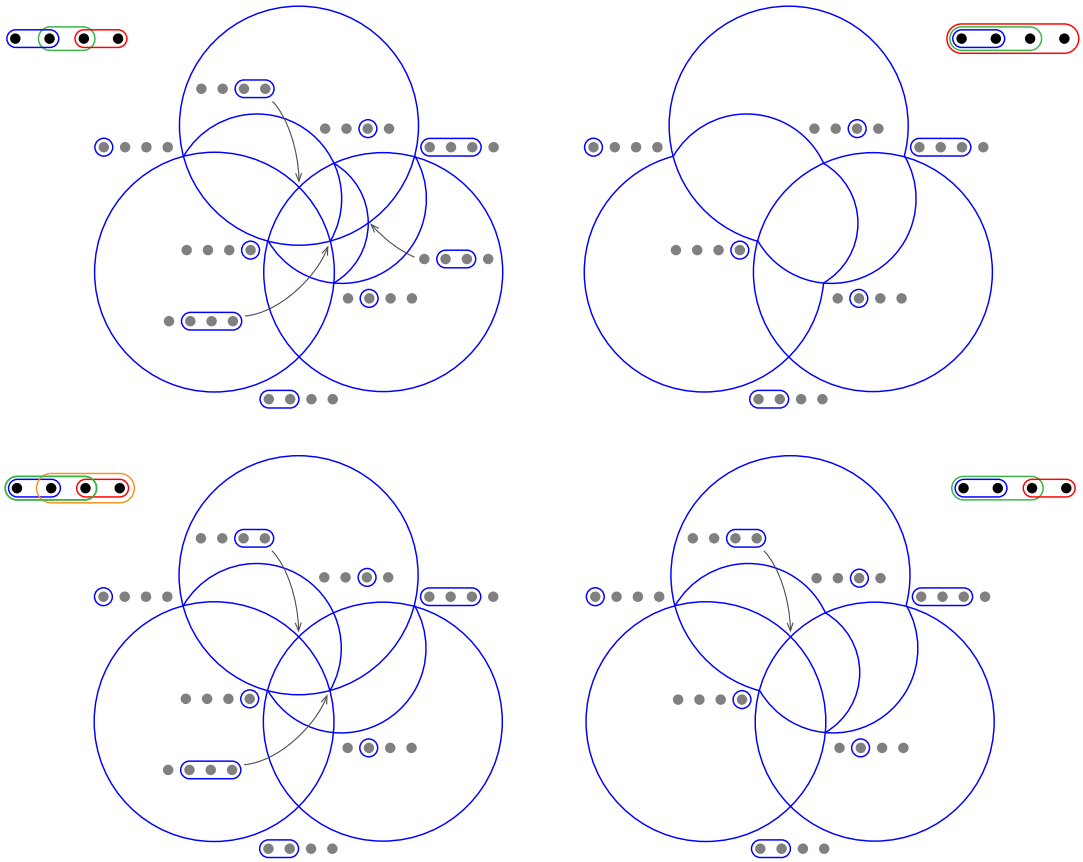

Figure 24: Four interval nested fans. The top left one is the sylvester fan, the top right one is the Pitman-Stanley fan, the bottom left one is the freehedron fan, and only the top right one is a fertilotope fan. The rays are labeled by the corresponding blocks. As the fans are 3-dimensional, we intersect them with the sphere and stereographically project them from the direction $(-1,-1,-1)$.

2.3.3 Simplicial deformation cones and interval building sets

To conclude this section, we characterize the building sets $\mathcal{B}$ whose nested fan $\mathcal{F}(\mathcal{B})$ has a simplicial deformation cone and study in more details a specific family of such building sets.

Proposition 2.66. *The deformation cone $\mathbb{DC}(\mathcal{F}(\mathcal{B}))$ is simplicial if and only if all blocks of $\mathcal{B}$ with at least three distinct maximal strict sub-blocks are elementary.*

Proof. Recall that the nested fan $\mathcal{F}(\mathcal{B})$ has dimension $|V|-|\kappa(\mathcal{B})|$ and has $|\mathcal{B}|-|\kappa(\mathcal{B})|$ rays. Hence, the deformation cone $\mathbb{DC}(\mathcal{F}(\mathcal{B}))$ is simplicial if and only if it has $|\mathcal{B}|-|V|$ facets. The statement thus immediately follows from Corollary 2.64. □

We conclude this section by focussing on the following special family of building sets which fulfills Proposition 2.66 and is illustrated in Figure 24.

Definition 2.67. An *interval building set* is a building set on $[n] := \{1,\dots,n\}$ whose blocks are some intervals. We call *interval nested fan* and *interval nestohedron* the nested fan and nestohedron of an interval building set.

Example 2.68. Particularly relevant examples of interval nestohedra include:

- the classical associahedron of [SS93, Lod04, PSZ23] for the building set with all intervals of $[n]$,

- the Pitman-Stanley polytope of [SP02] for the building set with all singletons $\{i\}$ and all initial intervals $[i]$ for $i \in [n]$,
- the freehedron of [San09] for the building set with all singletons $\{i\}$, all initial intervals $[i]$ for $i \in [n]$, and all final intervals $[n] \smallsetminus [i]$ for $i \in [n-1]$,
- the fertilotopes of [Def21] for the binary building sets defined as the interval building sets where any two intervals are either nested or disjoint.

Note that, by definition, any interval nested fan coarsens the associahedron nested fan, so all the above examples are deformations of the associahedron.

Proposition 2.69. *For any interval building set $\mathcal{B}$, the deformation cone $\mathbb{DC}(\mathcal{F}(\mathcal{B}))$ is simplicial.*

Proof. We give two proofs of this fact.

(Proof with the tools of this section). Assume that $\mathcal{B}$ has a non-elementary block $[i,j]$, with at least three distinct maximal strict sub-blocks $[a,b]$, $[c,d]$ and $[e,f]$. Since $[a,b]$, $[c,d]$ and $[e,f]$ are pairwise non nested, we can assume up to permutation that $a < c < e$ and $b < d < f$. Since $[i,j]$ is not elementary, $[a,b] \cap [c,d] \neq \varnothing$ and thus $[a,b] \cup [c,d] = [a,d]$ is a block of $\mathcal{B}$. This contradicts the maximality of $[a,b]$ since $[a,b] \subsetneq [a,d] \subsetneq [i,j]$ as $b < d < f \leq j$.

(Proof with using deformations). As interval nestohedra are deformation of the associahedron, by Proposition 2.4 their deformation cone is a face of the deformation cone of the associahedron which is simplicial (see Proposition 2.35). □

Remark 2.70. Note that there are building sets $\mathcal{B}$ for which the deformation cone $\mathbb{DC}(\mathcal{F}(\mathcal{B}))$ is simplicial, but which are not (isomorphic to) interval building sets. See *e.g.* Figure 19(Left).

We now translate the facet description of Corollary 2.63 to the specific case of interval building sets. We need a few additional notations. Consider an interval building set $\mathcal{B}$ on $[n]$. For $1 \leq i < j \leq n$, define

$$\ell(i,j) := \min\{k \in [i+1, j] \;;\; [k,j] \in \mathcal{B}\} \qquad \text{and} \qquad r(i,j) := \max\{k \in [i, j-1] \;;\; [i,k] \in \mathcal{B}\}.$$

Note that $\ell(i,j)$ and $r(i,j)$ are well-defined since $\mathcal{B}$ contain all singletons. Observe that $[i, r(i,j)]$ and $[\ell(i,j), j]$ are maximal strict subblocs of $[i,j]$. Therefore,

- if $[i,j] \in \mathcal{B}$ is elementary, then we have $r(i,j) < \ell(i,j)$ and the maximal strict sub-blocks of $[i,j]$ are the intervals $[s_{k-1}(i,j), s_k(i,j) - 1]$ for $k \in [p]$ where the sequence $s_0(i,j) < s_1(i,j) < \cdots < s_p(i,j)$ is defined by the boundary conditions $s_0(i,j) := i$ and $s_1(i,j) = r(i,j) + 1$ and $s_p(i,j) := j+1$, and the induction $s_k(i,j) := r(s_{k-1}(i,j), j+1) + 1$.
- if $[i,j] \in \mathcal{B}$ is not elementary, we have $\ell(i,j) \leq r(i,j)$ so that

  $$[i, r(i,j)] \cup [\ell(i,j), j] = [i,j] \qquad \text{and} \qquad [i, r(i,j)] \cap [\ell(i,j), j] = [\ell(i,j), r(i,j)].$$

  Thus $[i, r(i,j)]$ and $[\ell(i,j), j]$ are the only maximal strict sub-blocks of $[i,j]$. Moreover, the connected components of $[i, r(i,j)] \cap [\ell(i,j), j] = [\ell(i,j), r(i,j)]$ are the intervals $[t_{k-1}(i,j), t_k(i,j) - 1]$ for $k \in [q]$ where the sequence $t_0(i,j) < t_1(i,j) < \cdots < t_q(i,j)$ is defined by the boundary conditions $t_0(i,j) := \ell(i,j)$ and $t_q(i,j) := r(i,j) + 1$, and the induction $t_k(i,j) := r(t_{k-1}(i,j), r(i,j) + 1) + 1$.

Using these notations, the following statement is just a translation of Corollary 2.63.

Proposition 2.71. *Consider an interval building set $\mathcal{B}$ on $[n]$ and let $\mathcal{B}^\star := \mathcal{B} \smallsetminus \{\{i\} \;;\; i \in [n]\}$ denote the blocks which are not singletons. Then the inequalities*

- $\sum_{k \in [p]} \boldsymbol{h}_{[s_{k-1}(i,j), s_k(i,j)-1]} \geq \boldsymbol{h}_{[i,j]}$ *for all* $[i,j] \in \mathcal{B}^\star$ *with* $r(i,j) < \ell(i,j)$,
- $\boldsymbol{h}_{[i,r(i,j)]} + \boldsymbol{h}_{[\ell(i,j),j]} \geq \boldsymbol{h}_{[i,j]} + \sum_{k \in [q]} \boldsymbol{h}_{[t_{k-1}(i,j), t_k(i,j)-1]}$ *for all* $[i,j] \in \mathcal{B}^\star$ *with* $\ell(i,j) \leq r(i,j)$,

provide an irredundant facet description of the deformation cone $\mathbb{DC}(\mathcal{F}(\mathcal{B}))$.

Example 2.72. For instance

- for the building set containing all intervals of $[n]$, we have $\ell(i,j) = i+1$ and $r(i,j) = j-1$, so that the facet defining inequalities of the deformation cone are $\boldsymbol{h}_{[i,j-1]} + \boldsymbol{h}_{[i+1,j]} \geq \boldsymbol{h}_{[i,j]} + \boldsymbol{h}_{[i+1,j-1]}$ for all $1 \leq i < j \leq n$ (with the convention that $\boldsymbol{h}_{[i+1,j-1]} = 0$ for $i+1 = j$), this is the facet description of the deformation cone of the associahedron;
- for the building set containing all singletons $\{i\}$ and all intervals $[i]$ for $i \in [n]$, we have $r(1,j) = j-1 < j = \ell(1,j)$, so that the facet defining inequalities of the deformation cone are $\boldsymbol{h}_{[j-1]} + \boldsymbol{h}_{\{j\}} \geq \boldsymbol{h}_{[j]}$ for all $1 < j \leq n$.

Generalizing Proposition 2.36, we finally combine Propositions 2.66 and 2.71 to define *kinematic nestohedra* for interval building sets, similar to the constructions of [AHBHY18, BMDM+18, PPPP19] for associahedra, cluster associahedra and gentle associahedra. Again, these polytopes are just affinely equivalent to the realizations in $\mathbb{R}^n$, but they should be more natural from a mathematical physics' perspective.

Proposition 2.73. *Consider an interval building set* $\mathcal{B}$ *on* $[n]$ *and let* $\mathcal{B}^\star := \mathcal{B} \smallsetminus \{\{i\} \,;\, i \in [n]\}$ *denote the blocks which are not singletons. Then for any* $\boldsymbol{p} \in \mathbb{R}^{\mathcal{B}^\star}_{>0}$*, the polytope* $R_{\boldsymbol{p}}(\mathcal{B}) \subseteq \mathbb{R}^{\mathcal{B}}$ *defined as the intersection of the positive orthant* $\{\boldsymbol{z} \in \mathbb{R}^{\mathcal{B}} \,;\, \boldsymbol{z} \geq 0\}$ *with the hyperplanes*

- $\boldsymbol{z}_K = 0$ *for* $K \in \kappa(\mathcal{B})$,
- $\sum_{k\in[p]} \boldsymbol{z}_{[s_{k-1}(i,j),s_k(i,j)-1]} - \boldsymbol{z}_{[i,j]} = \boldsymbol{p}_{[i,j]}$ *for* $[i,j] \in \mathcal{B}^\star$ *with* $r(i,j) < \ell(i,j)$,
- $\boldsymbol{z}_{[i,r(i,j)]} + \boldsymbol{z}_{[\ell(i,j),j]} - \boldsymbol{z}_{[i,j]} - \sum_{k\in[q]} \boldsymbol{z}_{[t_{k-1}(i,j),t_k(i,j)-1]} = \boldsymbol{p}_{[i,j]}$ *for* $[i,j] \in \mathcal{B}^\star$ *with* $\ell(i,j) \leq r(i,j)$,

is a nestohedron whose normal fan is the nested fan $\mathcal{F}(\mathcal{B})$*. Moreover, the polytopes* $R_{\boldsymbol{p}}(\mathcal{B})$ *for* $\boldsymbol{p} \in \mathbb{R}^{\mathcal{B}^\star}_{>0}$ *describe all polytopal realizations of* $\mathcal{F}(\mathcal{B})$ *(up to translations).*

We end this discussion on nestohedra with a simplicial deformation cone by proving the equivalent of Corollary 2.17 in this setting, and thanking Vic Reiner for pointing us the question:

Theorem 2.74. *For a building set* $\mathcal{B}$*, all deformations of its nestohedron* $\mathsf{Nest}_{\mathcal{B}}$ *are nestohedra if and only if* $\mathcal{B}$ *has only elementary blocks. In this case, its deformations are exactly all (the polytopes normally equivalent to) the* $\mathsf{Nest}_{\mathcal{C}}$ *for* $\mathcal{C}$ *a sub-building set of* $\mathcal{B}$*.*

Proof. It is straitghforward that all $\mathsf{Nest}_{\mathcal{C}}$ for $\mathcal{C}$ a sub-building set of $\mathcal{B}$ are deformations of $\mathsf{Nest}_{\mathcal{B}}$, as they appear as Minkowski summand: $\mathsf{Nest}_{\mathcal{B}} = \sum_{B\in\mathcal{B}} \Delta_B = \mathsf{Nest}_{\mathcal{C}} + \sum_{B\in\mathcal{B}\smallsetminus\mathcal{C}} \Delta_B$. On the other hand, if $\mathcal{C}$ is a building set that is not a sub-building set of $\mathcal{B}$, then it contains a block $C \in \mathcal{C} \smallsetminus \mathcal{B}$, so Δ_C is a deformation of $\mathsf{Nest}_{\mathcal{C}}$ but not of $\mathsf{Nest}_{\mathcal{B}}$ (the faces of the standard simplex that are deformations of $\mathsf{Nest}_{\mathcal{B}}$ are precisely the Δ_B for $B \in \mathcal{B}$). This proves that the only deformations of $\mathsf{Nest}_{\mathcal{B}}$ that are nestohedra are the $\mathsf{Nest}_{\mathcal{C}}$ for $\mathcal{C}$ a sub-building set of $\mathcal{B}$.

Besides, note that if $\mathbb{DC}(\mathcal{F}(\mathcal{B}))$ is not simplicial, then some of its rays correspond to deformations of $\mathsf{Nest}_{\mathcal{B}}$ that are not (sums of) faces of the standard simplex, hence not nestohedra. Thus, we consider the case where $\mathbb{DC}(\mathcal{F}(\mathcal{B}))$ is simplicial. It has $2^{|\mathcal{B}|-|V|}$ faces, so all deformations of $\mathsf{Nest}_{\mathcal{B}}$ are nestohedra if and only if $\mathcal{B}$ has $2^{|\mathcal{B}|-|V|}$ sub-building sets. That is only the case when all blocks of $\mathcal{B}$ are elementary. Indeed, if $B \in \mathcal{B}$ is not elementary, then $\mathcal{B} \smallsetminus \{B\}$ is not a building set (it does not respect the intersection property), so $\mathcal{B}$ has strictly less than $2^{|\mathcal{B}|-|V|}$ sub-building sets. □

2.3.4 Perspectives and open questions

Computational remarks The computation of deformation cones of nestohedra have been implemented with Sage, allowing us to construct numerous examples that helped us to build the main proofs of this section. Thanks to this code, one can input a building set $\mathcal{B}$ and compute the deformation cone of is nestohedron as the cone of heights in $\mathbb{R}^{\mathcal{B}}$, illustrating Corollary 2.63. As the fan $\mathcal{F}(\mathcal{B})$ is simplicial, the direct implementation of Proposition 2.2 can be used for this computation.

Assets and limits of the current approach, open questions We have computed in this section the deformation cones of two families of generalized permutahedra: graphical zonotopes on the one side, and nestohedra on the other. The final goal would be to understand the full submodular cone, *i.e.* the deformation cone of the permutahedron, answering a longstanding question opened since the 70s [Edm70]. However, two intermediate questions seem to be particularly interesting.

The first one is the computation of the deformation cone of hypergraphic polytopes. Hypergraphic polytopes are the pendant of graphical zonotopes for general hypergraphs: fix a collection H of subsets of $[n]$ and define the associated hypergaphic polytope as the Minkowski sum of the corresponding face of the standard simplex: $\mathsf{P}_H := \sum_{C \in H} \Delta_C$. This family encapsulates both graphical zonotopes and nestohedra. The deformation of a hypergraphic polytope is again a hypergraphic polytope, and this family can be thought of as the sub-cone of the submodular cone generated by the faces of the standard simplex. However, deformations of hypergraphic polytopes are more difficult to handle than the families studied in this section, as their normal fan is not in general simplicial, and the combinatorial resources we can use are not as rich as in the case of graphs. As stated in [PPP22a], we are able to give an explicit basis of the linear span of the deformation cone of the hypergraphic polytopes: as in the case of graphical zonotopes (see Theorem 2.11), it is formed by the *induced cliques* of the hypergraph. We also applied Proposition 2.3 to hypergraphic polytopes, but only obtained a highly redundant description of the deformation cone of hypergraphic polytopes.

Generalized permutahedra go beyond hypergraphic polytopes, and some other families could be both not-too-hard to tackle, and rich enough to improve our knowledge of the submodular cone. In particular, quotientopes [PS19] seem to fall in this category. We have already determined which quotientopes have a simplicial deformation cone, but giving a facet description of their deformation cone in general seems more involved.

Last but not least, even if we focused here on giving a facet-description of interesting faces of the submodular cone, the question of computing its rays remain open since Edmonds [Edm70], even in the cases we studied. It is worth noting that the facet-description we provide allow for computer experiments in higher dimensions than before (for the specific cases of graphical zonotopes and nestohedra), and may help to find new examples of rays for the submodular cone. These rays can be thought of as explicit height vectors, or looked upon as their polytopal counterpart.

3 Max-slope pivot rule polytopes

J'ai appris que la voie du progrès n'était ni rapide ni facile.
Dans la vie, rien n'est à craindre, tout est à comprendre.
– Marie Curie

3.1 Max-slope pivot rule and max-slope pivot polytope

For a linear program $(\mathsf{P}, \boldsymbol{c})$, the choice of a $\boldsymbol{c}$-improving neighbor of a vertex $\boldsymbol{v} \in V(\mathsf{P})$ is determined by the pivot rule adopted by the simplex method, see Section 1.3. Beside varying the objective function of a linear program, one can wonder about the behavior of different pivot rules. Recall that the pivot rule is called *memoryless* if the choice is deterministic and based only on the knowledge of $\boldsymbol{v}$. Among pivot rules, max-slope pivot rules are of a great theoretical and practical importance. First observe that linear programming is easy in dimension 2: for a polygon in the plane, the monotone path chosen by the simplex method is either the upper path of the polygon or its lower path, see the exterior of Figure 25(Left). Thus, for a linear program $(\mathsf{P}, \boldsymbol{c})$, the idea of a *max-slope pivot rule* is to choose a secondary vector $\boldsymbol{\omega}$, linearly independent with $\boldsymbol{c}$, then to project P onto the plane defined by $(\boldsymbol{c}, \boldsymbol{\omega})$. The path chosen by the simplex method is defined, by convention, to be the upper path of this 2-dimensional projection of P.

Thereby, a max-slope pivot rule depends on one parameter $\boldsymbol{\omega}$, but several $\boldsymbol{\omega}$ can give the same monotone path. A monotone path $\mathcal{P}$ on P is said to be coherent if there exists $\boldsymbol{\omega}$ such that $\mathcal{P}$ is the path followed by the simplex method with the max-slope pivot rule associated to $\boldsymbol{\omega}$, see Figure 25(Left). The set of coherent paths on P can be seen as the set of vertices of a polytope, called its *monotone path polytope* $\mathsf{M}_{\boldsymbol{c}}(\mathsf{P})$, we will discuss this construction in more details in Section 4.2.1.

When studying the monotone path polytope, one focuses on the behavior of the pivot rule only on the monotone path that the simplex method walks on when starting from the worst vertex (the vertex $\boldsymbol{v}_0$ minimizing $\langle \boldsymbol{v}, \boldsymbol{c} \rangle$), and going towards the optimal vertex (the vertex $\boldsymbol{v}_{\text{opt}}$ maximizing $\langle \boldsymbol{v}, \boldsymbol{c} \rangle$). But besides this, one can also look at all the monotone paths at once, *i.e.* the combinatorial behavior the pivot rule has on all the vertices of the polytope, see [BDLLS22]: each vertex points towards the one of its neighbor improving $\langle \boldsymbol{v}, \boldsymbol{c} \rangle$ that maximizes the slope $\frac{\langle \boldsymbol{\omega}, \boldsymbol{u}-\boldsymbol{v} \rangle}{\langle \boldsymbol{c}, \boldsymbol{u}-\boldsymbol{v} \rangle}$. As depicted in Figure 25(Right), for a given linear program $(\mathsf{P}, \boldsymbol{c})$, and a secondary direction $\boldsymbol{\omega}$, the associated arborescence is a function $A^{\boldsymbol{\omega}} : V(\mathsf{P}) \smallsetminus \{\boldsymbol{v}_{\text{opt}}\} \to V(\mathsf{P})$ defined by (where "argmax" designate the unique maximizer of the studied quantity):

$$A^{\boldsymbol{\omega}}(\boldsymbol{v}) = \operatorname{argmax} \left\{ \frac{\langle \boldsymbol{\omega}, \boldsymbol{u} - \boldsymbol{v} \rangle}{\langle \boldsymbol{c}, \boldsymbol{u} - \boldsymbol{v} \rangle} \ ; \ \boldsymbol{u} \text{ improving neighbor of } \boldsymbol{v} \right\}$$

Conversely, a function $A : V(\mathsf{P}) \smallsetminus \{\boldsymbol{v}_{\text{opt}}\} \to V(\mathsf{P})$ is said to be a *coherent arborescence* or a *max-slope arborescence* when there exists $\boldsymbol{\omega}$ such that $A = A^{\boldsymbol{\omega}}$. Note that coherent arborescences are necessary monotone in the sense that $\langle A(\boldsymbol{v}), \boldsymbol{c} \rangle > \langle \boldsymbol{v}, \boldsymbol{c} \rangle$ for all $\boldsymbol{v} \in V(P) \smallsetminus \{\boldsymbol{v}_{\text{opt}}\}$, we call *arborescence* a function that satisfies this monotonicity property, and extend A to $V(\mathsf{P})$ by setting $A(\boldsymbol{v}_{\text{opt}}) = \boldsymbol{v}_{\text{opt}}$ when convenient. As for coherent monotone paths, the set of coherent arborescences can be embedded as the vertices of a polytope. We give several ways to construct this polytope. To begin with, one can construct a fan whose maximal cones are $\mathsf{C}_A = \{\boldsymbol{\omega} \ ; \ A^{\boldsymbol{\omega}} = A\}$ for A a (coherent) arborescence on P: Figure 26 shows how to gather all coherent arborescences for the case of the 3-dimensional simplex, while Figure 27 pictures the resulting fan.

For a fixed linear program $(\mathsf{P}, \boldsymbol{c})$ and an arborescence $A : V(\mathsf{P}) \to V(\mathsf{P})$ define

$$\Psi(A) \ := \sum_{v \neq \boldsymbol{v}_{\text{opt}}} \frac{1}{\langle \boldsymbol{c}, A(v) - v \rangle} (A(v) - v) \, .$$

The *max-slope pivot rule polytope* is defined as

$$\Pi(\mathsf{P}, \boldsymbol{c}) \ := \ \operatorname{conv}\{\Psi(A) : A \text{ arborescence of } (\mathsf{P}, \boldsymbol{c})\} \, .$$

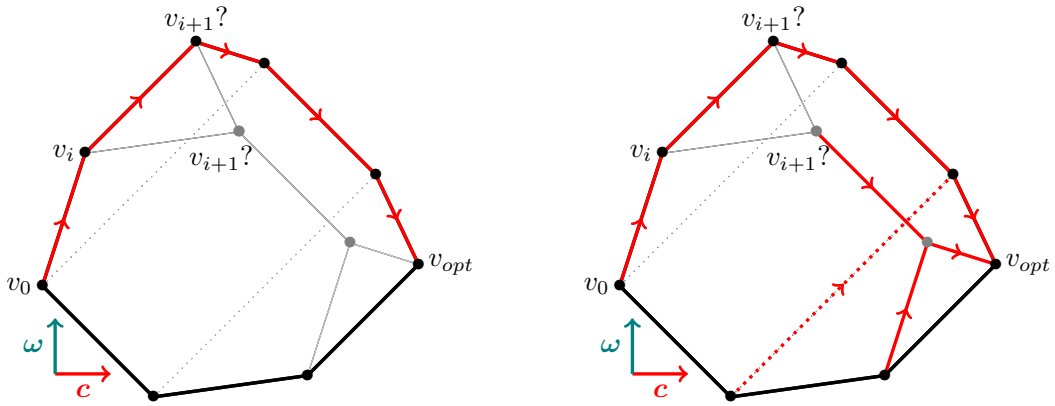

Figure 25: (Left) In red, the coherent monotone path associated to the parameter $\boldsymbol{\omega}$ for the linear problem $(\mathsf{P}, \boldsymbol{c})$. (Right) In red, the coherent arborescence associated to the same parameter. In both figures, to each vertex, the pivot rule associates the one of its neighbors that maximizes the slope in the plane $(\boldsymbol{c}, \boldsymbol{\omega})$.

The following special case of [BDLLS22, Theorem 1.4] states that the pivot rule polytope captures the combinatorics of max-slope arborescences, as its normal fan is the fan constructed above. For a polytope $\mathsf{Q} \subset \mathbb{R}^d$ and $\boldsymbol{\omega} \in \mathbb{R}^d$, we denote as usual (see Section 1.2) $\mathsf{Q}^{\boldsymbol{\omega}} = \{x \in \mathsf{Q} \ ; \ \langle \boldsymbol{\omega}, x\rangle \geq \langle \boldsymbol{\omega}, y\rangle \text{ for all } y \in \mathsf{Q}\}$ the face of Q that maximizes $\boldsymbol{\omega}$.

Theorem 3.1 ([BDLLS22])**.** *Let $\mathsf{P} \subset \mathbb{R}^d$ be a polytope of dimension k and $\boldsymbol{c} \in \mathbb{R}^d$ a generic objective function. The polytope $\Pi(\mathsf{P}, \boldsymbol{c})$ is of dimension $k-1$ and for any generic $\boldsymbol{\omega} \in \mathbb{R}^d$: $\Pi(\mathsf{P}, \boldsymbol{c})^{\boldsymbol{\omega}} = \{\Psi(A^{\boldsymbol{\omega}})\}$.*

In particular, the vertices of $\Pi(\mathsf{P}, \boldsymbol{c})$ are in bijection to max-slope arborescences of $(\mathsf{P}, \boldsymbol{c})$. The faces of $\Pi(\mathsf{P}, \boldsymbol{c})$ are in correspondence to certain *multi-arborescences*, that is, maps $\mathcal{A} : V(\mathsf{P}) \to 2^{V(\mathsf{P})}$ such that for all $\boldsymbol{v} \neq \boldsymbol{v}_{\text{opt}}$, $\mathcal{A}(\boldsymbol{v})$ is a nonempty subset of $\boldsymbol{c}$-improving neighbors of $\boldsymbol{v}$, see Section 3.3.

The max-slope pivot polytope can also be constructed as a sum of sections of P, see Figure 28: for each vertex $\boldsymbol{v} \in V(\mathsf{P})$, consider the convex hull $\operatorname{conv}\big(\{\boldsymbol{v}\} \cup \{\boldsymbol{u} \ ; \ \boldsymbol{u} \text{ improving neighbor of } \boldsymbol{v}\}\big)$ and take a section orthogonal to $\boldsymbol{c}$ close to $\boldsymbol{v}$ (which correspond to the vertex figure at $\boldsymbol{v}$). The Minkowski sum of these sections for $\boldsymbol{v} \in V(\mathsf{P}) \smallsetminus \{\boldsymbol{v}_{\text{opt}}\}$ is (a dilate of) $\Pi(\mathsf{P}, \boldsymbol{c})$. For instance, Figure 28 illustrates the fact that the max-slope pivot polytope of any simplex (for any generic objective function) is an associahedron [BDLLSon], see also Section 3.3.1 for a self-contained proof of this fact. We give here a first description of this result. Let S be a simplex of dimension $n-1$. We may assume that the vertices $\boldsymbol{v}_1, \boldsymbol{v}_2, \dots, \boldsymbol{v}_n$ are labelled in such a way that $\langle \boldsymbol{c}, \boldsymbol{v}_1\rangle < \langle \boldsymbol{c}, \boldsymbol{v}_2\rangle < \cdots < \langle \boldsymbol{c}, \boldsymbol{v}_n\rangle$. As $V(\mathsf{S})$ is in bijection with $[n]$, an arborescence of $(\mathsf{S}, \boldsymbol{c})$ is encoded by a map $A : [n] \to [n]$ such that $A(n) = n$ and $A(i) > i$ for $i = 1, \dots, n-1$. We sometimes identify A with the collection of pairs $(i, A(i))$ and write $(i,k) \in A$ if $A(i) = k$. We call an arborescence $A : [n] \to [n]$ *non-crossing* if for all $i < j$ if $j < A(i)$, then $A(j) \leq A(i)$. In other words, there are no $i < a < j < b$ such that $(i,j), (a,b) \in A$, see Figure 32(Right) for an example. Non-crossing arborescences form a Catalan family in the sense of Section 1.2.4, we detail here some of their properties. It is straightforward, that for any polytope P whose graph is the complete graph, all coherent arborescences on P are non-crossing, see Figure 29 for an illustration.

Theorem 3.2 ([BDLLSon])**.** *Let S be an $(n-1)$-simplex and $\boldsymbol{c}$ a generic objective function. An arborescence A is a max-slope arborescence for $(\mathsf{S}, \boldsymbol{c})$ if and only if A is non-crossing. Moreover, $\Pi(\mathsf{S}, \boldsymbol{c})$ is combinatorially isomorphic to Asso_{n-2}.*

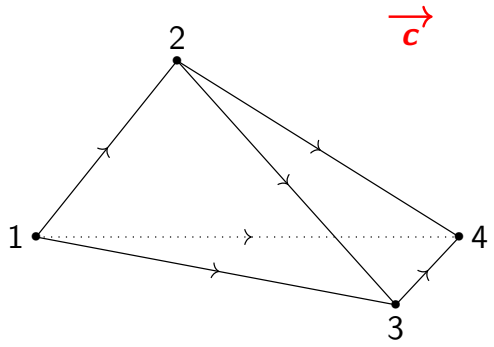

Figure 26: Animated construction of the normal fan of the max-slope pivot polytope of the 3-dimensional simplex. For each $\boldsymbol{\omega} \in \mathbb{R}^3$ orthogonal to $\boldsymbol{c}$, we project Δ_3 onto the plane $(\boldsymbol{c}, \boldsymbol{\omega})$ (Left), and record the corresponding coherent arborescence (Right). *(Animated figures obviously do not display on paper, and some PDF readers do not support the format: it is advised to use Adobe Acrobat Reader. If no solution is suitable, the animation can be found on my website or asked by email.)*

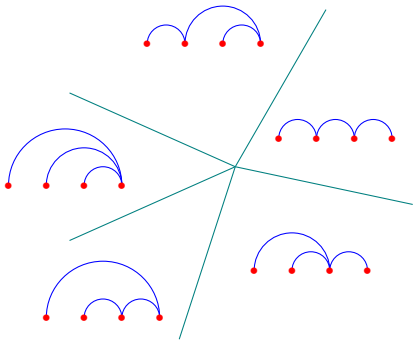

Figure 27: Normal fan of $\Pi(\Delta_3, \boldsymbol{c})$ where each maximal cone is labelled by the corresponding coherent arborescence.

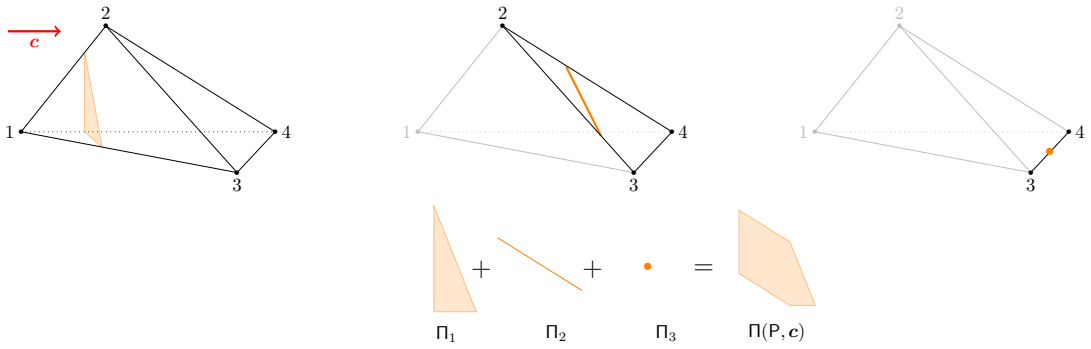

Figure 28: The max-slope pivot rule polytope $\Pi(\mathsf{P}, \boldsymbol{c})$ can be obtained as (a dilate of) the Minkowski sum of sections, here illustrated for the tetrahedron $\mathsf{P} = \Delta_3$. For each vertex $\boldsymbol{v} \in V(\mathsf{P})$, consider the convex hull that $\boldsymbol{v}$ forms with its improving neighbors, and take a section of it orthogonal to $\boldsymbol{c}$ (close to $\boldsymbol{v}$). Their sum is normally equivalent to $\Pi(\mathsf{P}, \boldsymbol{c})$.

Example 4.3 in [BDLLS22] illustrates the max-slope polytope of a simplex. Theorem 3.2 is discussed in the more general context of pivot associahedra in [BDLLSon]. Here, we give the main results and ideas. We will use the following simple decomposition of non-crossing arborescences.

Proposition 3.3. *For a non-crossing arborescence $A : [n] \to [n]$ define $r(A)$ as the minimal $r \geq 1$ such that $A(r) = n$. Restricting A to $[r]$ and to $[r+1, n] := \{r+1, \dots, n\}$ yields two non-crossing arborescences A' and A'' and A is uniquely determined by (r, A', A'').*

Proposition 3.3 immediately gives a recursive way to compute the number of non-crossing arborescences (identical to the recursive formula of Section 1.2.4), which shows that there are Catalan-many non-crossing arborescences. To check that $\Pi(\mathsf{P}, \boldsymbol{c})$ is indeed combinatorially isomorphic to the associahedron, it suffices to determine the graph of $\Pi(\mathsf{P}, \boldsymbol{c})$ and use the fact that simple polytopes are determined by their graph [BML87]; see also [Zie98, Chapter 3.4]. We call an $i < n$ *forward-sliding* if $A(i) \neq n$ and there is no $j < i$ with $A(j) = A(i)$. We call i *backward-sliding* if $A(i) \neq i + 1$. If i is forward-sliding, then define $F_i A$ by $F_i A(i) := A(A(i))$ and $F_i A(k) := A(k)$ for all $k \neq i$. Likewise, if i is backward-sliding, then define $B_i A(i) := j$ where $j > i$ is minimal with $A(j) = A(i)$ and $B_i A(k) = A(k)$ for $k \neq i$. A quick scribble reveals that both $B_i A$ and $F_i A$ are non-crossing, and that $B_i F_i A = A$ and $F_i B_i A = A$. As for all Catalan families, we say that $B_i A$ and $F_i A$ differ from A by a *flip*. To summarize, non-crossing arborescences form a Catalan family, and flips in this family are forward- or backward-slide.

The following proposition is adapted from [BDLLSon] or Theorem 3.69.

Proposition 3.4. *Let $A_1, A_2 : [n] \to [n]$ be non-crossing arborescences. Then $[\Psi(A_1), \Psi(A_2)]$ is an edge of $\Pi(\mathsf{S}, \boldsymbol{c})$ if and only if A_1, A_2 differ by a flip.*

As for the proof's strategy of Theorem 3.2, let us first note that up to linear transformation, we may assume that $\mathsf{S} = \Delta_{n-1} := \operatorname{conv}(\boldsymbol{e}_1, \dots, \boldsymbol{e}_n) \subset \mathbb{R}^n$. For a given $\boldsymbol{\omega} \in \mathbb{R}^n$, define $p_i = (c_i, \omega_i)$ for $i \in [n]$ and the *slope* $\tau(i, j) = \frac{\omega_j - \omega_i}{c_j - c_i}$ for all $1 \leq i < j \leq n$. Then A is a max-slope arborescence on S if and only if there is $\boldsymbol{\omega} \in \mathbb{R}^n$ such that

$$\tau(i, A(i)) \;>\; \tau(i, k) \quad \text{for all } k > i \text{ and } k \neq A(i)$$

Pictorially, consider the points $p_1, \dots, p_n \in \mathbb{R}^2$. Then $A(i) = j$ if all points p_k for $i < k \neq j$ are strictly below the line $\overline{p_i p_j}$, see Figure 32(Left). This perspective yields the following key insight:

Lemma 3.5. *For $1 \leq r < s < t \leq n$*

$$\tau(r, t) > \tau(r, s) \iff \tau(s, t) > \tau(r, t) \quad \text{and} \quad \tau(r, t) < \tau(r, s) \iff \tau(s, t) < \tau(r, t)$$

Proof. The following convex combination gives the result: $\tau(r, t) = \frac{c_r - c_s}{c_t - c_r} \tau(r, s) + \frac{c_t - c_r}{c_t - c_r} \tau(s, t)$. □

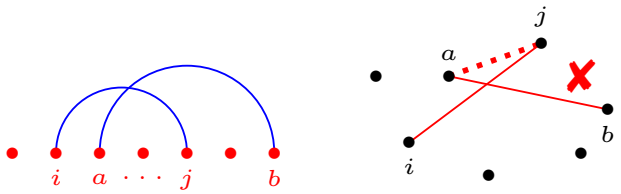

Figure 29: Coherent arborescences on a polytope whose graph is complete are non-crossing. For $i < a < j < b$ with $A(i) = j$, then Lemma 3.5 ensures that $\frac{\langle \boldsymbol{\omega}, \boldsymbol{v}_j - \boldsymbol{v}_a \rangle}{\langle \boldsymbol{\omega}, \boldsymbol{v}_j - \boldsymbol{v}_a \rangle} > \frac{\langle \boldsymbol{\omega}, \boldsymbol{v}_b - \boldsymbol{v}_a \rangle}{\langle \boldsymbol{\omega}, \boldsymbol{v}_b - \boldsymbol{v}_a \rangle}$, so $A(a) = b$ is impossible.

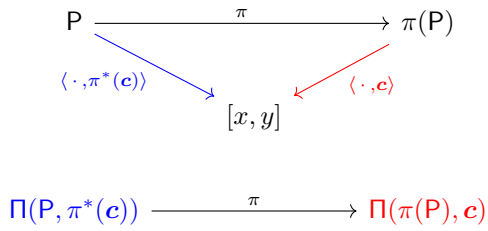

Figure 30: **When the graph of P is isomorphic to the graph of $\pi(\mathsf{P})$**, then the max-slope polytope of $\pi(\mathsf{P})$ is a projection of the one of P. We denote $x = \langle \boldsymbol{v}_0, \boldsymbol{c} \rangle$ and $y = \langle \boldsymbol{v}_{\text{opt}}, \boldsymbol{c} \rangle$.

The monotone path polytope construction behaves functorially with respect to linear projections, see Section 4.1, that is, if $\pi : \mathsf{P} \to \mathsf{Q}$ is a projection of polytopes, then the monotone path polytope of Q is a projection of the one of P. This does not hold for max-slope pivot polytopes in general. However, it does hold in the special case when graphs are retained under projection, see Figure 30. This first new result will help us link the max-slope pivot rule polytope of cyclic polytopes with the associahedron (as the max-slope pivot rule polytope of the simplex).

Theorem 3.6. *Let $\mathsf{P} \subset \mathbb{R}^d$ be a polytope and $\pi : \mathbb{R}^d \to \mathbb{R}^e$ a linear projection. If $\pi(\mathsf{P})$ has the same graph as P, then for every linear function $\boldsymbol{c}$ that is generic for $\pi(\mathsf{P})$, denoting π^* the adjoint of π:*

$$\Pi(\pi(\mathsf{P}), \boldsymbol{c}) \;=\; \pi(\Pi(\mathsf{P}, \pi^*(\boldsymbol{c})))$$

Proof. Let $\mathsf{P}' = \pi(\mathsf{P})$. If P and P' have the same graph, then $\pi : V(\mathsf{P}) \to V(\mathsf{P}')$ is a bijection and we write $\pi(v) = v'$. In particular, A is an arborescence of P if and only if $A' := \pi \circ A \circ \pi^{-1}$ is an arborescence of P'. For an arborescence A on P we compute

$$\pi(\Psi(A)) = \sum_{v \in V(\mathsf{P})} \langle \pi^*(\boldsymbol{c}), A(v) - v \rangle^{-1} \, \pi(A(v) - v) = \sum_{v \in V(\mathsf{P})} \langle \boldsymbol{c}, A'(v') - v' \rangle^{-1} \, (A'(v') - v') = \Psi(A')$$

and hence $\pi(\Pi(\mathsf{P}, \pi^*(\boldsymbol{c}))) = \operatorname{conv}(\Psi(A') : A) = \Pi(\mathsf{P}', \boldsymbol{c})$. □

A polytope P is called *2-neighborly* if any two vertices of P share an edge, that is to say when the graph of P is the complete graph.

Corollary 3.7. *Let P be a 2-neighborly polytope. Then, for any generic linear function $\boldsymbol{c}$, $\Pi(\mathsf{P}, \boldsymbol{c})$ is the projection of an associahedron.*

Proof. Every polytope $\mathsf{P} = \operatorname{conv}(\boldsymbol{v}_1, \ldots, \boldsymbol{v}_n) \subset \mathbb{R}^d$ is the projection of Δ_{n-1} under the linear map $\pi : \mathbb{R}^n \to \mathbb{R}^d$ with $\pi(\boldsymbol{e}_i) = \boldsymbol{v}_i$ for $i \in [n]$. Since P is 2-neighborly, the projection π retains the graph of Δ_{n-1} and the result follows from Theorem 3.6 and Theorem 3.2. □

This result motivates the next section. We will study the max-slope pivot polytopes of a well-known family of 2-neighborly polytopes: cyclic polytopes.

3.2 Max-slope pivot polytope of cyclic polytopes

This section is a joint work with Aenne Benjes and Raman Sanyal. An article is in preparation, containing this section together with Section 4.3.

For a linear program $(\mathsf{P}, \boldsymbol{c})$, we have seen that when the graph of P is the complete graph on n nodes, that is, if P is 2-*neighborly*, then its max-lope pivot polytope is a projection of the associahedron Asso_{n-2}. This implies that the arborescences corresponding to the vertices of $\Pi(\mathsf{P}, \boldsymbol{c})$ will be *non-crossing*, meaning that there are no $i < j < k < l$ such that $A(i) = k$ and $A(j) = l$. Note that not all non-crossing arborescences will show up as a vertex of $\Pi(\mathsf{P}, \boldsymbol{c})$, but only a sub-family of them. Stronger even, Corollary 3.7 shows that when the vertices of P are sufficiently generic, then the faces of $\Pi(\mathsf{P}, \boldsymbol{c})$ are products of associahedra.

For $n > d \geq 4$ and $\boldsymbol{t} = (t_1 < t_2 < \cdots < t_n) \in \mathbb{R}^n$, the d-dimensional *cyclic polytope* is $\mathsf{Cyc}_d(\boldsymbol{t}) := \mathrm{conv}\{(t_i, t_i^2, \ldots, t_i^d) : i = 1, \ldots, n\}$, see Figure 31. Cyclic polytopes play the main role in the Upper Bound Theorem for polytopes [McM70] and they exhibit a number of remarkable properties. In particular, for $d \geq 4$, $\mathsf{Cyc}_d(\boldsymbol{t})$ is 2-neighborly and simplicial. Moreover, its vertices are in general position: no $d+1$ of them belong to the same hyperplane. The linear function $\boldsymbol{x} \mapsto \langle \boldsymbol{e}_1, \boldsymbol{x} \rangle = x_1$ is generic with respect to $\mathsf{Cyc}_d(\boldsymbol{t})$. Corollary 3.7 yields that $\Pi(\mathsf{Cyc}_d(\boldsymbol{t}), \boldsymbol{e}_1)$ is a projection of Asso_{n-2} defined in terms of $\boldsymbol{t}$. Thus, for generic $\boldsymbol{t}$, its combinatorial structure corresponds to a subposet of the lattice of faces of Asso_{n-2}, and justifies the following definition.

Definition 3.8. For $n > d \geq 4$ and $\boldsymbol{t} = (t_1 < t_2 < \cdots < t_n)$, the $(d-1)$-dimensional *cyclic associahedron* $\mathsf{Asso}_{d-1}(\boldsymbol{t})$ is the max-slope pivot polytope $\Pi(\mathsf{Cyc}_d(\boldsymbol{t}), \boldsymbol{e}_1)$.

The following section is devoted to the study of cyclic associahedra. In particular, a quick numerical implementation reveals that the combinatorics of $\mathsf{Asso}_{d-1}(\boldsymbol{t})$ depends on $\boldsymbol{t}$, whereas Athanasiadis, De Loera, Reiner and Santos have shown in [ALRS00] that the combinatorics of the monotone path polytope of the cyclic polytope does not depend on $\boldsymbol{t}$. A first result (Corollary 3.13) determines the vertices of $\mathsf{Asso}_{d-1}(\boldsymbol{t})$ *as if it were not depending on* $\boldsymbol{t}$, that is we indicate which non-crossing arborescence appears as a vertex of $\mathsf{Asso}_{d-1}(\boldsymbol{t})$ for at least a $\boldsymbol{t}$. Then, in Theorem 3.16, we give a general but complex criterion for a non-crossing arborescence to appear as a vertex of $\mathsf{Asso}_{d-1}(\boldsymbol{t})$ for a given $\boldsymbol{t}$. These two theorems allow a full description of the case $d = 3$: intriguingly, the number of vertices of $\mathsf{Asso}_2(\boldsymbol{t})$ does not depend on $\boldsymbol{t}$, see Corollaries 3.37 and 3.49.

To determine which non-crossing arborescences correspond to a vertex of $\mathsf{Asso}_{d-1}(\boldsymbol{t})$, we propose a general perspective in elementary geometric terms: For a univariate polynomial $P(t) = w_1 t + w_2 t^2 + \cdots + w_d t^d$, consider the n points $p_i = (t_i, P(t_i)) \in \mathbb{R}^2$. Define $A : [n] \to [n]$ by the property that $A(i) = j$ if $j > i$ and all points p_k for $i < k \neq j$ are below the line $\overline{p_i p_j}$; see Figure 32 for an illustration. This defines a non-crossing arborescence, and we say that P *captures* A on $\boldsymbol{t}$. Thus, if $d \geq 4$, a non-crossing arborescence A correspond to a vertex of $\mathsf{Asso}_{d-1}(\boldsymbol{t})$ if and only if it can be captured on $\boldsymbol{t}$ by a polynomial of degree at most d.

Since $\mathsf{Cyc}_n(\boldsymbol{t})$ is a $(n-1)$-simplex, every non-crossing arborescence is captured by some polynomial on $\boldsymbol{t}$. We define the *degree* $\mu(A, \boldsymbol{t})$ of a non-crossing arborescence A as the minimal degree of a polynomial P that captures A on $\boldsymbol{t}$. In general, the degree of A depends on the choice of $\boldsymbol{t} = (t_1 < \cdots < t_n)$. We define the *intrinsic degree* of A as $\mu(A) := \min_{\boldsymbol{t}} \mu(A, \boldsymbol{t})$. The intrinsic degree defines a natural complexity measure on non-crossing arborescences and hence on Catalan families. We show that $\mu(A)$ can be determined directly from the combinatorics of A, see Corollary 3.13.

Even though our motivation originally comes from the study of the geometry of pivot rules, it also advocates for new ways to think about the associahedron. In fact, (combinatorial) understandings and realizations of the associahedron already naturally arise in a wide variety of domains: the associahedron occurs as a secondary polytope [Lee89], as a generalized permutahedron [Lod04, Pos09], or as a polytope of expansive motions [RSS03]. In this section, the realizations of the associahedron we introduce are parametrized by $\boldsymbol{t} \in \mathbb{R}^n$, and generalized to more convoluted structures whose genesis prompts a natural complexity parameter on Catalan families (parenthe-

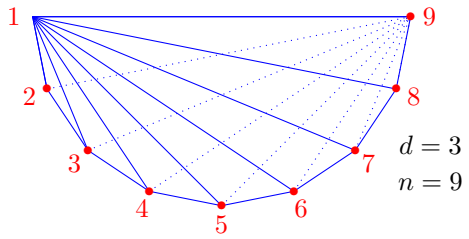

Figure 31: The cyclic polytope $\mathsf{Cyc}_3(\boldsymbol{t})$ for $n = 9$. Note that its graph is not complete (the graph of $\mathsf{Cyc}_d(\boldsymbol{t})$ is complete for $d \geq 4$).

sations, binary search trees, triangulations of polygons...). Moreover, the tools developed here will be of prime importance for the study of fiber polytopes in Section 4.3.

If A is a max-slope arborescence of $(\mathsf{P}, \boldsymbol{c})$, then the leading path from the minimal to the maximal vertex of $\boldsymbol{c}$ over P is a coherent $\boldsymbol{c}$-monotone path in the sense of Billera–Sturmfels [BS92]. The monotone path polytope $\mathsf{M}_{\boldsymbol{c}}(\mathsf{P})$ gives a geometric model for coherent monotone paths, and one can prove it captures the homotopy type of the Baues poset [BKS94]. It was shown in [BDLLS22] that $\mathsf{M}_{\boldsymbol{c}}(\mathsf{P})$ is a weak Minkowski summand of $\Pi(\mathsf{P}, \boldsymbol{c})$: the monotone path polytope is a deformation of the max-slope pivot polytope, see Section 4.2.1 for the details. On the combinatorial level, this implies that $\mathsf{Asso}_{d-1}(\boldsymbol{t})$ refines the combinatorics of $\mathsf{M}_{\boldsymbol{e}_1}(\mathsf{Cyc}_d(\boldsymbol{t}))$. The latter was studied by Athanasiadis, De Loera, Reiner and Santos in [ALRS00]: the proof of Corollary 3.13 is related to the relative locations of roots of $P''(t)$ induced by the combinatorics of A and is inspired by their work. There, the authors show that the combinatorics of $\mathsf{M}_{\boldsymbol{e}_1}(\mathsf{Cyc}_d(\boldsymbol{t}))$ is that of cyclic zonotopes and, in particular, independent of $\boldsymbol{t}$. In our case, the combinatorics of the polytope $\mathsf{Asso}_{d-1}(\boldsymbol{t})$ will depend on $\boldsymbol{t}$. This motivates the notion of universal non-crossing arborescences.

A non-crossing arborescence A is *universal* if for any $\boldsymbol{t} = (t_1 < t_2 < \cdots < t_n)$ there is a polynomial of degree $\mu(A)$ that captures A on $\boldsymbol{t}$ (that is $\mu(A, \boldsymbol{t}) = \mu(A)$ for all $\boldsymbol{t}$). For $d \geq \max(4, \mu(A))$ this implies that A is always a vertex of $\mathsf{Asso}_{d-1}(\boldsymbol{t})$ whatever $\boldsymbol{t}$. In Section 3.2.2 we completely classify universal arborescences of intrinsic degree 3 and smaller. To that end, we study realization sets of A, that is, the set of $\boldsymbol{t} = (t_1 < \cdots < t_n)$ such that A is captured by a polynomial of a given degree. Moreover, we prove in Corollary 3.37 that the number of non-crossing arborescence A captured on $\boldsymbol{t}$ in degree 3 or smaller is $\binom{n}{2} - 1$, independently of $\boldsymbol{t}$.

Note however that when $d \leq 3$, the max-slope pivot polytope $\mathsf{Asso}_{d-1}(\boldsymbol{t})$ is not a projection of the associahedron, the special cases $\mathsf{Asso}_1(\boldsymbol{t})$ and $\mathsf{Asso}_2(\boldsymbol{t})$ will be studied in Section 3.2.3. We prove there that the number of vertices of $\mathsf{Asso}_1(\boldsymbol{t})$ and $\mathsf{Asso}_2(\boldsymbol{t})$ are independent from $\boldsymbol{t}$: they are respectively 2 and $3n - 7$, see Theorem 3.39 and Corollary 3.49.

3.2.1 Cyclic associahedra and the intrinsic degree

We start by fixing the notations of what we have swiftly introduced above.

For $d \geq 2$ and $\boldsymbol{t} = (t_1, t_2, \ldots, t_n) \in \mathbb{R}^n$ with $t_1 < t_2 < \cdots < t_n$, the d-dimensional *cyclic polytope* $\mathsf{Cyc}_d(\boldsymbol{t})$ is defined as the convex hull of $\boldsymbol{\gamma}_d(t_1), \ldots, \boldsymbol{\gamma}_d(t_n)$ where $\boldsymbol{\gamma}_d(t) := (t, t^2, \ldots, t^d)$. It is well-known that for $d \geq 4$, the cyclic polytope $\mathsf{Cyc}_d(\boldsymbol{t})$ is 2-neighborly [Zie98, Cor. 0.8]. For $\boldsymbol{c} = \boldsymbol{e}_1 = (1, 0, \ldots, 0)$, we have $\langle \boldsymbol{e}_1, \boldsymbol{\gamma}_d(t) \rangle = t$ for all $t \in \mathbb{R}$ and hence $\boldsymbol{e}_1$ is a generic linear function for $\mathsf{Cyc}_d(\boldsymbol{t})$. For $d \geq 4$, we call $\mathsf{Asso}_{d-1}(\boldsymbol{t}) := \Pi(\mathsf{Cyc}_d(\boldsymbol{t}), \boldsymbol{e}_1)$ a *cyclic associahedron*.

Proposition 3.9. *For any $d \geq 4$, if $\boldsymbol{t}$ is sufficiently generic, then the faces of $\mathsf{Asso}_{d-1}(\boldsymbol{t})$ are combinatorially isomorphic to products of associahedra.*

Proof. When $d \geq 4$, $\mathsf{Cyc}_d(\boldsymbol{t})$ is 2-neighborly for any $\boldsymbol{t}$. By Corollary 3.7, $\mathsf{Asso}_{d-1}(\boldsymbol{t})$ is the image of $\Pi(\Delta_{n-1}, \boldsymbol{t}) = \mathsf{Asso}_{n-2}$ under the projection $\pi(\boldsymbol{e}_i) = \boldsymbol{\gamma}_d(t_i)$ for $i = 1, \ldots, n$. For every $(d-2)$-face $G \subset \mathsf{Asso}_{n-2}$ let U_G be the $(d-2)$-dimensional linear subspace parallel to G. This gives a finite collection of $(d-2)$-linear subspaces. The collection of $\boldsymbol{t}$ such that π is not injective on the union

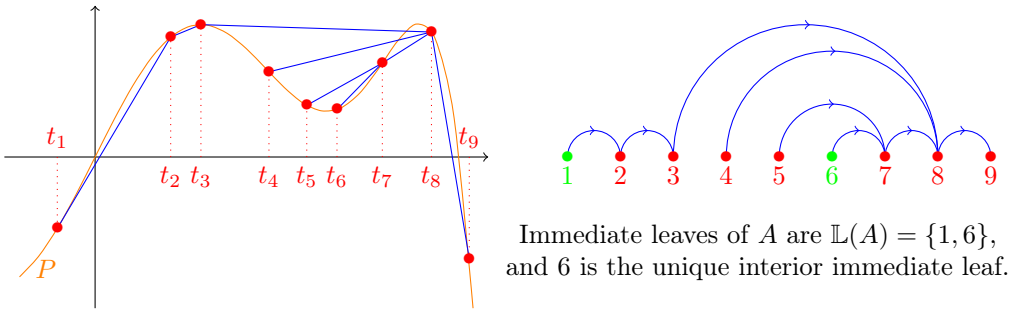

Figure 32: (Left) A 5-degree polynomial with the points p_i in red and the (pieces of) lines $\overline{p_i p_{A(i)}}$ in blue; (Right) the non-crossing arborescence A captured by P on $\boldsymbol{t}$.

of these subspaces is Zariski closed. For any $\boldsymbol{t}$ in the complement, for any facet $F \subset \mathsf{Asso}_{d-1}(\boldsymbol{t})$, the face $\pi^{-1}(F) \subset \mathsf{Asso}_{n-2}$ is linearly isomorphic to F. This proves the claim. □

Proposition 3.9 also implies that for generic $\boldsymbol{t}$ and $d \geq 4$, the vertices of $\mathsf{Asso}_{d-1}(\boldsymbol{t})$ correspond to certain non-crossing arborescences $A : [n] \to [n]$ that depend on $\boldsymbol{t}$ and d. For a given (generic) $\boldsymbol{w} = (w_1, \ldots, w_d)$, there is a simple way to determine the associated non-crossing arborescence. We note that $\langle \boldsymbol{w}, \boldsymbol{\gamma}_d(t) \rangle = w_1 t + w_2 t^2 + \cdots + w_d t^d =: P_{\boldsymbol{w}}(t)$ is a univariate polynomial in t of degree at most d. Consider the graph of the function $P_{\boldsymbol{w}}(t)$ with the marked points $p_i(\boldsymbol{t}) = (t_i, P(t_i))$ for $i = 1, \ldots, n$. As in the previous section, we note that $A(i) = j$ if and only if $p_k(\boldsymbol{t})$ is below the line $\overline{p_i(\boldsymbol{t}) p_j(\boldsymbol{t})}$ for all $k > i$ with $k \neq j$. Figure 32 illustrates the construction. We say that the non-crossing arborescence A is *captured* by the polynomial $P_{\boldsymbol{w}}$ on $\boldsymbol{t}$. For $d \geq 4$, A is captured by a polynomial of degree d on $\boldsymbol{t}$ if and only if $\Psi(A)$ appears as a vertex of $\mathsf{Asso}_{d-1}(\boldsymbol{t})$. The following fact is immediate from this geometric perspective, as 'being below' a line is an open condition.

Corollary 3.10. *Let A be a non-crossing arborescence that is captured by P on $\boldsymbol{t}$. Then there is an $\varepsilon > 0$ such that A is captured by P on $\boldsymbol{t}'$ for all $\boldsymbol{t}'$ with $\|\boldsymbol{t} - \boldsymbol{t}'\|_\infty < \varepsilon$.*

Recall that the *degree* of a non-crossing arborescence A with respect to $\boldsymbol{t}$ is

$$\mu(A, \boldsymbol{t}) \;:=\; \min\{\deg P \;;\; A \text{ is captured by } P \text{ on } \boldsymbol{t}\}\,.$$

For fixed $\boldsymbol{t}$, the degree defines a filtration on non-crossing arborescences. However, as we will see in the next section, the degree of A depends on $\boldsymbol{t}$. This motivates the definition of the *intrinsic degree* of A as

$$\mu(A) \;:=\; \min\{\mu(A, \boldsymbol{t}) \;;\; \boldsymbol{t} = (t_1 < t_2 < \cdots < t_n) \in \mathbb{R}^n\}\,.$$

In the remainder of this section, we prove that the intrinsic degree can be computed efficiently and easily from the non-crossing arborescence, see Corollary 3.13. A $j \in [n-1]$ is a *leaf* of A if there is no i with $A(i) = j$. We call j an *immediate leaf* if, additionally, $A(j) = j + 1$ and denote by $\mathbb{L}(A)$ the set of immediate leaves. An immediate leaf $j \in \mathbb{L}(A)$ is *interior* if $1 < j < n - 1$, and we write $\mathbb{L}^\circ(A)$ for the interior leafs. We first prove that a lower bound on the degree $\mu(A)$:

Theorem 3.11. *Let A be a non-crossing arborescence. Then*

$$\mu(A) \;\geq\; |\mathbb{L}(A)| + |\mathbb{L}^\circ(A)| + 1\,.$$

Proof. Let P be a polynomial and $\boldsymbol{t} = (t_1 < t_2 < \cdots < t_n)$ so that P captures A on $\boldsymbol{t}$. Recall that for $i < j$, $\tau(i, j) = \frac{P(t_j) - P(t_i)}{t_j - t_i}$ is the slope of the line connecting $(t_i, P(t_i))$ to $(t_j, P(t_j))$. Applying the mean-value theorem to $t \mapsto P(t)$, we get that for every $i = 1, \ldots, n-1$, there is $t_i < \theta_i < t_{i+1}$ with $P'(\theta_i) = \tau(i, i+1)$.

Let $i \in \mathbb{L}(A)$ with $i > 1$ and set $j = A(i-1)$. Since i is a leaf, we know that $j \geq i + 1$ and $\tau(i-1, j) > \tau(i-1, i)$. From Lemma 3.5 we obtain $\tau(i, j) > \tau(i-1, j)$. From $A(i) = i + 1$, we

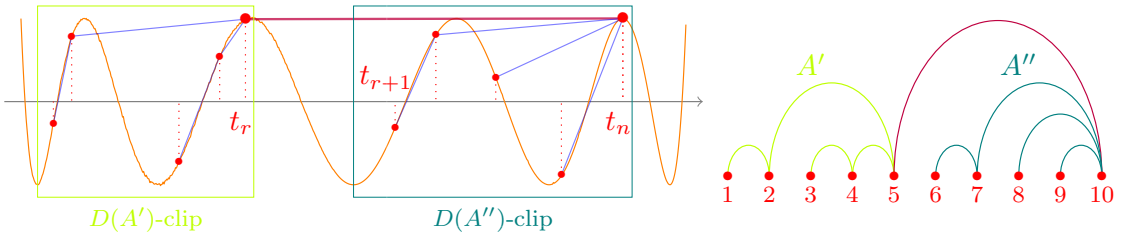

Figure 33: Decomposition of a $D(A)$-clip into $D(A')$-clip and $D(A'')$-clip for $r+1 \in \mathbb{L}(A)$.

deduce that $\tau(i,i+1) \geq \tau(i,j)$ and therefore $\tau(i,i+1) > \tau(i-1,i)$. Applying the mean-value theorem to $t \mapsto P'(t)$, we find $\theta_{i-1} < \alpha_i < \theta_i$ with $P''(\alpha_i) = \frac{P'(\theta_i)-P'(\theta_{i-1})}{\theta_i-\theta_{i-1}} = \frac{\tau(i,i+1)-\tau(i-1,i)}{\theta_i-\theta_{i-1}} > 0$.

On the other hand, for every $i < n-1$, if $A(i) = i+1$, then $\tau(i,i+1) > \tau(i,i+2)$. Lemma 3.5 yields $\tau(i,i+1) > \tau(i,i+2) > \tau(i+1,i+2)$ and there is $\theta_i < \beta_i < \theta_{i+1}$ such that $P''(\beta_i) < 0$.

If $i,j \in \mathbb{L}(A)$ with $i < j$, then $P''(\beta_i) < 0 < P''(\alpha_j)$ and, since $i \leq j-2$, we have $\beta_i < \theta_{j-1} < \alpha_j$. If there is no immediate leaf between i and j, then there is a root in the open interval (β_i, α_j). So far, this gives $|\mathbb{L}(A)| - 1$ roots of P''.

For every interior immediate leaf $1 < j < n-1$, we have $P''(\beta_j) < 0 < P''(\alpha_j)$ and $\alpha_j < \theta_j < \beta_j$ and P'' has a root in (α_j, β_j). This gives an additional $|\mathbb{L}^\circ(A)|$ roots of P''. To finish the proof, we compute $\deg P = \deg P'' + 2 \geq |\mathrm{roots}(P'')| + 2 \geq |\mathbb{L}(A)| + |\mathbb{L}^\circ(A)| + 1$. □

The idea for the proof was inspired by the proof of Theorem 3.1 in [ALRS00], where the authors study monotone path polytopes of cyclic polytopes. The coherence of a $\boldsymbol{e}_1$-monotone path of $\mathsf{Cyc}_d(\boldsymbol{t})$ depends on the degree, but it was shown that it does not depend on the choice of $\boldsymbol{t}$. Unfortunately, the degree of A depends on the choice of $\boldsymbol{t}$, and in order to prove $\mu(A) \leq |\mathbb{L}(A)| + |\mathbb{L}^\circ(A)| + 1$ we need to exhibit a concrete polynomial P and $\boldsymbol{t}$ to capture A.

For $d \geq 1$, the *Chebychev polynomial* T_d of the first kind is the polynomial of degree d with the property that $T_d(\cos(\alpha)) = \cos(d\alpha)$ for all $\alpha \in [0,\pi]$. It follows that all d roots of T_d are distinct and real, and lie in the open interval $(-1,1)$. Moreover, T_d has $d+1$ extrema in the interval $[-1,1]$ and the extrema alternate between -1 and 1. In particular, $T_d(1) = 1$ and $T_d(-1) = (-1)^d$. We also note that $T_d''(1) > 0$ and $(-1)^d T_d''(-1) > 0$. Hence $(-1)^d T_d(t)$ and $T_d(t)$ are convex in a neighborhood of $t = -1$ and $t = 1$, respectively.

For $D \geq 0$, a *D-clip* of T_d is an interval $[m,M] \subseteq [-1,1]$ that contains $D+1$ extrema including m and M and M is a maximum ($T_d(M) = 1$). We call the D-clip *concave* if T_d is concave on $[M-\varepsilon, M]$ for some $\varepsilon > 0$. Any D-clip with $M < 1$ is concave.

For a non-crossing arborescence on $n \geq 1$ nodes we define $D(A) := 2|\mathbb{L}(A)|$ if $1 \notin \mathbb{L}(A)$ and $D(A) := 2|\mathbb{L}(A)| - 1$ if $1 \in \mathbb{L}(A)$. If $n = 1$, then set $D(A) := 0$.

Proposition 3.12. *Let A be a non-crossing arborescence on n nodes. For any concave $D(A)$-clip $[m,M]$ of T_d there are $m \leq t_1 < t_2 < \cdots < t_n = M$ such that A is captured by T_d on $\boldsymbol{t} = (t_1,\ldots,t_n)$ and $T_d(t_i) < 1 = T_d(t_n)$ for $i = 1,\ldots,n-1$.*

Proof. We prove the claim by induction on n. Let $[m,M]$ be a fixed concave $D(A)$-clip of T_d. For $n \leq 2$, this is clearly true. Let $n \geq 3$ and consider the decomposition of A into (r, A', A'') of Proposition 3.3. We distinguish three cases.

If $r = 1$, then A' has a single node. Moreover, $D(A) = 2|\mathbb{L}(A)|$ is even and thus m is a maximum. If $2 \in \mathbb{L}(A)$, then $D(A'') = D(A) - 1$ is odd. Let m'' be the first minimum of the concave $D(A)$-clip $[m,M]$. By induction, A'' can be captured on $[m'',M]$. The condition $T_d(t_i) < 1$ for $i < n$ ensures that for $t_1 = m + \varepsilon$ with $\varepsilon > 0$ sufficiently small, the points $p_i(\boldsymbol{t}) = (t_i, T_d(t_i))$ for $1 < i < n$ are below the line $\overline{p_1(\boldsymbol{t})p_n(\boldsymbol{t})}$. If $2 \notin \mathbb{L}(A)$, then $D(A'') = D(A)$ and A'' can be captured on $[m,M]$. Since $D(A)$ is even, m is a maximum and $m < t_2$. The same argument as before shows that choosing $t_1 \in (m,t_2)$ close enough to m suffices.

If $r = n-1$, then $D(A') = D(A)$ and A' can be captured on the concave $D(A)$-clip $[m, M]$ with $m \le t_1 < t_2 < \cdots < t_{n-1} = M$. By Corollary 3.10, we can change t_{n-1} to $t_{n-1} - \varepsilon$ for some small $\varepsilon > 0$. For $t_n = M$, the line $\overline{p_{n-1}(\boldsymbol{t})p_n(\boldsymbol{t})}$ is close to the tangent of T_d at t_n and by the concavity of the maximum, $p_n(\boldsymbol{t})$ is below all lines $\overline{p_i(\boldsymbol{t})p_{n-1}(\boldsymbol{t})}$ for $i < n-1$.

Thus, we can assume $1 < r < n-1$. If $r+1 \notin \mathbb{L}(A)$, then $D(A) = D(A') + D(A'')$ and $D(A'')$ is even. Let $y \in [m, M]$ such that $[m, y]$ is a concave $D(A')$-clip and $[y, M]$ is a concave $D(A'')$-clip. By induction there are $m \le t_1 < \cdots < t_r = y < \cdots < t_n = M$ that capture A' and A'' on their clips. Again by Corollary 3.10, $t_1 < \cdots < t_r = y - \varepsilon$ still captures A' for $\varepsilon > 0$ sufficiently small. Since $T_d(t_j) < 1$ for all $j < r$, the points $p_i(\boldsymbol{t})$ for $i > r$ are all below the lines $\overline{p_j(\boldsymbol{t})p_r(\boldsymbol{t})}$ as well as below the line $\overline{p_r(\boldsymbol{t})p_n(\boldsymbol{t})}$. If $r+1 \in \mathbb{L}(A)$, then $D(A) = D(A') + D(A'') + 1$ and $D(A'')$ is odd, see Figure 33. Choose $y \in [m, M]$ so that $[y, M]$ is a concave $D(A'')$-clip. Since $D(A'')$ is odd, y is a minimum and let x be the maximum before y. We can capture A' on $[m, x]$ and again changing t_r to $t_r = x - \varepsilon$, the resulting $t_1 < \cdots < t_n$ capture A on the concave $D(A)$-clip $[m, M]$. □

Corollary 3.13. *Let $A : [n] \to [n]$ be a non-crossing arborescence. Then*

$$\mu(A) \;=\; |\mathbb{L}(A)| + |\mathbb{L}^\circ(A)| + 1\,.$$

Proof. Let $A : [n] \to [n]$ be a non-crossing arborescence. By Theorem 3.11 it suffices to prove that A is captured by a polynomial P of degree $d = |\mathbb{L}(A)| + |\mathbb{L}^\circ(A)| + 1$ on some $\boldsymbol{t} = (t_1 < \cdots < t_n)$. If $n-1$ is not an immediate leaf of A, then $D(A) = |\mathbb{L}(A)| + |\mathbb{L}^\circ(A)| = d - 1$ and $-T_d$ has a concave $D(A)$-clip. If $n-1 \in \mathbb{L}(A)$, then $D(A) = |\mathbb{L}(A)| + |\mathbb{L}^\circ(A)| + 1 = d$. We note that if $n-1$ is an immediate leaf, then in a $D(A)$-clip $[m, M]$ the maximum M does not have to be concave and we can choose $M = 1$ to capture A on T_d. □

3.2.2 Realization sets and universal arborescence

In this section, we now investigate the collection of vectors $\boldsymbol{t} = (t_1 < t_2 < \cdots < t_n)$ for which a non-crossing arborescence A can be captured on $\boldsymbol{t}$ by a polynomial P of degree at most d. We use these realization sets to characterize universal non-crossing arborescences A (i.e. $\mu(A, \boldsymbol{t}) = \mu(A)$ for all $\boldsymbol{t}$) of intrinsic degree $\mu(A) \le 3$. These universal arborescences will correspond to vertices of the cyclic associahedron $\mathsf{Asso}_{d-1}(\boldsymbol{t})$ for every $d \ge \max(\mu(A), 4)$.

Realization sets

Definition 3.14. For a non-crossing arborescence $A : [n] \to [n]$ and any d, we define the *realization set* $\mathcal{T}_d^\circ(A)$ of A as the collection of $\boldsymbol{t} = (t_1 < t_2 < \cdots < t_n) \in \mathbb{R}^n$ such that A can be captured on $\boldsymbol{t}$ by some polynomial P of degree at most d.

If A is captured on $\boldsymbol{t}$ by P, then for $\lambda > 0$, A is captured on $\lambda\boldsymbol{t}$ by $P(\frac{t}{\lambda})$. Likewise, A is captured on $(c, \dots, c) + \boldsymbol{t}$ by $P(t - c)$. With Corollary 3.10, this shows the closure $\mathcal{T}_d(A)$ of $\mathcal{T}_d^\circ(A)$ is a (generally non-convex) full-dimensional subcone of the *order cone* $\mathsf{O}_n = \{\boldsymbol{t} \in \mathbb{R}^n : t_1 \le \cdots \le t_n\}$.

In particular, when convenient, we can assume $t_1 = 0$ and $t_n = 1$. By definition, remark that

$$\mathcal{T}_1(A) \subseteq \mathcal{T}_2(A) \subseteq \cdots \subseteq \mathcal{T}_n(A) = \mathsf{O}_n.$$

In order to give a description of $\mathcal{T}_d(A)$, let $\mathcal{I}_A^b, \mathcal{I}_A^f \subseteq [n-2]$ be the sets of backward-sliding and forward-sliding nodes of A. We start with a description of the collection of polynomials P that capture A on a given $\boldsymbol{t}$. If $i \in \mathcal{I}_A^f$ is forward-sliding, we write $i^* := A(i)$. If $i \in \mathcal{I}_A^b$ is backward-sliding, we write i^* for minimal $j > i$ with $A(j) = A(i)$. See Figure 34.

Lemma 3.15. *Let $A : [n] \to [n]$ be a non-crossing arborescence and $\boldsymbol{t} \in \mathsf{O}_n^\circ$. A polynomial P captures A on $\boldsymbol{t}$ if and only if for all forward-sliding $i \in \mathcal{I}_A^f$*

$$(t_{A(i^*)} - t_i)(P(t_{i^*}) - P(t_i)) - (t_{i^*} - t_i)(P(t_{A(i^*)}) - P(t_i)) \;>\; 0$$

and for all backward-sliding $i \in \mathcal{I}_A^b$

$$(t_{A(i^*)} - t_i)(P(t_{i^*}) - P(t_i)) - (t_{i^*} - t_i)(P(t_{A(i^*)}) - P(t_i)) \;<\; 0\,,$$

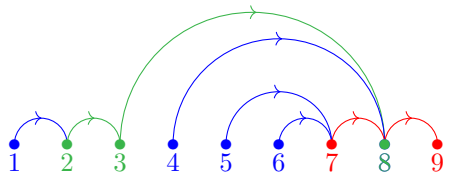

2 is forward-sliding.
7 is not forward-sliding.

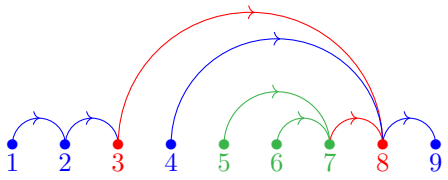

5 is backward sliding.
3 is backward-sliding, but $3^* \neq 7$

Figure 34: Here, $\mathcal{I}_A^f = \{1,2,3,5\}$ is the set of forward-sliding nodes, and $\mathcal{I}_A^b = \{3,4,5\}$ is the set of backward-sliding nodes.

Proof. Let $P(t) = w_d t^d + w_{d-1} t^{d-1} + \cdots + w_1 t = \langle \boldsymbol{w}, \boldsymbol{\gamma}_d(t) \rangle$. Then P captures A on $\boldsymbol{t}$ if and only if $\langle \boldsymbol{w}, \Psi(A) \rangle > \langle \boldsymbol{w}, \Psi(A') \rangle$ for all non-crossing arborescences $A' \neq A$. By convexity, it suffices to consider only those A' such that $[\Psi(A), \Psi(A')]$ is an edge. By Proposition 3.4 this boils down to

$$\langle \boldsymbol{w}, \Psi(A) \rangle - \langle \boldsymbol{w}, \Psi(F_i A) \rangle \;=\; \frac{P(t_{i^*}) - P(t_i)}{t_{i^*} - t_i} - \frac{P(t_{A(i^*)}) - P(t_i)}{t_{A(i^*)} - t_i} \;>\; 0\,,$$

when $i \in \mathcal{I}_A^f$; and when $i \in \mathcal{I}_A^b$ to

$$\langle \boldsymbol{w}, \Psi(A) \rangle - \langle \boldsymbol{w}, \Psi(B_i A) \rangle \;=\; \frac{P(t_{A(i)}) - P(t_i)}{t_{A(i)} - t_i} - \frac{P(t_{i^*}) - P(t_i)}{t_{i^*} - t_i} \;>\; 0 \qquad \square$$

We can write Lemma 3.15 as follows. Define the *complete symmetric polynomial* of degree s:

$$h_s(x_1, x_2, x_3) \;:=\; \sum_{a+b+c=s} x_1^a x_2^b x_3^c$$

For $i \in \mathcal{I}_A^b \cup \mathcal{I}_A^f$, we construct $\Phi_i^d(\boldsymbol{t}) \in \mathbb{R}^d$ with $\Phi_i^d(\boldsymbol{t})_j = h_{j-2}\left(t_i, t_{i^*}, t_{A(i^*)}\right)$.

Observe that $\Phi_i^d(\boldsymbol{t})_1 = 0$ and $\Phi_i^d(\boldsymbol{t})_2 = 1$. We set $\overline{\Phi}_i^d(\boldsymbol{t}) := \left(h_j(t_i, t_{i^*}, t_{A(i^*)})\right)_{j=1,\ldots,d-2} \in \mathbb{R}^{d-2}$.

Theorem 3.16. *Let $A : [n] \to [n]$ be a non-crossing arborescence. For $\boldsymbol{t} \in \mathsf{O}_n^\circ$ and $d \geq 2$, define the polytopes*

$$\mathsf{P}_d^f(A, \boldsymbol{t}) \;:=\; \operatorname{conv}\left\{\overline{\Phi}_i^d(\boldsymbol{t}) : i \in \mathcal{I}_A^f\right\} \qquad \text{and} \qquad \mathsf{P}_d^b(A, \boldsymbol{t}) \;:=\; \operatorname{conv}\left\{\overline{\Phi}_i^d(\boldsymbol{t}) : i \in \mathcal{I}_A^b\right\}.$$

Then A is captured on $\boldsymbol{t}$ by some P of degree at most d if and only if $\mathsf{P}_d^f(A, \boldsymbol{t}) \cap \mathsf{P}_d^b(A, \boldsymbol{t}) = \varnothing$.

Proof. Let $P(t) = w_1 t + \cdots + w_d t^d = \langle \boldsymbol{w}, \boldsymbol{\gamma}_d(t) \rangle$, and $\boldsymbol{t} \in \mathsf{O}_n^\circ$. By Lemma 3.15, A is captured on $\boldsymbol{t}$ by some polynomial P of degree at most d if and only if $\langle \boldsymbol{w}, \Psi(A) - \Psi(F_i A) \rangle > 0$ for all $i \in \mathcal{I}_A^f$ and $\langle \boldsymbol{w}, \Psi(A) - \Psi(B_i A) \rangle > 0$ for all $i \in \mathcal{I}_A^b$. For $i \in \mathcal{I}_A^f$, let $j = A(i)$ and $k = A(j)$. We compute

$$\Psi(F_i A)_{r+1} - \Psi(A)_{r+1} \;=\; \frac{t_k^{r+1} - t_i^{r+1}}{t_k - t_i} - \frac{t_j^{r+1} - t_i^{r+1}}{t_j - t_i} \;=\; \sum_{s=0}^{r} t_k^s t_i^{r-s} - \sum_{s=0}^{r} t_j^s t_i^{r-s} \;=\; \sum_{s=0}^{r} (t_k^s - t_j^s) t_i^{r-s}\,.$$

This implies that $\Phi_i^d(\boldsymbol{t}) = \frac{1}{t_k - t_j}(\Psi(F_i A) - \Psi(A))$, and as $t_j < t_k$, the inequality $\langle \boldsymbol{w}, \Psi(A) - \Psi(F_i A) \rangle > 0$ is equivalent to $\left\langle \boldsymbol{w}, \Phi_i^d(\boldsymbol{t}) \right\rangle < 0$. For $i \in \mathcal{I}_A^b$ we can prove analogously, that $\langle \boldsymbol{w}, \Psi(A) - \Psi(B_i A) \rangle > 0$ is equivalent to $\left\langle \boldsymbol{w}, \Phi_i^d(\boldsymbol{t}) \right\rangle > 0$. This gives us a system of strict linear inequalities that by Gordan's lemma, a variant of Farkas' lemma (cf. [Sch98, Sect. 7.8]), has a solution if and only if there are $\lambda_i \geq 0$ for $i \in \mathcal{I}_A^f$ and $\mu_j \geq 0$ for $j \in \mathcal{I}_A^b$ not identically zero and

$$\sum_{i \in \mathcal{I}_A^f} \lambda_i \Phi_i^d(\boldsymbol{t}) \;=\; \sum_{i \in \mathcal{I}_A^b} \mu_i \Phi_i^d(\boldsymbol{t})\,.$$

Since $\Phi_i^d(\boldsymbol{t})_2 = 1$, it follows that $\Lambda := \sum_{i \in \mathcal{I}_A^f} \lambda_i = \sum_{i \in \mathcal{I}_A^b} \mu_i > 0$. Dividing both sides of the above equality by Λ yields a point in $\mathsf{P}_d^f(A, \boldsymbol{t}) \cap \mathsf{P}_d^b(A, \boldsymbol{t})$. $\square$

Example 3.17. For $n = 5$, one can consider $\boldsymbol{t} = (1, 2, 3, 4, 5)$. In Figure 35 are drawn $\mathsf{P}_d^b(A, \boldsymbol{t})$ and $\mathsf{P}_d^f(A, \boldsymbol{t})$ for $d = 3$ and $d = 4$ for the two given non-crossing arborescences. None of the polytopes intersects for $d = 4$, indicating that both arborescences are captured in degree 4 (what was already known, as $d = 4 = n - 1$, and all non-crossing arborescences on n nodes are captured in degree d). However, for $d = 3$, the left arborescence is not captured while the right one is.

The situation is inverted for $\boldsymbol{t} = (-1, 2, 3, 4, 5)$, as shown in Figure 36.

Non-crossing arborescences with $\mu(A) \leq 3$ In this section, we will characterize realization sets of non-crossing arborescences of intrinsic degree at most 3. We call a non-crossing arborescence A *quadratic* if $\mu(A) = 2$, and *cubic* if $\mu(A) = 3$. We start with a classification of quadratic and cubic arborescences, obtained from Corollary 3.13. Quadratic non-crossing arborescences have exactly 1 exterior immediate leave (and no interior one), while cubic ones have either 1 interior and no exterior, or 2 exterior ones. Consequently, their non-crossing property gives:

Corollary 3.18. *The two non-crossing arborescences of intrinsic degree 2 on $n \geq 3$ nodes are A_m and A_M, defined by $A_m(i) = i + 1$ for $1 \leq i \leq n - 1$ and $A_M(i) = n$ for $1 \leq i \leq n - 1$. See Figure 37.*

Corollary 3.19. *For $n \geq 4$, there are precisely $2^{n-2} + n - 5$ non-crossing arborescences A on n nodes with $\mu(A) = 3$. They come in two types:*

(i) *For $1 < k < n - 1$, define $A(i) = i + 1$ for $1 \leq i < k$ and $A(i) = n$ for $k \leq i < n$. These are $n - 3$ non-crossing arborescences with $\mathbb{L}(A) = \{1, n - 1\}$.*

(ii) *For $1 < k < n - 1$ and $n \geq j_1 \geq j_2 \geq \cdots \geq j_{k-1} > k$, define $A(i) = j_i$ for $1 \leq i < k$ and $A(i) = i + 1$ for $k \leq i < n$. These are $2^{n-2} - 2$ non-crossing arborescences with $\mathbb{L}(A) = \{k\}$.*

We call a non-crossing arborescence $A : [n] \to [n]$ *universal* if A can be captured by a polynomial of degree $\mu(A)$ on all $\boldsymbol{t} \in \mathsf{O}_n^\circ$, that is: $\mathcal{T}_{\mu(A)}(A) = \mathsf{O}_n$. Note that this implies that $\mathcal{T}_d(A) = \mathsf{O}_n$ for all $d \geq \mu(A)$. We next determine all universal arborescences A with $\mu(A) \leq 3$, giving a description of the realization set of any non-crossing arborescence A with $\mu(A) \leq 3$.

Lemma 3.20. *Let $A : [n] \to [n]$ be a non-crossing arborescence with $\mu(A) = 3$ and $\mathbb{L}(A) = \{k\}$, $1 < k < n - 1$. Then for all $\boldsymbol{t} \in \mathsf{O}_n^\circ$,*

$$\min\{t_i + t_{i^*} + t_{A(i^*)} : i \in \mathcal{I}_A^b\} < \max\{t_i + t_{i^*} + t_{A(i^*)} : i \in \mathcal{I}_A^f\}.$$

Proof. As $k \neq n - 1$ there is an $i \in \mathcal{I}_A^f \cap [n - 2]$ with $i^* = n - 1$. Recall that A is of the form Corollary 3.19(ii). If $j_1 \leq n - 2$, then for all $j \in \mathcal{I}_A^b$ we have $A(j^*) \leq n - 2$ and the statement follows. Otherwise, either $j \in \mathcal{I}_A^b$ exists with $j^* = n-1$ and $j < i$, or $j^* = n-2$ and $i \leq j$. In both cases, for all $\boldsymbol{t} \in \mathsf{O}_n^\circ$, we have $\min\{t_i + t_{i^*} + t_{A(i^*)} : i \in \mathcal{I}_A^b\} \leq t_j + t_{j^*} + t_{A(j^*)} < t_i + t_{i^*} + t_{A(i^*)} \leq \max\{t_i + t_{i^*} + t_{A(i^*)} : i \in \mathcal{I}_A^f\}$. □

Theorem 3.21. *Let $A : [n] \to [n]$ be a non-crossing arborescence with $\mu(A) \leq 3$. Then A is universal if and only if $\mu(A) = 2$, or if $\mu(A) = 3$ and*

(a) $\mathbb{L}(A) = \{1, n - 1\}$, *or*

(b) $\mathbb{L}(A) = \{n - 2\}$, $A(i) = n$ *for* $i = 1, \ldots, n - 4$, *and* $A(n - 3) \in \{n - 1, n\}$, *or*

(c) $\mathbb{L}(A) = \{2\}$ *and* $A(1) \in \{3, 4\}$.

Proof. Using Theorem 3.16 it suffices to show that $\mathsf{P}_d^f(A, \boldsymbol{t}) \cap \mathsf{P}_d^b(A, \boldsymbol{t}) = \varnothing$ for all choices of $\boldsymbol{t}$ holds in precisely the situations stipulated above.

When $\mu(A) = 2$, $\mathsf{P}_d^f(A, \boldsymbol{t})$ and $\mathsf{P}_d^b(A, \boldsymbol{t})$ are polytopes in $\mathbb{R}^0$. Hence, the claim holds if and only if $\mathcal{I}_A^b = \varnothing$ or $\mathcal{I}_A^f = \varnothing$. By Corollary 3.18 this is the case for both A_m and A_M.

If $\mu(A) = 3$, then $\mathsf{P}_d^f(A, \boldsymbol{t}) = [x_f, y_f]$, $\mathsf{P}_d^b(A, \boldsymbol{t}) = [x_b, y_b] \subset \mathbb{R}$ with (x_f, y_f) the minimum and maximum of $\{t_i + t_{i^*} + t_{A(i^*)} : i \in \mathcal{I}_A^f\}$ and likewise for (x_b, y_b).

Let A an arborescence with $\mu(A) = 3$. If $\mathbb{L}(A) = \{1, n - 1\}$, then A satisfies Corollary 3.19 (i) for some $1 < k < n - 1$. Thus $\mathcal{I}_A^f = \{1, 2, \ldots, k - 1\}$ and $\mathcal{I}_A^b = \{k, \ldots, n - 2\}$. It follows that

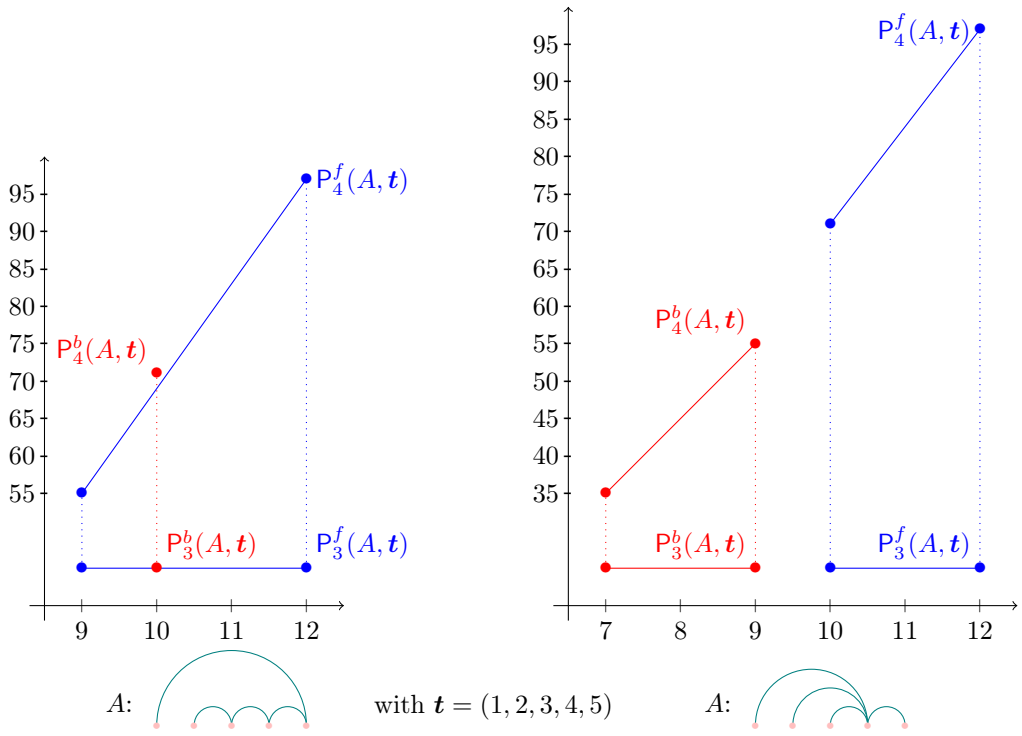

Figure 35: The polytopes $\mathsf{P}_d^b(A,\boldsymbol{t})$ and $\mathsf{P}_d^f(A,\boldsymbol{t})$ with $\boldsymbol{t} = (1,2,3,4,5)$, for $d = 3$ (Bottom, 1-dimensional drawing) and $d = 4$ (Top, 2-dimensional drawing), for the two non-crossing arborescences drawn (Left and Right).

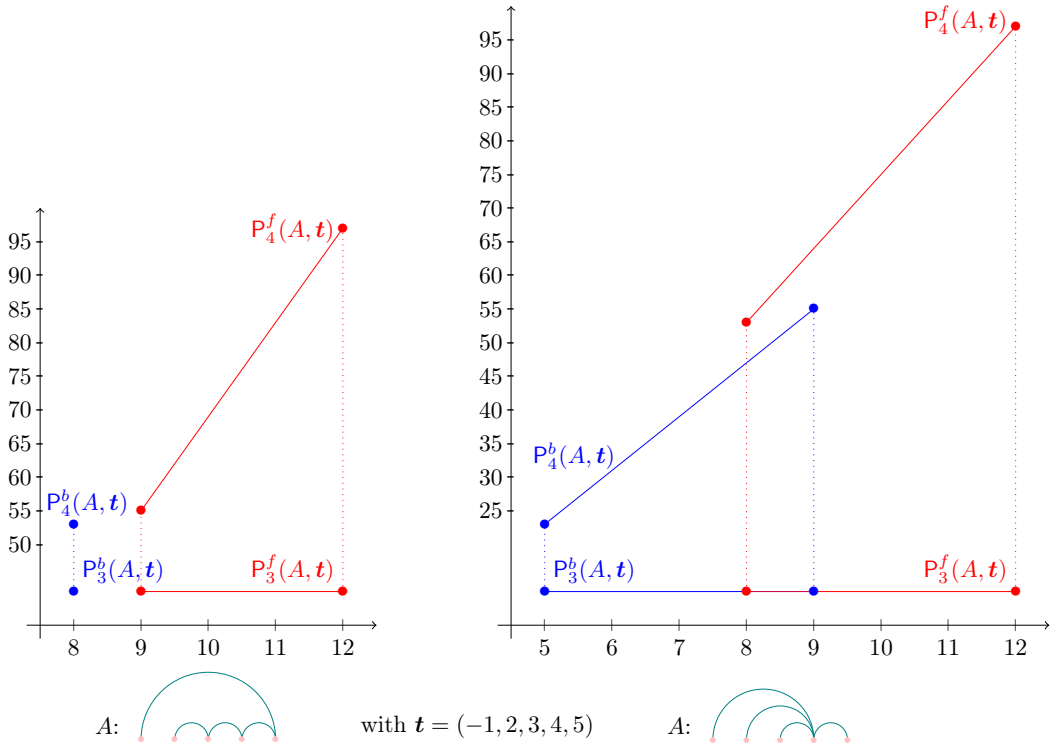

Figure 36: The polytopes $\mathsf{P}_d^b(A,\boldsymbol{t})$ and $\mathsf{P}_d^f(A,\boldsymbol{t})$ with $\boldsymbol{t} = (-1,2,3,4,5)$, for $d = 3$ (Bottom) and $d = 4$ (Top), for the two non-crossing arborescences drawn (Left and Right).

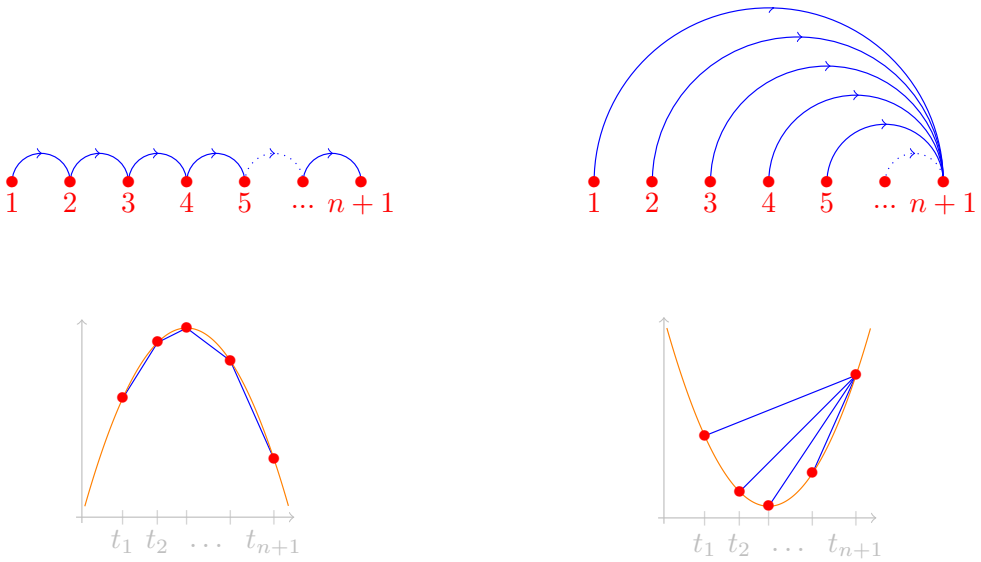

Figure 37: The two (universal) non-crossing arborescences of intrinsic degree 2, and degree 2 polynomials capturing them.

$y_f = t_{k-1} + t_k + t_{n+1} < t_k + t_{k+1} + t_n = x_b$. This proves (a). Otherwise, A satisfies Corollary 3.19 (ii) for some $1 < k < n-1$ and $n \geq j_1 \geq j_2 \geq \cdots \geq j_{k-1} > k$. Note that $\mathcal{I}_A^b \subseteq [k-1]$ and they are all leaves. For (b), $k = n-2$ and $j_1 = \cdots = j_{n-4} = n$. If $j_{n-3} = n$, then $n-2$ is the only forward-sliding node and $x_f = y_f = t_{n-2} + t_{n-1} + t_n > t_{n-3} + t_{n-1} + t_n = y_b$. If $j_{n-3} = n-1$, then $x_f = y_f = t_{n-3} + t_{n-1} + t_n > \max(t_{n-3} + t_{n-1} + t_{n-2},\ t_{n-4} + t_{n-1} + t_n) = y_f$. Likewise, for (c) we have $k = 2$. If $A(1) = 3$, then $x_b = y_b = t_1 + t_2 + t_3 < t_1 + t_3 + t_4 = x_f$. If $A(1) = 4$, then $x_b = y_b = t_1 + t_3 + t_4 < \min(t_2 + t_3 + t_4, t_1 + t_4 + t_5) = x_f$.

Assume A satisfies Corollary 3.19 (ii) with $\mathbb{L}(A) = \{k\}$, but neither (b) nor (c). In this case, we will find $\boldsymbol{t}$ with $\mathsf{P}_d^f(A, \boldsymbol{t}) \cap \mathsf{P}_d^b(A, \boldsymbol{t}) \neq \varnothing$, which proves A is not universal. By Lemma 3.20, $\mathsf{P}_d^f(A, \boldsymbol{t}) \cap \mathsf{P}_d^b(A, \boldsymbol{t}) = \varnothing$ if and only if $y_b < x_f$.

If k is forward-sliding, then $k^* = k+1$ and either there is $i < k$ with $j_i > A(k^*) = k+2$, or $j_1 = \cdots = j_{k-1} = k+2 < n$ and $1 < k-1$. In the first case, choose the maximal $i < k$ with $j_i > k+2$: i is backward-sliding and $i^* = A(i^*) - 1 = j_i - 1 > k+1$. For any $\boldsymbol{t} \in \mathsf{O}_n^\circ$ with $t_{i^*} > t_k + t_{k+1}$ it follows $x_f \leq t_k + t_{k+1} + t_{k+2} < t_i + t_{i^*} + t_{A(i^*)} \leq y_b$. In the second case, $i = 1$ is forward-sliding with $i^* = k+2$, and $k-1$ is backward-sliding with $(k-1)^* = k+1$. Choosing $\boldsymbol{t} \in \mathsf{O}_n^\circ$ with t_1 small enough, ensures $x_f \leq t_1 + t_{1^*} + t_{A(1^*)} < t_{k-1} + t_{k-1^*} + t_{A(k-1^*)} \leq y_b$.

If k is not forward-sliding, then $k-1$ is backward-sliding with $(k-1)^* = k$ and there is a minimal forward-sliding $i < k$ with $i^* = k+1$. If $i < k-1$ then we can find $\boldsymbol{t} \in \mathsf{O}_n^\circ$ with t_i small enough so that $x_f \leq t_i + t_{k+1} + t_{k+2} < t_{k-1} + t_k + t_{k+1} \leq y_b$. If $i = k-1$, then $1 < k-1$ and we can choose $j < k-1$ forward-sliding. Similarly, we can find $\boldsymbol{t} \in \mathsf{O}_n^\circ$, with t_j small enough and thus $x_f \leq t_j + t_{j^*} + t_{A(j^*)} < t_{k-1} + t_k + t_{k+1} \leq y_b$. □

Corollary 3.22. *The number of universal non-crossing arborescences $A : [n] \to [n]$ with $\mu(A) \leq 3$ is $n+3$.*

Proof. The universal non-crossing arborescences on $[n]$ are characterized by Theorem 3.21. There are exactly two non-crossing arborescences with $\mu(A) = 2$. Moreover, there are $n-3$ arborescences of the form (a), 2 of the form (b) and 2 of the form (c). □

Example 3.23. In Figure 38(Left), you can see all non-crossing arborescences $A : [5] \to [5]$ with $\mu(A) \leq 3$. Two arborescences A, A' are connected by an edge if and only if they differ by a flip.

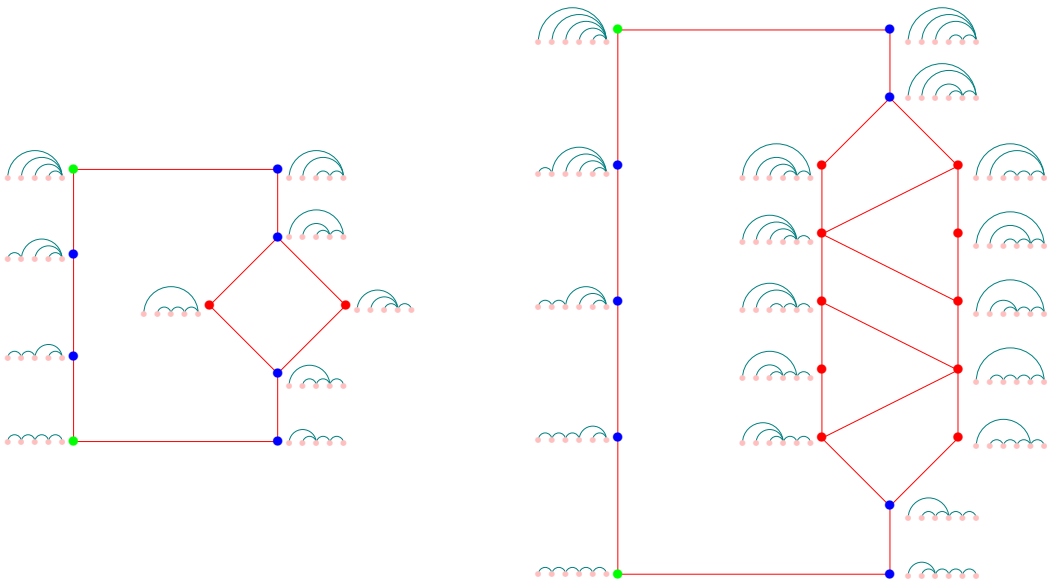

Figure 38: All non-crossing arborescences A on $n = 5$ (Left) and $n = 6$ (Right) nodes with $\mu(A) \leq 3$. Green and blue dots represent universal arborescences, red dots non-universal ones.

The arborescences at the green dots are the two universal arborescences of intrinsic degree 2, the ones at the blue dots are the universal arborescences of intrinsic degree 3. The two remaining arborescences at the red dots are the two non-universal arborescences of intrinsic degree 3, see Example 3.17.

One can construct the same graph for $n = 6$, see Figure 38(Right), and $n = 7$, see Figure 39. Note that these graphs are oriented from top to bottom by the Tamari orientation of flips. For $d \geq 4$ and fixed $\boldsymbol{t}$, one can consider the graph $G_{\boldsymbol{t}}$ whose set of vertices is the set of A with $\mu(A, \boldsymbol{t}) \leq 3$, and the edges are the flips between them. This forms a sub-graph of the graph of $\mathsf{Asso}_{d-1}(\boldsymbol{t})$, and hence a sub-graph of the graph of the associahedron. The projection principle of Proposition 3.9 ensures that $G_{\boldsymbol{t}}$ is the graph of a polygon, thus $G_{\boldsymbol{t}}$ is a cycle. The idea behind the rest of this section will be to prove that $G_{\boldsymbol{t}}$ is a *great cycle* in Figures 38 and 39 (and of the corresponding graph for greater n), meaning that $G_{\boldsymbol{t}}$ is composed by two paths from A_M to A_m: the left path of universal arborescences, and a right path that is increasing for the Tamari orientation. Not all increasing right paths will correspond to a $G_{\boldsymbol{t}}$ for some $\boldsymbol{t}$, but this will allow us to prove that the number of vertices of $G_{\boldsymbol{t}}$ is independent from $\boldsymbol{t}$.

Remark 3.24. Applying the bijection between non-crossing arborescences and triangulations to Figure 38 we obtain the graph of the fiber polytope for the canonical projection from $\mathsf{Cyc}_4(\boldsymbol{t})$ to $\mathsf{Cyc}_2(\boldsymbol{t})$ for $\boldsymbol{t} \in \mathsf{O}_n^\circ$ as pictured in Figure [ALRS00, Figure 1]. The study of this phenomenon will be at the heart of Section 4.3.

In the remaining of the section, we are going to use the properties of cubic arborescences and the first property we have given of their realization set in order to count the number of cubic arborescences that can be captured for a given $\boldsymbol{t} \in \mathsf{O}_n^\circ$. Even though it will be notationally heavy, most of it will boil down to proving that what our previous drawings indicates holds in general.

Definition 3.25. For a non-crossing arborescence A, a forward-sliding i is called *minimal* when i is a leaf, and a backward-sliding i is called *maximal* when $i^* + 1 = A(i^*)$.

Lemma 3.26. *Let $A : [n] \to [n]$ be a non-universal cubic arborescence, and $\mathbb{L}^\circ(A) = \{k\}$. For any minimal forward-sliding i, $i^* + 1 = A(i^*)$ with $i \leq k$ and $i^* > k$. Any maximal backward-sliding j is a leaf, $j < k$ and $j^* \geq k$.*

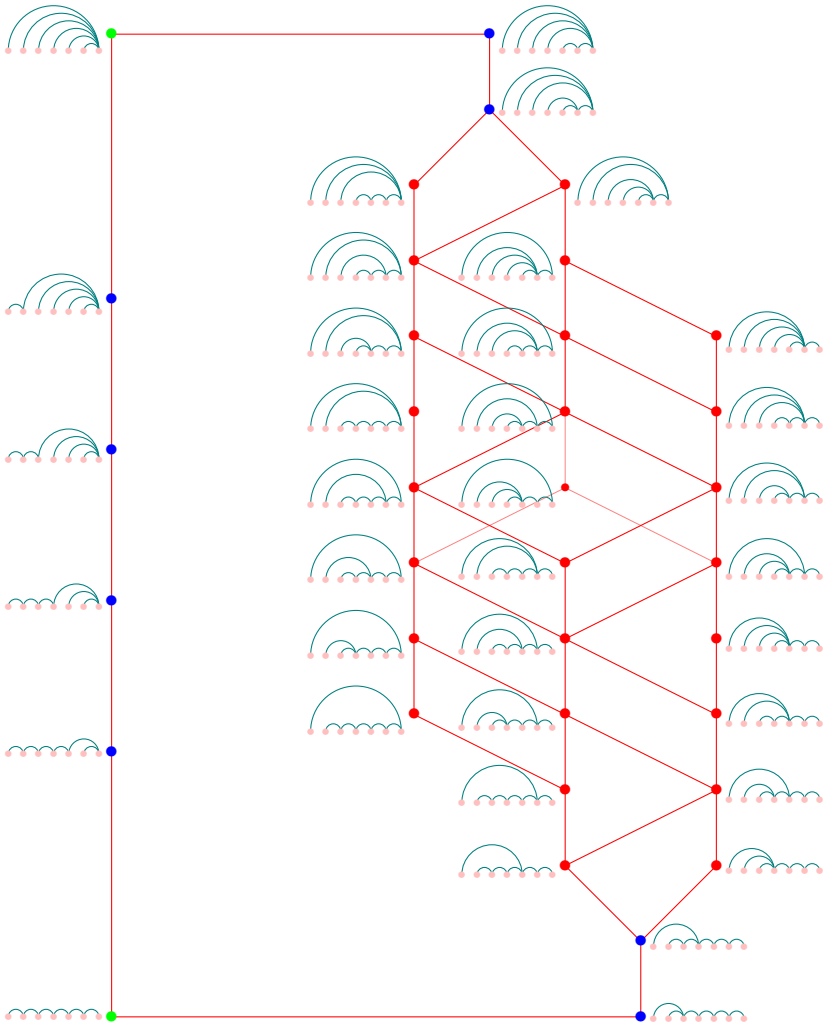

Figure 39: All non-crossing arborescences A on $n = 7$ nodes with $\mu(A) \leq 3$. Green and blue dots represent universal arborescences, red dots non-universal ones.

Proof. Since A is non-universal and cubic, A is of the form described in Corollary 3.19(ii). For any $i > k$, one has $A(i-1) = i$; thus any minimal forward-sliding i has to be smaller or equal to k. Moreover this ensures that $i^* > k$ and $A(i^*) = i^* + 1$.

Suppose j is backward-sliding and maximal. The fact that $A(j) > j+1$, forces $j < k$. Thus j is a leaf. By Corollary 3.19(ii), $j^* > k$. □

Theorem 3.27. *Let $A : [n] \to [n]$ be a cubic arborescence and $\boldsymbol{t} \in \mathsf{O}_n^\circ$. If A is non-universal, then $\boldsymbol{t} \in \mathcal{T}_3^\circ(A)$ if and only if*

(i) $t_i < t_{i+1}$ for all $1 \leq i < n$,

(ii) $t_j + t_{j^*} + t_{A(j^*)} < t_i + t_{i^*} + t_{A(i^*)}$ for all $j \in \mathcal{I}_A^b$ maximal and $i \in \mathcal{I}_A^f$ minimal.

Proof. Let A be cubic non-universal. By Theorem 3.16, it suffices to show that $\mathsf{P}_d^f(A, \boldsymbol{t}) \cap \mathsf{P}_d^b(A, \boldsymbol{t}) = \varnothing$ and $\boldsymbol{t} \in \mathsf{O}_n^\circ$ precisely when $\boldsymbol{t}$ satisfies the conditions (i) and (ii). Let $\mathsf{P}_d^f(A, \boldsymbol{t}) = [x_f, y_f]$ and $\mathsf{P}_d^b(A, \boldsymbol{t}) = [x_b, y_b]$. By Lemma 3.20 we conclude that for $\boldsymbol{t} \in \mathsf{O}_n^\circ$, $\mathsf{P}_d^f(A, \boldsymbol{t}) \cap \mathsf{P}_d^b(A, \boldsymbol{t}) = \varnothing$ if and only if $y_b < x_f$. As a consequence any $\boldsymbol{t} \in \mathcal{T}_3^\circ(A)$ satisfies (i) and (ii).

Conversely, let $\boldsymbol{t} \in \mathbb{R}^n$ fulfil (i) and (ii). Obviously $t \in \mathsf{O}_n^\circ$.

Assume that $i \in \mathcal{I}_A^f$ is not minimal. Then there is a forward-sliding leaf $a < i$ and $m > 1$ such that $A^m(a) = i$. This shows $x_f \leq t_a + t_{a^*} + t_{A(a^*)} < t_i + t_{i^*} + t_{A(i^*)}$. Hence $t_j + t_{j^*} + t_{A(j^*)} < t_i + t_{i^*} + t_{A(i^*)}$ is implied by $t_j + t_{j^*} + t_{A(j^*)} < t_a + t_{a^*} + t_{A(a^*)}$.

Assume that $j \in \mathcal{I}_A^b$ is not maximal. Then $j^* < A(j^*) - 1$ implies that there exists a backward-sliding b with $j^* \leq b < A(j^*)$ and $A(j^*) = A(b^*) = b^* + 1$. This shows $t_i + t_{i^*} + t_{A(i^*)} < t_j + t_{j^*} + t_{A(j^*)} \leq y_b$. We conclude that $t_j + t_{j^*} + t_{A(j^*)} < t_i + t_{i^*} + t_{A(i^*)}$ is implied by $t_b + t_{b^*} + t_{A(b^*)} < t_i + t_{i^*} + t_{A(i^*)}$.

□

Example 3.28. For $n = 5$, there are 10 non-crossing arborescences A with $\mu(A) \leq 3$, see Figure 38(Left). Among them, 8 are universal and 2 are not. We have discussed the 2 non-universal ones in Example 3.17. Theorem 3.27 allows us to compute the realizations sets of theses 2 non-universal arborescences: besides facets of O_5, they have a facet on the hyperplane $\{\boldsymbol{t} \in \mathbb{R}^5 \ ; \ t_2 + t_3 + t_4 = t_1 + t_4 + t_5\}$. In Figure 40(Bottom) are drawn these two realization sets, embedded inside the order cone O_5. As this cone is 5-dimensional, we intersect it with the two hyperplanes $\{\boldsymbol{t} \in \mathbb{R}^5 \ ; \ t_1 = 0\}$ and $\{\boldsymbol{t} \in \mathbb{R}^5 \ ; \ t_5 = 1\}$, making the picture 3-dimensional. For each realization sets, we have drawn in blue $\mathsf{Asso}_{d-1}(\boldsymbol{t})$ for $d = 4$ which is an associahedron, and highlighted in red the non-crossing arborescences A with $\mu(A, \boldsymbol{t}) \leq 3$ for the corresponding $\boldsymbol{t}$.

Remark 3.29. Note that different cases of Theorem 3.27 lead to the same inequality (see Figure 41):

(i) For example, if $i \in \mathcal{I}_A^b \cap [1, k-1]$, $i+1 \in \mathcal{I}_A^f$ and $A(i+1) < i^*$. Since $i+1 \leq k$, $i+1$ is a leaf and thus minimal. By $A(i+1) < i^*$ and thus $i^* > k$ follows that i is maximal. Moreover, $i < i+1 < k < A(i+1) < A(A(i+1)) \leq i^* < A(i^*)$. By (ii), $t_{A(i+1)} < t_{A(A(i+1))} \leq t_{i^*} < t_{A(i^*)}$ and so (iii) implies $t_i < t_{i+1}$.

(ii) If $i \in \mathcal{I}_A^b$, $j \in \mathcal{I}_A^f$ and $i = j$, then $A(i^*) = j^*$ and thus the inequality $t_i + t_{i^*} + t_{A(i^*)} < t_j + t_{j^*} + t_{A(j^*)}$ is implied by $t_{i^*} < t_{A(j^*)}$.

(iii) If $i \in \mathcal{I}_A^b$, $j \in \mathcal{I}_A^f$ and $i^* = j^*$, then $j < i$ as A is non-crossing. As i is forward-sliding and j is maximal, $i = j + 1$ and the inequality corresponding to i and j follows from $t_j < t_i$.

Now we want a closer look at the realization set and describe, which of the inequalities in Theorem 3.27 of the form (ii) give a facet for $\mathcal{T}_3(A)$.

Let $A : [n] \to [n]$ be a non-crossing arborescence, $i \in [n-2]$ forward-sliding and $j \in [n-2]$ backward-sliding. Recall the definitions of flips ($F_i A$ and $B_j A$ are non-crossing arborescences):

$$F_i A(k) = \begin{cases} A(i^*) & k = i \\ A(k) & k \neq i \end{cases} \quad \text{and} \quad B_j A(k) = \begin{cases} j^* & k = j \\ A(k) & k \neq i. \end{cases}$$

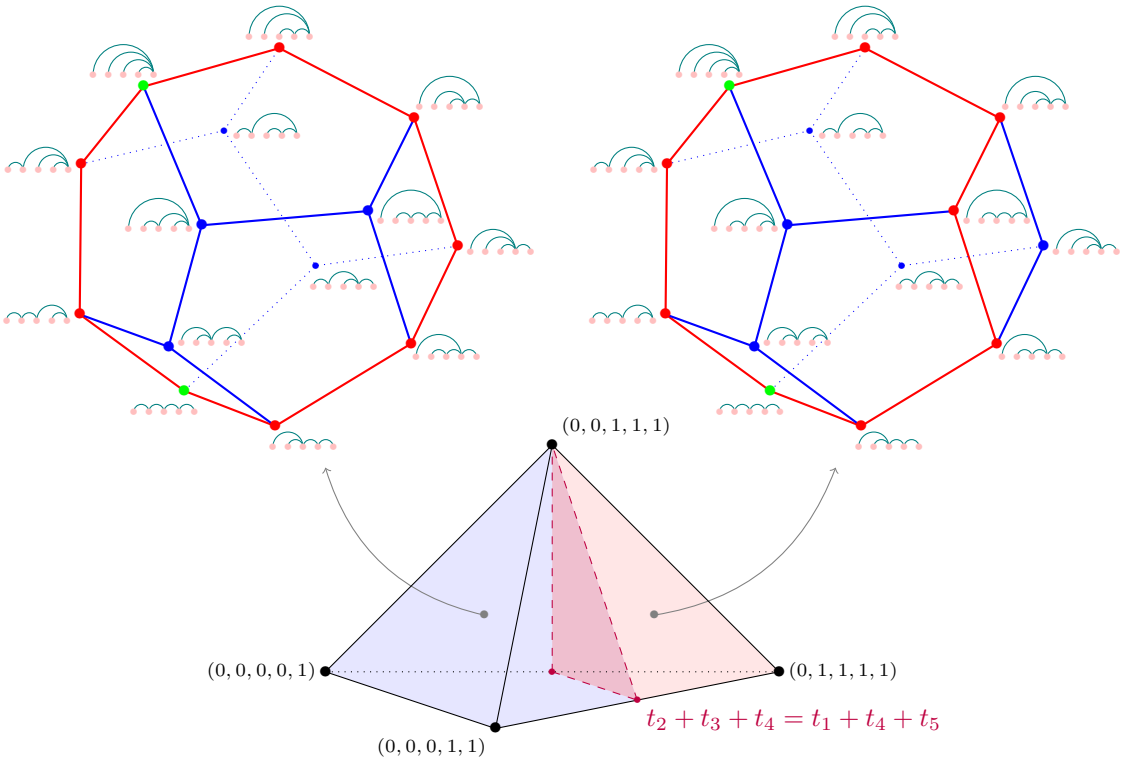

Figure 40: The order cone O_5 intersected by the hyperplanes $\{\boldsymbol{t}\ ;\ t_1 = 0\}$ and $\{\boldsymbol{t}\ ;\ t_5 = 1\}$, and subdivided into the different realization sets for non-crossing arborescences A with $\mu(A) \leq 3$. For each realization sets, the cyclic associahedron $\mathsf{Asso}_3(\boldsymbol{t})$ with, highlighted in red, the non-crossing arborescences A with $\mu(A, \boldsymbol{t}) \leq 3$.

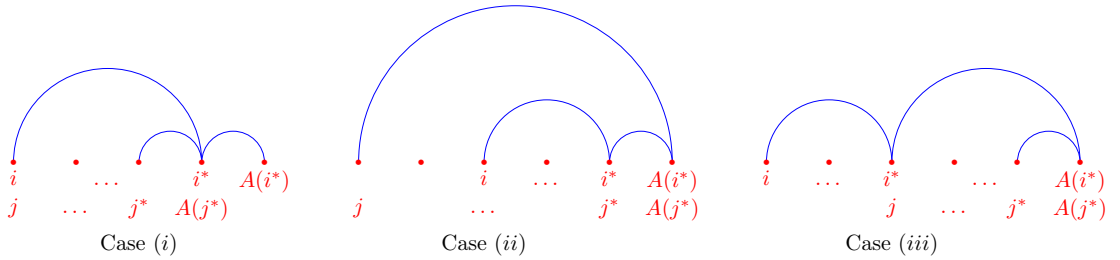

Figure 41: Some diagonal switches are forbidden due to the relative positions of i, j, i^* and j^*.

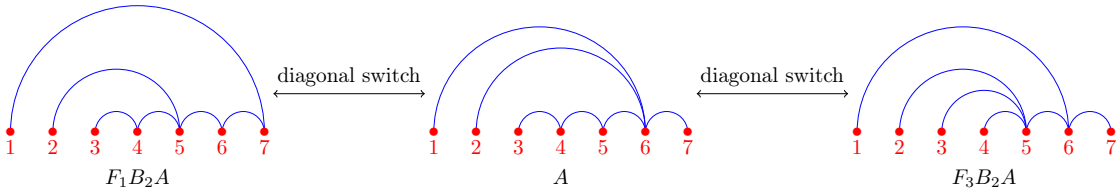

Figure 42: A non-crossing arborescence $A : [7] \to [7]$ and two diagonal switches.

If j is backward-sliding in F_iA and i is forward-sliding in B_jA then we could consider the combination of the two flips. We say that A and A' differ by a *diagonal switch* if $A' = F_iB_jA = B_jF_iA \neq A$, equivalently we say that we perform a diagonal switch with respect to i and j on A.

The notion *diagonal* switch is motivated by the fact that A, F_iA, B_jA and F_iB_jA form a square face[8] of Asso_{n-2}, and switching from A to F_iB_jA corresponds to switching along the diagonal of the square that contains A. In the directed graph $G_{\boldsymbol{t}}$ defined in Example 3.23, a diagonal flip amounts to travelling through two edges: one respecting the Tamari orientation and the other not (in Figure 38 and Figure 39, two arborescences are linked by a diagonal switch when there are at the same height and at distance 2).

Lemma 3.30. *Let $A : [n] \to [n]$ be a non-crossing arborescence, i forward-sliding and j backward-sliding. We can perform a diagonal switch with respect to i and j on A, if and only if the following conditions are fulfilled, see Figure 41:*

(i) $i \neq j$
(ii) $j^* \neq i^*$
(iii) $j \neq i^*$

Proof. Suppose one of the conditions is not fulfilled. If $i = j$, then $F_iB_jA = B_jF_iA = A$. If $j^* = i^*$, then $A(j^*) = A(i^*)$ and as $A(j) = A(j^*) > A(i) = i^*$, we need $j < i$. Hence $B_jA(j) = j^* = i^*$, and thus i is not forward-sliding in B_jA. If $j = i^*$, then $F_iB_jA(i) = j^* \neq B_jF_iA(i) = A(i^*)$.

Suppose $(i) - (iii)$ are fulfilled. Notice that (i) implies $i^* \neq A(j^*)$, (ii) and (iii) imply $A(i^*) \neq A(j^*)$. It cannot happen that $j^* = i$, as then i would not be forward-sliding. If $i = A(j^*), j = A(i^*)$ or $j^* = A(i^*)$, then the diagonal switch can be performed. Otherwise, $\{i, i^*, A(i^*)\} \cap \{j, j^*, A(j^*)\} = \varnothing$ and thus the diagonal switch can be performed as well. □

Corollary 3.31. *Let $A : [n] \to [n]$ be a non-crossing arborescence, $1 \leq i \leq n-2$ forward-sliding and $1 \leq j \leq n-2$ backward-sliding. If $j = i^*$, then either $\mathbb{L}(A) = \{1, n-1\}$ or $\mu(A) > 3$.*

Proof. From $j = i^*$ follows that $A(i^*) = A(j^*)$. As $i^* < A(i^*) - 1$, there is an immediate leaf $i^* < \ell_1 < A(i^*) \leq n-1$. Furthermore either $A(1) = 2$ and thus $1 \in \mathbb{L}(A)$, or there is an interior immediate leaf $1 < \ell_2 < i^*$. □

[8] All induced 3-, 4- and 5-cycles in the graph of a simple polytope are 2-faces, thus the four vertices associated to A, F_iA, B_jA and F_iB_jA form a square **face** of Asso_{n-2}.

Proposition 3.32. *Let $A : [n] \to [n]$ be a cubic non-universal non-crossing arborescence. Let $1 \leq i \leq n-2$ be forward-sliding and minimal and $1 \leq j \leq n-2$ backward-sliding and maximal. If $i \neq j$ and $i^* \neq j^*$, then $A' = F_i B_j A = B_j F_i A$ is cubic and non-universal.*

Proof. As A is non-universal and cubic, by Theorem 3.21 A satisfies $\mathbb{L}(A) = \{\ell\}$, $1 < \ell < n-1$. If i is minimal, then, by Corollary 3.19 and Lemma 3.26, either $i = \ell$ or $i < \ell$. If $i = \ell$, then this implies $i^* = \ell + 1$ and $A(i^*) = \ell + 2$ and thus $\mathbb{L}(F_i A) = \mathbb{L}(F_l A) = \{\ell + 1\}$. If $i < \ell$, then as $A(i^*) = i^* + 1 \geq \ell + 1$, it follows that $\mathbb{L}(F_i A) = \mathbb{L}(A) = \{\ell\}$.

If j is maximal, then, by Corollary 3.19, either $j = \ell - 1$ or $j < \ell < j^*$. In the first case, $j^* = \ell$, $A(j^*) = \ell + 1$ and $\mathbb{L}(B_j A) = \{\ell - 1\}$. In the second case, $\mathbb{L}(B_j A) = \mathbb{L}(A) = \{\ell\}$.

Moreover, we observe, that ℓ can not be forward-sliding and $\ell - 1$ is backward-sliding at the same time. We conclude, that $\mathbb{L}(F_i B_j A) \subseteq [2, n-2]$ and thus $F_i B_j A$ is cubic. If $3 \leq \ell \leq n-3$ this almost shows that $F_i B_j A$ is non-universal. We only have to consider two special cases.
Suppose $\ell = 3$ and $A(1) = 4$. Then only 2 is backward-sliding and maximal and only 1 is forward-sliding and minimal. Thus $\mathbb{L}(B_2 F_1 A) = \{2\}$, but with $A(1) = 5$, implying that $B_2 F_1 A$ is non-universal. Similarly, if $\ell = n-3$ and $A(k) = n$ for all $k < n-3$, then as only $n-3$ is forward-sliding and minimal and only $n-4$ is backward-sliding and maximal. We have $\mathbb{L}(B_{n-4} F_{n-3} A) = \{n-2\}$. Moreover, $B_{n-4} F_{n-3} A(n-4) = n-1$ and thus $B_{n-4} F_{n-3} A$ is non-universal.

If $\ell = 2$, as A is non-universal, we have $A(1) > 4$. Thus only 1 is backward-sliding and maximal, and only 2 is forward-sliding and minimal, which leads to $\mathbb{L}(B_1 F_2 A) = 3$ and hence $B_1 F_2 A$ is non-universal. If $\ell = n-2$, as A is non-universal, we have $A(n-4) = A(n-3) = n-1$. Then the smallest $i < n-4$ such that $A(i) = n-1$ is the only forward-sliding and minimal choice, and only $n-3$ is backward-sliding and maximal. This leads to $\mathbb{L}(F_i B_{n-3} A) = \{n-3\}$ and thus A is non-universal. □

Now we want to highlight some inequalities of Theorem 3.27. Let $A : [n] \to [n]$ be a cubic arborescence. We call a facet of $\mathcal{T}_3(A)$ *internal*, if it is not contained in any facet of O_n. By definition, universal arborescences have no internal facets.

Theorem 3.33. *Let A be a cubic, non-crossing and non-universal arborescence. Any internal facet of $\mathcal{T}_3(A)$ is of the form*

$$\mathcal{T}_3(A) \cap \{\boldsymbol{t} \in \mathbb{R}^n \ ; \ t_j + t_{j^*} + t_{A(j^*)} = t_i + t_{i^*} + t_{A(i^*)}\},$$

where i is forward-sliding and minimal and j is backward-sliding and maximal, and a diagonal switch can be performed on A with respect to i and j.

Proof. In the inequality description given by Theorem 3.27, the inequalities of the form (i) come from facets of O_n. By Lemma 3.30 and Corollary 3.31, a diagonal switch can be performed with respect to i and j if and only if $i \neq j$ and $i^* \neq j^*$. If $i = j$ or $i^* = j^*$, then the associated inequality gives rise to a facet of O_n, Remark 3.29(ii) and (iii). □

Remark 3.34. The above Theorem 3.33 almost gives a facet-description of $\mathcal{T}_3(A)$. Indeed, we know that its facets are associated to pairs of compatible **minimal** forward-sliding and **maximal** backward-sliding nodes, but it is not mandatory that all such couples are associated to a facet. Nonetheless, the collection of such couples is far smaller than the collection of all couples of forward-sliding and backward-sliding nodes, and will reveal to be far more manageable thanks to the diagonal flip.

Definition 3.35. The *switching arrangement* $\mathcal{H}_n$ is the collection of hyperplanes

$$H_{(i,j)} = \{\boldsymbol{t} \in \mathbb{R}^n : t_j + t_{j^*} + t_{A(j^*)} = t_i + t_{i^*} + t_{A(i^*)}\}$$

for all couples (i, j) such that there exists a non-crossing non-universal cubic arborescence $A : [n] \to [n]$ with i forward-sliding and minimal, and j backward-sliding and maximal and a diagonal switch can be performed with respect to i and j.

For $\boldsymbol{t} \in \mathbb{R}^n$, let $\mathcal{A}(\boldsymbol{t})$ be the collection of non-crossing arborescences $A : [n] \to [n]$ such that $\boldsymbol{t} \in \mathcal{T}_3^\circ(A)$. Observe, that $A \in \mathcal{A}(\boldsymbol{t})$ for any universal $A : [n] \to [n]$ and any $\boldsymbol{t} \in \mathsf{O}_n^\circ$. We can prove the last main theorem of this section:

Theorem 3.36. *For all $\boldsymbol{t}, \boldsymbol{t}' \in \mathsf{O}_n^\circ \setminus \bigcup_{H \in \mathcal{H}_n} H$, one has $|\mathcal{A}(\boldsymbol{t})| = |\mathcal{A}(\boldsymbol{t}')|$.*

Proof. By Theorem 3.33, if $\boldsymbol{t}$ and $\boldsymbol{t}'$ belong to the same maximal cone of $\mathsf{O}_n^\circ \setminus \bigcup_{H \in \mathcal{H}_n} H$, then $\mathcal{A}(\boldsymbol{t}) = \mathcal{A}(\boldsymbol{t}')$.

Suppose $\boldsymbol{t} \in \mathsf{C}$ and $\boldsymbol{t}' \in \mathsf{C}'$ where C and C' are two adjacent maximal cones of $\mathsf{O}_n^\circ \setminus \bigcup_{H \in \mathcal{H}_n} H$. Then C and C' are separated by a hyperplane $H_{(i,j)}$.

For $A \in \mathcal{A}(\boldsymbol{t})$, if (i, j) is not a couple with i minimal forward-sliding in A and j maximal backward-sliding in A such that a diagonal switch can be performed, then $A \in \mathcal{A}(\boldsymbol{t}')$, as the segment $[\boldsymbol{t}, \boldsymbol{t}']$ does cross any facet of $\mathcal{T}_3(A)$.

Suppose the converse. Then $A \notin \mathcal{A}(\boldsymbol{t}')$, but we can perform a diagonal switch on A with respect to i and j to obtain $A' = F_i B_j A$. We are going to prove that $A' \in \mathcal{A}(\boldsymbol{t}')$. For a minimal forward-sliding in A', then one can list the possibilities: either $a = j$, or $a^* = i$, or $a^* = j^*$, or a is forward-sliding in A (all other possibilities contradict the minimality of a or the fact that $\mu(A') = 3$). In all these cases, as A is captured on $\boldsymbol{t}$, we have $t_i + t_{i^*} + t_{A(i^*)} \leq t_a + t_{a^*} + t_{A'(a^*)}$. By adjacency of C and C', the segment $[\boldsymbol{t}, \boldsymbol{t}']$ does not cross any hyperplane of $\mathcal{H}_n$ other than $H_{(i,j)}$, so $t'_j + t'_{j^*} + t'_{A'(j^*)} \leq t'_a + t'_{a^*} + t'_{A'(a^*)}$. The same arguments ensure that $t'_i + t'_{i^*} + t'_{A'(i^*)} \leq t'_b + t'_{b^*} + t'_{A'(b^*)}$ for all b maximal back-sliding in A'. By construction of $\boldsymbol{t}'$, we have $t'_i + t'_{i^*} + t'_{A'(i^*)} \leq t'_j + t'_{j^*} + t'_{A'(j^*)}$. Consequently, $\boldsymbol{t}' \in \mathcal{T}_3(A')$, meaning that $A' \in \mathcal{A}(\boldsymbol{t}')$.

We have proven that $|\mathcal{A}(\boldsymbol{t})| \geq |\mathcal{A}(\boldsymbol{t}')|$. By symmetry, both quantities are equal. The theorem results from the fact that the graph of maximal cones of $\mathsf{O}_n^\circ \setminus \bigcup_{H \in \mathcal{H}_n} H$ is connected. □

Corollary 3.37. *If $\boldsymbol{t} \in \mathsf{O}_n^\circ \setminus \bigcup_{H \in \mathcal{H}_n} H$, then $|\mathcal{A}(\boldsymbol{t})| = \binom{n}{2} - 1$.*

Proof. By Theorem 3.36 it is enough to show $|\mathcal{A}(\boldsymbol{t})| = \binom{n}{2} - 1$ for some $\boldsymbol{t} \in \mathsf{O}_n^\circ \setminus \bigcup_{H \in \mathcal{H}_n} H$. Let $\boldsymbol{t}_{lex} = (2, 2^2, \ldots, 2^n)$. Recall that for $m \in \mathbb{N}$, $2^m - 1 = \sum_{i=0}^{m-1} 2^i$ and thus $2^m > \sum_{i=0}^{m-1} 2^i$. Thus for any triples $(i_1, i_2, i_3), (j_1, j_2, j_3)$ with $1 \leq i_1 < i_2 < i_3 \leq n$ and $1 \leq j_1 < j_2 < j_3 \leq n$, $2^{i_1} + 2^{i_2} + 2^{i_3} = 2^{j_1} + 2^{j_2} + 2^{j_3}$ if and only if $(i_1, i_2, i_3) = (j_1, j_2, j_3)$. This implies that $\boldsymbol{t}_{lex} \in \mathsf{O}_n^\circ \setminus \bigcup_{H \in \mathcal{H}_n} H$.

Let $A : [n] \to [n]$ be a non-crossing arborescence with $\mu(A) \leq 3$. If A is universal, then $A \in \mathcal{A}(\boldsymbol{t}_{lex})$. There are two such arborescences of intrinsic degree 2 by Corollary 3.18 and $n - 3$ of intrinsic degree 3 by Corollary 3.19(i). Otherwise, $\mathbb{L}(A) = \mathbb{L}^\circ(A) = \{\ell\} \subseteq [2, n-2]$, see Corollary 3.19. By Lemma 3.26, if j is backward-sliding and maximal, then $j < \ell$, $j^* > \ell$ and $A(j^*) = j^* + 1$. If i is forward-sliding and minimal, then $i \leq \ell$ and $A(i^*) - 1 = i^* > \ell$. Consequently, $A \in \mathcal{A}(\boldsymbol{t}_{lex})$ if and only if for all i minimal forward and j maximal backward:

$$2^j + 2^{j^*} + 2^{A(j^*)} < 2^i + 2^{i^*} + 2^{A(i^*)}. \tag{12}$$

As A is non-crossing, if $j < i$, then $j^* \geq i^*$. Assume $j^* \geq i^* + 1$. Then $2^{A(j^*)} > 2^i + 2^{i^*} + 2^{A(i^*)}$ and thus $A \notin \mathcal{A}(\boldsymbol{t}_{lex})$. Otherwise, if $i^* = j^*$, then Equation (12) holds. If $j \geq i$, then $A(i^*) > j^*$ and thus Equation (12) also holds. Consequently, if $A \in \mathcal{A}(\boldsymbol{t}_{lex})$, then there is $p \in [\ell]$ and $k \in [\ell + 1, n - 1]$ such that for all $i < p$, $A(i) = k$ and for all $p \leq i < \ell$, $A(i) = k + 1$. If $k > \ell + 1$, then ℓ is forward-sliding and minimal and $2^{k+1} > 2^\ell + 2^{\ell+1} + 2^{\ell+2}$. Thus $A \in \mathcal{A}(\boldsymbol{t}_{lex})$ if and only if $k = \ell + 1$. The number of those arborescences is

$$\sum_{\ell=2}^{n-2} \sum_{p=1}^{\ell} 1 = \sum_{\ell=2}^{n-2} \ell = \binom{n-1}{2} - 1.$$

Hence in total

$$|\mathcal{A}(\boldsymbol{t}_{lex})| = \binom{n-1}{2} - 1 + (n-1) = \binom{n}{2} - 1.$$

□

Example 3.38. We consider the subdivision of O_n induced by $\mathcal{H}_n$, and then merge the maximal cones C and C' such that $\mathcal{A}(\boldsymbol{t}) = \mathcal{A}(\boldsymbol{t}')$ for $\boldsymbol{t} \in \mathsf{C}$ and $\boldsymbol{t}' \in \mathsf{C}'$. Said differently, we consider the subdivision $\boldsymbol{S}_n$ of O_n induced by the family of polytopes $\mathcal{T}_3(A)$ for A with $\mu(A) \leq 3$.

For $n = 6$, thanks to a computer analysis, we can show that $\boldsymbol{S}_6$ is composed of 12 cones, separated by the 5 hyperplanes of $\mathcal{H}_6$. Corollary 3.37 ensures that to each cone C correspond a 14-gon whose vertices are in bijection with the 14 non-crossing arborescences A with $\mu(A, \boldsymbol{t}) \leq 3$ for all $\boldsymbol{t} \in \mathsf{C}$. In Figure 43 is pictured the dual graph of $\boldsymbol{S}_6$: each maximal cone is represented by its 14-gon whose vertices are labelled by the corresponding non-crossing arborescence. The edges of the dual graph are colored according to the hyperplane of $\mathcal{H}_6$ they correspond to. Moreover, the vertices of the 14-gons are colored with the same colors: hence, following the cyan edge amounts to performing a diagonal switch on the label of the cyan vertex (and similarly for the other colors). As before, green vertices correspond to non-crossing arborescences A with $\mu(A) = 2$, and blue vertices to universal ones with $\mu(A) = 3$.

3.2.3 Pivot polytopes of cyclic polytopes of dimension 2 and 3

The cyclic polytope $\mathsf{Cyc}_d(\boldsymbol{t})$ has a complete graph for $d \geq 4$, but for $d = 2$ and $d = 3$, one can also define the max-slope pivot polytope $\Pi(\mathsf{Cyc}_d(\boldsymbol{t}), \boldsymbol{e}_1)$, even though it will not be the projection of an associahedron. Hence, its vertices will not be associated (in general) to non-crossing arborescences, but just to arborescences on n nodes. For the sake of completeness, we present here the study of the cases $d = 2$ and $d = 3$. To this end, we make use of the method developed in the previous sections (and the proof will be exposed in a more concise way).

Dimension 2 In dimension 2, whatever the chosen $\boldsymbol{t} \in \mathbb{R}^n$, $n \geq 4$, the cyclic polytope $\mathsf{Cyc}_2(\boldsymbol{t})$ is not neighborly: as it is a polygon, its graph is not complete. Thus, its max-slope pivot polytope is not in general the projection of an associahedron. In this section, we describe the max-slope pivot polytope of $\mathsf{Cyc}_2(\boldsymbol{t})$ for the objective function $\boldsymbol{e}_1$.

Theorem 3.39. *For all $\boldsymbol{t} \in \mathsf{O}_n^\circ$, the 1-dimensional polytope $\Pi(\mathsf{Cyc}_2(\boldsymbol{t}), \boldsymbol{e}_1)$ has two vertices, one corresponding to the arborescence $A_m^{(2)}$ defined by $A_m^{(2)}(i) = i+1$ for all $i \in [n]$, and one corresponding to $A_M^{(2)}$ defined by $A_M^{(2)}(1) = n$ and $A_M^{(2)}(i) = i + 1$ for $i \neq 1$, see Figure 44.*

Proof. As $\mathsf{Cyc}_2(\boldsymbol{t})$ is 2-dimensional, $\Pi(\mathsf{Cyc}_2(\boldsymbol{t}), \boldsymbol{e}_1)$ is 1-dimensional and has precisely two vertices.

Fix $\boldsymbol{t} \in \mathsf{O}_n^\circ$. When orienting $\mathsf{Cyc}_2(\boldsymbol{t})$ along $\boldsymbol{e}_1$, the only improving neighbor of $\boldsymbol{\gamma}_d(t_i)$ is $\boldsymbol{\gamma}_d(t_{i+1})$ for $i \neq 1$; on the other hand, $\boldsymbol{\gamma}_d(t_1)$ has two improving neighbors: $\boldsymbol{\gamma}_d(t_2)$ and $\boldsymbol{\gamma}_d(t_n)$. Thus, there are exactly two possible arborescences on $\mathsf{Cyc}_2(\boldsymbol{t})$: $A_m^{(2)}$ and $A_M^{(2)}$. Consequently $A_m^{(2)}$ and $A_M^{(2)}$ correspond to the two vertices of $\Pi(\mathsf{Cyc}_2(\boldsymbol{t}), \boldsymbol{e}_1)$. □

Remark 3.40. The arborescences $A_m^{(2)}$ and $A_M^{(2)}$ are universal in the sense that they appear as vertices of $\Pi(\mathsf{Cyc}_2(\boldsymbol{t}), \boldsymbol{e}_1)$ for all $\boldsymbol{t} \in \mathsf{O}_n^\circ$. Note that $A_m^{(2)}$ is captured on all $\boldsymbol{t} \in \mathsf{O}_n^\circ$ by any polynomial $P(t) = a_2t^2 + a_1t + a_0$ with $a_2 < 0$ whereas $A_M^{(2)}$ is captured when $a_2 > 0$.

Last but not least, although $A_m^{(2)} = A_m$ is a non-crossing arborescence of degree 2 in the sense of the previous section, this is not the case of $A_M^{(2)} \neq A_M$.

Dimension 3 In dimension $d = 3$, whatever the chosen $\boldsymbol{t} \in \mathsf{O}_n$, $n \geq 5$, the cyclic polytope $\mathsf{Cyc}_3(\boldsymbol{t})$ is not neighborly: its graph is not complete. Thus, its max-slope pivot polytope is not in general the projection of an associahedron. In this section, we will explore the max-slope pivot polytope of the cyclic polytope $\mathsf{Cyc}_3(\boldsymbol{t})$. First, we need to understand the edges of $\mathsf{Cyc}_3(\boldsymbol{t})$.

Lemma 3.41. *When orienting $\mathsf{Cyc}_3(\boldsymbol{t})$ along $\boldsymbol{e}_1$, the vertex $\boldsymbol{\gamma}_d(t_i)$ has at most 2 improving neighbors for $i \neq 1$: $\boldsymbol{\gamma}_d(t_j)$ with $j \in \{i+1, n\}$. Moreover, every $\boldsymbol{\gamma}_d(t_j)$ for $1 < j \leq n$ is an improving neighbor of $\boldsymbol{\gamma}_d(t_1)$.*

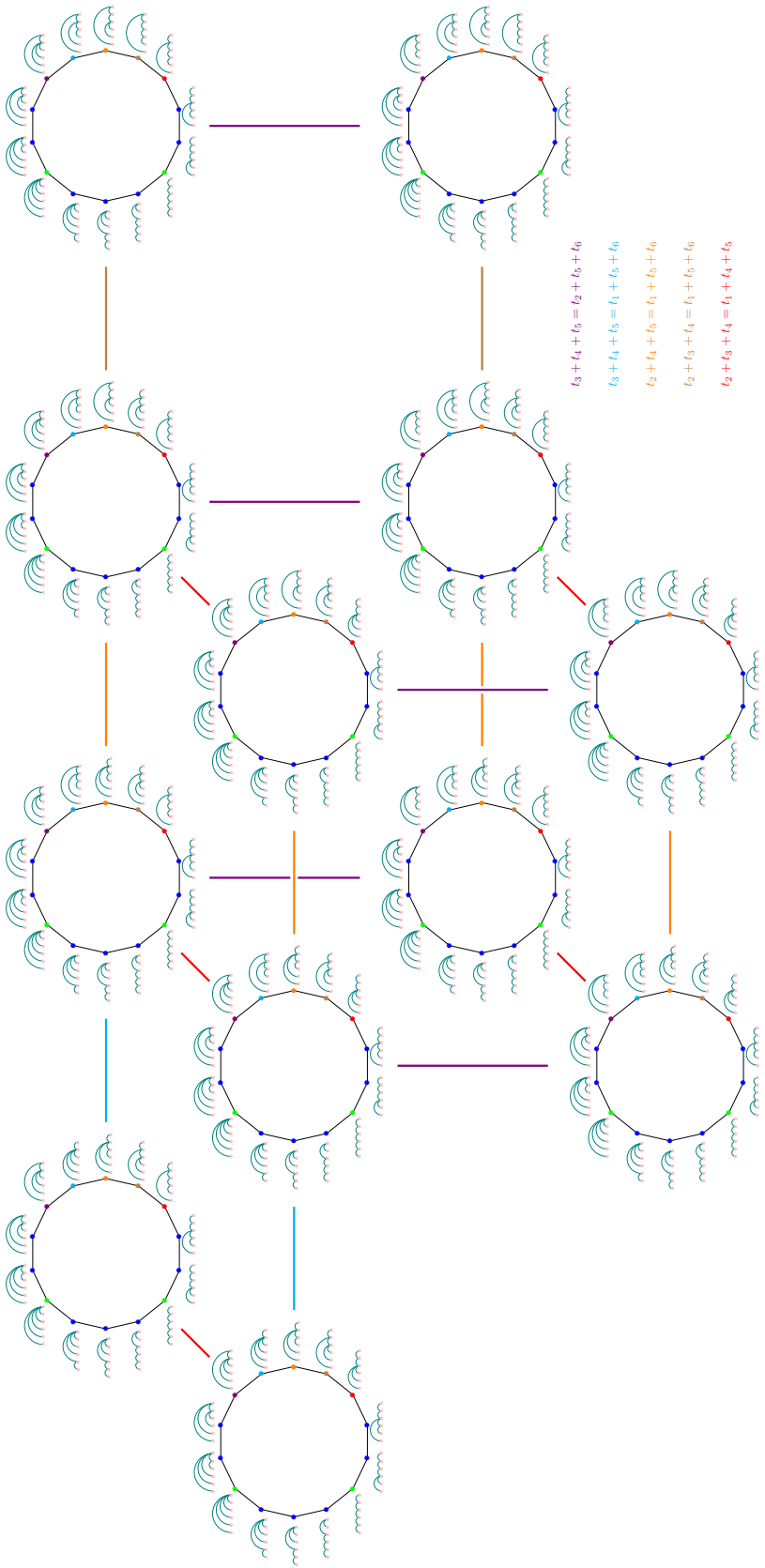

Figure 43: Dual graph of the subdivision of O_6 induced by $\mathcal{T}_3(A)$ for A non-crossing with $\mu(A) \leq 3$.

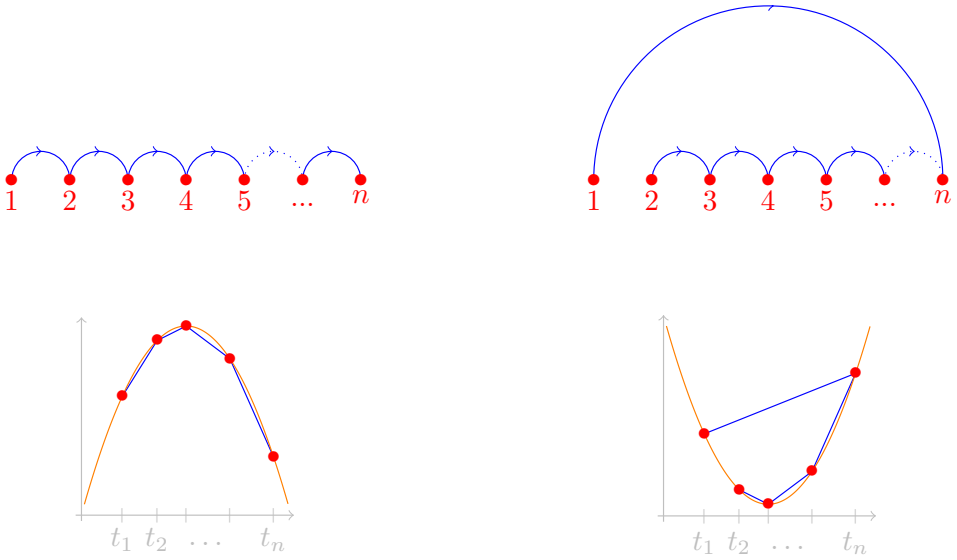

Figure 44: The two arborescences $A_m^{(2)}$ (Left) and $A_M^{(2)}$ (Right) appearing as vertices of $\Pi(\mathsf{Cyc}_2(\boldsymbol{t}), \boldsymbol{e}_1)$ for all $\boldsymbol{t} \in \mathsf{O}_n^\circ$, and degree 2 polynomials capturing them.

Proof. As $\mathsf{Cyc}_3(\boldsymbol{t})$ is a simplicial 3-dimensional polytope, its facets are triangles. By Gale's evenness condition (see [Zie98] Theorem 0.7), the vertices $\boldsymbol{\gamma}_d(t_a)$, $\boldsymbol{\gamma}_d(t_b)$ and $\boldsymbol{\gamma}_d(t_c)$ form a facet when there is an even number of elements from $\{a, b, c\}$ between the elements of $[n]\backslash\{a, b, c\}$. This means either $\{a, b, c\} = \{1, i, i+1\}$ for some $1 < i < n$, or $\{a, b, c\} = \{i, i+1, n\}$ for some $1 < i < n$. Thus, edges of $\mathsf{Cyc}_3(\boldsymbol{t})$ are $[\boldsymbol{\gamma}_d(t_i), \boldsymbol{\gamma}_d(t_{i+1})]$, $[\boldsymbol{\gamma}_d(t_1), \boldsymbol{\gamma}_d(t_i)]$ and $[\boldsymbol{\gamma}_d(t_i), \boldsymbol{\gamma}_d(t_n)]$. Orienting them along $\boldsymbol{e}_1$ yields the lemma. □

Definition 3.42. A *3-arborescence* is a map $A : [n] \to [n]$ with $A(i) \in \{i+1, n\}$ for $i \neq 1$ (and $A(1) \in [n]$).

Hence, by Lemma 3.41, each vertex of $\Pi(\mathsf{Cyc}_3(\boldsymbol{t}), \boldsymbol{e}_1)$ can be associated to a 3-arborescence. Note that such arborescences can have crossings, contrarily to what we discussed so far.

The fact that $\mathsf{Cyc}_3(\boldsymbol{t})$ is not neighborly also modifies the notion of capturing an arborescence.

Proposition 3.43. *A 3-arborescence A corresponds to a vertex of $\Pi(\mathsf{Cyc}_3(\boldsymbol{t}), \boldsymbol{e}_1)$ if and only if there exists a polynomial P of degree at most 3 such that (denoting $\tau(a, b) = \frac{P(b)-P(a)}{b-a}$ as usual):*

- *for all $j \notin \{1, A(1)\}$, $\tau(1, A(1)) > \tau(1, j)$.*
- *for all $i \neq 1$, if $A(i) = i+1$, then $\tau(i, i+1) > \tau(i, n)$, else if $A(i) = n$, then $\tau(i, n) > \tau(i, i+1)$.*

Proof. Fix $\boldsymbol{t} = (t_1, ..., t_n)$. A 3-arborescence A corresponds to a max-slope arborescence for the linear program $(\mathsf{Cyc}_3(\boldsymbol{t}), \boldsymbol{e}_1)$ if there exists $\boldsymbol{w} = (w_1, w_2, w_3) \in \mathbb{R}^3$ such that $A(i) = A^{\boldsymbol{w}}(\boldsymbol{\gamma}_d(t_i))$ for all $i \in [n]$, with $A^{\boldsymbol{w}}(\boldsymbol{v}) = \operatorname{argmax}\left\{ \frac{\langle \boldsymbol{w}, \boldsymbol{u}-\boldsymbol{v} \rangle}{\langle \boldsymbol{e}_1, \boldsymbol{u}-\boldsymbol{v} \rangle} : u \ \boldsymbol{e}_1\text{-improving neighbor of } v \right\}$. Denoting by P the univariate polynomial $P(t) = w_3 t^3 + w_2 t^2 + w_1 t$, then $\langle \boldsymbol{\gamma}_d(t_i), \boldsymbol{w} \rangle = P(t_i)$, and the conditions of the proposition precisely describe $A^{\boldsymbol{w}}$. □

Corollary 3.44. *For all $\boldsymbol{t} \in \mathsf{O}_n^\circ$, a 3-arborescence corresponding to one of the vertices of $\Pi(\mathsf{Cyc}_3(\boldsymbol{t}), \boldsymbol{e}_1)$ can have one of the following forms:*

(i) *For $k \in [n-1]$, define $A_k^{(3)}$ by $A_k^{(3)}(i) = i+1$ for $1 \leq i < k$ and $A(i) = n$ for $k \leq i < n$, see Figure 45. There are $n-1$ such arborescences.*

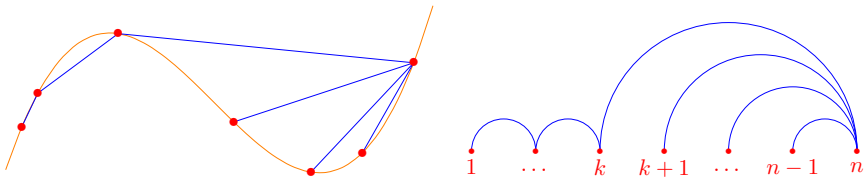

Figure 45: 3-arborescences captured by a degree 3 polynomial with **positive** leading coefficient.

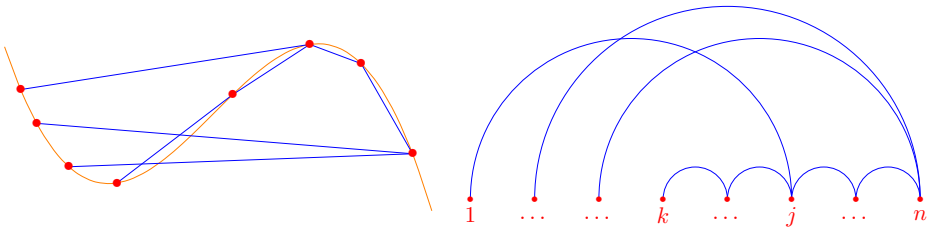

Figure 46: 3-arborescences captured by a degree 3 polynomial with **negative** leading coefficient.

(ii) *For* $1 < k \leq j-1 \leq n-1$ *and* $(j,k) \neq (n,-1)$, *define* $A^{(3)}_{j,k}$ *by* $A^{(3)}_{j,k}(1) = j$, $A^{(3)}_{j,k}(i) = n$ *for* $1 \leq i < k$ *and* $A^{(3)}_{j,k}(i) = i+1$ *for* $k \leq i < n$, *see Figure 46. There are* $\sum_{j=3}^{n}(j-2) - 1 = \binom{n-1}{2} - 1$ *such arborescences.*

Proof. Fix $\boldsymbol{t} \in \mathsf{O}_n^\circ$. Write $P(t) = w_3t^3 + w_2t^2 + w_1t$. If $w_3 = 0$, then P is of degree 2: it can capture A_1 (when $w_2 > 0$) or A_{n-1} (when $w_2 < 0$). There remain two cases.

First, suppose that the leading coefficient of P is positive, *i.e.* $w_3 > 0$. We are going to prove that a 3-arborescence captured by P is necessarily of the form $A^{(3)}_k$ for some $k \in [n-1]$. Indeed, let A be the arborescence captured by P on $\boldsymbol{t}$. By Lemma 3.41, we know that A is a 3-arborescence. Suppose that there exists $i \neq 1$ such that $A(i) = n$ and $A(i+1) = i+2$. Then $\tau(i,n) > \tau(i,i+1)$ and $\tau(i+1,i+2) > \tau(i+1,n)$. By Lemma 3.5, the first inequality gives $\tau(i+1,n) > \tau(i,i+1)$ and the second $\tau(i+2,n) > \tau(i+1,i+2)$. Then $\tau(i+1,i+2) > \tau(i,i+1)$. Thus, as in the proof of Theorem 3.11, there is $\alpha \in]\theta_i, \theta_{i+2}[$ with $P''(\alpha) > 0$ and $\beta \in]\theta_{i+1}, \theta_n[$ with $P''(\beta) < 0$, where $\theta_i < \theta_{i+1} < \theta_n$. But this means that $\alpha < \beta$, which contradicts the fact that the leading coefficient of P is positive.

Consequently, if $A(i) = i+1$, then $A(i') = i'+1$ for all $i' \geq i$. If $A(1) \neq 2$, then the same reasoning applies (with $i = 1$). This proves that $A = A^{(3)}_k$ for some k.

On the other side, if the leading coefficient of P is negative, *i.e.* $w_3 < 0$, then similar arguments apply to prove that, in the 3-arborescence A captured, if $A(i) = i+1$, then $A(i') = i'+1$ for all $i' \geq i$. Suppose that $A(1) = j$ for some $j \in [2,n]$, then $A(j-1) = j$, because, with Lemma 3.5, $\tau(1,j) > \tau(j,n)$, and $\tau(1,j) < \tau(j-1,j)$, thus $\tau(j-1,j) > \tau(j,n)$. This proves that $A = A^{(3)}_{j,k}$ for some $1 < k \leq j-1 \leq n-1$.

As $A_{n-1} = B_{n,n-1}$, we avoid double counting by requiring $(j,k) \neq (n,n-1)$. □

We now want to mimic Theorem 3.16.

Theorem 3.45. *For* $k \in [n-1]$, *we define:*

$$\begin{aligned} \mathsf{P}_3^f\left(A^{(3)}_k, \boldsymbol{t}\right) &= [t_1+t_2+t_3, \quad t_{k-1}+t_k+t_n] \\ \mathsf{P}_3^b\left(A^{(3)}_k, \boldsymbol{t}\right) &= [t_k+t_{k+1}+t_n, \quad t_{n-2}+t_{n-1}+t_n] \end{aligned}$$

For $1 < k \leq j-1 \leq n-1$, we define:

$$\begin{array}{rcl} \mathsf{P}_3^f\left(A_{j,k}^{(3)}, \boldsymbol{t}\right) & = & [\min(t_1+t_j+t_{j+1},\ t_k+t_{k+1}+t_n),\quad t_{n-2}+t_{n-1}+t_n] \\ \mathsf{P}_3^b\left(A_{j,k}^{(3)}, \boldsymbol{t}\right) & = & [t_1+t_2+t_3,\quad \max(t_1+t_{j-1}+t_j,\ t_{k-1}+t_k+t_n)] \end{array}$$

For $\boldsymbol{t} \in \mathsf{O}_n^\circ$, a 3-arborescence A with $A = A_k^{(3)}$ (for some $k \in [n-1]$) or $A = A_{j,k}^{(3)}$ (for some $1 < k \leq j-1 \leq n-1$), A corresponds to a vertex of $\Pi(\mathsf{Cyc}_3(\boldsymbol{t}), \boldsymbol{e}_1)$ if and only if $\mathsf{P}_d^f(A, \boldsymbol{t}) \cap \mathsf{P}_d^b(A, \boldsymbol{t}) = \varnothing$.

Proof. This proof is slightly different from the one of Theorem 3.16 because we can not benefit from Lemma 3.15, as $\Pi(\mathsf{Cyc}_3(\boldsymbol{t}), \boldsymbol{e}_1)$ is not the projection of an associahedron. Nevertheless, the same proof than for Theorem 3.16, applying Gordan's lemma to the inequalities of Proposition 3.43, gives that A can be captured on $\boldsymbol{t}$ if and only if $\mathsf{P}_3^f(A, \boldsymbol{t}) \cap \mathsf{P}_3^b(A, \boldsymbol{t}) = \varnothing$ where:

$$\begin{array}{rcl} \mathsf{P}_3^f(A, \boldsymbol{t}) & = & \operatorname{conv}\{t_x + t_y + t_z \ :\ x < y < z \text{ all triples such that } A \text{ imposes } \tau(x,y) > \tau(x,z)\} \\ \mathsf{P}_3^b(A, \boldsymbol{t}) & = & \operatorname{conv}\{t_x + t_y + t_z \ :\ x < y < z \text{ all triples such that } A \text{ imposes } \tau(x,y) < \tau(x,z)\} \end{array}$$

On the one hand, $A_k^{(3)}$ imposes $\tau(x,y) > \tau(x,z)$ for $(x,y,z) \in \{(1,2,i)\}_{i \geq 3} \cup \{(i,i+1,n)\}_{i \leq k-1}$; and $\tau(x,y) < \tau(x,z)$ for $(x,y,z) \in \{(a,a+1,n)\}_{a \geq k}$. Analyzing the minimum and maximum possible sums of triplets gives the desired endpoints of both segments.

On the other hand, $A_{j,k}^{(3)}$ imposes $\tau(x,y) > \tau(x,z)$ for $(x,y,z) \in \{(1,j,i)\}_{i>j} \cup \{(i,i+1,n)\}_{i \geq k}$; and $\tau(x,y) < \tau(x,z)$ for $(x,y,z) \in \{(1,a,j)\}_{a<j} \cup \{(a,a+1,n)\}_{1<a<k}$. Analyzing the minimum and maximum possible sums of triplets give the desired endpoints of both segments. □

This result allows us to determine which 3-arborescences are *universal* in the sense that they correspond to a vertex of $\Pi(\mathsf{Cyc}_3(\boldsymbol{t}), \boldsymbol{e}_1)$ for all $\boldsymbol{t} \in \mathsf{O}_n^\circ$, and to give an inequality description of their realization set otherwise.

Corollary 3.46. *For all $k \in [n-1]$, the 3-arborescence $A_k^{(3)}$ is universal. For $(j,k) \in \{(3,2),(4,2),(n,n-2)\}$, the 3-arborescence $A_{j,k}^{(3)}$ is universal.*

For $1 < k \leq j-1 \leq n-1$ with $(j,k) \notin \{(3,2),(4,2),(n,n-2),(n,n-1)\}$, the 3-arborescence $A_{j,k}^{(3)}$ is not universal, and corresponds to a vertex of $\Pi(\mathsf{Cyc}_3(\boldsymbol{t}), \boldsymbol{e}_1)$ if and only if

$$\boldsymbol{t} \in \mathsf{O}_n^\circ \ \cap\ \left\{ \boldsymbol{t} \in \mathbb{R}^n \ ;\ \begin{array}{rcll} t_{k-1}+t_k+t_n & < & t_1+t_j+t_{j+1} & \text{when } k \neq 2 \text{ and } j \neq n \\ t_1+t_{j-1}+t_j & < & t_k+t_{k+1}+t_n & \end{array} \right\} \subsetneq \mathsf{O}_n^\circ$$

Proof. For all $\boldsymbol{t} \in \mathsf{O}_n^\circ$, and $k \in [n-1]$, it is easily seen that $\mathsf{P}_3^f\left(A_k^{(3)}, \boldsymbol{t}\right)$ and $\mathsf{P}_3^b\left(A_k^{(3)}, \boldsymbol{t}\right)$ do not intersect.

For $\boldsymbol{t} \in \mathsf{O}_n^\circ$ and $1 < k \leq j-1 \leq n-1$, $\mathsf{P}_3^f\left(A_{j,k}^{(3)}, \boldsymbol{t}\right)$ and $\mathsf{P}_3^b\left(A_{j,k}^{(3)}, \boldsymbol{t}\right)$ do not intersect if and only if $t_{k-1}+t_k+t_n < t_1+t_j+t_{j+1}$ and $t_1+t_{j-1}+t_j < t_k+t_{k+1}+t_n$. The first inequality is defined only when $k \neq 2$ and $j \neq n$. This gives the last part of the above corollary.

Furthermore, the above inequalities are redundant with respect to the ones of O_n° if and only if $(j,k) \in \{(3,2),(4,2),(n,n-2)\}$. □

Definition 3.47. For n, the *3-switching arrangement* $\mathcal{H}_n^{(3)}$ is the collection of hyperplanes defined for $1 < k \leq j-1 \leq n-1$ by:

$$H_{j,k} = \{\boldsymbol{t} \in \mathbb{R}^n \ ;\ t_k + t_{k+1} + t_n = t_1 + t_j + t_{j+1}\}$$

Remark that the two inequalities of the above corollary correspond to the hyperplanes $H_{j,k-1}$ and $H_{j-1,k}$. Consequently, the same ideas as for Corollary 3.37 allows us to prove the following main results:

Theorem 3.48. *The number of vertices of $\Pi(\mathsf{Cyc}_3(\boldsymbol{t}), \boldsymbol{e}_1)$ is the same for all $\boldsymbol{t} \in \mathsf{O}_n^\circ \setminus \bigcup_{H \in \mathcal{H}_n^{(3)}} H$.*

Proof. By Corollary 3.46, if $\boldsymbol{t}$ and $\boldsymbol{t}'$ belong to the same maximal cone of $\mathsf{O}_n^\circ \setminus \bigcup_{H\in\mathcal{H}_n^{(3)}} H$, then the 3-arborescences captured on $\boldsymbol{t}$ and $\boldsymbol{t}'$ are the same. Thus the number of vertices of $\Pi(\mathsf{Cyc}_3(\boldsymbol{t}), \boldsymbol{e}_1)$ and $\Pi(\mathsf{Cyc}_3(\boldsymbol{t}'), \boldsymbol{e}_1)$ are the same.

For a maximal cone C of the arrangement $\mathcal{H}_n^{(3)}$, we denote by $\mathcal{A}^{(3)}(\mathsf{C})$ the set of 3-arborescences captured on (any) $\boldsymbol{t} \in \mathsf{C}$. Take two adjacent maximal cones C and C'. Suppose that, for some $1 < k \leq j-1 \leq n-1$ with $(j,k) \notin \{(3,2),(4,2),(n,n-2),(n,n-1)\}$, $A^{(3)}_{j,k} \in \mathcal{A}^{(3)}(\mathsf{C})$ but $A^{(3)}_{j,k} \notin \mathcal{A}^{(3)}(\mathsf{C}')$. Then the hyperplane separating C and C' is either $H_{j-1,k}$ or $H_{j,k-1}$. Suppose it is $H_{j-1,k}$, then $A^{(3)}_{j+1,k-1} \notin \mathcal{A}^{(3)}(\mathsf{C})$ (as C is not on the side of $H_{j-1,k}$ where $A^{(3)}_{j+1,k-1}$ can be captured) but $A^{(3)}_{j+1,k-1} \in \mathcal{A}^{(3)}(\mathsf{C}')$ because C' is on the side of $H_{j-1,k}$ where $A^{(3)}_{j+1,k-1}$ can be captured, and on the same side of $H_{j+1,k-2}$ as C, where $A^{(3)}_{j+1,k-1}$ can be captured. If it were $H_{j,k-1}$, then $A^{(3)}_{j-1,k+1} \in \mathcal{A}^{(3)}(\mathsf{C}) \setminus \mathcal{A}^{(3)}(\mathsf{C}')$ for the same reasons.

As all other 3-arborescences can be captured both in C and C', we deduce that $|\mathcal{A}^{(3)}(\mathsf{C}')| \geq |\mathcal{A}^{(3)}(\mathsf{C})|$. This proves that the cardinal $|\mathcal{A}^{(3)}(\mathsf{C})|$ is the same for all maximal cone C of the hyperplane arrangement $\mathcal{H}_n^{(3)}$ (as the graph of adjacency of its maximal cones is connected). □

Corollary 3.49. *For all $\boldsymbol{t} \in \mathsf{O}_n^\circ \setminus \bigcup_{H\in\mathcal{H}_n^{(3)}} H$, the number of vertices of $\Pi(\mathsf{Cyc}_3(\boldsymbol{t}), \boldsymbol{e}_1)$ is $3n-7$.*

Proof. By Theorem 3.48, it is enough to compute the number of vertices of $\Pi(\mathsf{Cyc}_3(\boldsymbol{t}), \boldsymbol{e}_1)$ for some $\boldsymbol{t} \in \mathsf{O}_n^\circ \setminus \bigcup_{H\in\mathcal{H}_n^{(3)}} H$. Take $\boldsymbol{t}_{lex} = (1, 2, ..., 2^{n-1}) \in \mathsf{O}_n^\circ$, then deciding if $t_a + t_b + t_c < t_x + t_y + t_z$ amount to knowing which triple of indices is lexicographically the greatest between (a,b,c) and (x,y,z). Thus, $\boldsymbol{t}_{lex} \notin \bigcup_{H\in\mathcal{H}_n^{(3)}} H$.

By the inequalities of Corollary 3.46, $A^{(3)}_{j,k}$ is captured on $\boldsymbol{t}_{lex}$ if and only if it falls into one of the following (mutually exclusive) cases:

- $k = 2$ and $j \in [3, n-1]$, accounting for $n-3$ possibilities
- $j = n-1$ and $k \in [3, n-2]$, accounting for $n-4$ possibilities
- $j = n$ and $k = n-2$, accounting for 1 possibility

These, plus the $n-1$ universal arborescences $A^{(3)}_k$ sum up to $3n-7$. □

Example 3.50. For $n = 5$, $\Pi(\mathsf{Cyc}_3(\boldsymbol{t}), \boldsymbol{e}_1)$ are octagons, all but 1 vertex of which correspond to universal 3-arborescences. There are 2 possible such octagons, depending on whether $t_2+t_3+t_5 < t_1+t_4+t_5$ or the converse, see Figure 47.

For $n = 6$, $\Pi(\mathsf{Cyc}_3(\boldsymbol{t}), \boldsymbol{e}_1)$ are 11-gons, all but 3 vertices of which correspond to universal 3-arborescences. There are 5 possible such 11-gons, depending on the position of $\boldsymbol{t}$ with respect to the 3 hyperplanes $\{\boldsymbol{t} \in \mathbb{R}^n \ ; \ t_2+t_3+t_6 = t_1+t_4+t_6\}$, $\{\boldsymbol{t} \in \mathbb{R}^n \ ; \ t_2+t_3+t_6 = t_1+t_5+t_6\}$ and $\{\boldsymbol{t} \in \mathbb{R}^n \ ; \ t_3+t_4+t_6 = t_1+t_5+t_6\}$, see Figure 48.

For $n = 7$, $\Pi(\mathsf{Cyc}_3(\boldsymbol{t}), \boldsymbol{e}_1)$ are 14-gons, all but 5 vertices of which correspond to universal 3-arborescences. There are 12 possible such 14-gons, depending on the position of $\boldsymbol{t}$ with respect to the 6 hyperplanes of $\mathcal{H}_6^{(3)}$.

In general, one can draw the graph whose vertices are all 3-arborescences on n nodes, and where A and A' are linked by an edge when there exists $\boldsymbol{t} \in \mathsf{O}_n^\circ$ such that the vertices of $\Pi(\mathsf{Cyc}_3(\boldsymbol{t}), \boldsymbol{e}_1)$ corresponding to A and A' appear and are linked by an edge. This amounts to consider the graph of "flips" of 3-arborescences: flipping a 3-arborescence $A^{(3)}_k$ gives $A^{(3)}_{k+1}$ for $k \in [n-2]$, flipping $A^{(3)}_{j,k}$ gives either $A^{(3)}_{j+1,k}$ or $A^{(3)}_{j,k+1}$, and flipping $A^{(3)}_{n-1}$ gives either $A^{(3)}_{3,2}$ or $A^{(3)}_{n-2}$. Though tedious, this definition of flips is made clear in the graph depicted in Figure 49 for $n = 7$. All max-slope pivot polytope $\Pi(\mathsf{Cyc}_3(\boldsymbol{t}), \boldsymbol{e}_1)$ correspond to a *great cycle* in this graph. To count these great cycles, we look at the paths from $A^{(3)}_1$ to $A^{(3)}_{n-1}$ that only uses 3-arborescences of the form $A^{(3)}_{j,k}$. These paths are in bijection with Dick paths of length $2(n-3)$, thus they are $\frac{1}{n-2}\binom{2(n-3)}{n-3}$ many (Catalan number). Note that for $n = 5$ and $n = 6$, all such paths do correspond to max-slope

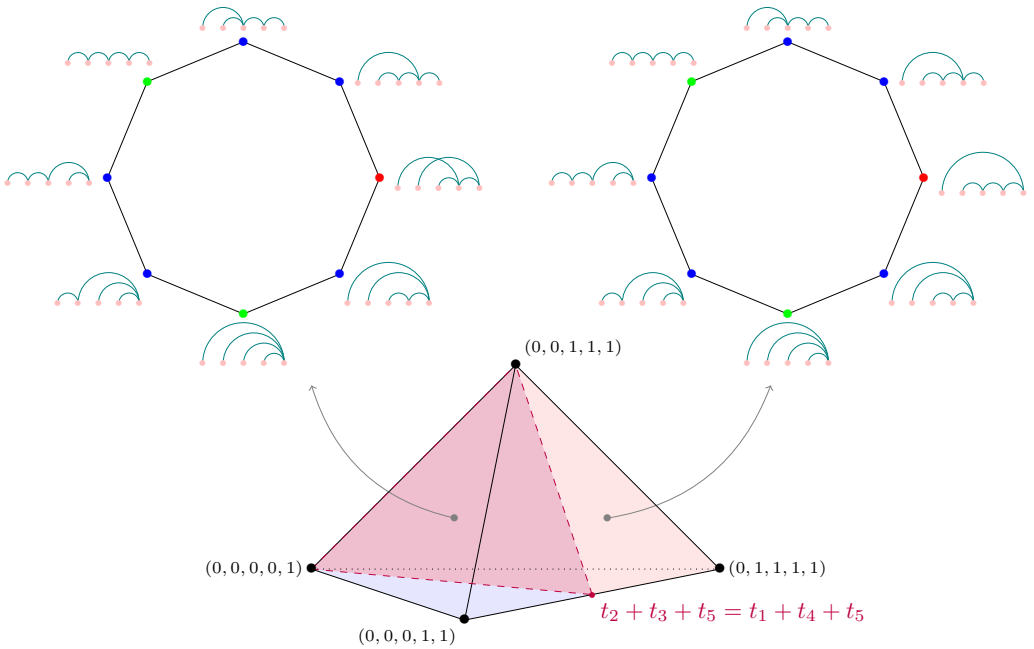

Figure 47: For $n = 5$, $\Pi(\mathsf{Cyc}_3(\boldsymbol{t}), \boldsymbol{e}_1)$ are octagons. Green and blue vertices represent universal 3-arborescences (green are captured by degree 2 polynomials), the red vertex is non-universal. For $\boldsymbol{t} \in \mathsf{O}_5^\circ$ with $t_2 + t_3 + t_5 < t_1 + t_4 + t_5$, the 3-arborescence $A^{(3)}_{4,3}$ can be captured, while $A^{(3)}_{5,2}$ can not (and conversely).

pivot polytopes (in the sense that there exists a $\boldsymbol{t} \in \mathsf{O}_n^\circ$ such that the vertices of $\Pi(\mathsf{Cyc}_3(\boldsymbol{t}), \boldsymbol{e}_1)$ correspond to the 3-arborescences appearing in this path). But for $n = 7$, there are only 12 possible max-slope pivot polytopes: not all 14 paths correspond to a max-slope pivot polytope, only 12 of them do. Again, one can wonder how many combinatorially different $\Pi(\mathsf{Cyc}_3(\boldsymbol{t}), \boldsymbol{e}_1)$ there are for all n.

This concludes this complementary section on 2- and 3-dimensional problems, and closes (almost completely) the case. As per usual, we devote the last sub-section to some perspectives and open questions. This sub-section will concern the general problem for $d \geq 4$, so the readers can forget what they just read and have a look again at Figures 38 to 40 and 43.

3.2.4 Perspectives and open questions

Computational remarks All the objects mentioned in this section have been implemented with Sage, allowing to compute the above examples. There are two possibilities for computing the maximal cones of the subdivision $\boldsymbol{S}_n$ mentioned in Example 3.38, and especially for counting the number of such cones. We say that two maximal cones correspond to two *combinatorially different* cyclic associahedra.

A straightforward way to do so is to take the hyperplane arrangement $\mathcal{H}_n$ and compute the maximal cones it induces, as topes of the corresponding oriented matroid. It is then easy to list the arborescences captured in each tope (it amounts to checking for each 3-arborescence if it respects the inequalities of its realization set), and to count how many different lists we get. To speed up this process, we use the *forcing poset* $\mathcal{F}_n$ of hyperplanes, that is the poset of inclusion of $H^+ \cap \mathsf{O}_n$ for $H \in \mathcal{H}_n$. Indeed, a tope corresponds to a down set of the forcing poset (but not all down sets correspond to topes).

On Figure 50 are the forcing posets $\mathcal{F}_6$ (Left) and $\mathcal{F}_7$ (Right, only the poset structure, without labeling). Quite remarkably, $\mathcal{F}_6$ has 12 down-sets which correspond to the 12 cyclic associahedra of Example 3.38. This explains the cubical structure of the dual graph of the polyhedral subdivision

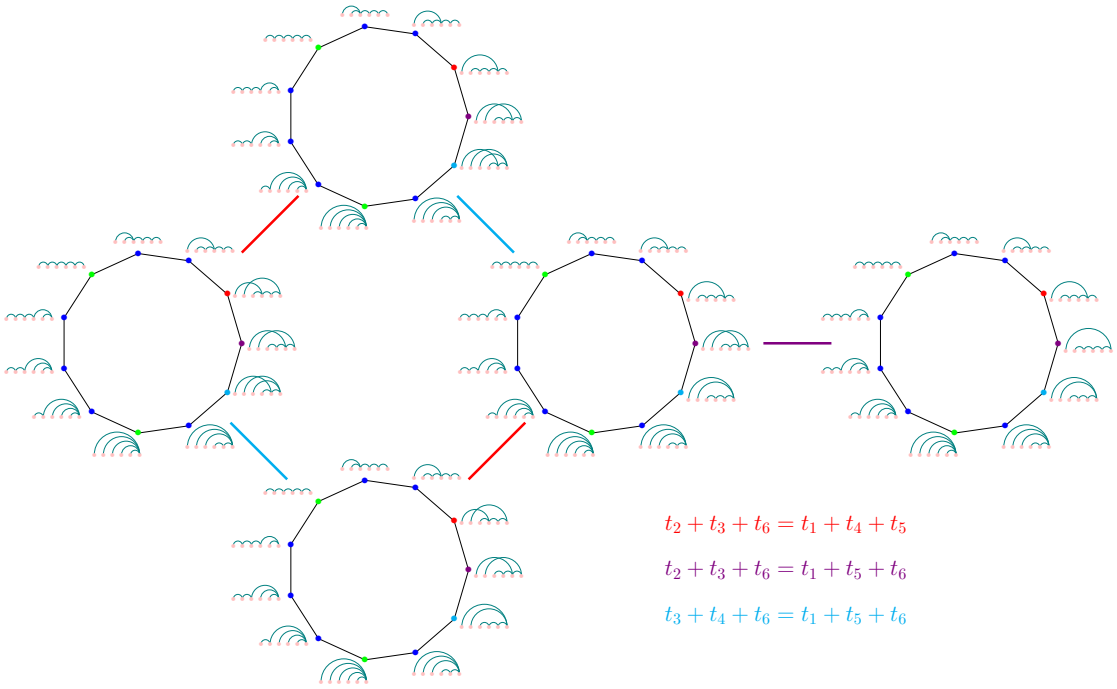

Figure 48: For $n = 6$, $\Pi(\mathsf{Cyc}_3(\boldsymbol{t}), \boldsymbol{e}_1)$ are 11-gons. Each 11-gon correspond to a subcone of O_6° on which its 3-arborescences are precisely the one captured. There are 5 such subcones, and the five colored edges figure the dual graph of this subdivision. For example, two 11-gons are linked by a red thick edge when their 11-gons differ only on the label of the red vertex.

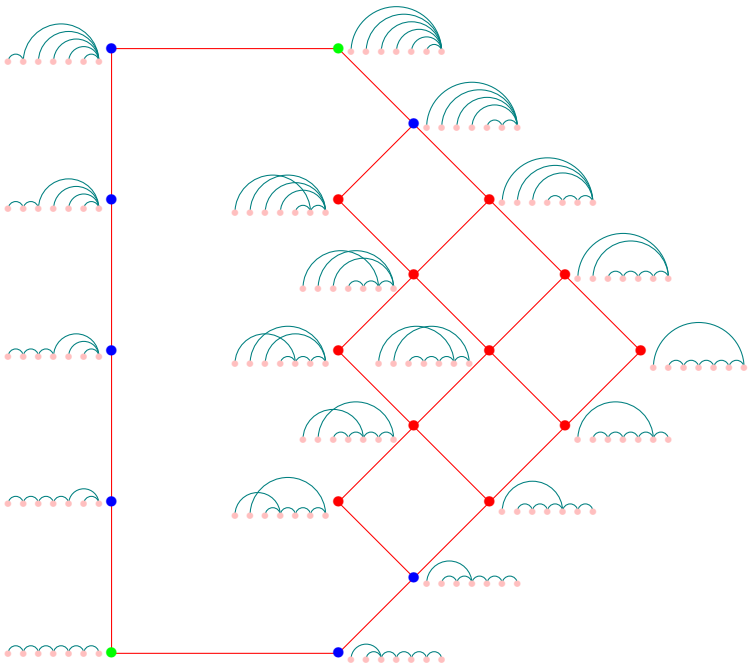

Figure 49: Green and blue dots represent universal arborescences, red dots non-universal ones. Each $\Pi(\mathsf{Cyc}_3(\boldsymbol{t}), \boldsymbol{e}_1)$ for $\boldsymbol{t} \in \mathsf{O}_7^\circ$ correspond to a great circle in this graph. A great circle is composed of the path from the green node to the other one on the left of the picture (using $A_k^{(3)}$s) and a path on the right of the picture (going from top to bottom). Not all great circles correspond to a $\Pi(\mathsf{Cyc}_3(\boldsymbol{t}), \boldsymbol{e}_1)$.

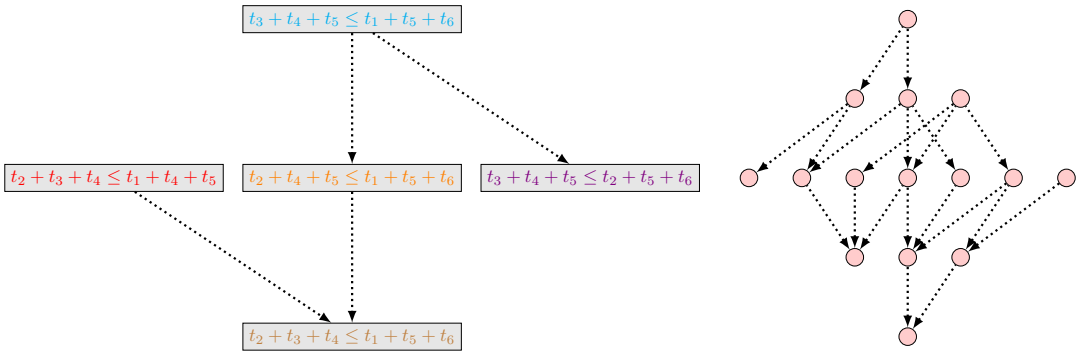

Figure 50: The forcing posets $\mathcal{F}_6$ (Left) and $\mathcal{F}_7$ (Right). Having only 1 element, $\mathcal{F}_5$ is not drawn.

for $n = 6$ in Figure 43: oriented from left to right and top to bottom, it is the graph of a lattice of ideals, which is a distributive lattice, hence cubical.

Unfortunately, not all down-sets of $\mathcal{F}_7$ do correspond to topes of the polyhedral subdivision for $n = 7$: $\mathcal{F}_7$ has 336 down-sets whereas there are only 187 topes in the polyhedral subdivision, each of them corresponding to a combinatorially different cyclic associahedron. This comes from the fact that being in some subsets of half-spaces forces to be in some other subsets, whereas the forcing poset only records if being in one half-space forces to be in another. But trying to construct the forcing relation for subsets of half-spaces would become impracticable, as there are already 15 elements in $\mathcal{F}_7$ (so 2^{15} subsets) and 35 in $\mathcal{F}_8$ (so 2^{35} subsets).

The failure of this first method advocates for a new one. Going back to Example 3.23, Corollary 3.37 implies that all cyclic associahedra come from a great cycle in the sub-graph of the Tamari graph induced by the non-crossing arborescences A with $\mu(A) \le 3$ (*i.e.* the graphs pictured in Figures 38 and 39 and their counterparts for greater n). We can run through all these great cycles, and for each of them compute the intersection of $\mathcal{T}_3(A)$ for the non-crossing arborescences in the great cycle. The family of arborescences forming the great cycle correspond to a cyclic associahedron if and only if this intersection is non-empty. This algorithmic solution gives the number of combinatorially different cyclic associahedra for $n = 8$ by testing "only" 33592 great cycles.

n	5	6	7	8
number of combinatorially different cyclic associahedra $\mathsf{Asso}_2(\boldsymbol{t})$	1	12	187	6179

Assets and limits of the current approach, open questions This computer experiment raises the following natural open question: How many combinatorially different cyclic associahedra $\mathsf{Asso}_2(\boldsymbol{t})$ are there for $n \ge 9$? We have proven that all cyclic associahedra $\mathsf{Asso}_2(\boldsymbol{t})$ have the same number of vertices $\binom{n}{2} - 1$ by Corollary 3.37. We know how to determine if a non-crossing arborescence A satisfies $\mu(A, \boldsymbol{t}) \le 3$ or not (by checking if a set of linear inequality has a solution, *i.e.* by solving a linear problem), but we do not know how to efficiently compute the number of combinatorially different cyclic associahedra.

On the other hand, the works presented so far only deal with the case $d \le 3$. Numerous questions are still open for $d \ge 4$. Indeed, Theorem 3.16 gives a way to check if, for a given $\boldsymbol{t}$, a non-crossing arborescence A satisfies $\mu(A, \boldsymbol{t}) \le \boldsymbol{t}$, but it remains difficult to compute $\mathcal{T}_d(A)$. To do so, one would need to determine for which $\boldsymbol{t}$ do some $(d-2)$-dimensional polytopes intersect, but these polytopes have coordinates of degree $d-2$ in $\boldsymbol{t}$, making the question (at least) as hard as computing a semi-algebraic set of degree $d-2$. With the help of the cylindrical algebraic decomposition, see [BPR06, Chapter 5], one can hope for dealing with the case $d = 4$ and $n = 6$, but going higher would require a better mathematical understanding of our problem.

Nonetheless, computer experiments indicate that the number of vertices of $\mathsf{Asso}_{d-1}(\boldsymbol{t})$ depends on $\boldsymbol{t}$ for $d = 4$. Moreover, given a set $\mathcal{A}$ of non-crossing arborescences, it is unclear whether the common realization set $\bigcap_{A \in \mathcal{A}} \mathcal{T}_d(A)$ is connected or not, and we believe that there exists $\mathcal{A}$ such that it is not connected, even for $d = 4$ (but have not found an example yet).

3.3 Max-slope pivot polytopes of products of polytopes

This section is an ongoing work on a conjecture of Vincent Pilaud and Raman Sanyal.

In the previous section, we have computed the max-slope pivot polytopes of cyclic polytopes. Especially, if one reviews the computation, he or she will notice that the key objects are the slopes in the plane $(\boldsymbol{c}, \boldsymbol{\omega})$ between the projection of adjacent vertices $\boldsymbol{u}, \boldsymbol{v} \in V(\mathsf{P})$, namely $\frac{\langle \boldsymbol{\omega}, \boldsymbol{u}-\boldsymbol{v}\rangle}{\langle \boldsymbol{c}, \boldsymbol{u}-\boldsymbol{v}\rangle}$. The comparisons between these slopes determine the arborescence associated to $\boldsymbol{\omega}$, and, for fixed $\boldsymbol{c}$, $\boldsymbol{u}$ and $\boldsymbol{v}$, these slopes are linear with respect to $\boldsymbol{\omega}$. In the present section, we will emphasize this idea by considering the partially ordered set that records only these comparisons and forgets the exact values of the slopes. Not only will this grant us, in Section 3.3.1, a second proof that the max-slope pivot polytope of the standard cube is the permutahedron [BDLLS22], and that the max-slope pivot polytope of a simplex is an associahedron [BDLLSon], but it will also give access, in Section 3.3.2, to the max-slope pivot polytope of a product of simplices (and grasp some hint about products of polytopes in general).

Generalized permutahedra will be at the center of this part, as we unveil the link between the normal fan of the max-slope pivot polytope and the braid fan. Besides Section 3.1 which introduces the preliminary notions concerning max-slope pivot rule polytopes, the useful definitions on pre-orders and braid fans are presented in Sections 1.1 and 1.2.3. We will directly use the notations defined in these preliminaries.

The watchword of this section is that max-slope pivot rule polytopes can be embedded in the braid fan and thought of as akin to generalized permutahedra. As a consequence, we will be able to detail max-slope pivot polytopes of products of simplices and prove that they are linked to the notion of shuffle defined in [CP22] on generalized permutahedra. In particular, this allows us to give new families of realizations of the multiplihedron and the constrainahedron in Example 3.75. These polytopes are generalizations of the permutahedron and the associahedron. Especially, the *constrainahedron* was introduced by Bottman and Poliakova [Bot19, Pol21] in order to study higher version of the A_∞ operad. The vertices of the constrainahedron are associated to bracketing on the 2-dimensional $m \times n$-grid, whereas the vertices of the usual associahedron correspond to usual bracketing (see Section 1.2.4). As to the *multiplihedron*, its vertices are in bijection with m-painted binary n-trees, and its combinatorics arises from the study of maps between A_∞-algebras, see [For08] for an historical presentation of the subject.

In this section, the central tools are only basic linear algebra (namely linear maps and dimensions of vector spaces), and (shuffle of) partially ordered set. Although these notions are well known to the reader, the notions will feel heavy and unwieldy, making the proofs technical. The reader is advised to first read the theorems and examples, and then to keep in mind that the idea is to prove that what the framework suggests is indeed true.

We start by exposing the general theory of how to embed max-slope pivot polytopes into the realm of generalized permutahedra. To this end, we need an elementary lemma:

Lemma 3.51. *The projection $\pi : \mathbb{R}^n \to \mathbb{R}^{n-1}$ that forgets the last coordinate sends the braid fan $\mathcal{B}_n$ onto the braid fan $\mathcal{B}_{n-1}$. For a surjection α of $[n-1]$, the pre-image of the cone C_α is exactly the union of cones: $\pi^{-1}(\mathsf{C}_\alpha) = \bigcup_{\sigma \text{ extends } \alpha} \mathsf{C}_\sigma$.*

Proof. This fact is straightforward from the definition of C_σ:

$$\mathsf{C}_\sigma = \left\{ \boldsymbol{x} \in \mathbb{R}^n \; ; \quad \begin{array}{lll} x_i < x_j & \text{if} & \sigma(i) < \sigma(j) \\ x_i = x_j & \text{if} & \sigma(i) = \sigma(j) \end{array} \right\}$$

□

As we want to discuss max-slope pivot polytopes as a whole and not only their vertices, we first detail the combinatorial interpretation of the faces of the max-slope pivot polytope, see [BDLLS22, Section 5]. For the rest of this discussion, we fix a linear program $(\mathsf{P}, \boldsymbol{c})$, on a polytope P of dimension d, n its number of vertices, and m its number of edges. As before, the set of vertices of P is $V(\mathsf{P})$, and $\boldsymbol{v}_{\text{opt}}$ is the vertex maximizing $\langle \boldsymbol{v}, \boldsymbol{c}\rangle$. Besides, $E_{\boldsymbol{c}}(\mathsf{P})$ will be the set of $\boldsymbol{c}$-improving edges of P, that is edges $\boldsymbol{uv}$ of P with $\langle \boldsymbol{u}, \boldsymbol{c}\rangle < \langle \boldsymbol{v}, \boldsymbol{c}\rangle$. As always: $\tau_{\boldsymbol{\omega}}(\boldsymbol{u}, \boldsymbol{v}) = \frac{\langle \boldsymbol{\omega}, \boldsymbol{u}-\boldsymbol{v}\rangle}{\langle \boldsymbol{c}, \boldsymbol{u}-\boldsymbol{v}\rangle}$

Definition 3.52. A *multi-arborescence* $\mathcal{A}$ is a function $\mathcal{A} : V(\mathsf{P}) \smallsetminus \{\boldsymbol{v}_{\mathrm{opt}}\} \to 2^{V(\mathsf{P})}$ such that $\mathcal{A}(\boldsymbol{v})$ is a non-empty subset of $\boldsymbol{c}$-improving neighbors of $\boldsymbol{v}$. By convention $\mathcal{A}(\boldsymbol{v}_{\mathrm{opt}}) = \{\boldsymbol{v}_{\mathrm{opt}}\}$ when needed.

A secondary direction $\boldsymbol{\omega}$ *captures* the following multi-arborescence (where "Argmax" designates the set of maximizers of the studied quantity) :

$$\mathcal{A}^{\boldsymbol{\omega}}(\boldsymbol{v}) = \mathrm{Argmax}\left\{ \frac{\langle \boldsymbol{\omega}, \boldsymbol{u} - \boldsymbol{v} \rangle}{\langle \boldsymbol{c}, \boldsymbol{u} - \boldsymbol{v} \rangle} \ ; \ \boldsymbol{uv} \in E_{\boldsymbol{c}}(\mathsf{P}) \right\}$$

A multi-arborescence $\mathcal{A}$ is *coherent* when there exists $\boldsymbol{\omega}$ such that $\mathcal{A} = \mathcal{A}^{\boldsymbol{\omega}}$, and we denote $\tau_{\boldsymbol{\omega}}(\mathcal{A}(\boldsymbol{u})) = \tau_{\boldsymbol{\omega}}(\boldsymbol{u}, \boldsymbol{v})$ for any[9] $\boldsymbol{v} \in \mathcal{A}(\boldsymbol{u})$.

We say that a multi-arborescence $\mathcal{A}$ *refines* a multi-arborescence $\mathcal{A}'$ when $\mathcal{A}(\boldsymbol{v}) \subseteq \mathcal{A}'(\boldsymbol{v})$ for all $\boldsymbol{v} \in V(\mathsf{P})$. In this case, we denote by $\mathcal{A} \subseteq \mathcal{A}'$ this relation, and by $\mathfrak{A}$ the corresponding partially ordered set completed by an arbitrary minimal element $\varnothing$. The following theorem gives access to the face lattice of the max-slope pivot polytope.

Theorem 3.53. ([BDLLS22, Theorem 5.4]) *For a linear program $(\mathsf{P}, \boldsymbol{c})$, the lattice of coherent multi-arborescences $\mathfrak{A}$ is isomorphic to the face lattice of the max-slope pivot polytope $\Pi(\mathsf{P}, \boldsymbol{c})$.*

Fix a linear program $(\mathsf{P}, \boldsymbol{c})$ and a coherent multi-arborescence $\mathcal{A}$ on it, we denote $\mathsf{F}_{\mathcal{A}}$ the corresponding face in the max-slope pivot polytope $\Pi(\mathsf{P}, \boldsymbol{c})$. By (a refined version of) Theorem 3.1, we know that the normal cone at $\mathsf{F}_{\mathcal{A}}$ is precisely the cone of $\boldsymbol{\omega}$ that captures $\mathcal{A}$. We call $\mathcal{N}(\mathcal{A})$ this cone, and set $\mathcal{N}(\mathcal{A}) = \varnothing$ when $\mathcal{A}$ is not coherent.

In order to know what multi-arborescence a given $\boldsymbol{\omega}$ captures, one does not need the exact value of $\boldsymbol{\omega}$, but only the comparisons between the slopes $\boldsymbol{\omega}$ gives to each improving edge $\boldsymbol{uv}$ of P (when projecting this edge into the plane $(\boldsymbol{c}, \boldsymbol{\omega})$). This invites us to define the two following pre-orders.

Definition 3.54. For a given $\boldsymbol{\omega} \in \mathbb{R}^d$, its *slope vector* is $\theta(\boldsymbol{\omega}) := \big(\tau_{\boldsymbol{\omega}}(\boldsymbol{u}, \boldsymbol{v}) \ ; \ \boldsymbol{uv} \in E_{\boldsymbol{c}}(\mathsf{P})\big) \in \mathbb{R}^{E_{\boldsymbol{c}}(\mathsf{P})}$.

Moreover, a given $\boldsymbol{\omega}$ induces a pre-order on $E_{\boldsymbol{c}}(\mathsf{P})$, called its *slope pre-order*, by considering $\boldsymbol{uv} \preccurlyeq_{\boldsymbol{\omega}} \boldsymbol{u'v'}$ when $\tau_{\boldsymbol{\omega}}(\boldsymbol{u}, \boldsymbol{v}) \leq \tau_{\boldsymbol{\omega}}(\boldsymbol{u'}, \boldsymbol{v'})$, or equivalently $\theta(\boldsymbol{\omega})_{\boldsymbol{uv}} \leq \theta(\boldsymbol{\omega})_{\boldsymbol{u'v'}}$.

The knowledge of the slope pre-order of $\boldsymbol{\omega}$ fully determines which multi-arborescence it captures, and this pre-order can be retrieved from comparison between coordinates of its slope vector. Note that the map $\boldsymbol{\omega} \mapsto \theta(\boldsymbol{\omega})$ is a linear map.

Furthermore, if $\boldsymbol{\omega} \in \mathbb{R}^d$ captures a multi-arborescence $\mathcal{A}$, it necessarily satisfies some slope inequalities, *i.e.* certain relations of its slope pre-order can be deduced from the capture of $\mathcal{A}$. For instance, if $\boldsymbol{\omega}$ captures $\mathcal{A}$, then the improving edges $\boldsymbol{uv}$ with $\boldsymbol{v} \in \mathcal{A}(\boldsymbol{u})$ are greater (for the slope pre-order of $\boldsymbol{\omega}$) than any improving edge $\boldsymbol{uv'}$. And we have seen in the previous Section 3.2 that Lemma 3.5 allows us to compare other slopes between them thanks to the triangles in the graph G_{P}.

We thus endow $\mathcal{A}$ with a pre-order of its own:

Definition 3.55. A multi-arborescence $\mathcal{A}$ induces an *utter slope pre-order* on the set $E_{\boldsymbol{c}}(\mathsf{P})$ by $\boldsymbol{uv} \preccurlyeq_{\mathcal{A}} \boldsymbol{u'v'}$ when $\tau_{\boldsymbol{\omega}}(\boldsymbol{u}, \boldsymbol{v}) \leq \tau_{\boldsymbol{\omega}}(\boldsymbol{u'}, \boldsymbol{v'})$ for all $\boldsymbol{\omega} \in \mathbb{R}^d$ capturing $\mathcal{A}$. Said equivalently:

$$\boldsymbol{uv} \preccurlyeq_{\mathcal{A}} \boldsymbol{u'v'} \iff \forall \boldsymbol{\omega} \in \mathcal{N}(\mathcal{A}),\ \boldsymbol{uv} \preccurlyeq_{\boldsymbol{\omega}} \boldsymbol{u'v'}$$

It is then immediate to see that:

Proposition 3.56. *A given $\boldsymbol{\omega} \in \mathbb{R}^d$ captures a multi-arborescence $\mathcal{A}$ if and only if $\preccurlyeq_{\boldsymbol{\omega}}$ extends $\preccurlyeq_{\mathcal{A}}$.*

The drawback of the utter slope pre-order of $\mathcal{A}$ is that it might encapsulate geometric constraints, while we would like to only care about the combinatorial constraints. Indeed, one could think that the utter slope pre-order is obtained by first enforcing, for all $\boldsymbol{u}$, that $\boldsymbol{uv'} \preccurlyeq_{\mathcal{A}} \boldsymbol{uv}$ when $\boldsymbol{v} \in \mathcal{A}(\boldsymbol{u})$, and then repeatedly applying Lemma 3.5 to deduce all possible slope inequalities.

[9] Note that the slope does not depend on $\boldsymbol{v} \in \mathcal{A}(\boldsymbol{u})$ by definition of the multi-arborescence.

Nevertheless, this is false: it can happen that all $\boldsymbol{\omega}$ capturing $\mathcal{A}$ respect a slope inequality that cannot be deduced by Lemma 3.5, see Example 3.76 and Figure 54(Bottom Right).

The other inconvenient of the slope vector is that it compares all the edges: not only have we seen that it implies comparisons that cannot be read from the multi-arborescence, but it also involves the slope vector which live in $\mathbb{R}^{E_{\boldsymbol{c}}(\mathsf{P})}$. We would like to keep less information and consequently embed our problem in a smaller dimension. To this end, we restrict the utter slope pre-order to the edges that are used by the multi-arborescence (and forget the other ones), this is easier done by considering the vertices of P instead of its edges:

Definition 3.57. For a multi-arborescence $\mathcal{A}$ and a given $\boldsymbol{\omega} \in \mathbb{R}^d$, the associated *restricted slope vector* is $\vartheta_{\mathcal{A}}(\boldsymbol{\omega}) := \big(\tau_{\boldsymbol{\omega}}(\mathcal{A}(\boldsymbol{v})) \ ; \ \boldsymbol{v} \in V(\mathsf{P}) \smallsetminus \{\boldsymbol{v}_{\text{opt}}\}\big) \in \mathbb{R}^{V(\mathsf{P})\smallsetminus\{\boldsymbol{v}_{\text{opt}}\}}$. A multi-arborescence $\mathcal{A}$ induces an *adapted slope pre-order* on the set $V(\mathsf{P})\smallsetminus\{\boldsymbol{v}_{\text{opt}}\}$ by $\boldsymbol{u} \trianglelefteq_{\mathcal{A}} \boldsymbol{v}$ when $\tau_{\boldsymbol{\omega}}(\mathcal{A}(\boldsymbol{u})) \leq \tau_{\boldsymbol{\omega}}(\mathcal{A}(\boldsymbol{v}))$ for all $\boldsymbol{\omega} \in \mathbb{R}^d$ capturing $\mathcal{A}$, or equivalently $\vartheta_{\mathcal{A}}(\boldsymbol{\omega})_{\boldsymbol{uv}} \leq \vartheta_{\mathcal{A}}(\boldsymbol{\omega})_{\boldsymbol{u'v'}}$ for all $\boldsymbol{\omega} \in \mathcal{N}(\mathcal{A})$.

Finally, we define a map to encompasses all the restricted slope vectors. All these maps are illustrated in Figure 51.

Definition 3.58. The *adapted slope vector* associated to $\boldsymbol{\omega} \in \mathbb{R}^d$ is defined by $\vartheta(\boldsymbol{\omega}) = \vartheta_{\mathcal{A}^{\boldsymbol{\omega}}}(\boldsymbol{\omega})$.

In the utter slope pre-order, the improving edges $\boldsymbol{uv}$ with $\boldsymbol{v} \in \mathcal{A}(\boldsymbol{u})$ are greater than any improving edge $\boldsymbol{uv'}$. Conversely, given a pre-order on $E_{\boldsymbol{c}}(\mathsf{P})$, such that for all $\boldsymbol{u} \in V(\mathsf{P})$ the maxima of $\big(\boldsymbol{uv}\big)_{\boldsymbol{v}\ ;\ \boldsymbol{uv}\in E_{\boldsymbol{c}}(\mathsf{P})}$ are equivalent, then this pre-order determines a unique multi-arborescence. Nevertheless, this is no longer true for the adapted slope pre-order: we will see that several coherent multi-arborescences share the same adapted slope pre-order.

Still, the adapted slope pre-order is a restriction of the utter one:

Lemma 3.59. *For a multi-arborescence $\mathcal{A}$ and a vertex $\boldsymbol{u} \in V(\mathsf{P}) \smallsetminus \{\boldsymbol{v}_{opt}\}$, fix arbitrarily a representative $\boldsymbol{v_u} \in \mathcal{A}(\boldsymbol{u})$. The map $\boldsymbol{u} \mapsto \boldsymbol{uv_u}$ is an injective (pre)order preserving map from the adapted pre-order to the utter pre-order.*

Proof. The map $\boldsymbol{u} \mapsto \boldsymbol{uv_u}$ is clearly injective. As $\tau_{\boldsymbol{\omega}}(\mathcal{A}(\boldsymbol{u})) = \tau_{\boldsymbol{\omega}}(\boldsymbol{u}, \boldsymbol{v_u})$ by definition, this map is (pre)order preserving. □

The utter and the adapted slope pre-orders are linked to the braid fan. Indeed, for each of them, we directly compare the slopes. The maps $\theta : \mathbb{R}^d \to \mathbb{R}^m$, $\vartheta_{\mathcal{A}} : \mathbb{R}^d \to \mathbb{R}^{n-1}$, and $\vartheta : \mathbb{R}^d \to \mathbb{R}^{n-1}$ will play a crucial role in what follows. The next theorem will show that the two first maps embed the pivot polytope into the realm of generalized permutahedra and braid fans, even though they have the undeniable handicap of raising the dimension. The last map ϑ is not, in general, well-behaved, but it will reveal powerful once the aforementioned handicap dealt with.

Definition 3.60. In a fan $\mathcal{F}$, a *great cone* is a cone that can be written as the union of cones of $\mathcal{F}$.

A fan $\mathcal{G}$ is *embedded into* a fan $\mathcal{F}$ when the cones of $\mathcal{G}$ are great cones of $\mathcal{F}$.

In the braid fan $\mathcal{B}_n$, a *pre-order cone* is a great cone associated to a pre-order $\leq$ and defined as $\mathsf{C}_{\leq} = \bigcup_{\sigma \text{ extends } \leq} \mathsf{C}_{\sigma}$ for σ surjection.

Theorem 3.61. *Fix a linear program $(\mathsf{P}, \boldsymbol{c})$, with $n = |V(\mathsf{P})|$ and $m = |E_{\boldsymbol{c}}(\mathsf{P})|$.*

(a) The map $\theta : \mathbb{R}^d \to \mathbb{R}^m$ is an injective linear map that sends the normal fan $\mathcal{N}_{\Pi(\mathsf{P},\boldsymbol{c})}$ of $\Pi(\mathsf{P}, \boldsymbol{c})$ onto a (complete) fan $\theta\big(\mathcal{N}_{\Pi(\mathsf{P},\boldsymbol{c})}\big)$ embedded into the sub-braid fan $\mathcal{B}_m \cap Im(\theta)$, inside $\mathbb{R}^m$. Moreover, a cone $\theta(\mathcal{N}(\mathcal{A}))$ is the intersection of $Im(\theta)$ with the pre-order cone $\mathsf{C}_{\preccurlyeq_{\mathcal{A}}}$.

(b) For a given multi-arborescence $\mathcal{A}$, the map $\vartheta_{\mathcal{A}} : \mathbb{R}^d \to \mathbb{R}^{n-1}$ is a linear map that sends the cone $\mathcal{N}(\mathcal{A})$ onto a great cone of the sub-braid fan $\mathcal{B}_{n-1} \cap Im(\vartheta_{\mathcal{A}})$ inside $\mathbb{R}^{n-1}$. Moreover, the cone $\vartheta_{\mathcal{A}}(\mathcal{N}(\mathcal{A}))$ is the intersection of $Im(\vartheta_{\mathcal{A}})$ with the pre-order cone $\mathsf{C}_{\trianglelefteq_{\mathcal{A}}}$.

Remark 3.62. A sub-braid fan is not necessary a braid fan: it is only a sub-fan of a braid fan, that is the intersection of a braid fan with a linear space (usually of lower dimension).

Proof of Theorem 3.61. (a) As the coordinate of $\theta(\boldsymbol{\omega})$ on $\boldsymbol{uv}$ is $\frac{\langle \boldsymbol{\omega}, \boldsymbol{v}-\boldsymbol{u}\rangle}{\langle \boldsymbol{c}, \boldsymbol{v}-\boldsymbol{u}\rangle}$, it is linear in $\boldsymbol{\omega}$. Furthermore, if $\theta(\boldsymbol{\omega}) = \mathbf{0}$, then $\boldsymbol{\omega}$ is orthogonal to all edges of P, so $\boldsymbol{\omega} = \mathbf{0}$ as P has dimension d. Consequently, θ is an injective linear map.

Fix a cone C in $\theta\big(\mathcal{N}_{\Pi(\mathsf{P},\boldsymbol{c})}\big)$ and consider its pre-image: by injectivity, it is a cone $\mathcal{N}(\mathcal{A})$ for some multi-arborescence $\mathcal{A}$. By Proposition 3.56, a vector $\boldsymbol{\omega} \in \mathbb{R}^d$ belongs to $\mathcal{N}(\mathcal{A})$ if and only if the slope pre-order of $\boldsymbol{\omega}$ is an extension of the utter slope pre-order of $\mathcal{A}$. This is equivalent to requiring that the entries of the slope vector $\theta(\boldsymbol{\omega})$ respect coordinate-wise equalities and inequalities. Consequently, $\boldsymbol{\omega} \in \mathcal{N}(\mathcal{A})$ if and only if $\theta(\boldsymbol{\omega})$ belongs to one of the cones C_σ for σ an extension of the utter slope pre-order, *i.e.* $\mathsf{C} = \mathrm{Im}(\theta) \cap \bigcup_{\sigma \text{ extends } \preccurlyeq_{\mathcal{A}}} \mathsf{C}_\sigma$. As each cone of $\theta\big(\mathcal{N}_{\Pi(\mathsf{P},\boldsymbol{c})}\big)$ is a union of cones of $\mathcal{B}_m$ intersected with $\mathrm{Im}(\theta)$, the embedding is proven.

(b) For a multi-arborescence $\mathcal{A}$ and a vertex $\boldsymbol{u} \in V(\mathsf{P}) \smallsetminus \{\boldsymbol{v}_{\mathrm{opt}}\}$, fix arbitrarily a representative $\boldsymbol{v_u} \in \mathcal{A}(\boldsymbol{u})$, then $\tau_{\boldsymbol{\omega}}(\mathcal{A}(\boldsymbol{u})) = \tau_{\boldsymbol{\omega}}(\boldsymbol{u}, \boldsymbol{v_u})$. Consider the projection $\pi_{\mathcal{A}} : \mathbb{R}^{E_{\boldsymbol{c}}(\mathsf{P})} \to \mathbb{R}^{V(\mathsf{P}) \smallsetminus \{\boldsymbol{v}_{\mathrm{opt}}\}}$ that forgets all coordinates but the ones associated to $(\boldsymbol{u}, \boldsymbol{v_u})$ for $\boldsymbol{u} \in V(\mathsf{P}) \smallsetminus \{\boldsymbol{v}_{\mathrm{opt}}\}$. Then, by definition, $\vartheta_{\mathcal{A}} = \pi_{\mathcal{A}} \circ \theta$, and $\pi_{\mathcal{A}}$ projects the cone $\theta(\mathcal{N}(\mathcal{A}))$ of $\theta\big(\mathcal{N}_{\Pi(\mathsf{P},\boldsymbol{c})}\big)$ onto the cone $\vartheta_{\mathcal{A}}(\mathcal{N}(\mathcal{A}))$. On top of that, by Lemma 3.51, this projection $\pi_{\mathcal{A}}$ projects $\mathcal{B}_m$ onto (a fan linearly isomorphic to) $\mathcal{B}_{n-1}$. Hence, $\vartheta_{\mathcal{A}}(\mathcal{N}(A))$ is a union of cones of $\mathcal{B}_{n-1}$. More precisely, $\vartheta_{\mathcal{A}}(\mathcal{N}(\mathcal{A})) = \mathrm{Im}(\vartheta_{\mathcal{A}}) \cap \bigcup_{\sigma \text{ extends } \preccurlyeq_{\mathcal{A}}} \pi_{\mathcal{A}}\big(\mathsf{C}_\sigma\big)$. As the projection $\pi_{\mathcal{A}}$ forgets all but the coordinates on $\boldsymbol{uv_u}$, Lemma 3.59 ensures that $\pi_{\mathcal{A}}\big(\mathsf{C}_\sigma\big) = \mathsf{C}_\alpha$ for some α that extends $\trianglelefteq_{\mathcal{A}}$, *i.e.* $\vartheta_{\mathcal{A}}(\mathcal{N}(A)) = \mathrm{Im}(\vartheta_{\mathcal{A}}) \cap \bigcup_{\alpha \text{ extends } \trianglelefteq_{\mathcal{A}}} \mathsf{C}_\alpha$. □

Remark 3.63. If P is not full dimensional but embedded into higher dimension, then the kernel of θ is the sub-space orthogonal to the affine hull of P. This does not change the core of the following results, but would overburden the notations.

In general, $\theta\big(\mathcal{N}_{\Pi(\mathsf{P},\boldsymbol{c})}\big)$ is not a complete fan in dimension m. As such, it does not coarsen the braid fan $\mathcal{B}_m$, and $\Pi(\mathsf{P}, \boldsymbol{c})$ is not a deformed permutahedron (in the sense of Section 2). Nonetheless, when Q is a projection of P, then $\mathcal{N}_{\mathsf{Q}}$ is the intersection of $\mathcal{N}_{\mathsf{P}}$ by a sub-space, see [Zie98, Lemma 7.11]. This motivates the following conjecture.

Conjecture 3.64. *For all polytopes $\mathsf{P} \subset \mathbb{R}^d$ with m edges, and objective function $\boldsymbol{c} \in \mathbb{R}^d$, the max-slope pivot polytope $\Pi(\mathsf{P}, \boldsymbol{c})$ is the orthogonal projection of a generalized permutahedron whose normal fan coarsens $\mathcal{B}_m$.*

The projection hinted at in the above conjecture would be the orthogonal projection onto $\mathrm{Im}(\theta)$. If a generalized permutahedron R exists that answers the conjecture, its normal fan $\mathcal{N}_R$ would satisfy $\mathcal{N}_{\mathsf{R}} \cap \mathrm{Im}(\theta) = \theta\big(\mathcal{N}_{\Pi(\mathsf{P},\boldsymbol{c})}\big)$. A natural way to introduce $\mathcal{N}_{\mathsf{R}}$ (as a coarsening of the braid fan $\mathcal{B}_m$) would be to require the maximal cones of $\mathcal{N}_{\mathsf{R}}$ to be exactly $\mathsf{C}_{\preccurlyeq_{\mathcal{A}}} = \bigcup_{\sigma \text{ extends } \preccurlyeq_{\mathcal{A}}} \mathsf{C}_\sigma$ for $\mathcal{A}$ a multi-arborescence on P, but two problems occur. Firstly, it is not mandatory, in general, that all σ extend a $\preccurlyeq_{\mathcal{A}}$ for some multi-arborescence $\mathcal{A}$: in order to properly define the coarsening $\mathcal{N}_{\mathsf{R}}$, one would need to choose what to do with the cones C_σ for σ that does not extend a $\preccurlyeq_{\mathcal{A}}$. On the other hand, it is not clear if there exists a way to choose this coarsening such that $\mathcal{N}_{\mathsf{R}}$ is a fan, and even less clear how to guarantee its polytopality.

Another consequence of the non-completeness of $\theta\big(\mathcal{N}_{\Pi(\mathsf{P},\boldsymbol{c})}\big)$ inside $\mathcal{B}_m$ is that it may happen that $\theta(\mathcal{N}(\mathcal{A}))$ does not intersect a cone C_σ, even though σ extends $\preccurlyeq_{\mathcal{A}}$. This implies that given a multi-arborescence $\mathcal{A}$ and a surjection σ that extends the utter slope pre-order $\preccurlyeq_{\mathcal{A}}$, it can be impossible to find $\boldsymbol{\omega}$ that captures $\mathcal{A}$ with slope pre-order σ.

To confront this non-completeness, one would like to drop dimension, and consider, for instance, the map ϑ, as it goes into $\mathbb{R}^{V(\mathsf{P}) \smallsetminus \{\boldsymbol{v}_{\mathrm{opt}}\}}$ instead of $\mathbb{R}^{E_{\boldsymbol{c}}(\mathsf{P})}$. Although the map θ is linear on the whole normal fan of $\Pi(\mathsf{P}, \boldsymbol{c})$, the map $\vartheta_{\mathcal{A}}$ depends on the chosen multi-arborescence $\mathcal{A}$. Therefore, even though two cones $\vartheta_{\mathcal{A}}(\mathcal{N}(\mathcal{A}))$ and $\vartheta_{\mathcal{A}'}(\mathcal{N}(\mathcal{A}'))$ live in the same braid fan $\mathcal{B}_{n-1}$, they may lie in different sub-spaces $\mathrm{Im}(\vartheta_{\mathcal{A}})$ and $\mathrm{Im}(\vartheta_{\mathcal{A}'})$. Moreover, they may also intersect, and the collection of cones $\big(\vartheta_{\mathcal{A}}(\mathcal{N}(\mathcal{A}))\big)$ for $\mathcal{A}$ a coherent multi-arborescence is not a fan in general. In a word: the map ϑ is not an injective (piece-wise) linear map in general.

Yet, Theorem 3.61 embeds max-slope pivot polytopes into the realm of generalized permutahedra. In particular, this allows us to study the capture of a multi-arborescence as a purely

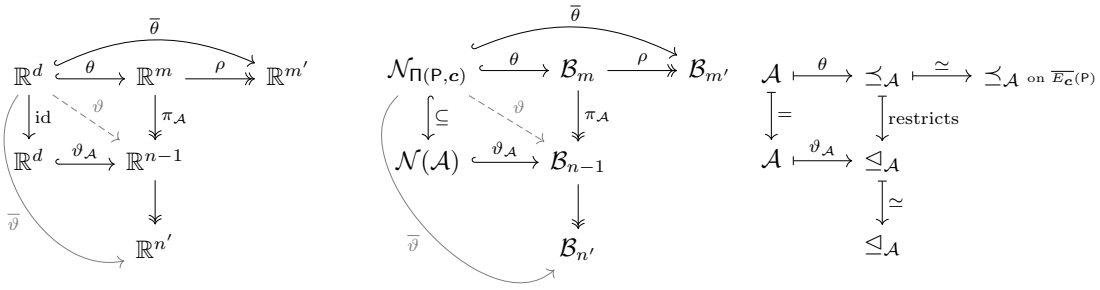

Figure 51: (Middle) The linear maps and projections that embeds the normal fan of $\Pi(\mathsf{P}, \boldsymbol{c})$ into braid fans of different dimensions. (Left) The real vector spaces these maps have for domains. (Right) Utter and adapted pre-orders associated to the multi-arborescence, and their restrictions.

combinatorial phenomenon. Before giving three different applications that benefits from this approach, we deal with parallelisms. As parallel edges always have the same slope when projected onto the plane $(\boldsymbol{c}, \boldsymbol{\omega})$, we can simply keep one edge per parallelism class. We make that precise:

Definition 3.65. In a polytope P, two edges $\boldsymbol{uv}$ and $\boldsymbol{u'v'}$ are *parallel* when $\boldsymbol{v} - \boldsymbol{u}$ and $\boldsymbol{v'} - \boldsymbol{u'}$ are linearly dependent. The set of parallelism classes of edges P is denoted $\overline{E_{\boldsymbol{c}}}(\mathsf{P})$, and the number of classes $\overline{m}$.

Theorem 3.66. *For a linear program $(\mathsf{P}, \boldsymbol{c})$, fix a representative $\boldsymbol{f}_X$ for each class X of parallelism of edges in $\overline{E_{\boldsymbol{c}}}(\mathsf{P})$. Let $\rho : \mathbb{R}^m \to \mathbb{R}^{\overline{m}}$ be the projection that forgets all but the coordinates associated to $(\boldsymbol{f}_X)_{X \in \overline{E_{\boldsymbol{c}}}(\mathsf{P})}$. Then $\overline{\theta} := \rho \circ \theta : \mathbb{R}^d \to \mathbb{R}^{\overline{m}}$ is a linear injection.*

Moreover, $\overline{\theta}(\mathcal{N}(\mathcal{A}))$ is the intersection of $Im(\overline{\theta})$ with the pre-order cone of $\mathcal{B}_{\overline{m}}$ associated to the pre-order that $\preccurlyeq_{\mathcal{A}}$ induces on $\overline{E_{\boldsymbol{c}}}(\mathsf{P})$.

Proof. If $\boldsymbol{uv}$ and $\boldsymbol{u'v'}$ are parallel, then $\theta(\boldsymbol{\omega})_{\boldsymbol{uv}} = \frac{\langle \boldsymbol{\omega}, \boldsymbol{v}-\boldsymbol{u} \rangle}{\langle \boldsymbol{c}, \boldsymbol{v}-\boldsymbol{u} \rangle} = \frac{\langle \boldsymbol{\omega}, \boldsymbol{v'}-\boldsymbol{u'} \rangle}{\langle \boldsymbol{c}, \boldsymbol{v'}-\boldsymbol{u'} \rangle} = \theta(\boldsymbol{\omega})_{\boldsymbol{u'v'}}$. Consequently, if $\pi \circ \theta(\boldsymbol{\omega}) = \mathbf{0}$, then all coordinates of $\theta(\boldsymbol{\omega})$ are zero, and $\boldsymbol{\omega} = \mathbf{0}$ by injectivity of θ.

The above equality also implies that $\boldsymbol{uv} \simeq_{\mathcal{A}} \boldsymbol{u'v'}$ when $\boldsymbol{uv}$ and $\boldsymbol{u'v'}$ are parallel. So Lemma 3.51 ensures that the projection ρ sends the (triangulation of the) great cone associated to $\preccurlyeq_{\mathcal{A}}$ in $\mathcal{B}_m \cap \mathrm{Im}(\theta)$ onto the (triangulation of the) great cone associated to the quotient of $\preccurlyeq_{\mathcal{A}}$ on parallelism classes. □

We now use the power of these embeddings inside (sections of) braid fans to study the max-slope pivot polytopes of cubes, simplices and products of simplices.

3.3.1 Max-slope pivot polytopes of the cube and the simplex

Max-slope pivot polytope of a cube The standard cube $\square_d$ has been introduced in Section 1.2.2. Note that applying an affine transformation to P and $\boldsymbol{c}$ amounts to applying the same linear transformation to $\Pi(\mathsf{P}, \boldsymbol{c})$, by Theorem 3.6, so the case of the standard cube enlightens the case of all cubes with parallel edges, and gives a hint for the case of zonotopes (as projections of the standard cube). We are going to prove the following:

Theorem 3.67. *For any generic $\boldsymbol{c} \in \mathbb{R}^d$, the affine map $\overline{\theta}$ sends the max-slope pivot polytope $\Pi(\square_d, \boldsymbol{c})$ to (a polytope normally equivalent to) the permutahedron Π_d. Moreover, the normal cone $\mathcal{N}_{\mathcal{A}}$ of the vertex of $\Pi(\square_d, \boldsymbol{c})$ associated to $\mathcal{A}$ is sent to the pre-order cone of the pre-order $\preccurlyeq_{\mathcal{A}}$ induced on $\overline{E_{\boldsymbol{c}}}(\mathsf{P})$.*

This case was already studied in [BDLLS22, Example 4.2]: there, the authors prove that $\Pi(\square_d, \boldsymbol{c})$ is a permutahedron in the sense that it is the convex hull of the $d!$ points obtained from

applying the action of the permutation group $\mathcal{S}_d$ on a starting point. Though the computations are similar, we give here a different perspective.

Fix P to be the standard cube $\square_d$ of dimension d and $\boldsymbol{c} \in \mathbb{R}^d$ any generic objective function. By symmetry, we can suppose $c_1 < \cdots < c_d$. The vertices of the cube $\square_d$ identify with the subsets of $[d]$ through the characteristic vector: $\boldsymbol{e}_I := \sum_{i \in I} \boldsymbol{e}_i$ for a subset $I \subseteq [d]$, and $V(\square_d) = \{\boldsymbol{e}_I \ ; \ I \subseteq [d]\}$. The optimal vertex is $\boldsymbol{e}_{[d]}$. Moreover, the improving edges are of the for $\boldsymbol{e}_I \boldsymbol{e}_{I \cup \{i\}}$ for $i \notin I \subsetneq [d]$, and their parallelism class is given by $\boldsymbol{e}_i$, see Figure 52(Top Right).

Hence, there are $\overline{m} = d$ classes of parallelism of edges of $\square_d$. The linear map $\overline{\theta} : \mathbb{R}^d \to \mathbb{R}^{\overline{m}}$ injects the normal fan of $\Pi(\square_d, \boldsymbol{c})$ into the braid fan $\mathcal{B}_d$. As $\overline{m} = d$, $\overline{\theta}$ is surjective. This implies that $\Pi(\square_d, \boldsymbol{c})$ is a generalized permutahedron.

It remains to understand the fan $\overline{\theta}(\mathcal{N}_{\Pi(\mathsf{P},\boldsymbol{c})})$. Fix a multi-arborescence $\mathcal{A}$ on $\square_d$. Let σ be a surjection on $[d]$ that extends the pre-order induced by $\preccurlyeq_{\mathcal{A}}$ on $[d]$. Then for $i \neq j$, looking at $\mathcal{A}([d] \smallsetminus \{i,j\})$, one concludes that $\sigma(i) \leq \sigma(j)$ if and only if $[d] \smallsetminus \{i\} \in \mathcal{A}([d] \smallsetminus \{i,j\})$. Thus σ is fully determined by $\mathcal{A}$: the image $\overline{\theta}(\mathcal{N}(\mathcal{A}))$ is a cone C_σ for some surjection σ of $[d]$.

Example 3.68. In Figure 52(Top Right) is depicted the standard 3-dimensional cube $\square_3$, where each vertex is labelled by the corresponding set I (denoted without comma nor bracket). The objective function corresponds to the left-to-right orientation. The max-slope pivot polytope $\Pi(\square_3, \boldsymbol{c}) \simeq \Pi_3$ is the hexagon drawn on the left. Each vertex and each edge is labelled by a representation of the corresponding multi-arborescence $\mathcal{A}$, and the ordered partition whose associated surjection is the pre-order $\preccurlyeq_{\mathcal{A}}$ on $\overline{E}_{\boldsymbol{c}}(\square_3)$. For instance, the vertical edge on the right side corresponds to the multi-arborescence $\mathcal{A}$ with (using the notations of the figure) $\mathcal{A}(\varnothing) = \{1,3\}$, $\mathcal{A}(1) = \mathcal{A}(3) = \{13\}$, $\mathcal{A}(2) = \{12, 23\}$, $\mathcal{A}(13) = \mathcal{A}(12) = \mathcal{A}(23) = \{123\}$. Such multi-arborescence imposes that if $\boldsymbol{\omega} \in \mathbb{R}^3$ captures $\mathcal{A}$, then $\omega_2 < \omega_1 = \omega_3$.

Max-slope pivot polytope of a simplex As all simplices are affinely equivalent, for all linear program $(\mathsf{P}, \boldsymbol{c}')$ with P a simplex, Theorem 3.6 ensures that the max-slope pivot polytope $\Pi(\mathsf{P}, \boldsymbol{c}')$ is linearly equivalent to $\Pi(\Delta_d, \boldsymbol{c})$ where Δ_d is the standard simplex $\Delta_d = \operatorname{conv}\{\boldsymbol{e}_1, \dots \boldsymbol{e}_{d+1}\}$, and $c_1 < \cdots < c_{d+1}$. Hence, we are going to prove the following:

Theorem 3.69. *For any $\boldsymbol{c} \in \mathbb{R}^{d+1}$, the map ϑ sends the max-slope pivot polytope $\Pi(\Delta_d, \boldsymbol{c})$ to (a polytope normally equivalent to) Loday's associahedron Asso_d (that is a deformed permutahedron, see Section 1.2.4). Moreover, the normal cone $\mathcal{N}(\mathcal{A})$ of the vertex of $\Pi(\Delta_d, \boldsymbol{c})$ associated to $\mathcal{A}$ is sent by ϑ to the pre-order cone of the pre-order $\trianglelefteq_{\mathcal{A}}$ on $V(\mathsf{P}) \smallsetminus \{\boldsymbol{e}_{d+1}\}$.*

This case was already studied in [BDLLSon]: there the authors prove that $\Pi(\Delta_d, \boldsymbol{c})$ is combinatorially equivalent to Asso_d.

Contrarily to the case of the cube, there are $\binom{d}{2}$ classes of parallelisms of edges, so $\overline{\theta} : \mathbb{R}^d \to \mathbb{R}^{\binom{d}{2}}$ is injective but not surjective. However, $n - 1 = d$ (where n is the number of vertices of Δ_d), so for a multi-arborescence $\mathcal{A}$ on Δ_d, the map $\vartheta_{\mathcal{A}}$ is an endomorphism of $\mathbb{R}^d = \operatorname{aff}(\Delta_d)$.

For the simplex Δ_d, one can recover $\theta(\boldsymbol{\omega})$ from $\vartheta_{\mathcal{A}}(\boldsymbol{\omega})$ for all $\boldsymbol{\omega} \in \mathbb{R}^{d+1}$. Indeed, $\vartheta_{\mathcal{A}}$ is an automorphism because if $\vartheta_{\mathcal{A}}(\boldsymbol{\omega}) = \mathbf{0}$, then $\boldsymbol{\omega}$ is orthogonal to d different edges of Δ_d, so $\boldsymbol{\omega} = \mathbf{0}$ as d different edges of Δ_d spans $\mathbb{R}^d$. Thus, as $\vartheta_{\mathcal{A}} = \pi_{\mathcal{A}} \circ \theta$, the dimensions indicate that the map $\pi_{\mathcal{A}}$ is a bijection between $\operatorname{Im}(\theta)$ and $\operatorname{Im}(\vartheta_{\mathcal{A}})$. Consequently, ϑ is injective: if $\vartheta(\boldsymbol{\omega}) = \vartheta(\boldsymbol{\omega}')$, then $\theta(\boldsymbol{\omega}) = \theta(\boldsymbol{\omega}')$ by the previous argument, so $\boldsymbol{\omega} = \boldsymbol{\omega}'$ as θ is injective.

Therefore, ϑ is an injective piece-wise linear map from $\operatorname{aff}(\Delta_d)$ to $\mathbb{R}^d$: it is a bijection as their dimensions are equal[10]. Thus, $\Pi(\Delta_d, \boldsymbol{c})$ is combinatorially isomorphic to a generalized permutahedron. It remains to understand the normal fan of $\vartheta\big(\Pi(\Delta_d, \boldsymbol{c})\big)$.

To this end, it is enough to focus on the maximal cones of the fan $\vartheta\big(\Pi(\Delta_d, \boldsymbol{c})\big)$, *i.e.* to arborescences captured on Δ_d. Each such arborescence A can be seen as a map $A : [d+1] \to [d+1]$ with $A(i) > i$. For a coherent arborescence A on Δ_d, we have $A(i) = \min\big(\{j \ ; \ j > i \text{ and } j \preccurlyeq_A$

[10]Such a map induces a continuous injective application $\boldsymbol{\omega} \mapsto \frac{\vartheta(\boldsymbol{\omega})}{\|\vartheta(\boldsymbol{\omega})\|}$ of the d-dimensional sphere $\mathbb{S}^d$ to itself. If it were not surjective, it would induce an injection from $\mathbb{S}^d$ to $\mathbb{R}^d$ (which is homeomorphic to a sphere minus a point): Borsuk–Ulam's theorem ensures it does not exist. As $\vartheta(\lambda\boldsymbol{\omega}) = \lambda\vartheta(\boldsymbol{\omega})$, the map ϑ is bijective.

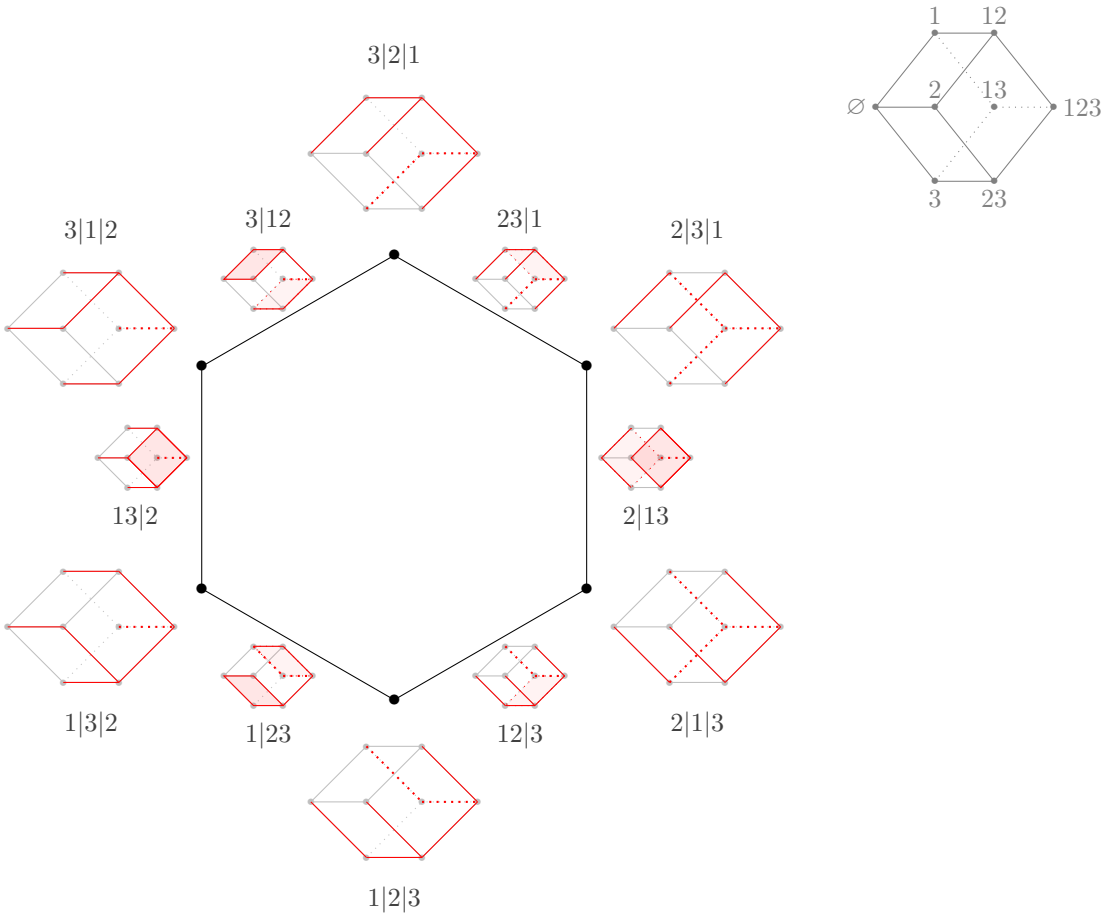

Figure 52: The max-slope pivot polytope of the cube $\square_3$ (the objective function is left to right). Each vertex is labelled by the corresponding multi-arborescence, and the surjection associated. For instance, the bottom vertex is associated with the arborescence $A^{\boldsymbol{\omega}}$ with $\omega_1 < \omega_2 < \omega_3$.

$i\} \cup \{d+1\}\big)$. Indeed, for a fixed i, on the one hand for all $i < j < A(i)$, Lemma 3.5 applied to the triangle (c_i, ω_i), (c_j, ω_j), $(c_{A(i)}, \omega_{A(i)})$ ensures that $i \preccurlyeq_A j$; and on the other hand, $A(i) \preccurlyeq_A i$ by Lemma 3.5 applied to the triangle (c_i, ω_i), $(c_{A(i)}, \omega_{A(i)})$, $(c_{A(A(i))}, \omega_{A(A(i))})$.

To a binary search tree T on $[d]$, one can associate the map $A_T : [d+1] \to [d+1]$ defined by $A_T(d+1) = d+1$ and $A_T(i) = \min\big(\{j \ ; \ j \notin T^i\} \cup \{d+1\}\big)$ where T^i is the sub-tree of root i in T. Fix a permutation σ and consider its binary search tree $T(\sigma)$, that is the binary search tree on $[d]$ in which i is inserted before j when $\sigma(i) < \sigma(j)$, see Section 1.2.4(paragraph Binary search trees). Then, $A_{T(\sigma)}$ is an arborescence such that σ extends $\trianglelefteq_{A_{T(\sigma)}}$. As ϑ is injective, $A_{T(\sigma)}$ is the unique arborescence with this property. Conversely, if two binary search trees T_1 and T_2 differ, then there exists i such that T_1^i and T_2^i differ, so $A_{T_1} \neq A_{T_2}$.

Hence, the map $T \mapsto A_T$ induces through ϑ a piece-wise linear isomorphism between $\mathcal{N}_{\Pi(\Delta_d, \boldsymbol{c})}$ and the coarsening of $\mathcal{B}_d$ defined by gluing C_σ and C_α when σ and α yield the same binary search tree, *i.e.* the sylvester fan. We have proven that $\Pi(\Delta_d, \boldsymbol{c})$ is piece-wise linearly equivalent to Loday's associahedron. Moreover, $\trianglelefteq_{\mathcal{A}}$ is precisely the pre-order associated to the normal cone $\vartheta(\mathcal{N}(\mathcal{A}))$.

Example 3.70. In Figure 53(Top Right) is depicted a 3-dimensional simplex Δ_3, where the vertices are labelled from 1 to 4 according to their scalar product against the (left-to-right oriented) objective function. The max-slope pivot polytope $\Pi(\Delta_3, \boldsymbol{c}) \simeq \mathsf{Asso}_3$ is drawn on the left. Each vertex is labelled three times. Firstly, by its non-crossing arborescence A (in the fashion of Sections 1.2.4 and 3.2). Secondly, by the pre-order $\trianglelefteq_A$ on $[3]$, figured as a binary search tree. Lastly, by the pre-order $\preccurlyeq_A$ on $E_{\boldsymbol{c}}(\Delta_3)$ (which has 6 edges, identified by the couple of vertices linked).

For instance, the rightmost vertex corresponds to the non-crossing arborescence A with $A(1) = 2$, $A(2) = A(3) = 4$, which adapted slope pre-order is defined by $2 \preccurlyeq_A 1$ and $2 \preccurlyeq_A 3$ (and no relation between 1 and 3), and utter slope pre-order can be read in increasing order from bottom to top on the rightmost part of Figure 53 (in red are the edges that A uses).

3.3.2 Max-slope pivot polytope of a product of simplices

The cartesian product of two polytopes $\mathsf{P} \subset \mathbb{R}^p$ and $\mathsf{Q} \subset \mathbb{R}^q$ is the polytope in $\mathbb{R}^{p+q} = \mathbb{R}^p \times \mathbb{R}^q$ defined as $\mathsf{P} \times \mathsf{Q} := \{(\boldsymbol{p}, \boldsymbol{q}) \ ; \ \boldsymbol{p} \in \mathsf{P}, \ \boldsymbol{q} \in \mathsf{Q}\}$. For two fixed polytopes P and Q and objective functions $\boldsymbol{c}_1 \in \mathbb{R}^p$ and $\boldsymbol{c}_2 \in \mathbb{R}^q$, suppose we know the max-slope pivot polytopes $\Pi(\mathsf{P}, \boldsymbol{c}_1)$ and $\Pi(\mathsf{Q}, \boldsymbol{c}_2)$: what can we say about the max-slope pivot polytope $\Pi(\mathsf{P} \times \mathsf{Q}, \boldsymbol{c})$ where $\boldsymbol{c} = (\boldsymbol{c}_1, \boldsymbol{c}_2)$?

We have already seen an instance of this problem: the standard cube $\square_d$ is the product of d segments $[0, 1]$, and its max-slope pivot polytope is the permutahedron. We will see that when P and Q are products of simplices, then $\Pi(\mathsf{P} \times \mathsf{Q}, \boldsymbol{c})$ is combinatorially isomorphic to the shuffle of $\Pi(\mathsf{P}, \boldsymbol{c}_1)$ and $\Pi(\mathsf{Q}, \boldsymbol{c}_2)$ as defined in [CP22, Section 2]. We will not be able to fully describe the general case, but some interesting general properties will spring from the discussion that follows.

Definition 3.71. ([CP22, Definition 75]). The *shuffle product* of two generalized permutahedra $\mathsf{P} \subset \mathbb{R}^p$ and $\mathsf{Q} \subset \mathbb{R}^q$ is the polytope $\mathsf{P} \star \mathsf{Q} \subset \mathbb{R}^{p+q}$ defined by:

$$\mathsf{P} \star \mathsf{Q} = \mathsf{P} \times \mathsf{Q} + \sum_{i \in [p], \ j \in [q]} [\boldsymbol{e}_i, \boldsymbol{e}_{p+j}]$$

Definition 3.72. Given two pre-orders $\leq$ on a set E and $\preccurlyeq$ on a set F, a pre-order $\trianglelefteq$ on $E \sqcup F$ is *shuffle of $\leq$ and $\preccurlyeq$* when the four following conditions hold:

- for all $e, e' \in E$, if $e \leq e'$ then $e \trianglelefteq e'$;
- for all $f, f' \in F$, if $f \preccurlyeq f'$, then $f \trianglelefteq f'$;
- for all $e \in E, f \in F$, either $e \trianglelefteq f$ or $f \trianglelefteq e$;
- $\trianglelefteq$ is the closure relation of the above (that is, for all $e, e' \in E$, if $e \trianglelefteq e'$, then either $e \leq e'$ or there exists $f \in F$ such that $e \trianglelefteq f \trianglelefteq e'$, and conversely for $f, f' \in F$).

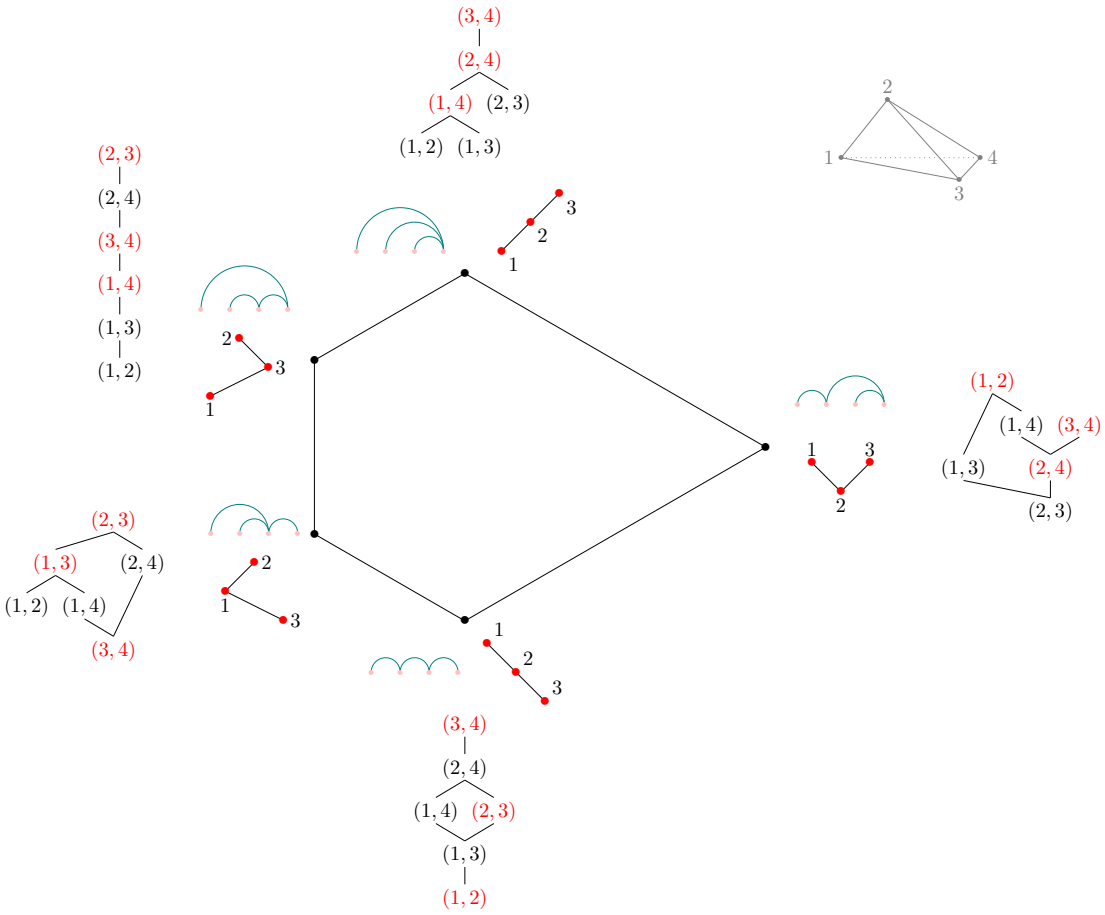

Figure 53: The max-slope pivot polytope of the simplex Δ_3. Each vertex is labelled by the corresponding (coherent) non-crossing arborescence A, the binary search tree T with $A = A_T$, and the pre-order $\preccurlyeq_A$ on the edges of Δ_3.

Recall that each cone of the normal fan of a deformed permutahedron is a pre-order cone.

Proposition 3.73. ([CP22, Proposition 79]). *For* P *and* Q *two deformed permutahedra, the normal fan of* $\mathsf{P} \star \mathsf{Q}$ *is precisely the set of pre-order cones* $\mathsf{C}_{\trianglelefteq}$ *where* $\trianglelefteq$ *runs over all shuffles between a pre-order* $\leq$ *corresponding to a normal cone of* P *and a pre-order* $\preccurlyeq$ *corresponding to a normal cone of* Q.

We are going to prove the following:

Theorem 3.74. *If* P *is (isomorphic to) a product of simplices* $\Delta_{d_1} \times \cdots \times \Delta_{d_r}$ *with* $d = \sum_{i=1}^{r} d_i$, *then for any generic objective function* $\boldsymbol{c}$, *there exists a piece-wise linear map* $\overline{\vartheta}$ *(explicitly defined hereafter) that sends the max-slope pivot polytope* $\Pi(\mathsf{P}, \boldsymbol{c})$, *to (a polytope normally equivalent to) the shuffle product* $\mathsf{Asso}_{d_1} \star \cdots \star \mathsf{Asso}_{d_r}$.

Moreover, the normal cone $\mathcal{N}(\mathcal{A})$ *of the vertex of* $\Pi(\mathsf{P}, \boldsymbol{c})$ *associated to* $\mathcal{A}$ *is sent by* $\overline{\vartheta}$ *to the pre-order cone of the pre-order that* $\trianglelefteq_{\mathcal{A}}$ *induces on* $\prod_{i=1}^{r} V(\Delta_{d_i}) \smallsetminus \{\boldsymbol{e}_{d_i+1}\}$.

Proof. Although the notations can feel heavy, we are simply going to work with (piece-wise) linear functions, and analyze which pre-orders are associated to which cones.

We first focus on classes of parallelism on $\mathsf{P} \times \mathsf{Q}$. Fix polytopes $\mathsf{P} \subset \mathbb{R}^p$ and $\mathsf{Q} \subset \mathbb{R}^q$ with generic objective functions $\boldsymbol{c}_1 \in \mathbb{R}^p$ and $\boldsymbol{c}_2 \in \mathbb{R}^q$. We denote $\boldsymbol{p}_{\mathrm{opt}}$ the optimal vertex of P with respect to $\boldsymbol{c}_1$, and $\boldsymbol{q}_{\mathrm{opt}}$ the optimal vertex of Q with respect to $\boldsymbol{c}_2$. Take a coherent multi-arborescence $\mathcal{A}$ on $\mathsf{P} \times \mathsf{Q}$ captured by $\boldsymbol{\omega} = (\boldsymbol{\omega}_1, \boldsymbol{\omega}_2) \in \mathbb{R}^p \times \mathbb{R}^q$. Remark that $\mathcal{A}$ induces a coherent multi-arborescence $\mathcal{A}_{\mathsf{P}}$ on P and a coherent multi-arborescence $\mathcal{A}_{\mathsf{Q}}$ on Q defined as follows: $\mathcal{A}_{\mathsf{P}}(\boldsymbol{u}) \times \{\boldsymbol{q}_{\mathrm{opt}}\} = \mathcal{A}((\boldsymbol{u}, \boldsymbol{q}_{\mathrm{opt}}))$ and $\{\boldsymbol{p}_{\mathrm{opt}}\} \times \mathcal{A}_{\mathsf{Q}}(\boldsymbol{v}) = \mathcal{A}((\boldsymbol{p}_{\mathrm{opt}}, \boldsymbol{v}))$. Manifestly, these multi-arborescences are coherent as they are captured by $\boldsymbol{\omega}_1$ and $\boldsymbol{\omega}_2$ respectively.

Then note that for any $\boldsymbol{p}, \boldsymbol{p}' \in V(\mathsf{P})$ and $\boldsymbol{q} \in V(\mathsf{Q})$, the edges $(\boldsymbol{p}, \boldsymbol{q})(\boldsymbol{p}', \boldsymbol{q})$ and $(\boldsymbol{p}, \boldsymbol{q}_{\mathrm{opt}})(\boldsymbol{p}', \boldsymbol{q}_{\mathrm{opt}})$ are parallel (and respectively for Q). Hence, there are three possibilities: either $\mathcal{A}((\boldsymbol{p}, \boldsymbol{q})) = \mathcal{A}_{\mathsf{P}}(\boldsymbol{p}) \times \{\boldsymbol{q}\}$, or $\mathcal{A}((\boldsymbol{p}, \boldsymbol{q})) = \{\boldsymbol{p}\} \times \mathcal{A}_{\mathsf{Q}}(\boldsymbol{q})$, or $\mathcal{A}((\boldsymbol{p}, \boldsymbol{q})) = \mathcal{A}_{\mathsf{P}}(\boldsymbol{p}) \times \mathcal{A}_{\mathsf{Q}}(\boldsymbol{q})$, depending on the (in)equality between $\tau_{\boldsymbol{\omega}_1}(\mathcal{A}_{\mathsf{P}}(\boldsymbol{p}))$ and $\tau_{\boldsymbol{\omega}_2}(\mathcal{A}_{\mathsf{Q}}(\boldsymbol{q}))$. This allows us to associate to $\mathcal{A}$ a pre-order $\trianglelefteq_{\mathcal{A},\|}$ on $\big(V(\mathsf{P}) \smallsetminus \{\boldsymbol{p}_{\mathrm{opt}}\}\big) \sqcup \big(V(\mathsf{Q}) \smallsetminus \{\boldsymbol{q}_{\mathrm{opt}}\}\big)$ defined by (the closure of):

$$\begin{cases} \boldsymbol{p} \trianglelefteq_{\mathcal{A},\|} \boldsymbol{p}' & \text{if} \quad (\boldsymbol{p}, \boldsymbol{q}_{\mathrm{opt}}) \trianglelefteq_{\mathcal{A}} (\boldsymbol{p}', \boldsymbol{q}_{\mathrm{opt}}) \\ \boldsymbol{q} \trianglelefteq_{\mathcal{A},\|} \boldsymbol{q}' & \text{if} \quad (\boldsymbol{p}_{\mathrm{opt}}, \boldsymbol{q}) \trianglelefteq_{\mathcal{A}} (\boldsymbol{p}_{\mathrm{opt}}, \boldsymbol{q}') \\ \boldsymbol{p} \triangleleft_{\mathcal{A},\|} \boldsymbol{q} & \text{if} \quad \mathcal{A}((\boldsymbol{p}, \boldsymbol{q})) = \{\boldsymbol{p}\} \times \mathcal{A}_{\mathsf{Q}}(\boldsymbol{q}) \\ \boldsymbol{q} \triangleleft_{\mathcal{A},\|} \boldsymbol{p} & \text{if} \quad \mathcal{A}((\boldsymbol{p}, \boldsymbol{q})) = \mathcal{A}_{\mathsf{P}}(\boldsymbol{p}) \times \{\boldsymbol{q}\} \\ \boldsymbol{p} \simeq_{\mathcal{A},\|} \boldsymbol{q} & \text{if} \quad \mathcal{A}((\boldsymbol{p}, \boldsymbol{q})) = \mathcal{A}_{\mathsf{P}}(\boldsymbol{p}) \times \mathcal{A}_{\mathsf{Q}}(\boldsymbol{q}) \end{cases}$$

The pre-order $\trianglelefteq_{\mathcal{A}}$ can be retrieved from the knowledge of $\trianglelefteq_{\mathcal{A},\|}$, as we only have quotiented (certain) equivalence classes: $(\boldsymbol{p}, \boldsymbol{q}) \simeq_{\mathcal{A}} (\boldsymbol{p}, \boldsymbol{q}_{\mathrm{opt}})$ when $\boldsymbol{q} \trianglelefteq_{\mathcal{A},\|} \boldsymbol{p}$; and $(\boldsymbol{p}, \boldsymbol{q}) \simeq_{\mathcal{A}} (\boldsymbol{p}_{\mathrm{opt}}, \boldsymbol{q})$ when $\boldsymbol{p} \trianglelefteq_{\mathcal{A},\|} \boldsymbol{q}$.

Consequently, when $\mathsf{P} = \Delta_{d_1} \times \cdots \times \Delta_{d_r}$ (where $\sum_i d_i = p = \dim(\mathsf{P})$) is a product of simplices, the above process allows us to associate injectively a pre-order $\trianglelefteq_{\mathcal{A},\|}$ on $\bigsqcup_i V(\Delta_{d_i}) \smallsetminus \{\boldsymbol{e}_{d_i+1}\}$ to the pre-order $\trianglelefteq_{\mathcal{A}}$, for each multi-arborescence $\mathcal{A}$ on P.

Now, we prove by induction on the number of factors that when P is a product of simplices $\Delta_{d_1} \times \cdots \times \Delta_{d_r}$, then there exists a piece-wise linear (continuous) bijection $\overline{\vartheta}_{\mathsf{P}} : \mathbb{R}^p \to \mathbb{R}^p$ that embeds $\mathcal{N}_{\Pi(\mathsf{P}, \boldsymbol{c}_1)}$ into $\mathcal{B}_p$ where $\overline{\vartheta}_{\mathsf{P}}(\mathcal{N}(\mathcal{A}_{\mathsf{P}}))$ is the pre-order cone $\mathsf{C}_{\trianglelefteq_{\mathcal{A}_{\mathsf{P}},\|}}$. Fix two products of simplices P and Q and suppose the statement holds, denoting $\overline{\vartheta}_{\mathsf{P}} : \mathbb{R}^p \to \mathbb{R}^p$ for P and $\overline{\vartheta}_{\mathsf{Q}} : \mathbb{R}^q \to \mathbb{R}^q$ for Q. Then define $\overline{\vartheta} : \mathbb{R}^{p+q} \to \mathbb{R}^{p+q}$ by setting $\overline{\vartheta}\big((\boldsymbol{\omega}_{\mathsf{P}}, \boldsymbol{\omega}_{\mathsf{Q}})\big) = \big(\overline{\vartheta}_{\mathsf{P}}(\boldsymbol{\omega}_{\mathsf{P}}),\ \overline{\vartheta}_{\mathsf{Q}}(\boldsymbol{\omega}_{\mathsf{Q}})\big)$. The application $\overline{\vartheta}$ is a piece-wise linear (continuous) bijection as $\overline{\vartheta}_{\mathsf{P}}$ and $\overline{\vartheta}_{\mathsf{Q}}$ are. It embeds $\overline{\vartheta}(\mathcal{N}_{\Pi(\mathsf{P} \times \mathsf{Q}, \boldsymbol{c})})$ into the braid fan $\mathcal{B}_{p+q}$. Moreover, for a multi-arborescence $\mathcal{A}$ on $\mathsf{P} \times \mathsf{Q}$, if σ is a surjection of $[p] \sqcup [q]$ that extends $\trianglelefteq_{\mathcal{A},\|}$, the definition of this pre-order ensures that if $\boldsymbol{\omega} \in \mathbb{R}^{p+q}$ satisfies $\overline{\vartheta}(\boldsymbol{\omega}) \in \mathsf{C}_{\sigma}$, then $\boldsymbol{\omega}$ captures $\mathcal{A}$. As $\overline{\vartheta}$ is bijective, the cone $\overline{\vartheta}(\mathcal{N}(\mathcal{A}))$ is the union of cones C_{σ} for σ that extends $\trianglelefteq_{\mathcal{A},\|}$. As the statement holds for any simplex by Theorem 3.69, the induction follows.

We have proven that $\Pi(\mathsf{P}\times\mathsf{Q},\boldsymbol{c})$ is a generalized permutahedron, as $\overline{\vartheta}$ sends bijectively the normal fan of $\Pi(\mathsf{P}\times\mathsf{Q},\boldsymbol{c})$ on a fan coarsening $\mathcal{B}_{p+q}$. It remains to understand this coarsening. As $\mathsf{P}=\Delta_{d_1}\times\dots\Delta_{d_r}$, we denote $\overline{V}(\mathsf{P}):=\bigsqcup_i V(\Delta_{d_i})\smallsetminus\{\boldsymbol{e}_{d_i+1}\}$. Fix a multi-arborescence $\mathcal{A}$ on $\mathsf{P}\times\mathsf{Q}$ and defined as before: $\mathcal{A}_{\mathsf{P}}(\boldsymbol{u})\times\{\boldsymbol{q}_{\mathrm{opt}}\}=\mathcal{A}((\boldsymbol{u},\boldsymbol{q}_{\mathrm{opt}}))$ and $\{\boldsymbol{p}_{\mathrm{opt}}\}\times\mathcal{A}_{\mathsf{Q}}(\boldsymbol{v})=\mathcal{A}((\boldsymbol{p}_{\mathrm{opt}},\boldsymbol{v}))$. Associate to $\mathcal{A}$ the pre-order $\trianglelefteq$ on $\overline{V}(\mathsf{P})\sqcup\overline{V}(\mathsf{Q})$ that is the shuffle of $\trianglelefteq_{\mathcal{A}_{\mathsf{P}},\|}$ and $\trianglelefteq_{\mathcal{A}_{\mathsf{Q}},\|}$ defined as the transitive closure of the following relations:

$$\begin{cases}\boldsymbol{p}\trianglelefteq\boldsymbol{p}' & \text{if}\quad \boldsymbol{p}\trianglelefteq_{\mathcal{A}_{\mathsf{P}},\|}\boldsymbol{p}'\\ \boldsymbol{q}\trianglelefteq\boldsymbol{q}' & \text{if}\quad \boldsymbol{q}\trianglelefteq_{\mathcal{A}_{\mathsf{Q}},\|}\boldsymbol{q}'\\ \boldsymbol{p}\trianglelefteq\boldsymbol{q} & \text{if}\quad \{\boldsymbol{p}\}\times\mathcal{A}_{\mathsf{Q}}(\boldsymbol{q})\subseteq\mathcal{A}((\boldsymbol{p},\boldsymbol{q}))\\ \boldsymbol{q}\trianglelefteq\boldsymbol{p} & \text{if}\quad \mathcal{A}_{\mathsf{P}}(\boldsymbol{q})\times\{\boldsymbol{q}\}\subseteq\mathcal{A}((\boldsymbol{p},\boldsymbol{q}))\end{cases}$$

If a surjection σ of $[p]\sqcup[q]$ extends this shuffle pre-order $\trianglelefteq$, then $\mathsf{C}_\sigma\subseteq\overline{\vartheta}(\mathcal{N}(\mathcal{A}))$. Indeed, as $\overline{\vartheta}$ is bijective, take $\boldsymbol{x}\in\mathsf{C}_\sigma$ and $\boldsymbol{\omega}=(\boldsymbol{\omega}_1,\boldsymbol{\omega}_2)$ with $\overline{\vartheta}(\boldsymbol{\omega})=\boldsymbol{x}$, then $\boldsymbol{\omega}_1$ captures $\mathcal{A}_{\mathsf{P}}$ on P, and $\boldsymbol{\omega}_2$ captures $\mathcal{A}_{\mathsf{Q}}$ on Q, by definitions of $\overline{\vartheta}_{\mathsf{P}}$ and $\overline{\vartheta}_{\mathsf{Q}}$. Furthermore, $\boldsymbol{p}\trianglelefteq\boldsymbol{q}$ if and only if $\{\boldsymbol{p}\}\times\mathcal{A}_{\mathsf{Q}}(\boldsymbol{q})\subseteq\mathcal{A}((\boldsymbol{p},\boldsymbol{q}))$, so $\boldsymbol{x}\in\overline{\vartheta}(\mathcal{N}(\mathcal{A}))$ as σ extends $\trianglelefteq$. Conversely, if $\boldsymbol{x}=\overline{\vartheta}((\boldsymbol{\omega}_1,\boldsymbol{\omega}_2))\in\mathsf{C}_\alpha$ for α that does not extend $\trianglelefteq$, then there exists $\boldsymbol{r},\boldsymbol{r}'\in\overline{V}(\mathsf{P})\sqcup\overline{V}(\mathsf{Q})$ such that $\boldsymbol{r}\trianglelefteq\boldsymbol{r}'$ but $\alpha(\boldsymbol{r})>\alpha(\boldsymbol{r}')$. If $\boldsymbol{r},\boldsymbol{r}'\in\overline{V}(\mathsf{P})$, then the definition of $\leq_{\mathcal{A}_{\mathsf{P}},\|}$ ensures that $\boldsymbol{\omega}_1$ does not capture P, and idem if $\boldsymbol{r},\boldsymbol{r}'\in\overline{V}(\mathsf{Q})$. And if $\boldsymbol{r}\in\overline{V}(\mathsf{P})$ while $\boldsymbol{r}'\in\overline{V}(\mathsf{Q})$, then $\tau_{\boldsymbol{\omega}_1}(\mathcal{A}_{\mathsf{P}}(\boldsymbol{p}))>\tau_{\boldsymbol{\omega}_2}(\mathcal{A}_{\mathsf{Q}}(\boldsymbol{q}))$, so $\{\boldsymbol{p}\}\times\mathcal{A}_{\mathsf{Q}}(\boldsymbol{q})\not\subseteq\mathcal{A}((\boldsymbol{p},\boldsymbol{q}))$. In any case, $\boldsymbol{x}\notin\overline{\vartheta}(\mathcal{N}(\mathcal{A}))$.

We have proven that $\mathsf{C}_\sigma\subseteq\overline{\vartheta}(\mathcal{N}(\mathcal{A}))$ if and only if σ extends the shuffle $\trianglelefteq_{\mathcal{A}_{\mathsf{P}},\|}$ and $\trianglelefteq_{\mathcal{A}_{\mathsf{Q}},\|}$ that $\trianglelefteq$ defines. Moreover, as Proposition 3.73 ensures that the shuffle product $\Pi(\mathsf{P},\boldsymbol{c}_1)\star\Pi(\mathsf{Q},\boldsymbol{c}_2)$ is realizable, we obtain that $\overline{\vartheta}(\mathcal{N}(\mathcal{A}))$ is the pre-order cone $\mathsf{C}_{\trianglelefteq}$. Together with Theorem 3.69, this proves the claimed theorem. □

Example 3.75. Theorem 3.74 grants access to several examples, studied in details in [CP22, Sections 3 & 4]. We briefly review the most prominent, and the combinatorial families they are associated to.

Let $\mathsf{P}=\Delta_{d_1}\times\dots\Delta_{d_r}$ be a product of simplices, then:

(a) When $r=1$, $\mathsf{P}=\Delta_d$ is a simplex, and $\Pi(\Delta_d,\boldsymbol{c})$ is an associahedron Asso_d (see Theorem 3.69). Its vertices correspond to binary trees.

(b) When $d_i=1$ for all i, $\mathsf{P}=\square_d$ is the standard cube and $\Pi(\square_d,\boldsymbol{c})$ is a permutahedron Π_d (see Theorem 3.67). Its vertices correspond to permutations.

(c) When $r=2$, $d_1=1$ and $d_2=n$, then $\mathsf{P}=\Delta_1\times\Delta_n$ is a prism over a simplex, and $\Pi(\Delta_1\times\Delta_n,\boldsymbol{c})$ is the *multiplihedron* (see [Sta70, For08]). More generally, when $r=m+1$, $d_1=\dots=d_m=1$ and $d_{m+1}=n$, then $\mathsf{P}=\square_m\times\Delta_n$ is the product of a cube and a simplex, and $\Pi(\square_m\times\Delta_n,\boldsymbol{c})$ is the *(m,n)-multiplihedron* as defined in [CP22, Section 3.2]. Its vertices correspond to painted trees.

(d) When $r=2$, $d_1=n$ and $d_2=m$, then $\mathsf{P}=\Delta_m\times\Delta_n$ is the product of two simplices, and $\Pi(\Delta_m\times\Delta_n,\boldsymbol{c})$ is the *(m,n)-constrainahedron* (see [Bot19, Pol21] and [CP22, Section 4]). Its vertices correspond to cotrees.

Example 3.76. For any P and Q, each coherent multi-arborescence $\mathcal{A}$ on $\mathsf{P}\times\mathsf{Q}$ is associated with a pre-order $\leq$ on $\big(V(\mathsf{P})\smallsetminus\{\boldsymbol{p}_{\mathrm{opt}}\}\big)\sqcup\big(V(\mathsf{Q})\smallsetminus\{\boldsymbol{q}_{\mathrm{opt}}\}\big)$ that is a shuffle between some pre-orders $\leq_{\mathcal{A}_{\mathsf{P}}}$ and $\leq_{\mathcal{A}_{\mathsf{Q}}}$ for $\mathcal{A}_{\mathsf{P}}$ and $\mathcal{A}_{\mathsf{Q}}$ as defined before. The map $\mathcal{A}\mapsto\leq$ is injective, as we have seen that the knowledge of all comparisons given by $\leq$ allows to recover the multi-arborescences. Nevertheless, $\trianglelefteq_{\mathcal{A}}$ is not necessarily isomorphic to $\leq$, but only extends it[11].

Moreover, in the general case when P or Q is not a product of simplicies, not all shuffles between coherent pre-orders on P and on Q are associated to a coherent pre-order on $\mathsf{P}\times\mathsf{Q}$ by this construction. To illustrate this fact, consider the following example. Fix $\boldsymbol{v}_1=\begin{pmatrix}0\\0\end{pmatrix}$, $\boldsymbol{v}_2=\begin{pmatrix}1\\0\end{pmatrix}$, $\boldsymbol{v}_3=\begin{pmatrix}0\\1\end{pmatrix}$ and $\boldsymbol{v}_4=\begin{pmatrix}2\\1\end{pmatrix}$ and let $\mathsf{P}=\operatorname{conv}\{\boldsymbol{v}_1,\boldsymbol{v}_2,\boldsymbol{v}_3,\boldsymbol{v}_4\}$ with $\boldsymbol{c}=(1,1)$, see

[11] The author sees no proof of isomorphism in general but is still trying to find a counter-example.

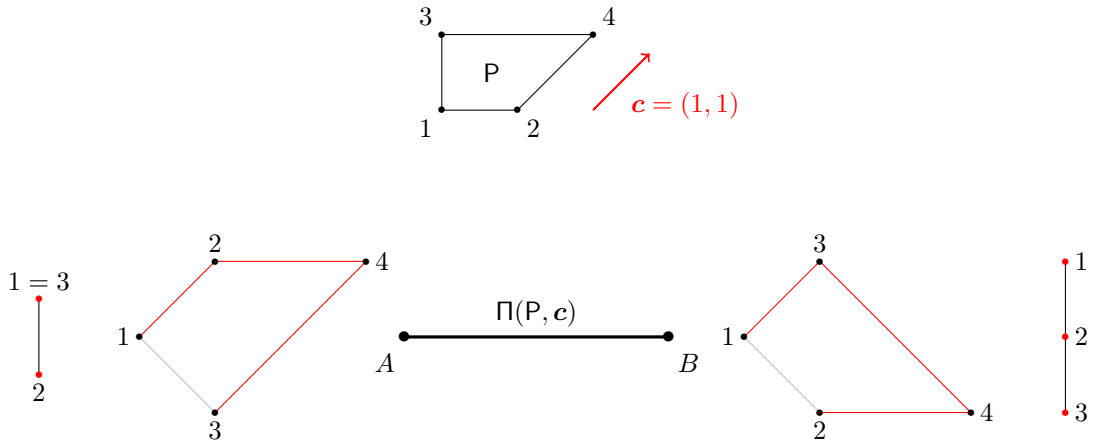

Figure 54: A non-standard square P (Top) and its max-slope pivot polytope (Bottom), labelled by its corresponding (coherent) arborescence A and B, together with their its adapted slope pre-orders $\trianglelefteq_A$ and $\trianglelefteq_B$.

Figure 54(Top). Note that the edges $\boldsymbol{v}_1\boldsymbol{v}_2$ and $\boldsymbol{v}_3\boldsymbol{v}_4$ are parallel, while $\boldsymbol{v}_1\boldsymbol{v}_3$ and $\boldsymbol{v}_2\boldsymbol{v}_4$ are not. As P is 2-dimensional, $\Pi(\mathsf{P}, \boldsymbol{c})$ is 1-dimensional and has two vertices. With the help of a computer, one can determine that the first vertex is associated with the arborescence (for convenience, we identify $\boldsymbol{v}_i$ with $i \in [4]$) A with $A(1) = 2$, $A(2) = 4$ and $A(3) = 4$, giving rise to the pre-order $\leq_A$ defined by $2 <_A 1 =_A 3$, see Figure 54(Bottom Left). The second vertex is associated with the arborescence B with $B(1) = 3$, $B(2) = 4$ and $B(3) = 4$, giving rise to the pre-order $\leq_B$ defined by $1 <_B 3 <_B 2$, see Figure 54(Bottom Right).

Define $\overline{\theta} : \mathbb{R}^2 \to \mathbb{R}^3$ by $\overline{\theta}(\boldsymbol{\omega}) = \big(\tau_{\boldsymbol{\omega}}(\boldsymbol{v}_1\boldsymbol{v}_2),\ \tau_{\boldsymbol{\omega}}(\boldsymbol{v}_2\boldsymbol{v}_4),\ \tau_{\boldsymbol{\omega}}(\boldsymbol{v}_1\boldsymbol{v}_3)\big)$. As we observe that $\boldsymbol{v}_4 - \boldsymbol{v}_2 = (\boldsymbol{v}_3 - \boldsymbol{v}_1) + (\boldsymbol{v}_2 - \boldsymbol{v}_1)$, one has that $\mathrm{Im}(\overline{\theta}) = \big\{(x, y, z) \in \mathbb{R}^3 \ ;\ z = \frac{x+y}{2}\big\}$, so in particular, for all $\boldsymbol{\omega} \in \mathbb{R}^2$, the second coordinate of $\overline{\theta}(\boldsymbol{\omega})$ is always in-between the two others: the only pre-order cones of $\mathcal{B}_3$ that intersects $\mathrm{Im}(\overline{\theta})$ are the ones associated with the pre-order $1 < 2 < 3$ (corresponding the arborescence B) and $3 < 2 < 1$ (corresponding to the arborescence A).

Now, we consider $\mathsf{P}^2 = \mathsf{P} \times \mathsf{P}$. Our computer experiment indicates that $\Pi(\mathsf{P}^2, (\boldsymbol{c}, \boldsymbol{c}))$ has 44 vertices. But there are 46 possible shuffles between $\leq_A$ and $\leq_B$, indeed:

$$\binom{2+2}{2} + \binom{2+3}{2} + \binom{3+2}{3} + \binom{3+3}{3} = 6 + 10 + 10 + 20 = 46$$

In the product P^2, we denote (i, j) for $i, j \in \{1, 2, 3, 4\}$ the vertex $(\boldsymbol{v}_i, \boldsymbol{v}_j)$. The couple $(4, 4)$ represents the optimal vertex $(\boldsymbol{v}_4, \boldsymbol{v}_4)$, and the support of the shuffles of A and B is $\{(i, 4)\}_{1 \leq i \leq 3} \sqcup \{(4, i)\}_{1 \leq i \leq 3}$. Thanks to our computer experiment, we can identify the two shuffles of A and B that do not correspond to vertices of $\Pi(\mathsf{P}^2, \boldsymbol{c})$: they are $(3, 4) < (4, 3) < (4, 2) < (2, 4) < (1, 4) < (4, 1)$ and its symmetric.

3.3.3 Perspectives and open questions

Computational remarks First of all, as for the other sections, I have implemented with Sage the main objects of the present section. To begin with, the computation of max-slope pivot polytopes is done as a sum of sections, see Figure 28. For a d-dimensional polytope P with $n = |V(\mathsf{P})|$, although this method seems efficient (as it does not require running through all possible arborescences and identify the coherent ones), it needs to construct $n - 1$ polytopes of dimension $d - 1$ and compute their Minkowski sum: even the max-slope pivot polytope of the product of two pentagons ($d = 4$

and $n = 25$) takes time. A better implementation of max-slope pivot polytopes would thus be important for more involved computations.

Besides, I have also implemented the computations of the utter and adapted slope pre-orders $\preccurlyeq_{\mathcal{A}}$ and $\trianglelefteq_{\mathcal{A}}$: for a linear program $(\mathsf{P}, \boldsymbol{c})$, my implementation can list the coherent arborescences together with their pre-orders, and determine (the coordinates and normal cone of) the associated vertex in $\Pi(\mathsf{P}, \boldsymbol{c})$.

Assets and limits of the current approach, open questions The above map $\overline{\vartheta}$ is very suitable for the study of product of simplices, but seems not exactly fit for products of other polytopes. Indeed, to replicate the proof of Theorem 3.69, the key point would be to decompose a polytope P as a product $\mathsf{P} = \mathsf{P}_1 \times \cdots \times \mathsf{P}_r$ (where each P_i can not be written as a product), and to have each P_i endowed with a piece-wise linear bijection $\vartheta_i : \mathbb{R}^d \to \mathbb{R}^{n-1}$. But this would mean that $n - 1 = d$, so P_i is a simplex.

Nevertheless, multiple ideas are to be retrieved from the study lead previously.

First, Conjecture 3.64 indicates that numerous links between the realm of max-slope pivot polytopes and generalized permutahedra are to be discovered. Especially, it advocates for a new way of thinking of slope comparisons, as comparisons between coordinates of a linear transformation.

Furthermore, this framework is efficient for quotienting parallelism of edges. For instance, all generalized permutahedra $\mathsf{P} \subset \mathbb{R}^n$ have (at most) $\binom{n}{2}$ classes of edge parallelism[12], indicating that all generalized permutahedra have *morally* the same complexity in terms of combinatorial behavior of the max-slope pivot rule (except for cubes, simplices, etc, which are simpler). It would be interesting to study the impact of other symmetries, for example by studying polytopes with central symmetry such as zonotopes, or classes of polytopes closed by taking faces such as hypersimplices.

Besides, the above Example 3.76 points out that, in general, the max-slope pivot polytope of a product $\mathsf{P} \times \mathsf{Q}$, even though not being the shuffle product of the max-slope pivot polytope of P and Q, is not far from being so. This shuffle product is not in general well-defined (as a polytope), as shuffle product is only defined for generalized permutahedra, but it is defined as a poset: it is the poset consisting of all shuffles between pre-orders of coherent multi-arborescences on P and pre-orders of coherent multi-arborescences on Q. The face lattice of $\Pi(\mathsf{P} \times \mathsf{Q}, (\boldsymbol{c}_1, \boldsymbol{c}_2))$ injects in this poset, and one can wonder how distinct the two can be.

Last but not least, an important open problem is to determine for which linear program $(\mathsf{P}, \boldsymbol{c})$ does the max-slope pivot polytope $\Pi(\mathsf{P}, \boldsymbol{c})$ is (combinatorially or piece-wise linearly isomorphic to) a generalized permutahedron. We have proven it happens for products of simplices. On the opposite, for cyclic polytopes it can not be the case in general, as the 2-dimensional $\Pi(\mathsf{Cyc}_3(\boldsymbol{t}), \boldsymbol{e}_1)$ and $\mathsf{Asso}_d(\boldsymbol{t})$ already have too many vertices, see Section 3.2 and Corollaries 3.37 and 3.49. However, the problem remains open, and finding a polytope P such that its max-slope pivot polytope is a generalized permutahedron would grant a powerful tool to study the behavior of the simplex method on P, while providing a very interesting example.

[12] As generalized permutahedra are (edge-)deformations of Π_n, all their edges are parallel to edges of Π_n, that is to say to $\boldsymbol{e}_j - \boldsymbol{e}_i$ for some $i, j \in [n]$ with $i \neq j$, limiting the number of classes of parallelism to at most $\binom{n}{2}$.

4 Fiber polytopes

Que mes claviers seront usés
D'avoir osé
Toujours vouloir tout essayer
Et recommencer
Là où le monde a commencé
– Michel Berger, *Le Paradis Blanc*

4.1 Preliminaries on fiber polytopes

In the following, we give a very brief introduction to fiber polytopes, secondary polytopes and π-coherent subdivisions arising from a polytope projection $\pi : \mathsf{P} \to \mathsf{Q}$. For an instructive and illustrated presentation of the subject, we advise the reader to look at [Zie98, Chapter 9], a more in depth explanation can be found in [ALRS00, Section 2] and [LRS10, Chapter 9.1], and the original articles [BS92] (for fiber polytopes) and [GKZ90, GKZ91] (for secondary polytopes) give the details of the proofs.

Definition 4.1. A *polytope projection* is a couple (P, π) where $\mathsf{P} \subset \mathbb{R}^d$ is a polytope and $\pi : \mathbb{R}^d \to \mathbb{R}^{d'}$ is a projection. When dimensions are obvious or irrelevant, we usually denote such a projection by $\pi : \mathsf{P} \to \mathsf{Q}$ assuming that $\mathsf{Q} := \pi(\mathsf{P})$.

In order to define fiber polytopes, we need to introduce (coherent) subdivisions. The notion of a complex is widely spread in mathematics, and we have already seen an instance of them, as fans are complexes. Here, we only focus on polyhedral complexes.

Definition 4.2. A *polyhedral complex* $\mathcal{C}$ is a collection of polytopes such that if $\mathsf{P} \in \mathcal{C}$, then all the faces of P are in $\mathcal{C}$, and if $\mathsf{P}, \mathsf{Q} \in \mathcal{C}$, then the intersection $\mathsf{P} \cap \mathsf{Q}$ is a face of both P and Q.

A *subdivision* of a polytope Q is a polyhedral complex $\mathcal{C}$ such that $\bigcup_{\mathsf{P} \in \mathcal{C}} \mathsf{P} = \mathsf{Q}$.

Definition 4.3. For a polytope projection $\pi : \mathsf{P} \to \mathsf{Q}$, a *$\pi$-induced subdivision* of Q is a subdivision $\pi(\mathcal{F})$ of Q where:
(i) $\pi(\mathcal{F}) = \{\pi(F) \ ; \ F \in \mathcal{F}\}$ for $\mathcal{F}$ a family of faces of P.
(ii) for $F, F' \in \mathcal{F}$, if $\pi(F) \subseteq \pi(F')$, then $F = F' \cap \pi^{-1}(\pi(F))$.

The set of π-induced subdivisions is ordered by refinement, forming the *Baues poset*: $\pi(\mathcal{F}_1) \preccurlyeq \pi(\mathcal{F}_2)$ when every polytope of $\pi(\mathcal{F}_2)$ is a union of polytopes of $\pi(\mathcal{F}_1)$. More conveniently, as $\mathcal{F}$ can be recovered from the knowledge of $\pi(\mathcal{F})$ (see [Zie98, Chapter 9]), one has that $\pi(\mathcal{F}_1) \preccurlyeq \pi(\mathcal{F}_2)$ if and only if $\bigcup_{F \in \mathcal{F}_1} F \subseteq \bigcup_{F \in \mathcal{F}_2} F$.

By convention, the empty family will be considered a π-induced subdivision. It is the minimal element of the Baues poset. Note that even if they are called *subdivisions*, the π-induced subdivisions are better thought of not as subdivisions of Q, but as polyhedral complexes that live in P (and whose projection by π is a subdivision of Q). Among π-induced subdivisions, some appear as special (regular) subdivisions, we follow here the reformulation of [Zie98].

Definition 4.4. ([Zie98, definition 9.2]) Let $\pi : \mathsf{P} \to \mathsf{Q}$ be a polytope projection with $\dim \mathsf{P} = d$ and $\dim \mathsf{Q} = d'$. For $\boldsymbol{\omega} \in \mathbb{R}^d$, define $\pi^{\boldsymbol{\omega}} : \mathbb{R}^d \to \mathbb{R}^{d'+1}$ by

$$\pi^{\boldsymbol{\omega}}(\boldsymbol{x}) = \begin{pmatrix} \pi(\boldsymbol{x}) \\ \langle \boldsymbol{\omega}, \boldsymbol{x} \rangle \end{pmatrix}$$

The family of lower faces[13] of $\pi^{\boldsymbol{\omega}}(\mathsf{P})$ projects down to Q by forgetting the last coordinate, giving rise to a π-induced subdivision of Q. The π-induced subdivisions of this form are called *π-coherent subdivisions*, and form a sub-poset of the Baues poset: the *lattice of π-coherent subdivisions*.

We say that $\boldsymbol{\omega}$ *captures* the subdivision.

[13] A face is a lower face when its normal cone contains a vector with a negative last coordinate.

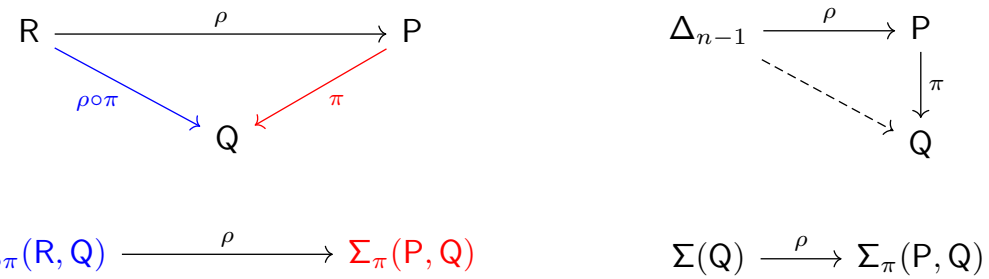

Figure 55: (Left) A projection $\rho : \mathsf{R} \to \mathsf{P}$ induces a projection between the fiber polytopes of R and P for their projections onto Q. Note that as ρ and π are projection $|V(\mathsf{R})| \geq |V(\mathsf{P})| \geq |V(\mathsf{Q})|$. (Right) If $n = |V(\mathsf{Q})|$, then $\Sigma_\pi(\mathsf{P}, \mathsf{Q})$ is a projection of $\Sigma(\mathsf{Q})$ when $|V(\mathsf{P})| = |V(\mathsf{Q})| = n$.

Note that when $\boldsymbol{\omega}$ is generic with respect to P, then the associated π-coherent subdivision is a finest π-coherent subdivision in the sense that it covers the empty subdivision in the Baues poset.

The fiber polytope has several (equivalent) definitions. In the present thesis, even though the formal definition is given here, we will not use the realization of the fiber polytope, but only focus on the characterization of its face lattice given in the following Theorem 4.6.

Definition 4.5. For a polytope projection $\pi : \mathsf{P} \to \mathsf{Q}$, a *section* of P is a continuous map $\gamma : \mathsf{Q} \to \mathsf{P}$ satisfying $\pi \circ \gamma = \mathrm{id}_\mathsf{Q}$. The *fiber polytope* $\Sigma_\pi(\mathsf{P}, \mathsf{Q})$ for the projection $\pi : \mathsf{P} \to \mathsf{Q}$ is defined by:

$$\Sigma_\pi(\mathsf{P}, \mathsf{Q}) = \left\{ \frac{1}{\mathrm{vol}(\mathsf{Q})} \int_\mathsf{Q} \gamma(\boldsymbol{x}) \mathrm{d}\boldsymbol{x} \ ; \ \gamma \text{ section of } \mathsf{P} \right\}$$

Theorem 4.6. ([BS92, Corollary 1.4]). *For a polytope projection $\pi : \mathsf{P} \to \mathsf{Q}$, the fiber polytope $\Sigma_\pi(\mathsf{P}, \mathsf{Q})$ is a polytope and its face lattice is (isomorphic to) the lattice of π-coherent subdivisions of Q.*

Note that $\Sigma_\pi(\mathsf{P}, \mathsf{Q})$ is of dimension $\dim(\mathsf{P}) - \dim(\mathsf{Q})$, though embedded in $\mathbb{R}^{\dim(\mathsf{P})}$.

The construction of fiber polytopes through Definition 4.5 is cumbersome for numerical computations and drawings. Fortunately, the following theorem provides a description of fiber polytopes as a **finite** Minkowski sum.

Theorem 4.7. ([BS92, Theorem 1.5]). *For the polytope projection $\pi : \mathsf{P} \to \mathsf{Q}$, consider the subdivision of Q defined as the common refinement of all $\pi(\mathsf{F})$ for F a face of P. For each maximal cell C of this subdivision, we denote $\boldsymbol{b}_\mathsf{C}$ the barycenter (or centroid) of C. Then:*

$$\Sigma_\pi(\mathsf{P}, \mathsf{Q}) = \frac{1}{\mathrm{vol}(\mathsf{Q})} \sum_{\mathsf{C} \text{ maximal cells}} \mathrm{vol}(\mathsf{C}) \ \pi^{-1}(\boldsymbol{b}_\mathsf{C})$$

Even though an adequate construction of a category of polytopes is still lacking, fiber polytopes have a categorical flavor. Indeed, if one would construct a category **Pol** in which objects are polytopes, and morphisms are (surjective) projections between polytopes, then the map $(\pi : \mathsf{P} \to \mathsf{Q}) \mapsto \Sigma_\pi(\mathsf{P}, \mathsf{Q})$ would resemble a functor from the category of morphisms of **Pol** to **Pol** itself. The commutative diagram of Figure 55(Left) indicates how the (categorical) cone over Q would be sent to **Pol** by this functor. Notably, the following proposition guaranties fiber polytopes are well-behaved with respect to projections:

Proposition 4.8. ([BS92, Lemma 2.3]). *For two polytopes projections $\rho : \mathsf{R} \to \mathsf{P}$ and $\pi : \mathsf{P} \to \mathsf{Q}$, one has:*

$$\Sigma_\pi(\mathsf{P}, \mathsf{Q}) = \rho\big(\Sigma_{\pi\circ\rho}(\mathsf{P}, \mathsf{R})\big)$$

Among all fiber polytopes, some are very special. For instance, when projecting a simplex onto a polytope, the finest π-coherent subdivisions are then in bijection with all regular triangulations of P. This motivates the construction of the following universal object.

Definition 4.9. Consider the standard simplex $\Delta_n = \text{conv}(\boldsymbol{e}_1, ..., \boldsymbol{e}_n) \subset \mathbb{R}^n$ and a polytope P of dimension d with vertices $(\boldsymbol{v}_1, ..., \boldsymbol{v}_n)$. Let $\pi : \mathbb{R}^n \to \mathbb{R}^d$ be the projection defined by $\pi(\boldsymbol{e}_i) = \boldsymbol{v}_i$. Then the dilate of the fiber polytope $\Sigma(\mathsf{P}) := (d+1)\text{vol}(\mathsf{P})\Sigma_\pi(\Delta_n, \mathsf{P})$ is called the *secondary polytope of* P. The vertices of $\Sigma(\mathsf{P})$ are in bijection with the set of regular triangulations of P.

In particular, if P and Q share the same number n of vertices, then there exists a polytope projection $\rho : \Delta_{n-1} \to \mathsf{P}$, see Figure 55(Right). In this setting, the previous proposition ensures:

Corollary 4.10. *If* P *and* Q *share the same number* n *of vertices, then* $\Sigma_\pi(\mathsf{P}, \mathsf{Q})$ *arises as a projection of the secondary polytope of* Q*, i.e. there exists a projection* ρ *such that:*

$$\Sigma_\pi(\mathsf{P}, \mathsf{Q}) = \rho\big(\Sigma(\mathsf{Q})\big)$$

This corollary is only a glint of the more general theory of secondary polytopes. They were defined to study triangulations of any points configuration. We limit ourselves to secondary polytopes of polytopes (*i.e.* points configuration in convex position), but the interested reader is referred to the original papers of Gelfand, Kapranov and Zelevinsky [GKZ90, GKZ91] for a global presentation. In particular, it is important to keep in mind that any fiber polytope is a projection of a secondary polytope of a points configuration, but only fiber polytopes for projections that retain the number of vertices are projections of secondary polytopes of polytopes.

4.2 Monotone path polytopes of the hypersimplices

This section is a work on my own on a question originally asked by Alex Black and a conjecture from Jesús De Loera. An article is in preparation.

After their introduction by Billera and Sturmfels in [BS92], fiber polytopes have received a lot of attention. Especially, the fiber polytope for the projection of a polytope P onto a segment encapsulates the combinatorics of monotone paths on P. For this reason, it is called the *monotone path polytope* of P [Ath99, AER00, BLL20]. The vertices of the monotone path polytopes are in bijection with the monotone paths that can be followed by a shadow vertex rule. As such, it links the world of linear optimization to the world of triangulations.

This, and the fact that monotone path polytopes stand among the easiest fiber polytopes to compute, have motivated numerous studies on the subject. Especially, the monotone path polytope of a simplex is a cube [BS92], the one of a cube is a permutahedron [BS92, Zie98, Example 9.8], the one of a cyclic polytope is a cyclic zonotope [ALRS00], the one of a cross-polytope is the signohedron [BL21], and the one of a S-hypersimplex is a permutahedron [MSS20].

However, the monotone path polytopes of the hypersimplices have not yet been explored. The (n,k)-*hypersimplex* $\Delta(n,k)$ can be equivalently defined as the section of the standard cube by the hyperplane $\{\boldsymbol{x} \in \mathbb{R}^n \ ; \ \sum_i x_i = k\}$, or as the convex hull of the $(0,1)$-vectors with k ones and $n-k$ zeros [Zie98, Example 0.11]. Hypersimplices appear as usual examples of various classes of examples ranging from generalized permutahedra [Pos09] to matroid polytopes of uniform matroids [ABD10], and alcove polytopes [LP07]. Moreover, triangulations of the second hypersimplex $\Delta(n,2)$ can be interpreted as through toric ideals of the complete graph [DLST95].

In the present section, we begin with a general introduction to monotone path polytopes (Section 4.2.1), and then examine the monotone path polytopes of hypersimplices, especially their vertices. We give a necessary criterion for a monotone path on $\Delta(n,k)$ to appear as a vertex of its monotone path polytope (Section 4.2.2). We prove that this criterion is furthermore sufficient in the case of the second hypersimplex (Section 4.2.3) and give the exact count of the vertices of the monotone path polytope of $\Delta(n,2)$ (Section 4.2.4).

4.2.1 Monotone paths polytopes in general

In general, fiber polytopes are, by construction, complicated to compute, even with the help of Theorem 4.7. As a simple case, fiber polytopes for projections onto a point are trivial, as $\Sigma_\pi(\mathsf{P}, \{\boldsymbol{q}\}) = \mathsf{P}$. Hence, among the first cases one would want to investigate are the fiber polytopes associated to projections onto a 1-dimensional polytope, *i.e.* a segment.

Definition 4.11. For a linear program $(\mathsf{P}, \boldsymbol{c})$, the *monotone path polytope* $\mathsf{M}_{\boldsymbol{c}}(\mathsf{P})$ is the fiber polytope for the projection $\pi_{\boldsymbol{c}} : \boldsymbol{x} \mapsto \langle \boldsymbol{x}, \boldsymbol{c} \rangle$. Denoting the image segment $\mathsf{Q} = \pi_{\boldsymbol{c}}(\mathsf{P}) = \{\langle \boldsymbol{x}, \boldsymbol{c} \rangle \ ; \ \boldsymbol{x} \in \mathsf{P}\}$, one has: $\mathsf{M}_{\boldsymbol{c}}(\mathsf{P}) := \Sigma_{\pi_{\boldsymbol{c}}}(\mathsf{P}, \mathsf{Q})$.

Note that $\mathsf{M}_{\boldsymbol{c}}(\mathsf{P})$ has dimension $\dim(\mathsf{P}) - 1$ but is embedded in $\mathbb{R}^{\dim(\mathsf{P})}$.

The monotone path polytope, though arising from a fiber polytope point of view, is deeply linked to linear programming. Indeed, fix a polytope $\mathsf{P} \subset \mathbb{R}^d$, and consider a finest $\pi_{\boldsymbol{c}}$-coherent subdivision $\mathcal{F}$ of P. By Definition 4.4, this amounts to taking a generic $\boldsymbol{\omega} \in \mathbb{R}^d$ and looking at the polygon $\pi^{\boldsymbol{\omega}}_{\boldsymbol{c}}(\mathsf{P}) = \big\{\big(\langle \boldsymbol{x}, \boldsymbol{c} \rangle, \ \langle \boldsymbol{x}, \boldsymbol{\omega} \rangle\big) \ ; \ \boldsymbol{x} \in \mathsf{P}\big\}$. The family of lower faces of $\pi^{\boldsymbol{\omega}}_{\boldsymbol{c}}(\mathsf{P})$ is at the same time the subdivision $\mathcal{F}$ at stake, and the monotone path followed by the simplex method for the shadow vertex rule with secondary direction $-\boldsymbol{\omega}$. Accordingly, this process gives a clever way to encompass in a polytope the combinatorial behavior of the shadow vertex rule. Note that, whereas pivot rule polytopes (see Section 3.1) cover the behavior the shadow vertex rule[14] has on each vertex of P, the monotone path polytopes only describe the possible coherent *leading paths* on P, that is the coherent paths from the worst vertex to the best, *i.e.* from the vertex $\boldsymbol{v}_{\min} \in V(\mathsf{P})$ minimizing $\langle \boldsymbol{v}, \boldsymbol{c} \rangle$ for $\boldsymbol{v} \in V(P)$ to the vertex $\boldsymbol{v}_{\text{opt}} \in V(\mathsf{P})$ maximizing it. Consequently, the face lattice of the monotone path polytope is the lattice of coherent cellular strings on P.

[14] Technically, max-slope pivot polytopes encompass max-slope pivot rules, a generalization of shadow vertex rules, see Sections 1.3 and 3.1.

Definition 4.12. For a linear program $(\mathsf{P}, \boldsymbol{c})$, a *cellular string* is a sequence $\sigma = (\mathsf{F}_1, \dots, \mathsf{F}_k)$ of faces of P such that $\min(\mathsf{F}_1) = \boldsymbol{v}_{\min}$, $\max(\mathsf{F}_k) = \boldsymbol{v}_{\text{opt}}$, and for all $i \in [k-1]$, $\max(\mathsf{F}_k) = \min(\mathsf{F}_{k+1})$, where minima and maxima are taken with respect to the scalar product against $\boldsymbol{c}$. As $\pi_{\boldsymbol{c}}$-induced subdivisions, cellular strings are ordered by containment of their union. A cellular string σ is *coherent* if there exists $\boldsymbol{\omega} \in \mathbb{R}^d$ such that $\mathsf{F} \in \sigma$ if F is the pre-image by $\pi_{\boldsymbol{c}}$ of a lower face of $\pi_{\boldsymbol{c}}(\mathsf{P})$.

To make the notations consistent and ease the drawings, we will keep for this section the convention of linear programming, saying a cellular string σ is captured by $\boldsymbol{\omega}$ when $\pi^{\boldsymbol{\omega}}_{\boldsymbol{c}}(\sigma)$ is the family of **upper faces** of $\pi^{\boldsymbol{\omega}}_{\boldsymbol{c}}(\mathsf{P})$ (instead of lower faces).

We now present two ways to visualize the monotone path polytope. First of all, Definition 4.4 invites us to focus on the space of all $\boldsymbol{\omega}$ and partition it depending on the coherent cellular strings they yield. Precisely, to a cellular string σ we associate $\mathcal{N}(\sigma) = \{\boldsymbol{\omega} \ ; \ \boldsymbol{\omega} \text{ captures } \sigma\}$. Then $\mathcal{N}(\sigma)$ is a polyhedral cone by linearity of $\pi^{\boldsymbol{\omega}}_{\boldsymbol{c}}$ in $\boldsymbol{\omega}$, and the family $\mathcal{N} = \big(\mathcal{N}(\sigma)\big)_\sigma$ is a fan. This fan is exactly the normal fan of $\mathsf{M}_{\boldsymbol{c}}(\mathsf{P})$. Hence, one can run through all possible $\boldsymbol{\omega} \in \mathbb{R}^d$, orthogonal to $\boldsymbol{c}$ (as all $\boldsymbol{\omega} + \lambda\boldsymbol{c}$ capture the same cellular string for any $\lambda \in \mathbb{R}$), to draw the normal fan of $\mathsf{M}_{\boldsymbol{c}}(\mathsf{P})$, see Figure 56.

This construction gives two interesting properties. On the one hand, it is clear that the normal fan of $\Pi(\mathsf{P}, \boldsymbol{c})$ coarsens the normal fan of $\mathsf{M}_{\boldsymbol{c}}(\mathsf{P})$: the cone associated to a coherent cellular string σ is the union of the cones associated to all coherent multi-arborescences whose leading cellular string is σ, see Figure 57. Consequently:

Proposition 4.13. ([BDLLS22, Proposition 6.2]). *The monotone path polytope $\mathsf{M}_{\boldsymbol{c}}(\mathsf{P})$ is a deformation of the pivot rule polytope $\Pi(\mathsf{P}, \boldsymbol{c})$.*

On the other hand, we have said that for a fixed $\boldsymbol{\omega}$, all $\boldsymbol{\omega}+\lambda\boldsymbol{c}$ for $\lambda \in \mathbb{R}$ capture the same cellular string. Consequently, one can obtain the normal fan of $\mathsf{M}_{\boldsymbol{c}}(\mathsf{P})$ by *projecting* the normal fan of P: to each normal cone $\mathsf{C} \in \mathcal{N}_{\mathsf{P}}$, associate its projection along $\boldsymbol{c}$, namely $\mathsf{C}_\perp := \{\boldsymbol{x} - \frac{\langle \boldsymbol{x}, \boldsymbol{c}\rangle}{\langle \boldsymbol{c}, \boldsymbol{c}\rangle}\boldsymbol{c} \ ; \ \boldsymbol{x} \in \mathsf{C}\}$. Then the common refinement of all $\big(\mathsf{C}_\perp \ ; \ \mathsf{C} \in \mathcal{N}_{\mathsf{P}}\big)$ is the normal fan[15] of $\mathsf{M}_{\boldsymbol{c}}(\mathsf{P})$.

A second way to visualize monotone path polytopes is to use Theorem 4.7. We begin by sorting the vertices of P according to the scalar product against $\boldsymbol{c}$: $V(\mathsf{P}) = \{\boldsymbol{v}_1, \dots, \boldsymbol{v}_n\}$ with $\langle \boldsymbol{v}_i, \boldsymbol{c}\rangle < \langle \boldsymbol{v}_{i+1}, \boldsymbol{c}\rangle$. The maximal cells of the segment $\mathsf{Q} = \pi_{\boldsymbol{c}}(\mathsf{P})$ are then the sub-segments $\mathsf{C}_i := [q_i, q_{i+1}]$ with $q_i = \langle \boldsymbol{v}_i, \boldsymbol{c}\rangle$, and the barycenter (*i.e.* middle) of C_i is trivially $b_i = \frac{q_i + q_{i+1}}{2}$. The monotone path polytope $\mathsf{M}_{\boldsymbol{c}}(\mathsf{P})$ is normally equivalent to the Minkowski sum of sections $\sum_{i=1}^n \pi_{\boldsymbol{c}}^{-1}(b_i)$.

Though exact, this construction is a bit unhandy. Yet, as we will prove in Theorem 4.14, one can forget about centers, as $\mathsf{M}_{\boldsymbol{c}}(\mathsf{P})$ is normally equivalent to $\sum_{i=2}^{n-1} \pi_{\boldsymbol{c}}^{-1}(q_i)$. This gives beautiful pictures, see Figure 58 for the case of the simplex.

Note that, between the two figures, a slight change of perspective happened: to see that the fan constructed in Figures 56 and 57(Left) is the normal fan of the $\mathsf{M}_{\boldsymbol{c}}(\mathsf{P})$ appearing in Figure 58(Right), rotate the latter clockwise slightly so that its bottom left corner fits in the cone with a right angle.

Theorem 4.14. *For a linear program $(\mathsf{P}, \boldsymbol{c})$, denote $V(\mathsf{P}) = \{\boldsymbol{v}_1, \dots, \boldsymbol{v}_n\}$ and $q_i = \langle \boldsymbol{v}_i, \boldsymbol{c}\rangle$ with $q_1 < \dots < q_n$. The monotone path polytope $\mathsf{M}_{\boldsymbol{c}}(\mathsf{P})$ is normally equivalent to the Minkowski sum of sections $\sum_{i=2}^{n-1}\{\boldsymbol{x} \in \mathsf{P} \ ; \ \langle \boldsymbol{x}, \boldsymbol{c}\rangle = q_i\}$.*

Remark 4.15. This theorem is not a new result, but is known in the folklore. We give here a self-contained proof, with the tools developed so far on sections and Minkowski sums, but the reader at ease with the subject shall rather think of it as an exercise on Cayley polytopes.

Proof of Theorem 4.14. For $i \in [1, n]$, we denote $\gamma_i = \{\boldsymbol{x} \in \mathsf{P} \ ; \ \langle \boldsymbol{x}, \boldsymbol{c}\rangle = q_i\}$ the section over q_i and $\zeta_i(\lambda) = \{\boldsymbol{x} \in \mathsf{P} \ ; \ \langle \boldsymbol{x}, \boldsymbol{c}\rangle = \lambda q_i + (1-\lambda)q_{i+1})\}$ for $\lambda \in]0, 1[$.

First, note that the sections γ_1 and γ_n are points, so adding them to $\sum_{i=2}^{n-1} \Gamma_i$ amounts to translating it (without changing its normal equivalence class). For this reason, we will prove by

[15] This construction embeds the fan $\mathcal{N}_{\mathsf{M}_{\boldsymbol{c}}(\mathsf{P})}$ directly into the hyperplane $\boldsymbol{c}^\perp$, instead of embedding it in $\mathbb{R}^{\dim(\mathsf{P})}$.

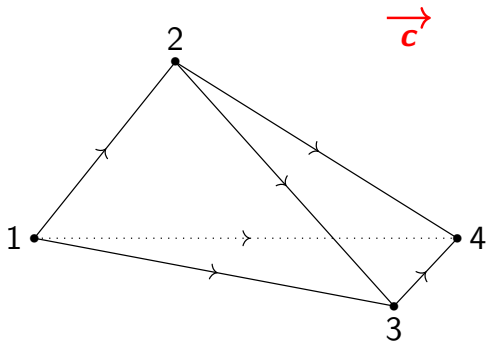

Figure 56: Animated construction of the normal fan of the monotone path polytope of the 3-dimensional simplex. For each $\boldsymbol{\omega} \in \mathbb{R}^3$ orthogonal to $\boldsymbol{c}$, we project Δ_3 onto the plane $(\boldsymbol{c}, \boldsymbol{\omega})$ (Left), and record the corresponding coherent monotone path (Right). note that, contrarily to Figure 26, we only score the upper path of each projection of the tetrahedron, not the full arborescence. *(Animated figures obviously do not display on paper, and some PDF readers do not support the format: it is advised to use Adobe Acrobat Reader. If no solution is suitable, the animation can be found on my website or asked by email.)*

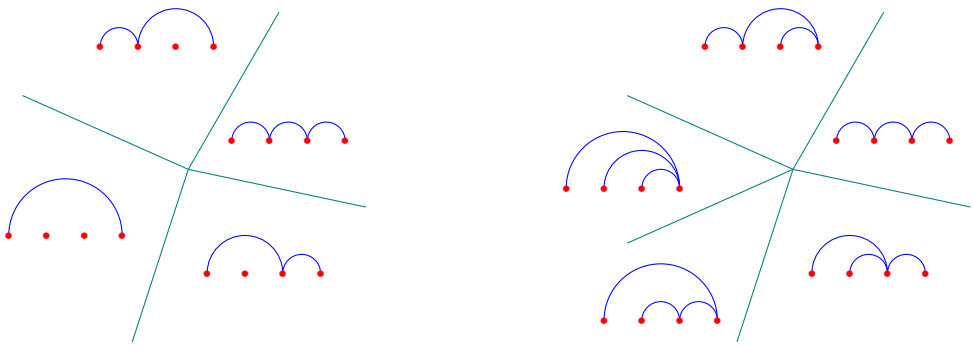

Fan of $\mathsf{M}_{\boldsymbol{c}}(\Delta_3)$ Fan of $\Pi(\Delta_3, \boldsymbol{c})$

Figure 57: The normal fan of $\mathsf{M}_{\boldsymbol{c}}(\mathsf{P})$ coarsens the one of $\Pi(\mathsf{P}, \boldsymbol{c})$. Here is drawn the example for the tetrahedron $\mathsf{P} = \Delta_3$.

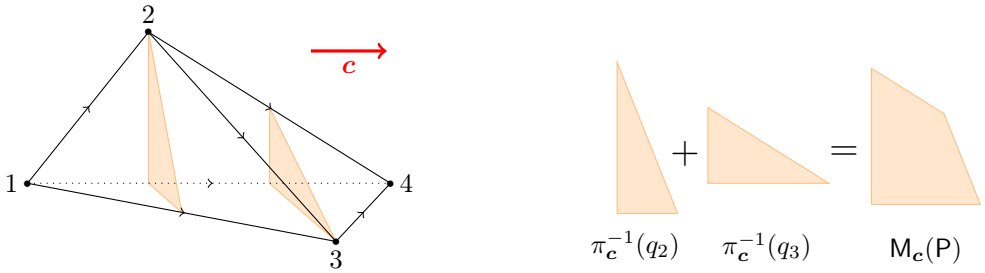

Figure 58: The construction of $\mathsf{M}_{\boldsymbol{c}}(\mathsf{P})$ as a sum of sections for the tetrahedron $\mathsf{P} = \Delta_3$. Each section is orthogonal to $\boldsymbol{c}$ and contains a vertex (except for $\boldsymbol{v}_{\min}$ and $\boldsymbol{v}_{\text{opt}}$).

induction that $\Gamma_{k+1} = \sum_{i=1}^{k+1} \gamma_i$ is normally equivalent to $Z_k = \sum_{i=1}^{k} \zeta_i(\frac{1}{2})$. As Z_{n-1} is normally equivalent to $M_{\boldsymbol{c}}(P)$ by Theorem 4.7, this will prove the theorem.

All $\zeta_i(\lambda)$ are normally equivalent for $\lambda \in]0,1[$, and γ_{i+1} is a deformation of $\zeta_i(\lambda)$. Thus Γ_n is a deformation of Z_n. Furthermore, suppose a face f of $\zeta_i(\lambda)$ does not appear in the deformation γ_{i+1} and let F be the corresponding intersected face in P. Then $\boldsymbol{v}_{i+1}$ is the last vertex of F, and there exists a vertex $\boldsymbol{v}_j$ with $j \leq i$ in F: then in γ_j, the face f appears.

This fact has two consequences. On one side, Γ_2 is normally equivalent to Z_1 as the only possible face with last vertex $\boldsymbol{v}_2$ is the edge $[\boldsymbol{v}_1, \boldsymbol{v}_2]$ which section is a point. On the other side, suppose Γ_{k+1} is normally equivalent to Z_k, and consider a face in $Z_k + \zeta_{k+1}$. This face either appears in one of the γ_i for $i \leq k+1$, or in γ_{k+2}. As the normal fan of a Minkowski sum is the common refinement of the normal fans of the summands, the polytopes Γ_{k+2} and Z_{k+1} are normally equivalent. □

The rest of this section is devoted to the monotone path polytopes of hypersimplices, and especially hypersimplices for $k = 2$. Before presenting new results on this subject, we shortly recall two former results from Billera and Sturmfels [BS92, end of Section 5].

Theorem 4.16 ([BS92]). *For any simplex Δ on $n+1$ vertices, and any generic direction $\boldsymbol{c}$, the monotone path polytope $M_{\boldsymbol{c}}(\Delta)$ is (isomorphic to) a cube of dimension $n-1$.*

Theorem 4.17 ([BS92]). *For the standard cube $\square_d = [0,1]^n$ of dimension n, and the direction $\boldsymbol{c} = (1, \dots, 1)$, the monotone path polytope $M_{\boldsymbol{c}}(\square_d)$ is (a dilation of) the permutahedron Π_n of dimension $n-1$.*

These two results motivate the study of the monotone path polytopes of hypersimplices. Indeed, hypersimplices are a generalization of simplices, and arise as sections of the standard cube.

Definition 4.18. For $n \geq 2$, $k \in [n]$, the *(n,k)-hypersimplex* is $\Delta(n,k) = \left\{\boldsymbol{x} \in [0,1]^n \ ; \ \sum_i x_i = k\right\}$. It is the section of the standard cube $\square_d = [0,1]^n$ by the hyperplane $\{\boldsymbol{x} \in \mathbb{R}^n \ ; \ \langle \boldsymbol{x}, (1, \dots, 1)\rangle = k\}$.

The vertices of $\Delta(n,k)$ are exactly its $(0,1)$-coordinate elements: the $(0,1)$-vectors with k ones and $n-k$ zeros. We denote the *support* of a vertex $\boldsymbol{v} \in V(\Delta(n,k))$ by $s(\boldsymbol{v}) := \{i \ ; \ v_i = 1\}$. Two vertices $\boldsymbol{u}, \boldsymbol{v} \in V(\Delta(n,k))$ share an edge when $|s(\boldsymbol{u}) \cap s(\boldsymbol{v})| = k-1$, *i.e.* to obtain $\boldsymbol{v}$ from $\boldsymbol{u}$, flip a zero to a one and a one to a zero.

Note that the hypersimplices $\Delta(n,1)$ and $\Delta(n,n-1)$ are simplices: in this sense, hypersimplices are a generalization of simplices.

We consider the linear problem $(\Delta(n,k), \boldsymbol{c})$ where $\boldsymbol{c} \in \mathbb{R}^n$ is generic with respect to $\Delta(n,k)$. The vector $\boldsymbol{c} \in \mathbb{R}^n$ will be fixed for the rest of this analysis of monotone path polytopes of the hypersimplices. See Figure 59(Left) for an example. We denote $M(n,k) := M_{\boldsymbol{c}}(\Delta(n,k))$ to ease notations. Such a $\boldsymbol{c}$ is generic for the hypersimplex when $c_i \neq c_j$ for all $i \neq j$, as each edge has direction $\boldsymbol{e}_i - \boldsymbol{e}_j$. Without lost of generality, as the hypersimplex is invariant under reordering coordinates, we suppose $c_1 < c_2 < \cdots < c_n$. Note however that there can exist $\boldsymbol{v}, \boldsymbol{w} \in V(\Delta(n,k))$ with $\langle \boldsymbol{v}, \boldsymbol{c}\rangle = \langle \boldsymbol{w}, \boldsymbol{c}\rangle$ (when $\boldsymbol{v}$ and $\boldsymbol{w}$ are not adjacent vertices). When drawing, we will take $\boldsymbol{c} = (1, 2, \dots, n)$.

We denote $\boldsymbol{v}_{\min} = (1, \dots, 1, 0, \dots, 0) \in V(\Delta(n,k))$ the vertex of $\Delta(n,k)$ minimizing $\langle \boldsymbol{v}, \boldsymbol{c}\rangle$ for $\boldsymbol{v} \in V(\Delta(n,k))$, and $\boldsymbol{v}_{\max} = (0, \dots, 0, 1, \dots, 1) \in V(\Delta(n,k))$ the vertex of $\Delta(n,k)$ maximizing $\langle \boldsymbol{v}, \boldsymbol{c}\rangle$ for $\boldsymbol{v} \in V(\Delta(n,k))$. We now interpret the conditions for being a coherent monotone path on a polytope for the case of the hypersimplex $\Delta(n,k)$.

Definition 4.19. A *monotone path of vertices* $P = (\boldsymbol{v}_1, ..., \boldsymbol{v}_r)$ on $\Delta(n,k)$ is an ordered list of vertices of $\Delta(n,k)$ such that $\boldsymbol{v}_1 = \boldsymbol{v}_{\min}$, $\boldsymbol{v}_r = \boldsymbol{v}_{\max}$ and for all $i \in [r-1]$, $(\boldsymbol{v}_i, \boldsymbol{v}_{i+1})$ is an *improving edge* of $\Delta(n,k)$ for $\boldsymbol{c}$, *i.e.* an edge of $\Delta(n,k)$ with $\langle \boldsymbol{v}_i, \boldsymbol{c}\rangle < \langle \boldsymbol{v}_{i+1}, \boldsymbol{c}\rangle$. The *length* of P is r.

For all $i \in [1, r-1]$, the vertices $\boldsymbol{v}_i$ and $\boldsymbol{v}_{i+1}$ form an edge of $\Delta(n,k)$. Thus, instead of considering the path P as a list of vertices, we emphasize what changes and what remains between $\boldsymbol{v}_i$ and $\boldsymbol{v}_{i+1}$ by storing the enhanced steps of P. The *i-th enhanced step* of P is denoted $x \xrightarrow{Z} y$ with:

- Z the common support, *i.e.* $Z = \mathrm{s}(\boldsymbol{v}_i) \cap \mathrm{s}(\boldsymbol{v}_{i+1})$.
- x the only index in the support of $\boldsymbol{v}_i$ that is not in the support of $\boldsymbol{v}_{i+1}$, *i.e.* $\{x\} = \mathrm{s}(\boldsymbol{v}_i) \smallsetminus \mathrm{s}(\boldsymbol{v}_{i+1})$.
- y the only index in the support of $\boldsymbol{v}_{i+1}$ that is not in the support of $\boldsymbol{v}_i$, *i.e.* $\{y\} = \mathrm{s}(\boldsymbol{v}_{i+1}) \smallsetminus \mathrm{s}(\boldsymbol{v}_i)$.

The list of enhanced steps of P is denoted $\mathcal{S}(P)$. The application $P \mapsto \mathcal{S}(P)$ is obviously injective. When $a \xrightarrow{C} b$ is the i-th enhanced step, and $x \xrightarrow{Z} y$ the j-th one, with $i < j$, we denote $a \xrightarrow{C} b \prec x \xrightarrow{Z} y$ and say that $a \xrightarrow{C} b$ *precedes* $x \xrightarrow{Z} y$.

A monotone path is said *coherent* when it corresponds to a vertex of $\mathsf{M}(n,k)$.

Proposition 4.20. *For $\boldsymbol{\omega} \in \mathbb{R}^n$, let $\pi^{\boldsymbol{\omega}} : \mathbb{R}^n \to \mathbb{R}^2$ be the projection $\pi^{\boldsymbol{\omega}}(\boldsymbol{x}) = \big(\langle \boldsymbol{x}, \boldsymbol{c}\rangle\,,\ \langle \boldsymbol{x}, \boldsymbol{\omega}\rangle\big)$. In particular, for a vertex $\boldsymbol{v} \in V(\Delta(n,k))$, then $\pi^{\boldsymbol{\omega}}(\boldsymbol{v}) = \big(\sum_{i\in s(\boldsymbol{v})} c_i,\ \sum_{i\in s(\boldsymbol{v})} \omega_i\big)$.*

A monotone path of vertices $P = (\boldsymbol{v}_1, \dots \boldsymbol{v}_r)$ is coherent if and only if there exists $\boldsymbol{\omega} \in \mathbb{R}^n$ such that for all $i \in [1, r-1]$:

$$\forall J \in \binom{[n]}{k}, \qquad \sum_{j\in J} c_j > \sum_{p\in s(\boldsymbol{v}_i)} c_p \implies \tau_{\boldsymbol{\omega}}\big(s(\boldsymbol{v}_i), J\big) < \tau_{\boldsymbol{\omega}}\big(s(\boldsymbol{v}_i), s(\boldsymbol{v}_{i+1})\big)$$

where $\tau_{\boldsymbol{\omega}}(I,J) = \frac{\sum_{j\in J}\omega_j - \sum_{i\in I}\omega_i}{\sum_{j\in J} c_j - \sum_{i\in I} c_i}$ is the slope between the point $\big(\sum_{i\in I} c_i,\ \sum_{i\in I}\omega_i\big)$ and the point $\big(\sum_{i\in J} c_j,\ \sum_{j\in J}\omega_j\big)$, see Figure 61(Top). We say that such $\boldsymbol{\omega}$ captures P.

Proof. By Definition 4.4, a monotone path of vertices P is coherent if and only if there exists $\boldsymbol{\omega} \in \mathbb{R}^n$ such that the upper path of the polygon $\pi^{\boldsymbol{\omega}}(\Delta(n,k))$ is precisely $\pi^{\boldsymbol{\omega}}(P) := \big(\pi^{\boldsymbol{\omega}}(\boldsymbol{v})\big)_{\boldsymbol{v}\in P}$ (remember we take the upper faces instead of the lower faces by convention in the section).

If $\boldsymbol{v} \in V(\Delta(n,k))$ is in the upper path of $\pi^{\boldsymbol{\omega}}(\Delta(n,k))$, then the next vertex in the upper path is the improving neighbor $\boldsymbol{v}'$ of $\boldsymbol{v}$ that maximizes the slope $\frac{\langle \boldsymbol{v}'-\boldsymbol{v}, \boldsymbol{\omega}\rangle}{\langle \boldsymbol{v}'-\boldsymbol{v}, \boldsymbol{c}\rangle}$. As $\boldsymbol{c}$ is generic for $\Delta(n,k)$, the vertex $\boldsymbol{u} \in V(\Delta(n,k))$ maximizing this slope is necessarily an improving neighbor of $\boldsymbol{v}$, as the pre-image of edge $\big[\pi^{\boldsymbol{\omega}}(\boldsymbol{v}), \pi^{\boldsymbol{\omega}}(\boldsymbol{u})\big]$ in the polygon $\pi^{\boldsymbol{\omega}}(\Delta(n,k))$ is an (improving) edge in $\Delta(n,k)$. Consequently, the condition stated in the proposition is both necessary and sufficient. □

Example 4.21. The hypersimplex $\Delta(3,2)$ is a triangle, that is to say a simplex of dimension 2. By Billera–Sturmfels' Theorem 4.16, for any $\boldsymbol{c} \in \mathbb{R}^3$, its monotone path polytope is a cube of dimension 1: it has 2 vertices, one corresponding to the path of length 3 and the other to the path of length 2.

Example 4.22. On the hypersimplex $\Delta(4,2)$, for $\boldsymbol{c} = (1,2,3,4)$ there are 8 coherent monotone paths, and 2 non-coherent monotone paths. The 8 coherent monotone paths correspond to the vertices of the octagon $\mathsf{M}(4,2)$ depicted on Figure 59(Right). There are 4 coherent monotone paths of length 3, and 4 coherent monotone paths of length 4. On the other side, the 2 non-coherent monotone paths are of length 5: $(1100, 1010, \mathbf{0110}, 0101, 0011)$ and $(1100, 1010, \mathbf{1001}, 0101, 0011)$, in bold are the vertices that differ between the two paths.

With a quick jotting, one can prove that for all $\boldsymbol{c} \in \mathbb{R}^4$, the same holds: for all $\boldsymbol{c} \in \mathbb{R}^4$, the coherent monotone paths are exactly the same. This can also be retrieved from [BL21, Theorem 3.2] as $\Delta(4,2)$ is the cross-polytope of dimension 3.

Example 4.23. To be able to draw the monotone path polytope $\mathsf{M}(n,k)$ of the hypersimplex $\Delta(n,k)$, we need that $\dim \Delta(n,k) \le 4$, so that $\dim \mathsf{M}(n,k) \le 3$. This implies $n \le 5$. Moreover, remember that $\Delta(n,k)$ is linearly isomorphic to $\Delta(n, n-k)$. For $n = 3$, Example 4.21 deals with $k = 2$ (and thus $k = 1$ by symmetry). For $n = 4$, Example 4.22 deals with $k = 2$, while $\Delta(4,k)$ with $k = 1$ and $k = 3$ are simplices and their monotone path polytopes are squares. For $n = 5$, $\Delta(5,k)$ with $k = 1$ and $k = 4$ are simplices and their monotone path polytopes are cubes, while $k = 2$ and $k = 3$ are equivalent and their monotone path polytope is depicted in Figure 60: it has 33 vertices, 52 edges, and 21 faces (5 octagons and 16 squares).

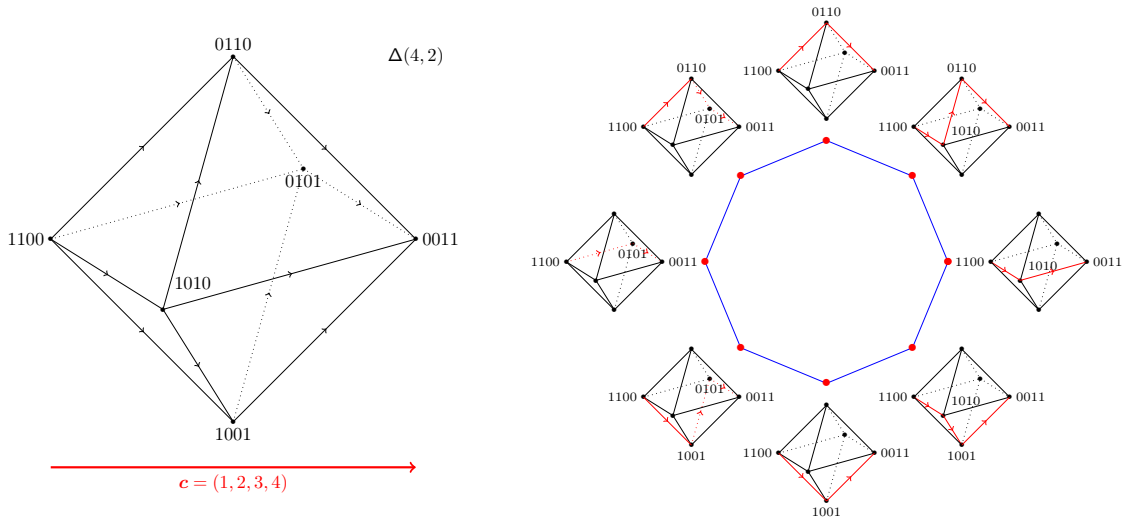

Figure 59: (Left) The $(4,2)$-hypersimplex lives in the hyperplane $\{\boldsymbol{x}\ ;\ \sum_{i=1}^{4} x_i = 2\}$ inside $\mathbb{R}^4$. (Right) The monotone path polytope $\mathsf{M}(4,2)$ is an octagon, each vertex of which is labelled by the corresponding monotone path (drawn on $\Delta(4,2)$).

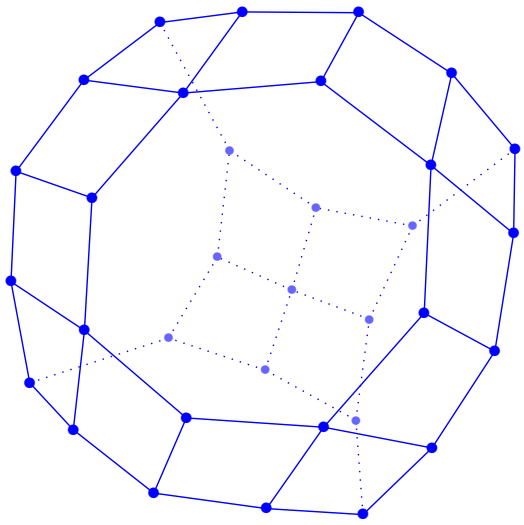

Figure 60: The monotone path polytope $\mathsf{M}(5,2)$ of the hypersimplex $\Delta(5,2)$. This hypersimplex is linearly equivalent to $\Delta(5,3)$. As $\Delta(5,2)$ has 5 facets linearly equivalent to $\Delta(4,2)$, its monotone path polytope $\mathsf{M}(5,2)$ has 5 facets which are isomorphic to $\mathsf{M}(4,2)$ *i.e.* octagons.

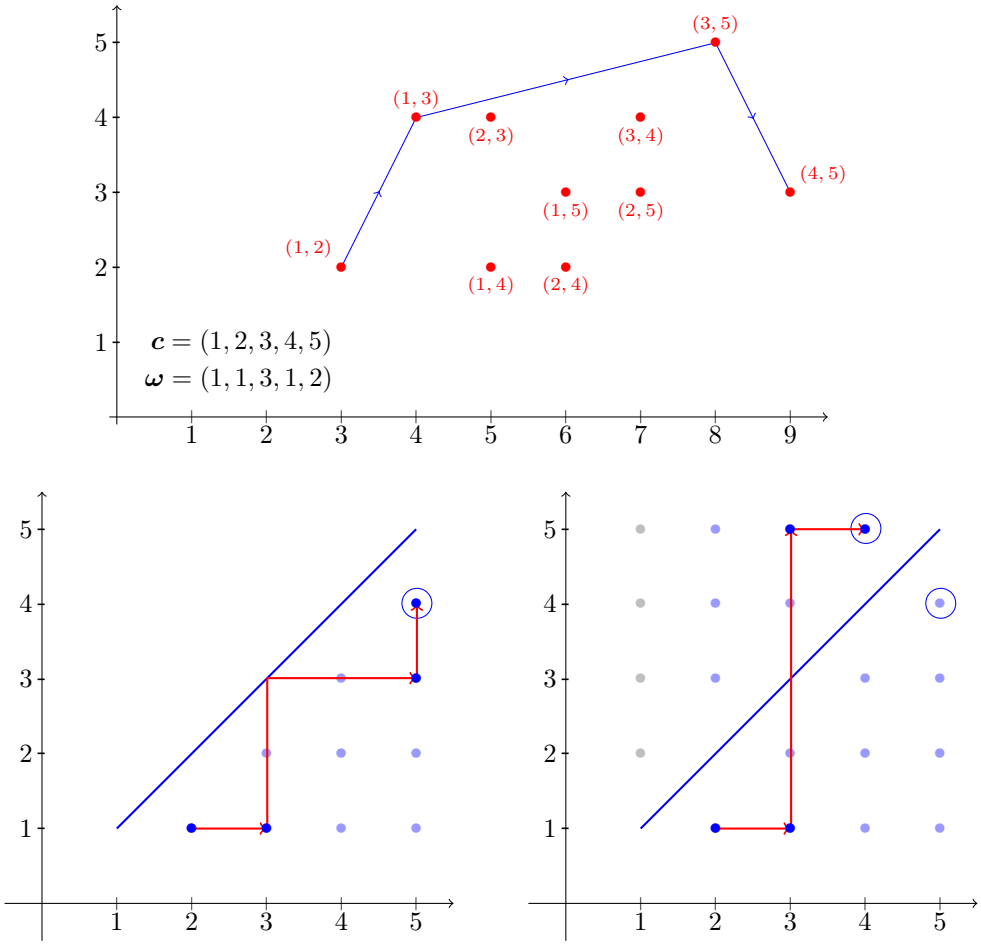

Figure 61: (Top) For the given $\boldsymbol{c}$ and $\boldsymbol{\omega}$, the hypersimplex $\Delta(5,2)$ is projected the 10 points drawn, where each vertex of $\Delta(5,2)$ is indicated by its support. The coherent path P captured is drawn in blue. (Bottom) P corresponds to the diagonal-avoiding path depicted on the right, while associating P to lattice points (x,y) with $x < y$ give the bottom left figure.

4.2.2 A necessary criterion for coherent paths on $\Delta(n,k)$

Even if Proposition 4.20 gives an efficient criterion for determining which monotone path a given $\boldsymbol{\omega}$ does capture, the question we want to answer is the converse one: how to characterize the coherent paths on the hypersimplex? In this section, we present a necessary criterion for a monotone path to be coherent, and in the next one, we prove this criterion is sufficient in the case of the $(n,2)$-hypersimplices (but not sufficient in general).

Theorem 4.24. *If path P is coherent, then for all couples of enhanced steps $i \xrightarrow{A} j \prec x \xrightarrow{Z} y$ with $x < j$, one has $j \in Z$ or $x \in A$.*

Before proving this criterion, we will introduce a simple but powerful lemma. In essence, this lemma states that there exist only two kinds of triangles in the plane: upwards pointing ones $\triangle$ and downwards pointing ones ∇. This lemma is equivalent to Lemma 3.5, but we give it here again to make the section self contained.

Lemma 4.25. *For three points in the plane (x_1,y_1), (x_2,y_2) and (x_3,y_3) with $x_1 < x_2 < x_3$, denote the slopes $\tau(1,2) = \frac{y_2-y_1}{x_2-x_1}$, $\tau(2,3) = \frac{y_3-y_2}{x_3-x_2}$ and $\tau(1,3) = \frac{y_3-y_1}{x_3-x_1}$. Then $\tau(1,3)$ is a convex combination of the slopes $\tau(1,2)$ and $\tau(2,3)$. In particular, if $\tau(1,2) < \tau(1,3)$, then $\tau(1,3) < \tau(2,3)$ (and conversely if $\tau(1,2) > \tau(1,3)$, then $\tau(1,3) > \tau(2,3)$).*

Proof. One has the convex combination: $\tau(1,3) = \frac{x_2-x_1}{x_3-x_1}\tau(1,2) + \frac{x_3-x_2}{x_3-x_1}\tau(2,3)$ □

Proof of Theorem 4.24. Suppose $i \xrightarrow{A} j \prec x \xrightarrow{Z} y \in \mathcal{S}(P)$ with $x < j$ (so $c_x < c_j$), $j \notin Z$ and $x \notin A$. Fix $\boldsymbol{\omega} \in \mathbb{R}^n$ that captures P. Then consider $\boldsymbol{v}_1$, $\boldsymbol{v}_2$ with $\mathrm{s}(\boldsymbol{v}_1) = A \cup \{i\}$, $\mathrm{s}(\boldsymbol{v}_2) = A \cup \{j\}$, and $\boldsymbol{v}_3$, $\boldsymbol{v}_4$ with $\mathrm{s}(\boldsymbol{v}_3) = Z \cup \{x\}$, $\mathrm{s}(\boldsymbol{v}_4) = Z \cup \{y\}$, see Figure 62. These are 4 vertices of $\Delta(n,k)$ in the path P. Abusing notation, we write $\tau_{\boldsymbol{\omega}}(\boldsymbol{u},\boldsymbol{v})$ instead of $\tau_{\boldsymbol{\omega}}\big(\mathrm{s}(\boldsymbol{u}),\mathrm{s}(\boldsymbol{v})\big)$ when the context is clear.

As $x \notin A$, there exists $\boldsymbol{u}_1 \in V(\Delta(n,k))$ with $\mathrm{s}(\boldsymbol{u}_1) = A \cup \{x\}$, thus $\boldsymbol{v}_2$ is an improving neighbor of $\boldsymbol{u}_1$. As $j \notin Z$, there exists $\boldsymbol{u}_2 \in V(\Delta(n,k))$ with $\mathrm{s}(\boldsymbol{u}_2) = Z \cup \{j\}$, thus $\boldsymbol{u}_2$ is an improving neighbor of $\boldsymbol{v}_3$. First observe that, $\tau_{\boldsymbol{\omega}}\big(\boldsymbol{v}_1,\boldsymbol{u}_1\big) < \tau_{\boldsymbol{\omega}}\big(\boldsymbol{v}_1,\boldsymbol{v}_2\big)$ by Proposition 4.20, thus $\tau_{\boldsymbol{\omega}}\big(\boldsymbol{u}_1,\boldsymbol{v}_2\big) > \tau_{\boldsymbol{\omega}}\big(\boldsymbol{v}_1,\boldsymbol{v}_2\big)$ by Lemma 4.25 applied in the triangle $\pi_{\boldsymbol{\omega}}(\boldsymbol{v}_1)$, $\pi_{\boldsymbol{\omega}}(\boldsymbol{v}_2)$, $\pi_{\boldsymbol{\omega}}(\boldsymbol{u}_1)$. Moreover, $\tau_{\boldsymbol{\omega}}\big(\boldsymbol{v}_3,\boldsymbol{u}_2\big) < \tau_{\boldsymbol{\omega}}\big(\boldsymbol{v}_3,\boldsymbol{v}_4\big)$ by Proposition 4.20. As $\pi_{\boldsymbol{\omega}}(P)$ is convex: $\tau_{\boldsymbol{\omega}}\big(\boldsymbol{v}_1,\boldsymbol{v}_2\big) > \tau_{\boldsymbol{\omega}}\big(\boldsymbol{v}_3,\boldsymbol{v}_4\big)$ because the second step comes later in the path. But then: $\tau_{\boldsymbol{\omega}}\big(\boldsymbol{u}_1,\boldsymbol{v}_2\big) < \tau_{\boldsymbol{\omega}}\big(\boldsymbol{v}_3,\boldsymbol{u}_2\big)$, while in the meantime: $\tau_{\boldsymbol{\omega}}\big(\boldsymbol{u}_1,\boldsymbol{v}_2\big) = \frac{\omega_j-\omega_x}{c_j-c_x} = \tau_{\boldsymbol{\omega}}\big(\boldsymbol{v}_3,\boldsymbol{u}_2\big)$. This contradiction proves the theorem. □

4.2.3 Sufficiency of this criterion in the case $\Delta(n,2)$

We are going to prove that for $\Delta(n,2)$, the criterion of Theorem 4.24 is actually sufficient. To this end, we want to associate monotone paths on $\Delta(n,k)$ with some lattice paths on the integer grid $[n]^k$. A first idea to do so would be to associate to each vertex $\boldsymbol{v}_i$ in the path $P = (\boldsymbol{v}_1,\dots\boldsymbol{v}_r)$ a point $\boldsymbol{\ell}_i = (\ell_{i,1},\dots,\ell_{i,k}) \in [n]^k$ satisfying $\{\ell_{i,1},\dots,\ell_{i,k}\} = \mathrm{s}(\boldsymbol{v}_i)$. This leaves $k!$ possible choices for $\boldsymbol{\ell}_i$. Even though a *natural* choice would be to impose $\ell_{i,1} < \cdots < \ell_{i,k}$, we will prefer another one. Indeed, as $\boldsymbol{v}_i$ and $\boldsymbol{v}_{i+1}$ form an edge of $\Delta(n,k)$, there is only one index differing between $\mathrm{s}(\boldsymbol{v}_i)$ and $\mathrm{s}(\boldsymbol{v}_{i+1})$, so we will impose that $\boldsymbol{\ell}_i$ and $\boldsymbol{\ell}_{i+1}$ differ at only one coordinate.

Although this idea allows us to embed our problem into the realm of lattice paths, it has for drawback to associate $k!$ different lattice points to a same vertex, see Figure 61(Bottom).

Definition 4.26. A *diagonal-avoiding lattice path* $\mathcal{L} = (\boldsymbol{\ell}_1,\dots,\boldsymbol{\ell}_r)$ of *size* n and *dimension* k is an ordered list of points $\boldsymbol{\ell}_i \in [n]^k$ such that:

- $\boldsymbol{\ell}_1 = (k, k-1, \dots, 1)$;
- $\boldsymbol{\ell}_r = (\ell_{r,1},\dots,\ell_{r,k})$ with $\{\ell_{r,1},\dots,\ell_{r,k}\} = \{n-k+1,\dots,n\}$;
- for all $i \in [r]$, $\ell_{i,p} \neq \ell_{i,q}$ for all $p,q \in [k]$ with $p \neq q$;

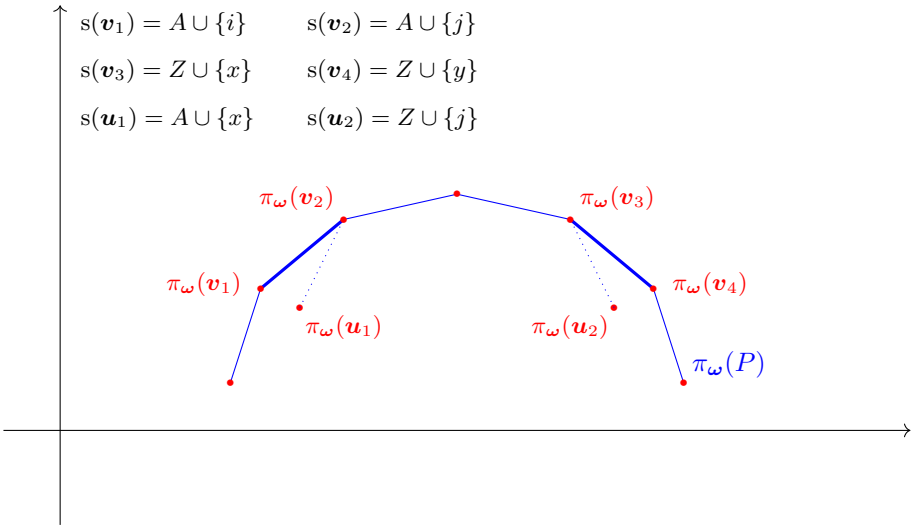

Figure 62: Dotted slopes shall be both equal to $\frac{\omega_j - \omega_x}{c_j - c_x}$: this is impossible if $\pi_{\boldsymbol{\omega}}(\boldsymbol{u}_1)$ and $\pi_{\boldsymbol{\omega}}(\boldsymbol{u}_2)$ are below $\pi_{\boldsymbol{\omega}}(P)$, thus either $\boldsymbol{u}_1$ or $\boldsymbol{u}_2$ is not a vertex of $\Delta(n,k)$ (*i.e.* $|s(\boldsymbol{u}_1)| \leq k-1$ or $|s(\boldsymbol{u}_2)| \leq k-1$).

- for all $i \in [r-1]$, there exists a $p \in [k]$ such that $\ell_{i,p} < \ell_{i+1,p}$, and $\ell_{i,q} = \ell_{i+1,q}$ for all $q \neq p$. The *i-th enhanced step* of $\mathcal{L}$ is denoted $\ell_{i,p} \xrightarrow{Z} \ell_{i+1,p}$ with $Z = \{\ell_{i,q} \ ; \ q \neq p\}$.

The ordered list of enhanced steps of $\mathcal{L}$ is denoted $\mathcal{S}(\mathcal{L})$. The *length* of $\mathcal{L}$ is r.

To a path $P = (\boldsymbol{v}_1, \dots \boldsymbol{v}_r)$ on $\Delta(n,k)$, one can associate a diagonal-avoiding lattice path $\mathscr{L}(P) = (\boldsymbol{\ell}_1, \dots, \boldsymbol{\ell}_r)$ of size n and dimension k defined by $\mathcal{S}(\mathscr{L}(P)) = \mathcal{S}(P)$, see Figure 63.

Proposition 4.27. *The map $P \mapsto \mathscr{L}(P)$ is a bijection from monotone paths on $\Delta(n,k)$ to diagonal-avoiding lattice paths of size n and dimension k.*

Proof. Fix a monotone path P on $\Delta(n,k)$. Starting at $\boldsymbol{\ell}_1 = (k, k-1, \dots, 1)$, the lattice path $\mathscr{L}(P) = (\boldsymbol{\ell}_1, \dots, \boldsymbol{\ell}_i, \dots, \boldsymbol{\ell}_r)$ can be defined by induction on i. Indeed, denote by $\mathscr{L}(P)_{\leq i} = (\boldsymbol{\ell}_1, \dots, \boldsymbol{\ell}_i)$, and suppose that for a fixed i: $\{\ell_{j,1}, \dots, \ell_{j,k}\} = s(\boldsymbol{v}_j)$ for all $j \leq i$, and the enhanced steps of $\mathscr{L}(P)_{\leq i}$ are the $(i-1)$ first enhanced steps of P. Consider the i-th enhanced step of P, say $x \xrightarrow{Z} y$. As $\{\ell_{i,1}, \dots, \ell_{i,k}\} = s(\boldsymbol{v}_j)$, there exists $p \in [k]$ such that $\ell_{i,p} = x$, and $\{\ell_{i,1}, \dots, \ell_{i,k}\} \smallsetminus \{\ell_{i,p}\} = Z$. By setting $\boldsymbol{\ell}_{i+1}$ with $\ell_{i+1,q} = \ell_{i,q}$ for $q \neq p$, and $\ell_{i+1,p} = y$, we construct $\mathscr{L}(P)_{\leq i+1}$ that fulfills the induction hypothesis. Hence, we can define $\mathscr{L}(P)$ such that $\mathcal{S}(\mathscr{L}(P)) = \mathcal{S}(P)$. By induction, $\mathscr{L}(P)$ satisfies that $\{\ell_{i,1}, \dots, \ell_{i,k}\} = s(\boldsymbol{v}_i)$. Moreover, as $|s(\boldsymbol{v}_i)| = k$, we know that $\ell_{i,p} \neq \ell_{i,q}$ for all $p \neq q$. Consequently, as $s(\boldsymbol{v}_i)$ and $s(\boldsymbol{v}_{i+1})$ differ by only one element, $\mathscr{L}(P)$ is a diagonal-avoiding path.

As $P \mapsto \mathcal{S}(P)$ is injective, it is immediate that $P \mapsto \mathscr{L}(P)$ is also injective.

Finally, for all diagonal-avoiding paths $\mathcal{L} = (\boldsymbol{\ell}_1, \dots, \boldsymbol{\ell}_r)$, one can construct by induction an ordered list of vertices $P_{\mathcal{L}} = (\boldsymbol{v}_1, \dots, \boldsymbol{v}_r)$ by taking $\boldsymbol{v}_i = \sum_{j \in \boldsymbol{\ell}_i} \boldsymbol{e}_j$. Such a path $P_{\mathcal{L}}$ is a monotone path on $\Delta(n,k)$ thanks to the properties of diagonal-avoiding paths. Moreover, as $\mathcal{S}(P_{\mathcal{L}}) = \mathcal{S}(\mathcal{L})$, the map $\mathcal{L} \mapsto P_{\mathcal{L}}$ is the reciprocal of $P \mapsto \mathscr{L}(P)$. □

Remark 4.28. It is straightforward to see that the length of P, *i.e.* the number of vertices contained in P, equals the length of $\mathscr{L}(P)$, *i.e.* the number of lattice points contained in $\mathscr{L}(P)$.

Example 4.29. For size $n = 3$, there are 2 diagonal-avoiding paths, one of length 1 and one of length 2. As seen in Example 4.21, all of them are images (by $\mathscr{L}$) of coherent paths on the simplex $\Delta(3,2)$.

$$\mathcal{S}(P) = \left(2 \xrightarrow{1} 4,\ \ 1 \xrightarrow{4} 5,\ \ 4 \xrightarrow{5} 6,\ \ 6 \xrightarrow{5} 7,\ \ 7 \xrightarrow{5} 8,\ \ 5 \xrightarrow{8} 7\right)$$

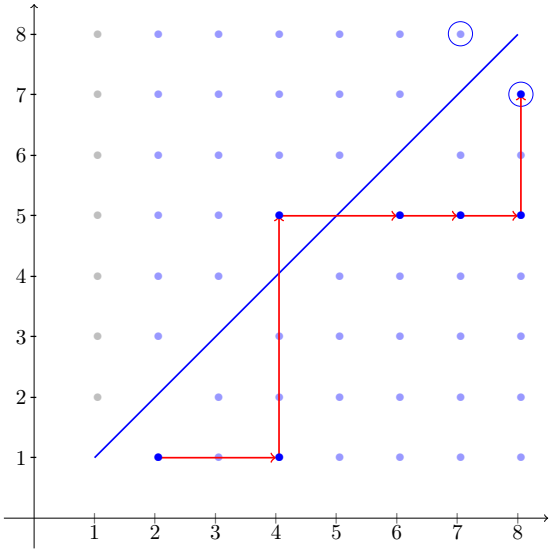

Figure 63: The lattice path associated to the ordered list of enhanced steps given on Top. It has size 8, dimension 2 and length 6.

For size $n = 4$, there are 10 diagonal-avoiding paths, see Figure 64. As seen in Example 4.22, 8 of them are images (by $\mathscr{L}$) of coherent paths on $\Delta(4, 2)$, while 2 come from monotone but not coherent paths on $\Delta(4, 2)$.

To ease notation, for an enhanced step of a path P on $\Delta(n, 2)$ or enhanced steps of diagonal-avoiding lattice paths of dimension 2, we will write $i \xrightarrow{a} j$ instead of $i \xrightarrow{\{a\}} j$. We will now study diagonal-avoiding paths of dimension 2. In particular, we will show that coherent monotone paths on $\Delta(n, 2)$ are associated with a certain family of diagonal-avoiding lattice paths, and that this family respects an induction process (which is cumbersome but powerful). To describe this induction process for our family, we need the notion of *restriction* of diagonal-avoiding lattice paths, which consists in shrinking the lattice grid $[n]^2$: suppose given a diagonal-avoiding lattice path on $[n+1]^2$, then erase the points of $[n+1]^2 \setminus [n]^2$; the path obtained on $[n]^2$ will probably not end at the right spot, but you can complete it to mimic the path you started with. The following definition formalizes this idea.

Definition 4.30. The *restriction* of a diagonal-avoiding lattice path $\mathcal{L} = (\boldsymbol{\ell}_1, \ldots, \boldsymbol{\ell}_r)$ of size $n + 1$ and dimension 2 is the diagonal-avoiding lattice path $\mathcal{L}' = (\boldsymbol{\ell}'_1, \ldots, \boldsymbol{\ell}'_s)$ of size n and dimension 2 defined by:

1. First, for all $i \in [r]$ define $\ell'_{i,p} = \begin{cases} \ell_{i,p} & \text{if } \ell_{i,p} \neq n+1 \\ n & \text{else} \end{cases}$ (for $p \in \{1, 2\}$) with $s = r$,
2. Next, as $\boldsymbol{\ell}'_r = (n, n)$: if $\boldsymbol{\ell}'_{r-1} = (x, n)$ then set $\boldsymbol{\ell}'_r = (n - 1, n)$, whereas if $\boldsymbol{\ell}'_{r-1} = (n, x)$ then set $\boldsymbol{\ell}'_r = (n, n - 1)$;
3. Finally, if $\boldsymbol{\ell}'_i = \boldsymbol{\ell}'_{i+1}$, then discard $\boldsymbol{\ell}'_{i+1}$ (and keep discarding until no doubles remain).

Even though this definition seems convoluted, it has a very straightforward illustration, see Figure 65: as explained before, draw the path $\mathcal{L}$ on the $(n + 1) \times (n + 1)$ grid, then $\mathcal{L}'$ is obtained by first restricting $\mathcal{L}$ to the $n \times n$ grid, then mimicking the steps $i \xrightarrow{n+1} j$ of $\mathcal{L}$ by introducing the steps $i \xrightarrow{n} j$ in $\mathcal{L}'$ (and slightly modifying $\mathcal{L}'$ to make it diagonal-avoiding).

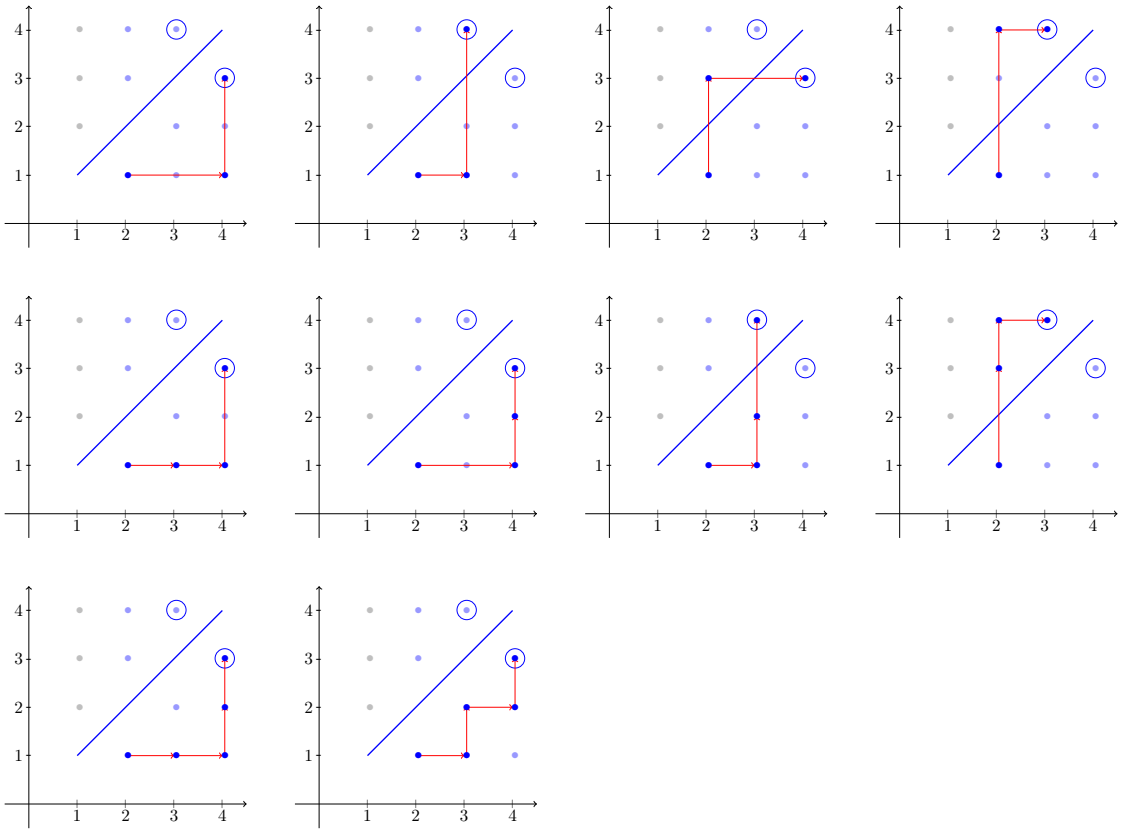

Figure 64: All 10 diagonal-avoiding lattice paths of size 4 and dimension 2, sorted by size.

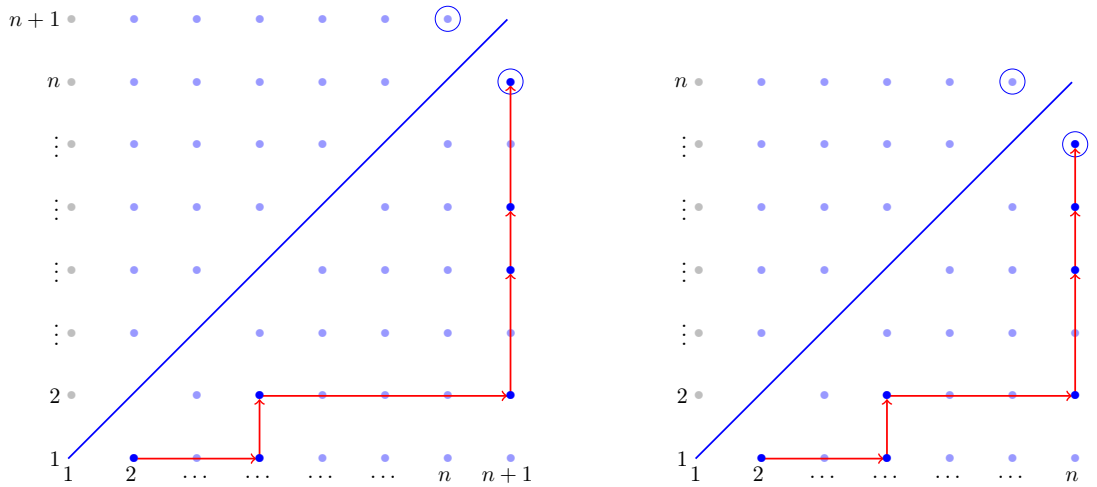

Figure 65: The restriction of $\mathcal{L}$ to $\mathcal{L}'$ restrict its enhanced steps from $\mathcal{S}(\mathcal{L}) = \big(2 \xrightarrow{1} 4,\ 1 \xrightarrow{4} 2,\ 4 \xrightarrow{2} n+1,\ 2 \xrightarrow{n+1} 4,\ 4 \xrightarrow{n+1} 5,\ 5 \xrightarrow{n+1} n\big)$ to $\mathcal{S}(\mathcal{L}') = \big(2 \xrightarrow{1} 4,\ 1 \xrightarrow{4} 2,\ 4 \xrightarrow{2} n,\ 2 \xrightarrow{n} 4,\ 4 \xrightarrow{n} 5,\ 5 \xrightarrow{n} n-1\big)$.

We can now introduce the main object of this section:

Definition 4.31. A diagonal-avoiding lattice path $\mathcal{L}$ of dimension 2 is said to be a *coherent lattice path* if for all couples of enhanced steps $i \xrightarrow{a} j \prec x \xrightarrow{z} y$ with $x < j$, we have $j = z$ or $x = a$.

Now, we will study the set of coherent lattice paths of size n. First, we will prove that such lattice paths can be constructed inductively. Then, we will show that the bijection $P \mapsto \mathscr{L}(P)$ (between monotone paths and diagonal-avoiding paths) bijectively sends coherent paths on $\Delta(n, 2)$ to coherent lattice paths. Finally, our inductive construction will allow us to count the number of coherent paths on $\Delta(n, 2)$.

Theorem 4.32. *For $n \geq 3$, let $\mathcal{L}$ be a coherent lattice path of size $n+1$ and $\mathcal{L}'$ its restriction of size n. Then $\mathcal{L}'$ is coherent and $\mathcal{L}$ can be reconstructed from $\mathcal{L}'$ as it belongs to one of these (mutually exclusive) 12 cases:*

(i) if $\mathcal{L}'$ ends by a step $x \xrightarrow{n-1} n$ with $x < n-1$, then denote $\mathcal{S}' = \mathcal{S}(\mathcal{L}') \smallsetminus \{x \xrightarrow{n-1} n\}$. One of the following holds (see Figure 66):

(a) $\mathcal{S}(\mathcal{L}) = \mathcal{S}(\mathcal{L}') \cup \{n-1 \xrightarrow{n} n+1\}$

(b) $\mathcal{S}(\mathcal{L}) = \mathcal{S}(\mathcal{L}') \cup \{n \xrightarrow{n-1} n+1,\ n-1 \xrightarrow{n+1} n\}$

(c) $\mathcal{S}(\mathcal{L}) = \mathcal{S}' \cup \{x \xrightarrow{n-1} n+1,\ n-1 \xrightarrow{n+1} n\}$

(ii) if $\mathcal{L}'$ ends by steps $x \xrightarrow{y_1} n$, $y_1 \xrightarrow{n} y_2, \ldots, y_{m-1} \xrightarrow{n} y_m$ with $x < n-1$, $m \geq 3$ and $y_1 < \cdots < y_m = n-1$, then denote $\mathcal{S}' = \mathcal{S}(\mathcal{L}') \smallsetminus \{x \xrightarrow{y_1} n,\ y_1 \xrightarrow{n} y_2,\ \ldots,\ y_{m-1} \xrightarrow{n} y_m\}$. One of the following holds (see Figure 67):

(a) $\mathcal{S}(\mathcal{L}) = \mathcal{S}(\mathcal{L}') \cup \{n-1 \xrightarrow{n} n+1\}$

(b) $\mathcal{S}(\mathcal{L}) = \big(\mathcal{S}(\mathcal{L}') \smallsetminus \{y_{m-1} \xrightarrow{n} n-1\}\big) \cup \{y_{m-1} \xrightarrow{n} n+1\}$

(c) $\mathcal{S}(\mathcal{L}) = \mathcal{S}' \cup \{x \xrightarrow{y_1} n+1,\ y_1 \xrightarrow{n+1} y_2,\ \ldots,\ y_{m-1} \xrightarrow{n+1} n-1,\ n-1 \xrightarrow{n+1} n\}$

(d) $\mathcal{S}(\mathcal{L}) = \mathcal{S}' \cup \{x \xrightarrow{y_1} n+1,\ y_1 \xrightarrow{n+1} y_2,\ \ldots,\ y_{m-1} \xrightarrow{n+1} n\}$

(iii) if $\mathcal{L}'$ ends by steps $x \xrightarrow{y} n$, $y \xrightarrow{n} n-1$ with $x < n$ and $y < n-1$, then denote $\mathcal{S}' = \mathcal{S}(\mathcal{L}') \smallsetminus \{x \xrightarrow{y} n,\ y \xrightarrow{n} n-1\}$. One of the following holds (see Figure 68):

(a) $\mathcal{S}(\mathcal{L}) = \mathcal{S}(\mathcal{L}') \cup \{n-1 \xrightarrow{n} n+1\}$

(b) $\mathcal{S}(\mathcal{L}) = \big(\mathcal{S}(\mathcal{L}') \smallsetminus \{y \xrightarrow{n} n-1\}\big) \cup \{y \xrightarrow{n} n+1\}$

(c) $\mathcal{S}(\mathcal{L}) = \big(\mathcal{S}(\mathcal{L}') \smallsetminus \{y \xrightarrow{n} n-1\}\big) \cup \{n \xrightarrow{y} n+1,\ y \xrightarrow{n+1} n\}$

(d) $\mathcal{S}(\mathcal{L}) = \mathcal{S}' \cup \{x \xrightarrow{y} n+1,\ y \xrightarrow{n+1} n-1,\ n-1 \xrightarrow{n+1} n\}$

(e) $\mathcal{S}(\mathcal{L}) = \mathcal{S}' \cup \{x \xrightarrow{y} n+1,\ y \xrightarrow{n+1} n\}$

Proof. Observe first that if $\mathcal{L}$ is a coherent lattice path of size $n+1$, then its restriction $\mathcal{L}'$ of size n is also coherent. Indeed, if $i \xrightarrow{a} j \prec x \xrightarrow{z} y \in \mathcal{S}(\mathcal{L}')$ with $x < j$, then the following two properties hold:

- either $i \xrightarrow{a} j \in \mathcal{S}(\mathcal{L})$, or $i \xrightarrow{a} n+1 \in \mathcal{S}(\mathcal{L})$ and $j = n$;
- either $x \xrightarrow{z} y \in \mathcal{S}(\mathcal{L})$, or $x \xrightarrow{z} n+1 \in \mathcal{S}(\mathcal{L})$ and $y = n$, or $x \xrightarrow{n+1} y' \in \mathcal{S}(\mathcal{L})$ and $z = n$ and $y' \in \{y, n\}$.

As $\mathcal{L}$ is coherent, this implies $x = a$ or $j = z$ in all cases except if $i \xrightarrow{a} j \in \mathcal{S}(\mathcal{L})$ with $j = n$ and $x \xrightarrow{n+1} y \in \mathcal{S}(\mathcal{L})$ with $x > a$. But in the latter, $x > a > j$ and $x \neq a$, $j \neq n+1$, contradicting the coherence of $\mathcal{L}$.

Now, we first prove that all 12 cases lead to coherent paths, and then that there is no other coherent path of size $n+1$.

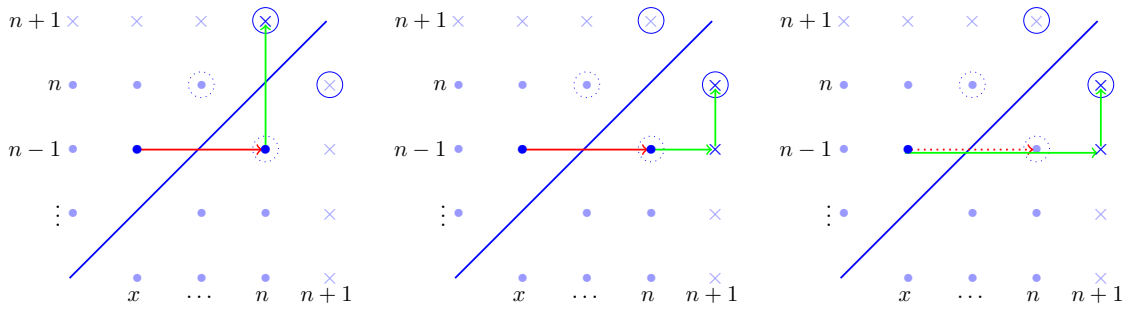

Figure 66: All 3 paths of size $n+1$ that restrict to a path of size n of type (i) in Theorem 4.32.

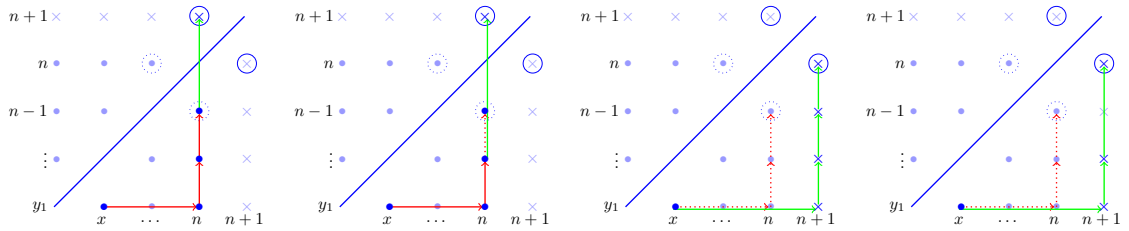

Figure 67: All 4 paths of size $n+1$ that restrict to a path of size n of type (ii) in Theorem 4.32.

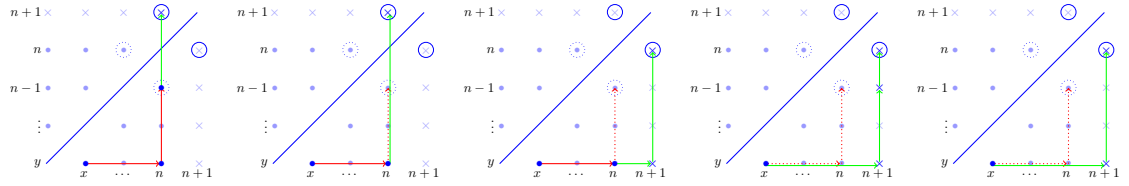

Figure 68: All 5 paths of size $n+1$ that restrict to a path of size n of type (iii) in Theorem 4.32.

We say that $i \xrightarrow{a} j \prec x \xrightarrow{z} y$ are *mutually coherent* if $x \geq j$, or if $x < j$ and $j = z$ or $x = a$.

Case $(i)(a)$, $(ii)(a)$ and $(iii)(a)$ If $i \xrightarrow{a} j \in \mathcal{S}(\mathcal{L}')$ satisfies $n-1 < j$, then $j = n$ so adding $n-1 \xrightarrow{n} n+1$ to $\mathcal{S}(\mathcal{L}')$ does not infringe coherence.

Case $(i)(b)$ $n \xrightarrow{n-1} n+1$ and $n-1 \xrightarrow{n+1} n$ are mutually coherent, and if $i \xrightarrow{a} j \in S(\mathcal{L}')$ satisfies $n-1 < j$, then $j = n$ and $a = n-1$, so $i \xrightarrow{a} j$ is mutually coherent with both $n \xrightarrow{n-1} n+1$ and $n-1 \xrightarrow{n+1} n$.

Case $(i)(c)$ and $(iii)(e)$ $x \xrightarrow{y} n+1$ and $y \xrightarrow{n+1} n$ are mutually coherent, and if $i \xrightarrow{a} j \in S'$ then $j \leq y$, so $i \xrightarrow{a} j$ is mutually coherent with both $x \xrightarrow{y} n+1$ and $y \xrightarrow{n+1} n$.

Case $(ii)(b)$ and $(iii)(b)$ Changing the endpoint of the last enhanced step doesn't interfere with mutual coherence (with previous steps).

Case $(ii)(c)$ and $(ii)(d)$ For $p \in [m-1]$, $x \xrightarrow{y_1} n+1$ and $y_p \xrightarrow{n+1} y_{p+1}$ are mutually coherent as $x \xrightarrow{y_1} n$ and $y_p \xrightarrow{n} y_{p+1}$ are in $\mathcal{S}(\mathcal{L}')$; if $i \xrightarrow{a} j \in \mathcal{S}'$, then $j \leq \max\{x, y_1\} \leq n-1$ and thus $i \xrightarrow{a} j$ is mutually coherent with $y_p \xrightarrow{n+1} y_{p+1}$, and mutually coherent with $x \xrightarrow{y_1} n+1$ as $x \xrightarrow{y_1} n \in \mathcal{S}(\mathcal{L}')$.

Case $(iii)(d)$ The above argument applies here, replacing y_1 by y.

Case $(iii)(c)$ The steps $x \xrightarrow{y} n$, $n \xrightarrow{y} n+1$ and $y \xrightarrow{n+1} n$ are mutually coherent, and if $i \xrightarrow{a} j \in \mathcal{S}(\mathcal{L}') \setminus \{y \xrightarrow{n} n-1\}$, then the above argument again applies.

Finally, we prove that there exists no other coherent paths of size $n+1$.

Case (i) If the last step of $\mathcal{L}'$ is $x \xrightarrow{n-1} n$, then the 3 claimed $\mathcal{L}$ are the only diagonal-avoiding lattice paths whose restriction is $\mathcal{L}'$ (as lattice paths must be North-East increasing).

Case (ii) If $\mathcal{L}$ restrict to $\mathcal{L}'$ whose last steps are $x \xrightarrow{y_1} n$, $y_1 \xrightarrow{n} y_2, \dots, y_{m-1} \xrightarrow{n} y_m$ with $x < n-1$, $m \geq 3$ and $y_1 < \cdots < y_m = n-1$, then consider the last step of the form $i \xrightarrow{a} n+1$ in $\mathcal{L}$. Either $a = n$ and $\mathcal{L}$ is necessarily in cases (a) or (b); or $(i, a) \in \{(x, y_1)\} \cup \{(n, y_p)\}_{p \in [m]}$. The first possibility leads necessarily to cases (c) and (d), while the latest lead to non-coherent paths, as $x \xrightarrow{y_1} n$ would be in $\mathcal{L}$ and is not mutually coherent with $y_p \xrightarrow{n+1} y_{p+1}$ for $p \geq 2$.

Case (iii) If the last steps of $\mathcal{L}'$ are $x \xrightarrow{n-1} n$ and $y \xrightarrow{n} n-1$, then there are 6 diagonal-avoiding lattice paths whose restriction is $\mathcal{L}'$ (as lattice paths must be North-East increasing). The only non-coherent one is given by $\mathcal{S}(\mathcal{L}) = \big(\mathcal{S}(\mathcal{L}') \setminus \{y \xrightarrow{n} n-1\}\big) \cup \{n \xrightarrow{y} n+1,\ y \xrightarrow{n+1} n-1,\ n-1 \xrightarrow{n+1} n\}$, which is not coherent as $n \xrightarrow{y} n+1$ and $n-1 \xrightarrow{n+1} n$ are not mutually coherent (as $y < n-1$). □

Now that we know how to inductively construct all coherent lattice paths, we are able to prove the reciprocal of Theorem 4.24. The proof of the following theorem will be cumbersome but not difficult: for each 12 cases of Theorem 4.32, we are going to exhibit a vector $\boldsymbol{\omega}$ that captures it.

Theorem 4.33. *Coherent paths on $\Delta(n, 2)$ are in bijection with coherent lattice paths of size n.*

Proof. Theorem 4.24 proves that the application $\mathscr{L}$ sends injectively coherent paths on $\Delta(n, 2)$ to coherent lattice paths of size n. We now prove the converse: if $\mathcal{L}$ is a coherent lattice path of size n, then there exists a coherent path P on $\Delta(n, 2)$ such that $\mathscr{L}(P) = \mathcal{L}$. To this end, we will use the induction process of Theorem 4.32. Thanks to Example 4.29, we know that all coherent lattice paths of size 3 and 4 are coherent paths on $\Delta(3, 2)$ and $\Delta(4, 2)$. We are going to prove that if $\mathcal{L}' = \mathscr{L}(P')$ for $\mathcal{L}'$ a coherent lattice path of size n, then for all coherent path $\mathcal{L}$ of size $n+1$ such that $\mathcal{L}$ restrict to $\mathcal{L}'$ (*i.e.* in all 12 cases of Theorem 4.32), we can find a coherent path P on $\Delta(n+1, 2)$ such that $\mathcal{L} = \mathscr{L}(P)$.

Let $\mathcal{L}'$ be a coherent lattice path of size n such that $\mathcal{L}' = \mathscr{L}(P')$ where P' is a coherent path and $\boldsymbol{\omega}' \in \mathbb{R}^n$ captures P'. We are going to find ω_{n+1} such that $\boldsymbol{\omega} := (\omega'_1, \dots, \omega'_n, \omega_{n+1}) \in \mathbb{R}^{n+1}$ captures a path P with $\mathscr{L}(P) = \mathcal{L}$ (in some cases, we will also modify ω_n slightly). We denote $\tau_{\boldsymbol{\omega}}(i \to j) = \frac{\omega_j - \omega_i}{c_j - c_i}$ as usual. As we will focus the behavior of the points $(c_i + c_j, \omega_i + \omega_{+j})$ for $(i, j) \in \mathcal{L}$, in order to ease notation, we say "the point (i, j)" instead of "the point $(c_i + c_j, \omega_i + \omega_j)$". We will distinguish three cases following the main cases of Theorem 4.32.

Case (i) Suppose the last step of $\mathcal{L}'$ is $x \xrightarrow{n-1} n$ with $x < n-1$. Remark that for $i \notin \{x, n-1, n\}$:

$$\tau_{\boldsymbol{\omega}}(n-1 \to n) < \tau_{\boldsymbol{\omega}}(x \to n) < \tau_{\boldsymbol{\omega}}(i \to n)$$

Indeed, the first inequality comes directly from the last step of $\mathcal{L}'$: if the inequality were reversed, the last step would have been $n-1 \xrightarrow{x} n$ instead. The second inequality follows from Lemma 4.25 applied to the triangle $(x, n-1)$, $(i, n-1)$, $(n, n-1)$.

Note first that, for $i < n$, if ω_{n+1} satisfies that $\tau_{\boldsymbol{\omega}}(n \to n+1) < \tau_{\boldsymbol{\omega}}(i \to n)$, then there can not be a step $i \xrightarrow{a} n+1$ in $\mathcal{S}(P)$ as $\tau_{\boldsymbol{\omega}}(i \to n+1) < \tau_{\boldsymbol{\omega}}(i \to n)$ by Lemma 4.25, thus the points associated to $(i, n+1)$ are all below the path P' and do not belong to P. As $\tau_{\boldsymbol{\omega}}(n \to n+1)$ is a continuous increasing function of ω_{n+1}, this gives three regimes.

Case $(i)(a)$: To obtain P with $\mathscr{L}(P)$ of form $(i)(a)$ in Theorem 4.32, choose ω_{n+1} small enough to satisfy $\tau_{\boldsymbol{\omega}}(n \to n+1) < \tau_{\boldsymbol{\omega}}(n-1 \to n)$, then the path P captured by $\boldsymbol{\omega}$ has $\mathcal{S}(P') \subset \mathcal{S}(P)$ by the above, and $n-1 \xrightarrow{n} n+1 \in \mathcal{S}(P)$ by applying Lemma 4.25 in the triangle $(n, n-1)$, $(n-1, n+1)$, $(n, n+1)$.

Case $(i)(b)$: To obtain P with $\mathscr{L}(P)$ of form $(i)(b)$ in Theorem 4.32, choose ω_{n+1} to satisfy $\tau_{\boldsymbol{\omega}}(n-1 \to n) < \tau_{\boldsymbol{\omega}}(n \to n+1) < \tau_{\boldsymbol{\omega}}(x \to n)$, then the path P captured by $\boldsymbol{\omega}$ has $\mathcal{S}(P') \subset \mathcal{S}(P)$ by the above, and $n \xrightarrow{n-1} n+1 \in \mathcal{S}(P)$ and $n-1 \xrightarrow{n+1} n \in \mathcal{S}(P)$ by applying Lemma 4.25 to the triangle $(n, n-1)$, $(n-1, n+1)$, $(n, n+1)$.

Case $(i)(c)$: To obtain P with $\mathscr{L}(P)$ of form $(i)(c)$ in Theorem 4.32, choose ω_{n+1} to satisfy $\tau_{\boldsymbol{\omega}}(x \to n) < \tau_{\boldsymbol{\omega}}(n \to n+1) < \min_{i \notin \{x,n\}} \tau_{\boldsymbol{\omega}}(i \to n)$, then the path P captured by $\boldsymbol{\omega}$ has $\mathcal{S}(P') \setminus \{x \xrightarrow{n-1} n\} \subset \mathcal{S}(P)$ by the above, and $x \xrightarrow{n-1} n+1 \in \mathcal{S}(P)$ and $n-1 \xrightarrow{n+1} n \in \mathcal{S}(P)$.

We have shown that if $\mathcal{L}'$ is in the case (i), then all the paths $\mathcal{L}$ that restrict to $\mathcal{L}'$ are of the form $\mathcal{L} = \mathscr{L}(P)$ for some coherent P.

Case (ii) Suppose the last steps of $\mathcal{L}'$ are $x \xrightarrow{y_1} n, y_1 \xrightarrow{n} y_2, \ldots, y_{m-1} \xrightarrow{n} n-1$ with $m \geq 3$. Then for all $i \notin \{x, y_1, n\}$, by the same argument as before:

$$\tau_{\boldsymbol{\omega}}(y_{m-1} \to n-1) < \tau_{\boldsymbol{\omega}}(y_{m-2} \to y_{m-1}) < \cdots < \tau_{\boldsymbol{\omega}}(y_1 \to y_2) < \tau_{\boldsymbol{\omega}}(x \to n) < \tau_{\boldsymbol{\omega}}(i \to n)$$

We distinguish three regimes.

Case $(ii)(a)$: To obtain P with $\mathscr{L}(P)$ of form $(ii)(a)$ in Theorem 4.32, choose ω_{n+1} small enough to satisfy $\tau_{\boldsymbol{\omega}}(n \to n+1) < \tau_{\boldsymbol{\omega}}(y_{m-1} \to n-1)$, then the path P captured by $\boldsymbol{\omega}$ has $\mathcal{S}(P') \subset \mathcal{S}(P)$, and $n-1 \xrightarrow{n} n+1 \in \mathcal{S}(P)$ by applying Lemma 4.25 to the triangle $(n, n-1)$, $(n-1, n+1)$ and $(n, n+1)$.

Case $(ii)(b)$: To obtain P with $\mathscr{L}(P)$ of form $(ii)(b)$ in Theorem 4.32, choose ω_{n+1} to satisfy $\tau_{\boldsymbol{\omega}}(y_{m-1} \to n-1) < \tau_{\boldsymbol{\omega}}(n \to n+1) < \tau_{\boldsymbol{\omega}}(y_{m-2} \to y_{m-1})$, then the path P captured by $\boldsymbol{\omega}$ has $\mathcal{S}(P') \setminus \{y_{m-1} \xrightarrow{n} n-1\} \subset \mathcal{S}(P)$, and $y_{m-1} \xrightarrow{n} n+1 \in \mathcal{S}(P)$ because applying Lemma 4.25 to the triangle (y_{m-1}, n), $(n, n-1)$ and $(n-1, n+1)$ gives that $\tau_{\boldsymbol{\omega}}(n-1 \to n+1) < \tau_{\boldsymbol{\omega}}(n-1 \to n)$, and applying it to (y_{m-1}, n), $(y_{m-1}, n+1)$ and $(n, n+1)$ gives that $\tau_{\boldsymbol{\omega}}(y_{m-1} \to n+1) > \tau_{\boldsymbol{\omega}}(n \to n+1)$.

Case $(ii)(d)$: To obtain P with $\mathscr{L}(P)$ of form $(ii)(d)$ in Theorem 4.32, choose ω_{n+1} to satisfy $\tau_{\boldsymbol{\omega}}(x \to n) < \tau_{\boldsymbol{\omega}}(n \to n+1) < \min_{i \notin \{x,n\}} \tau_{\boldsymbol{\omega}}(i \to n)$, then the path P captured by $\boldsymbol{\omega}$ has $\mathcal{S}' \subset \mathcal{S}(P)$, and by applying Lemma 4.25 to the triangle (x, y_1), (n, y_1) and $(n+1, y_1)$, one gets that $x \xrightarrow{y_1} n+1 \in \mathcal{S}(P)$. Moreover, the projected path $\big((n+1, y_1), (n+1, y_2), \ldots, (n+1, y_{m-1}), (n+1, n-1)\big)$ is parallel and higher than the projected path $\big((n, y_1), (n, y_2), \ldots, (n, y_{m-1}), (n, n-1)\big)$, thus $y_i \xrightarrow{n+1} y_{i+1} \in \mathcal{S}(P)$ for $i \in [1, m-2]$. As $\tau_{\boldsymbol{\omega}}(y_{m-1} \to n-1) < \tau_{\boldsymbol{\omega}}(x \to n) \leq \tau_{\boldsymbol{\omega}}(n-1 \to n)$ in P', Lemma 4.25 ensures that $y_{m-1} \xrightarrow{n+1} n \in \mathcal{S}(P)$.

Case $(ii)(c)$: To obtain P with $\mathscr{L}(P)$ of form $(ii)(c)$ in Theorem 4.32, note that in the previous sub-case there is no point (i, n) in P except from $(n, n+1)$. So lowering the value of ω_n (with the same fixed ω_{n+1} as in the previous sub-case) will not affect the path except in the last triangle $(y_{m-1}, n+1)$, $(n-1, n+1)$, $(n, n+1)$. Taking ω_n low enough to satisfy $\tau_{\boldsymbol{\omega}}(y_{m-1} \to n-1) > \tau_{\boldsymbol{\omega}}(n-1 \to n)$, we obtain a path $\tilde{P}$ with $\mathcal{S}(P) \setminus \{y_{m-1} \xrightarrow{n+1} n\} \subset \mathcal{S}(\tilde{P})$ and $\{y_{m-1} \xrightarrow{n+1} n-1,\ n-1 \xrightarrow{n+1} n\} \in \mathcal{S}(\tilde{P})$.

Case (*iii*) Suppose that the last steps of $\mathcal{L}'$ are $x \xrightarrow{n} y$, $y \xrightarrow{n} n-1$. Then for $i \notin \{x, y, n\}$:

$$\tau_{\boldsymbol{\omega}}(y \to n-1) < \tau_{\boldsymbol{\omega}}(y \to n) < \tau_{\boldsymbol{\omega}}(x \to n) < \tau_{\boldsymbol{\omega}}(i \to n)$$

Indeed, $\tau_{\boldsymbol{\omega}}(y \to n) < \tau_{\boldsymbol{\omega}}(x \to n)$ otherwise $x \xrightarrow{y} n \notin \mathcal{S}(P')$, and $\tau_{\boldsymbol{\omega}}(y \to n-1) < \tau_{\boldsymbol{\omega}}(y \to n)$ as already $\tau_{\boldsymbol{\omega}}(y \to n-1) < \tau_{\boldsymbol{\omega}}(n-1 \to n)$.

Case (iii)(a): To obtain P with $\mathscr{L}(P)$ of form (*iii*)(*a*) in Theorem 4.32, choose ω_{n+1} small enough to satisfy $\tau_{\boldsymbol{\omega}}(n \to n+1) < \tau_{\boldsymbol{\omega}}(y \to n-1)$, then $\mathcal{S}(P') \subset \mathcal{S}(P)$ and $n-1 \xrightarrow{n} n+1 \in \mathcal{S}(P)$.

Case (iii)(b): To obtain P with $\mathscr{L}(P)$ of form (*iii*)(*b*) in Theorem 4.32, choose ω_{n+1} to satisfy $\tau_{\boldsymbol{\omega}}(y \to n-1) < \tau_{\boldsymbol{\omega}}(n \to n+1) < \tau_{\boldsymbol{\omega}}(y \to n)$, then $\mathcal{S}(P') \setminus \{y \xrightarrow{n} n-1\} \subset \mathcal{S}(P)$, and as $\tau_{\boldsymbol{\omega}}(n \to n+1) < \tau_{\boldsymbol{\omega}}(y \to n)$, Lemma 4.25 ensures $y \xrightarrow{n} n+1 \in \mathcal{S}(P)$.

Case (iii)(c): To obtain P with $\mathscr{L}(P)$ of form (*iii*)(*c*) in Theorem 4.32, choose ω_{n+1} to satisfy $\tau_{\boldsymbol{\omega}}(y \to n) < \tau_{\boldsymbol{\omega}}(n \to n+1) < \tau_{\boldsymbol{\omega}}(x \to n)$, then $\mathcal{S}(P') \setminus \{y \xrightarrow{n} n-1\} \subset \mathcal{S}(P)$, and as $\tau_{\boldsymbol{\omega}}(n \to n+1) > \tau_{\boldsymbol{\omega}}(y \to n)$, Lemma 4.25 ensures $\{n \xrightarrow{y} n+1,\ y \xrightarrow{n+1} n\} \subset \mathcal{S}(P)$.

Case (iii)(e): To obtain P with $\mathscr{L}(P)$ of form (*iii*)(*e*) in Theorem 4.32, choose ω_{n+1} to satisfy $\tau_{\boldsymbol{\omega}}(x \to n) < \tau_{\boldsymbol{\omega}}(n \to n+1) < \min_{i \notin \{x,n\}} \tau_{\boldsymbol{\omega}}(i \to n)$, then $\mathcal{S}' \cup \{x \xrightarrow{y} n+1\} \subset \mathcal{S}(P)$, and $y \xrightarrow{n} n+1 \in \mathcal{S}(P)$ as $\tau_{\boldsymbol{\omega}}(y \to n-1) < \tau_{\boldsymbol{\omega}}(n-1 \to n)$.

Case (iii)(d): To obtain P with $\mathscr{L}(P)$ of form (*iii*)(*d*) in Theorem 4.32, from the previous value of ω_{n+1}, we lower the value of ω_n until $\tau_{\boldsymbol{\omega}}(y \to n-1) > \tau_{\boldsymbol{\omega}}(n-1 \to n)$. As no other point of the form (i, n) belongs to P, this new $\boldsymbol{\omega}$ captures a path $\tilde{P}$ with $\mathcal{S}(P) \setminus \{y \xrightarrow{n+1} n\} \subset \mathcal{S}(\tilde{P})$ and $\{y \xrightarrow{n+1} n-1,\ n-1 \xrightarrow{n+1} n\} \subset \mathcal{S}(\tilde{P})$.

We have proven that in all 12 cases, if the restriction of $\mathcal{L}$ is the image by $\mathscr{L}$ of a coherent path on $\Delta(n-1, 2)$, then $\mathcal{L}$ is the image by $\mathscr{L}$ of a coherent path on $\Delta(n, 2)$. This shows the surjectivity of $\mathscr{L}$. □

4.2.4 Counting the number of coherent monotone paths on $\Delta(n, 2)$

The induction process of Theorem 4.32 allows us to count precisely the number of coherent lattice paths, which is the number of vertices of $\mathsf{M}(n, 2)$ thanks to Theorem 4.33.

Let t_n be the number of coherent paths $\mathcal{L}$ of size n such that the last step of $\mathcal{L}$ is $x \xrightarrow{n-1} n$ (*i.e.* of type (*i*) in Theorem 4.32). Let q_n be the number of these finishing by steps $x \xrightarrow{y_1} n, y_1 \xrightarrow{n} y_2, \ldots, y_{m-1} \xrightarrow{n} n-1$ with $m \geq 3$ (*i.e.* of type (*ii*) in Theorem 4.32). Let c_n be the number of these finishing by $x \xrightarrow{y} n, y \xrightarrow{n} n-1$ (*i.e.* of type (*iii*) in Theorem 4.32).

Observing the induction process of Theorem 4.32 gives the following:

Proposition 4.34. *The sequences t_n, q_n and c_n satisfy the following recursive formula:*

$$\forall n \geq 4,\ \begin{pmatrix} t_{n+1} \\ q_{n+1} \\ c_{n+1} \end{pmatrix} = M \begin{pmatrix} t_n \\ q_n \\ c_n \end{pmatrix} \quad \textit{with} \quad M = \begin{pmatrix} 1 & 2 & 2 \\ 0 & 2 & 1 \\ 2 & 0 & 2 \end{pmatrix} \quad \textit{and} \quad \begin{pmatrix} t_4 \\ q_4 \\ c_4 \end{pmatrix} = \begin{pmatrix} 3 \\ 1 \\ 4 \end{pmatrix}$$

Proof. The values for t_4, q_4 and c_4 follow from Example 4.29.

Looking at the induction process in Theorem 4.32, for each case (*i*)(*a*) to (*iii*)(*e*), one can identify if the created coherent path of size $n+1$ is of the type of case (*i*), (*ii*) or (*iii*). For example, if $\mathcal{L}'$ of size n ends by a step $x \xrightarrow{n-1} n$, then there are three $\mathcal{L}$ of size $n+1$ that restrict to $\mathcal{L}'$: in case (*i*)(*a*), $\mathcal{L}$ ends with $y \xrightarrow{n} n+1$ (with $y = n-1$) so it belongs to type (*i*). The case analysis is summarized in the following table:

	(*a*)	(*b*)	(*c*)	(*d*)	(*e*)
(*i*)	(*i*)	(*iii*)	(*iii*)		
(*ii*)	(*i*)	(*i*)	(*ii*)	(*ii*)	
(*iii*)	(*i*)	(*i*)	(*iii*)	(*ii*)	(*iii*)

Reading off the table gives the matrix M. □

Theorem 4.35. *For $n \geq 4$, there are $\frac{1}{3}\left(25 \times 4^{n-4} - 1\right)$ coherent paths of size n.*

Proof. By definition, the total number of coherent paths of size n is $t_n + q_n + c_n$.

A quick analysis of M shows that $\mathrm{Sp}(M) = \{0, 1, 4\}$ with $(2, -2, -1)M = (0, 0, 0)$. Thus for all n: $2t_n = 2q_n + c_n$. It follows that if $c_n = t_n + 1$, then $t_n = 2q_n + 1$ and thus $c_{n+1} = 2t_n + 2c_n = t_n + 2q_n + 2c_n + 1 = t_{n+1} + 1$. By induction: $\forall n \geq 4, c_n = t_n + 1$. This gives: $t_{n+1} + q_{n+1} + c_{n+1} = 4(t_n + q_n + c_n) + 1$

With $t_4 + q_4 + c_4 = 8$, this recursive formula gives the number of coherent paths of size n. □

This formula solves the question we started with: determine the vertices of $\mathsf{M}(n, 2)$ and count them. Notwithstanding, one can go even further in the analysis of the induction process. Let $t_{n,\ell}$ be the number of coherent path of size n and length ℓ that end with a step $x \xrightarrow{n-1} n$ and let $q_{n,\ell}$, $c_{n,\ell}$ be the counterparts for the two other main cases of the induction. Let $T_n = \sum_\ell t_{n,\ell} z^\ell$, $Q_n = \sum_\ell q_{n,\ell} z^\ell$ and $C_n = \sum_\ell c_{n,\ell} z^\ell$ be the associated generating polynomials, then observing Theorem 4.32 gives the following:

Proposition 4.36. *The sequences of polynomials T_n, Q_n and C_n satisfy the following recursive formula:*

$$\forall n \geq 4,\ \begin{pmatrix} T_{n+1} \\ Q_{n+1} \\ C_{n+1} \end{pmatrix} = \mathcal{M} \begin{pmatrix} T_n \\ Q_n \\ C_n \end{pmatrix} \quad \textit{with} \quad \mathcal{M} = \begin{pmatrix} z & 1+z & 1+z \\ 0 & 1+z & z \\ z+z^2 & 0 & 1+z \end{pmatrix}, \quad \begin{pmatrix} T_4 \\ Q_4 \\ C_4 \end{pmatrix} = \begin{pmatrix} z^4 + 2z^3 \\ z^4 \\ 2z^4 + 2z^3 \end{pmatrix}$$

Remark 4.37. Note that evaluating the previous relation at $z = 1$ gives back Proposition 4.34.

Proof of Proposition 4.36. The values for T_4, Q_4 and C_4 have been explored in Example 4.29.

Looking at the induction process, for each case $(i)(a)$ to $(iii)(e)$, one can identify the length of the created coherent path of size $n+1$. For example, if $\mathcal{L}'$ of size n and length ℓ ends by a step $x \xrightarrow{n-1} n$, then there are three $\mathcal{L}$ of size $n+1$ that restricts to $\mathcal{L}'$: in case $(i)(a)$, $\mathcal{L}$ contains 1 step more than $\mathcal{L}'$ so it has length $\ell + 1$. The case analysis is summarized in the following table, assuming the restricted path is of length ℓ:

	(a)	(b)	(c)	(d)	(e)
(i)	$\ell+1$	$\ell+2$	$\ell+1$		
(ii)	$\ell+1$	ℓ	$\ell+1$	ℓ	
(iii)	$\ell+1$	ℓ	$\ell+1$	$\ell+1$	ℓ

Reading off this table together with the one of the proof of Proposition 4.34 yields $\mathcal{M}$. □

The matrix $\mathcal{M}$ (over the polynomial ring) has three eigenvalues $\lambda_0 = 0$, $\lambda_+ = 1 + \frac{3}{2}z + \frac{1}{2}z\sqrt{4z+5}$, and $\lambda_- = 1 + \frac{3}{2}z - \frac{1}{2}z\sqrt{4z+5}$ with associated (left) eigenvectors:

$$\boldsymbol{x}_0 = \begin{pmatrix} -1 & 1 & \frac{1}{1+z} \end{pmatrix}, \ \boldsymbol{x}_+ = \begin{pmatrix} 1 & \frac{\sqrt{4z+5}-1}{2z} & \frac{z\sqrt{4z+5}+z+2}{2(z^2+z)} \end{pmatrix}, \ \boldsymbol{x}_- = \begin{pmatrix} 1 & -\frac{\sqrt{4z+5}+1}{2z} & \frac{-z\sqrt{4z+5}+z+2}{2(z^2+z)} \end{pmatrix}$$

Unfortunately, the square roots in the eigenvalues and eigenvectors make it very difficult to derive an explicit formula as simple as in Theorem 4.35, but we can prove two very interesting properties on the number of coherent paths of a given length.

Theorem 4.38. *For a fixed size n with $n \geq 4$, the longest coherent path of size n is of length $\ell_{\max} = \left\lfloor \frac{3}{2}(n-1) \right\rfloor$. The number of coherent paths of size n and length $\ell_{\max}$ is 1 if n is odd, and $\left\lfloor \frac{3}{2}(n-1) \right\rfloor$ if n is even.*

Proof. We will prove by induction the slightly stronger following statement on the degrees and leading coefficients of T_n, Q_n and C_n. Denote $\nu_n = \left\lfloor \frac{3}{2}(n-1) \right\rfloor$:

$$\begin{cases} \text{if } n \text{ odd}, & T_n = (\nu_n - 2)z^{\nu_n - 1} + o(z^{\nu_n - 1}), & Q_n = O(z^{\nu_n - 1}), & C_n = z^{\nu_n} + o(z^{\nu_n}) \\ \text{if } n \text{ even}, & T_n = z^{\nu_n} + o(z^{\nu_n}), & Q_n = z^{\nu_n} + o(z^{\nu_n}), & C_n = (\nu_n - 2)z^{\nu_n} + o(z^{\nu_n}) \end{cases}$$

This statement holds for $n = 4$ as $\nu_4 = 4$, $T_4 = z^4 + o(z^4)$, $Q_4 = z^4$ and $C_4 = 2z^4 + o(z^4)$. Now, it is just a matter of multiplying by $\mathcal{M}$. Suppose n is odd and the statement holds, then:

$$\begin{aligned} T_{n+1} &= zT_n + (1+z)Q_n + (1+z)C_n \\ &= O(z^{\nu_n}) + O(z^{\nu_n}) + z^{\nu_n+1} + o(z^{\nu_n+1}) \\ &= z^{\nu_{n+1}} + o(z^{\nu_{n+1}}) && \text{as } \nu_{n+1} = \nu_n + 1 \end{aligned}$$

$$\begin{aligned} Q_{n+1} &= (1+z)Q_n + zC_n \\ &= O(z^{\nu_n}) + z^{\nu_n+1} + o(z^{\nu_n+1}) \\ &= z^{\nu_{n+1}} + o(z^{\nu_{n+1}}) && \text{as } \nu_{n+1} = \nu_n + 1 \end{aligned}$$

$$\begin{aligned} C_{n+1} &= (z^2+z)T_n + (1+z)C_n \\ &= (\nu_n - 2)z^{\nu_n+1} + o(z^{\nu_n+1}) + z^{\nu_n+1} + o(z^{\nu_n+1}) \\ &= (\nu_{n+1} - 2)z^{\nu_{n+1}} + o(z^{\nu_{n+1}}) && \text{as } \nu_{n+1} = \nu_n + 1 \end{aligned}$$

Suppose n is even, and the statement holds, then:

$$\begin{aligned} T_{n+1} &= zT_n + (1+z)Q_n + (1+z)C_n \\ &= z^{\nu_n+1} + z^{\nu_n+1} + (\nu_n - 2)z^{\nu_n+1} + o(z^{\nu_n+1}) \\ &= (\nu_{n+1} - 2)z^{\nu_{n+1}-1} + o(z^{\nu_{n+1}-1}) && \text{as } \nu_{n+1} = \nu_n + 2 \end{aligned}$$

$$\begin{aligned} Q_{n+1} &= (1+z)Q_n + zC_n \\ &= O(z^{\nu_n+1}) + O(z^{\nu_n+1}) \\ &= O(z^{\nu_{n+1}-1}) && \text{as } \nu_{n+1} = \nu_n + 2 \end{aligned}$$

$$\begin{aligned} C_{n+1} &= (z^2+z)T_n + (1+z)C_n \\ &= z^{\nu_n+2} + o(z^{\nu_n+2}) + O(z^{\nu_n+1}) \\ &= z^{\nu_{n+1}} + o(z^{\nu_{n+1}}) && \text{as } \nu_{n+1} = \nu_n + 2 \end{aligned}$$

Thus, by induction the polynomial $T_n + Q_n + C_n$ has degree ν_n and leading coefficient 1 if n is odd, and ν_n if n is even, which proves the theorem. □

Theorem 4.39. *For a fixed length ℓ, the number of coherent paths of size $n \geq \left\lceil \frac{2}{3}\ell + 1 \right\rceil$ is a polynomial in n of degree $\ell - 3$.*

Proof. Let $v_{n,\ell}$ be the total number of coherent paths of size n and length ℓ, then $V_n = \sum_\ell v_{n,\ell} z^\ell = T_n + Q_n + C_n$. We can compute V_n thanks to the powers of $\mathcal{M}$:

$$V_{n+4} = \begin{pmatrix} 1 & 1 & 1 \end{pmatrix} \mathcal{M}^n \begin{pmatrix} T_4 \\ Q_4 \\ C_4 \end{pmatrix}$$

With the eigenvalues and eigenvectors given above, one can compute:

$$V_{n+4} = \frac{\lambda_+^n - \lambda_-^n}{\sqrt{4z+5}} z^5 + \left(2(\lambda_+^n + \lambda_-^n) + 6\frac{\lambda_+^n - \lambda_-^n}{\sqrt{4z+5}} \right)(z^4 + z^3)$$

Note that as λ_+ and λ_- depend on z. Indeed:

$$\frac{\lambda_+^n - \lambda_-^n}{\sqrt{4z+5}} = \sum_k \binom{n}{2k+1} \left(1 + \frac{3}{2}z\right)^{n-(2k+1)} \left(\frac{5}{4} + z\right)^k z^{2k+1}$$

and

$$\lambda_+^n + \lambda_-^n = 2\sum_k \binom{n}{2k} \left(1 + \frac{3}{2}z\right)^{n-2k} \left(\frac{5}{4} + z\right)^k z^{2k}$$

Not only they are polynomials in z (which was expected as V_n is a polynomial by definition), but we can investigate their coefficients. It allows us to re-write:

$$V_{n+4} = \sum_{(a,b,c)\in\mathbb{N}^3} \alpha_{n,a,b,c} \left(1+\frac{3}{2}z\right)^a \left(\frac{5}{4}+z\right)^b z^c$$

where $\alpha_{n,a,b,c}$ is a sum of binomial coefficient $\binom{n}{f(a,b,c)}$ with f a function of a, b and c. This coefficient is thus a polynomial in n.

By Theorem 4.38, we know that the polynomial V_n has degree $\left\lfloor \frac{3}{2}(n-1) \right\rfloor$, thus for a fixed ℓ, the coefficient of V_n on z^ℓ is non-zero when $n \geq \left\lceil \frac{2}{3}\ell + 1 \right\rceil$. This coefficient can be seen as (a multiple of) the evaluation at $z=0$ of the polynomial $\frac{\partial^\ell}{\partial z^\ell} V_n$. But this derivative is again a sum of (products of) powers of $\left(1+\frac{3}{2}z\right)$, of $\left(\frac{5}{4}+z\right)$ and of z, with no new dependencies in n. Evaluating at $z=0$ gives that $v_{n,\ell}$ is a sum (which coefficients depend on ℓ) of $\binom{n}{f(a,b,c)}$: a polynomial in n.

To obtain the degree of this polynomial, we look for the greatest κ such that $\binom{n}{\kappa}$ appears in the coefficient of z^ℓ. In the developments of both $\frac{\lambda_+^n - \lambda_-^n}{\sqrt{4z+5}}$ and $\left(\lambda_+^n + \lambda_-^n\right)$, remark that κ is the power on the factor z. For a fixed ℓ, the greatest power on the factor z appearing in $\frac{\lambda_+^n - \lambda_-^n}{\sqrt{4z+5}} z^5$ is $\ell - 5$, the greatest in $\left(2(\lambda_+^n + \lambda_-^n) + 6\frac{\lambda_+^n - \lambda_-^n}{\sqrt{4z+5}}\right)(z^4+z^3)$ is $\ell-3$. Thus, the degree of the polynomial $v_{n,\ell}$, as a polynomial in n, is $\ell - 3$. □

Example 4.40. With the help of Proposition 4.36, one can compute the number of coherent paths of size n and length ℓ:

$n\vert\ell$	3	4	5	6	7	8	9	10	11	12	13	14	15
4	4	4											
5	4	16	12	1									
6	4	28	56	38	7								
7	4	40	132	195	129	32	1						
8	4	52	240	556	694	448	129	10					
9	4	64	380	1205	2250	2496	1571	501	61	1			
10	4	76	552	2226	5565	8896	9019	5564	1914	304	13		
11	4	88	756	3703	11627	21416	34622	32725	19881	7236	1375	99	1

In this table, one can read out Theorem 4.38 (for $n \leq 11$) by looking at the right-most value in each line. Furthermore, Theorem 4.39 ensures that each column ℓ is a polynomial in n of degree $\ell - 3$, observing the rows given, the following holds for $n \geq 1$:

- for $\ell = 3$: $v_{n+3,3} = 4$ is also the number of diagonal-avoiding paths of length 3.
- for $\ell = 4$: $v_{n+3,4} = 12n - 8$ is also the number of diagonal-avoiding paths of length 4.
- for $\ell = 5$: $v_{n+4,5} = 4n(4n-1)$ is **not** the number of diagonal-avoiding paths of length 5.
- for $\ell = 6$: $v_{n+5,6} = 14n^3 - 24n^2 + 11n$.
- for $\ell = 7$: $v_{n+6,7} = \frac{1}{6}(55n^4 - 2n^3 - 34n^2 + 23n)$.

And one can easily continue this list with a computer.

4.2.5 Perspectives and open questions

Computational remarks As usual, all the objects present in this section have been implemented with Sage. Namely, I am able to compute monotone path polytopes and label their vertices by the corresponding monotone paths and their normal cones (*i.e.* the cone of $\boldsymbol{\omega}$ that captures the

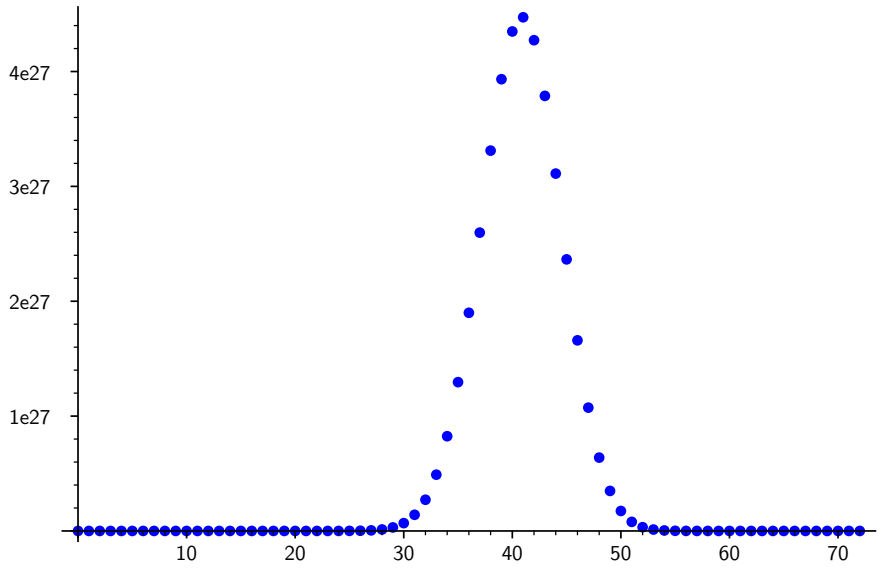

Figure 69: Number of coherent paths on $\Delta(50, 2)$ for length $\ell \in [3, 73]$

corresponding monotone path). Monotone path polytopes are computed as a Minkowski sum of sections, one at each vertex, however the same remark as for max-slope pivot rule polytopes holds: computing Minkowski sums in high dimension and with a lot of vertices takes time.

Furthermore, in the case of the monotone path polytope of the hypersimplices $\Delta(n, 2)$, all numerical statements have been checked by (i) constructing the monotone path polytope and counting its vertices (up to dimension 8); (ii) constructing all possible monotone paths and solving the linear system to know whether it can be captured or not (up to dimension 9); (iii) generating all paths that respect the criterion of Theorem 4.24 and verifying if they are coherent (up to dimension 12); (iv) implementing the matrix recursion (up to dimension 300). Fortunately, all these methods lead to the same result. We also have implemented similar methods for counting the paths by their length.

Besides, the diagonalization of matrices were done with the help of Sage (and latter checked by hand and with Wolfram Alpha), which benefits from excellent and easy-to-use tools to deal with matrices over any rings (especially the ring of symbolic expressions, *i.e.* of polynomials and more).

Assets and limits of the current approach, open questions We have detailed the behavior of $v_{n,\ell}$ for a fixed length ℓ. But on the other side, for a fixed size n, one can look at the sequence $\big(v_{n,\ell}\ ;\ \ell \in [3, \lfloor \frac{3}{2}(n-1) \rfloor]\big)$. Jesús De Loera conjectured the following for all polytopes:

Conjecture 4.41 (De Loera)**.** *For any polytope* P *and generic objective function* $\mathbf{c}$*, the sequence* $\big(N_\ell\ ;\ \ell \geq 1\big)$ *of the number of coherent monotone paths on* P *of length* ℓ *is a log-concave sequence.*

Especially, in our case, this conjectures states that for a fixed dimension n, the sequence $\big(v_{n,\ell}\ ;\ \ell \geq 3\big)$ is log-concave. Thanks to Proposition 4.36, we can compute these sequences for large n, for example $n = 50$ in Figure 69. All the computations done so far tend to confirm this conjecture, in particular it holds true for all $n \leq 150$. Moreover, note that the archetypal sequence $\big(\binom{n}{\ell}\ ;\ \ell \in [0, n]\big)$ is log-concave and shares a property similar to Theorem 4.39: for a fixed ℓ, the value $\binom{n}{\ell}$ is a polynomial in n of degree ℓ. Even though we have not been able to prove this conjecture for hypersimplices $\Delta(n, 2)$, there may be a way to extract this property from the matrix recursion presented in Proposition 4.36.

Moreover, one can count the number of monotone path according to their length (without restricting to coherent monotone paths), which amounts to counting the total number of diagonal-avoiding lattice paths. This exercise of enumerative combinatorics will be carried out in the future. Given the type of combinatorics at stake, it does not seem senseless to think that the sequence of total number of monotone paths will be log-concave, although it remains non-trivial to prove it is.

Besides, Theorem 4.24 gives a necessary criterion for a monotone path on $\Delta(n,k)$ to be coherent. We have shown that this criterion is sufficient for the case $k=2$, but computer experiments shows that is it no longer sufficient when $k \geq 3$. The encoding of monotone paths on $\Delta(n,k)$ through lattice paths on the grid $[n]^k$ seems a good framework for studying this problem further.

Last but not least, we only give here a description of the vertices of $\mathsf{M}(n,2)$, it would be of prime interest to investigate the (higher-dimensional) faces of it. A first idea to do so is to introduce a notion of adjacencies between coherent lattice paths in order to describe the edges of $\mathsf{M}(n,2)$, but the drawings this notion gives birth to are not easy to interpret. A second idea would be to use the fact that faces of the hypersimplex are again hypersimplices (of lower dimensions): one could try to "see" $\mathsf{M}(n-1,k)$ inside $\mathsf{M}(n,k)$, and recover (properties of) the face lattice of $\mathsf{M}(n,k)$ from there. A glimpse of this is depicted in Figures 59 and 60: the 5 octagons appearing in the polytope of the second figure shall be thought of as 5 copies of the octagon on the right of the first figure (but it remains hard to explain where the 16 squares come from, and how the faces fit together).

4.3 Fiber polytopes for the projection from $\mathsf{Cyc}_d(\boldsymbol{t})$ to $\mathsf{Cyc}_2(\boldsymbol{t})$

This section is a joint work with Aenne Benjes and Raman Sanyal. An article is in preparation, containing this section, together with Section 3.2.

We have seen that the study of fiber polytopes has drawn a lot of attention in recent years. They were, at the beginning, constructed in order to give a positive answer to the generalized Baues problem [BS92, Rei99] which can be thought of as the problem of structuring the set of subdivisions of a given polytope. From there, fiber polytopes made an appearance in a myriad of domains, ranging from linear optimization up to triangulations, and the search for a category of polytopes. We have already discussed their link with linear programming in Section 4.2, and briefly mentioned the longing for a category of polytope in Section 4.1, and we emphasize here their relationship with triangulations.

In particular, the secondary polytope introduced by Gelfand, Kapranov and Zelevinsky [GKZ90, GKZ91] (see also [BFS90]) encapsulates (regular) triangulations of a point configuration into the vertices of a polytope. It is worth noting that when the points of the configuration are in convex position, *i.e.* when looking at a polytope, the secondary polytope is (a dilation of) the fiber polytope for the projection of a simplex onto these points. In this context, the associahedron again appears, as the secondary polytope of a polygon [DRS10, Chapter 5]. Polygons and simplices are the two extreme cases of cyclic polytopes, so the aim of the section is to factor the projection from a simplex onto a polygon by an intermediate projection from a cyclic polytope onto a polygon: for $\boldsymbol{t} = (t_1, \dots, t_n)$, one consider the sequence of projections $\mathsf{Cyc}_n(\boldsymbol{t}) \to \mathsf{Cyc}_d(\boldsymbol{t}) \to \mathsf{Cyc}_2(\boldsymbol{t})$ where $\mathsf{Cyc}_n(\boldsymbol{t}) \simeq \Delta_n$ and $\mathsf{Cyc}_2(\boldsymbol{t})$ is a n-gon (and $2 \leq d \leq n$). The vertices of the fiber polytope for the projection $\mathsf{Cyc}_d(\boldsymbol{t}) \to \mathsf{Cyc}_2(\boldsymbol{t})$ will naturally associate to triangulations of $\mathsf{Cyc}_2(\boldsymbol{t})$, prompting a notion of degree on triangulation (and hence Catalan families). This way, we will analyze a fiber polytope that is not a monotone path polytope (projection onto a segment), nor a secondary polytope (projection from a simplex), but a more general case.

It is not an accident that the present framework resemble the one of Section 3.2: even if the motivations and context are different, the tools and techniques developed are the same, and the results similar. We will widely reuse the material of this section and the ideas of [ALRS00] who began the exploration of fiber polytopes between cyclic polytopes. The present section starts with a short preliminary on triangulations (Section 4.3.1), gathering the useful vocabulary and constructing the bijection from triangulations to non-crossing arborescences. We pursue with the main result (Section 4.3.2) that determines how to know if a triangulation appears or not as a vertex of the fiber polytope for the projection $\mathsf{Cyc}_d(\boldsymbol{t}) \to \mathsf{Cyc}_2(\boldsymbol{t})$, and we then focus on the case $d = 4$ (Section 4.3.3). Again, quite surprisingly, we obtain that the number of vertices of the fiber polytope $\Sigma_\pi(\mathsf{Cyc}_4(\boldsymbol{t}), \mathsf{Cyc}_2(\boldsymbol{t}))$ is $\binom{n}{2} - 1$, independently of $\boldsymbol{t}$, see Theorem 4.60.

4.3.1 Bijection between triangulations and non-crossing arborescences

Triangulations of a $(n+1)$-gon and non-crossing arborescences on n nodes are both Catalan families, as presented in Section 1.2.4. We exhibit an explicit bijection between these families that will allow us to link fiber polytope for the projection from $\mathsf{Cyc}_d(\boldsymbol{t})$ to $\mathsf{Cyc}_2(\boldsymbol{t})$ and cyclic associahedra $\Pi^d_{\boldsymbol{t}}$ of Section 3.2.

A vast study of triangulations, adorned by plenty of figures, can be found in [LRS10], especially Chapters 3 and 5 for what concerns us here.

Definition 4.42. Let P be a $(n+1)$-gon whose vertices are labelled clockwise from 0 to n in circular order. A *triangle* in P is a triplet of distinct indices $\delta = (i, j, k) \in [0, n]^3$ with $i < j < k$. Such a triangle splits the (cyclic) interval $[n]$ into three *pieces of circle*: $[i, j]$, $[j, k]$ and $[k, n] \cup [0, i]$. Two triangles δ_1, δ_2 in P don't intersect when all three indices of δ_2 belong to the same piece of circle of δ_1. A *triangulation* T of P is a family of $n-1$ (pairwise) non-intersecting triangles, see Figure 70 ($n-1$ being the maximum number of non-intersecting triangles that a $(n+1)$-gon can welcome).

An *edge* of a triangulation T is a couple (x, y) with $x < y$ that appears in a triangle of T: $(x, y) \subset \delta$ for some $\delta \in T$. An edge (x, y) is *exterior* when $y = x + 1$ or $(x, y) = (0, n)$ (meaning

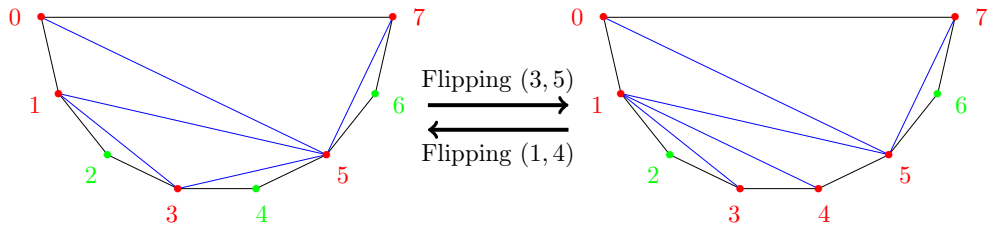

Figure 70: (Left) The triangulation $T = \big((0,5,7),(0,1,5),(1,3,5),(1,2,3),(3,4,5),(5,6,7)\big)$. Its 8 exterior edges are in black, while its 5 interior ones are in blue. It has 2 positive quadrangles and 3 negative ones: $Q^+(T) = \big((0,1,5,7),(1,2,3,5)\big)$ and $Q^-(T) = \big((0,1,3,5),(0,5,6,7),(1,3,4,5)\big)$. Its immediate vertices are in green: $\mathbb{L}(T) = \{2,4,6\}$. Flipping the edge $(3,5)$ gives the triangulation T' on the Right. The new quadrangles are $Q^+(T') = \big((0,1,5,7),(1,3,4,5),(1,2,3,4)\big)$ and $Q^-(T') = \big((0,5,6,7),(0,1,4,5)\big)$, and new immediate vertices are $\mathbb{L}(T') = \{2,6\}$. Flipping the edge $(1,4)$ in T' gives back T.

it is an edge of the polygon P), *interior* otherwise. We denote by $E(T)$ the set of edges of T and $E^\circ(T)$ the set of interior edges of T. Note that in a triangulation, interior edges appear in exactly two triangles, while exterior ones appear in exactly one triangle.

A *quadrangle* in a triangulation T is a quadruplet of indices $\kappa = \delta_1 \cup \delta_2$ corresponding to two adjacent triangles $\delta_1, \delta_2 \in T$, *i.e.* $|\kappa| = 4$. The *edge e_κ of the quadrangle κ* is the (interior) edge shared by the two adjacent triangles. Note that $\kappa \mapsto e_\kappa$ is a bijection between interior edges $E^\circ(T)$ and the set of quadrangles of T. A quadrangle (i,j,k,l) is *positive* when its edge is (i,k), and *negative* when its edge is (j,l). The family of positive quadrangles is denoted $Q^+(T)$, and the family of negative ones $Q^-(T)$.

A *flip* in a triangulation T consists in removing one interior edge and adding back the only other interior edge possible. Namely, if $(x,y) \in E^\circ(T)$, then (x,y) belongs to two triangles, forming a quadrangle κ: flipping (x,y) amounts to changing κ from positive to negative or the reverse (the Tamari orientation consists in changing from negative to positive). This changes one edge, two triangles and at most five quadrangles. It is well known that the graph of flips of the triangulations of a $(n+1)$-gon is precisely the graph of the associahedron Asso_{n-1}.

An *immediate vertex* of T is some index $\ell \in [n-1]$ such that $(\ell-1, \ell, \ell+1) \in T$. When immediate vertices, 1 and $n-1$ are called *exterior*, while other immediate vertices are called *interior* ones. We denote by $\mathbb{L}(T)$ the set of all immediate vertices of T, and by $\mathbb{L}^\circ(T)$ the set of interior ones.

The corresponding super-Catalan family is the family of all subdivisions of P.

There is a very easy way to construct a bijection from the set of triangulations of a $(n+1)$-gon to the set of non-crossing arborescences on n nodes:

Proposition 4.43. *Let T be a triangulation of a $(n+1)$-gon and $E(T)$ its set of edges. Then the map $A_T : [n-1] \to [n-1]$ defined by $A_T(i) = \max\{j \ ; \ j > i \text{ and } (i,j) \in E(T)\}$ is a non-crossing arborescence on n nodes[16], see Figure 71. The application $T \mapsto A_T$ is a bijection between the set of triangulations of a $(n+1)$-gon and the set of non-crossing arborescences on n nodes.*[17]

Proof. First, notice that $T \mapsto A_T$ sends a triangulation of a $(n+1)$-gon to a non-crossing arborescence on n nodes. Indeed, edges of A_T are (some) edges of T, so if A_T were crossing, then two triangles of T would intersect. Furthermore, flipping the edge (j,l) in a negative quadrangle (i,j,k,l) of T changes the (j,l) in A_T to (j,k) because of the non-intersecting property: flips for triangulations correspond to flips for non-crossing arborescences. Thus, the application $T \mapsto A_T$

[16] As usual, it shall be complete with $A_T(n) = n$.
[17] Triangulations are defined on $[0,n]$ while arborescences are defined on $[1,n]$: 0 is not mapped by A_T.

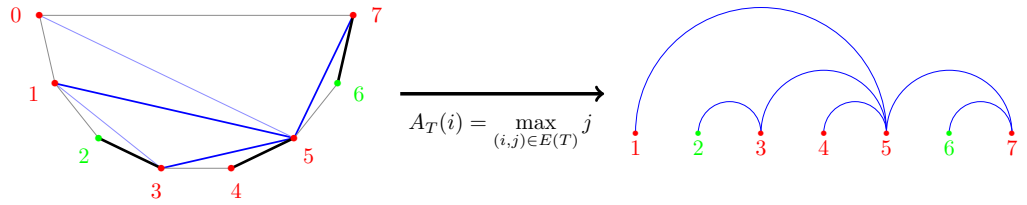

Figure 71: The bijection $T \mapsto A_T$ between triangulations of a $(n+1)$-gon and non-crossing arborescences on n nodes. (Left) In bold are drawn the edges of the triangulation kept in the non-crossing arborescence.

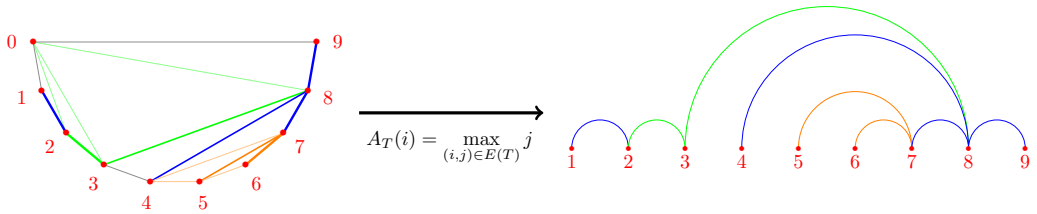

Figure 72: In the left triangulation T, the positive quadrangle $(0,2,3,8) \in Q^+(T)$ is sent to the forward-sliding node $2 \in \mathcal{I}^f_{A_T}$, while the negative quadrangle $(4,5,6,7) \in Q^-(T)$ is sent to the backward-sliding node $5 \in \mathcal{I}^b_{A_T}$.

is surjective as the graph of flips of non-crossing arborescences is connected. As the numbers of triangulations of a $(n+1)$-gon and the number of non-crossing arborescences on n nodes is the same, $T \mapsto A_T$ is a bijection. □

Note that, in particular, immediate vertices of T are sent bijectively through the bijection $T \mapsto A_T$ to immediate leaves of A_T. We refer to Section 3.2.2 for the definitions of forward- and backward-sliding nodes (and consort).

Lemma 4.44. *Let T be triangulation and A_T the associated non-crossing arborescence. Positive quadrangles of T are sent bijectively to forward-sliding nodes A_T through $(i,j,k,l) \mapsto j$; and negative quadrangles of T are sent bijectively to backward-sliding nodes A_T through $(i,j,k,l) \mapsto j$, see Figure 72.*

Proof. Fix $(i,j,k,l) \in Q^+(T)$. Then $k = \max\{y \ ; \ (j,y) \in E(T)\}$ because otherwise (j,y) would cross the edge (i,k). Thus $A_T(j) = k$. Besides $l = \max\{y \ ; \ (k,y) \in E(T)\}$ because otherwise (k,y) would cross the edge (i,l). Thus $A_T(k) = l$. Finally, an edge (a,k) with $a < j$ would cross either the edge (i,j) or the edge (i,l). So $j = \min\{x \ ; \ A_T(x) = k\}$, which fulfills the definition for $j \in \mathcal{I}^f_{A_T}$.

The proof is similar for the negative quadrangles. As $|Q^+(T)|+|Q^-(T)| = n-1 = |\mathcal{I}^f_{A_T}|+|\mathcal{I}^b_{A_T}|$, the two bijections holds. □

4.3.2 Fiber polytopes for the projection $\mathsf{Cyc}_d(\boldsymbol{t}) \xrightarrow{\pi} \mathsf{Cyc}_2(\boldsymbol{t})$

In the remaining of this section, we present some new results on a family of fiber polytopes associated to cyclic polytopes. These results extend the one of [ALRS00]. It will be the opportunity to use the tools and ideas developed in Section 3.2.

In the latter, we designated the order cone by $\mathsf{O}_n = \{\boldsymbol{t} \in \mathbb{R}^n \ ; \ t_1 \le \cdots \le t_n\}$. In what follows, we will slightly abuse notations: for a fixed $n \ge 1$, if $\boldsymbol{t} \in \mathsf{O}_{n+1}$, then its coordinates will be denoted $\boldsymbol{t} = (t_0, t_1, \ldots, t_n)$, and triangulations will be on a $(n+1)$-gon ; while if $\boldsymbol{t} \in \mathsf{O}_n$, then

its coordinates will be denoted $\boldsymbol{t} = (t_1, \dots, t_n)$ and non-crossing arborescences will take place on n nodes.

Definition 4.45. For $d \geq 2$ and $\boldsymbol{t} \in \mathsf{O}^\circ_{n+1}$, the *fiber associahedron* $\Sigma^d_2(\boldsymbol{t})$ is the fiber polytope $\Sigma_\pi(\mathsf{Cyc}_d(\boldsymbol{t}), \mathsf{Cyc}_2(\boldsymbol{t}))$ where π is the projection that forgets all but the two first coordinates: $\pi(\boldsymbol{x}) = (\langle \boldsymbol{x}, \boldsymbol{e}_1 \rangle\,,\ \langle \boldsymbol{x}, \boldsymbol{e}_2 \rangle)$.

By Corollary 4.10, $\Sigma^d_2(\boldsymbol{t})$ is a projection of the secondary polytope $\Sigma(\mathsf{Cyc}_2(\boldsymbol{t}))$. As $\mathsf{Cyc}_2(\boldsymbol{t})$ is a polygon with n vertices, its secondary polytope $\Sigma(\mathsf{Cyc}_2(\boldsymbol{t}))$ is an associahedron Asso_{n-2}, see [LRS10]. For $\boldsymbol{t} \in \mathsf{O}^\circ_{n+1}$, as vertices of $\Sigma(\mathsf{Cyc}_2(\boldsymbol{t}))$ are naturally associated to triangulations of $\mathsf{Cyc}_2(\boldsymbol{t})$, one can associate a triangulation to each vertex of $\Sigma^d_2(\boldsymbol{t})$. We now establish a criterion for a triangulation to be associated to a vertex of $\Sigma^d_2(\boldsymbol{t})$.

Proposition 4.46. *For $(i,j,k,l) \in [0,n]^4$ with $i<j<k<l$, $\boldsymbol{t} \in \mathsf{O}^\circ_n$ and a polynomial P, we denote*

$$\tau(i,j,k,l) = \det \begin{pmatrix} 1 & 1 & 1 & 1 \\ t_i & t_j & t_k & t_l \\ t_i^2 & t_j^2 & t_k^2 & t_l^2 \\ P(t_i) & P(t_j) & P(t_k) & P(t_l) \end{pmatrix}$$

For $\boldsymbol{t} \in \mathsf{O}^\circ_{n+1}$ and $d \geq 2$, a triangulation T of $\mathsf{Cyc}_2(\boldsymbol{t})$ corresponds to a vertex of $\Sigma^d_2(\boldsymbol{t})$ if and only if there exists a polynomial P of degree at most d such that $\tau(\kappa) > 0$ for all $\kappa \in Q^+(T)$ and $\tau(\kappa) < 0$ for all $\kappa \in Q^-(T)$.

When these conditions are satisfied, we say that P captures the triangulation T on $\boldsymbol{t}$.

To prove this property, we need a classical lemma, of which we give a short proof for the sake of completeness.

Lemma 4.47. *For a 3-dimensional polytope P with vertices $\boldsymbol{v}_0 = \begin{pmatrix} x_0 \\ y_0 \\ z_0 \end{pmatrix}, \dots, \boldsymbol{v}_n = \begin{pmatrix} x_n \\ y_n \\ z_n \end{pmatrix}$, a triangle (i,j,k) corresponds to a lower face of P if and only if, for all $l \in [0,n] \smallsetminus \{i,j,k\}$ one has:*

$$\det \begin{pmatrix} 1 & 1 & 1 & 1 \\ x_i & x_j & x_k & x_l \\ y_i & y_j & y_k & y_l \\ z_i & z_j & z_k & z_l \end{pmatrix} > 0$$

Proof of Lemma 4.47. The positivity of this determinant is equivalent to the fact that $\boldsymbol{v}_l \in H^+_{(i,j,k)}$ where $H_{(i,j,k)}$ is the plane of $\mathbb{R}^3$ containing the points $\boldsymbol{v}_i$, $\boldsymbol{v}_j$ and $\boldsymbol{v}_k$. □

Proof of Proposition 4.46. Fix $\boldsymbol{t} \in \mathsf{O}^\circ_{n+1}$. By Theorem 4.6, vertices of $\Sigma^d_2(\boldsymbol{t})$ are in bijection with π-coherent triangulations of $\mathsf{Cyc}_2(\boldsymbol{t})$. Pick $\boldsymbol{w} = (w_1, ..., w_d) \in \mathbb{R}^d$ generic with respect to $\mathsf{Cyc}_d(\boldsymbol{t})$ and construct $\pi^{\boldsymbol{w}} : \boldsymbol{x} \mapsto \begin{pmatrix} \pi(\boldsymbol{x}) \\ \langle \boldsymbol{w}, \boldsymbol{x} \rangle \end{pmatrix}$ as in Definition 4.4. Then the vertices of $\pi^{\boldsymbol{w}}(\mathsf{Cyc}_d(\boldsymbol{t}))$ come from vertices $\boldsymbol{\gamma}_d(t_i)$ of $\mathsf{Cyc}_d(\boldsymbol{t})$: they are thus of the form $p_i := \begin{pmatrix} t_i \\ t_i^2 \\ \langle \boldsymbol{w}, \boldsymbol{\gamma}_d(t_i) \rangle \end{pmatrix}$. Denoting $P(t) = w_1 t + \cdots + w_d t^d$, one has $\langle \boldsymbol{w}, \boldsymbol{\gamma}_d(t_i) \rangle = P(t_i)$. The family of lower faces of $\pi^{\boldsymbol{w}}(\mathsf{Cyc}_d(\boldsymbol{t}))$ projects down to a triangulation of $\mathsf{Cyc}_2(\boldsymbol{t})$ (by forgetting the last coordinate).

Consequently, a triangulation T of $\mathsf{Cyc}_2(\boldsymbol{t})$ appears as such a projection if and only if there exists a polynomial P of degree at most d satisfying that for all triangle $\delta = (j,k,l) \in T$, the points $\boldsymbol{p}_j, \boldsymbol{p}_k, \boldsymbol{p}_l$ are the vertices of a lower face of $\mathrm{conv}\{\boldsymbol{p}_i \ ;\ i \in [0,n]\}$. By Lemma 4.47, this amount to having $\tau(j,k,l,m) > 0$ for all $m \in [0,n] \smallsetminus \{j,k,l\}$.

In the associahedron Asso_{n-2}, the vertex associated with T is adjacent to the vertices associated with the triangulations T' obtained by flipping any quadrangle in T. Hence, by convexity, it is

equivalent to test the positivity of $\tau(j,k,l,m)$ for (j,k,l,m) a quadrangle of T, than to test the positivity of $\tau(j,k,l,m)$ for all $(j,k,l) \in T$ and $m \in [0,n] \smallsetminus \{j,k,l\}$.

Thus, by re-ordering the columns of the determinant $\tau(\kappa)$, the triangulation T appears if and only P satisfies that $\tau(\kappa) > 0$ for all $\kappa \in Q^+(T)$ and $\tau(\kappa) < 0$ for all $\kappa \in Q^-(T)$. □

The above Proposition 4.20 gives a simple criterion for determining the triangulation captured by a polynomial on a given $\boldsymbol{t}$. Also, Lemma 4.47 ensures that if P captures T on $\boldsymbol{t}$, then we know the value of $\tau(i,j,k,l)$ for all quadruples $(i,j,k,l) \in [0,n]^4$, not only for the quadrangles of T.

Recall from Section 3.2.2 the complete symmetric polynomial of degree s on 4 variables:

$$h_s(X,Y,Z,U) = \sum_{a+b+c+d=s} X^a Y^b Z^c U^d$$

For a quadrangle $\kappa = (i,j,k,l)$ in a triangulation T and $\boldsymbol{t} \in \mathsf{O}^\circ_{n+1}$, we construct $\Omega^d_\kappa(\boldsymbol{t}) \in \mathbb{R}^d$ defined by $\Omega^d_\kappa(\boldsymbol{t})_s = h_{s-3}(t_i,t_j,t_k,t_l)$, together with $\overline{\Omega}^d_\kappa(\boldsymbol{t}) = \big(h_s(t_i,t_j,t_k,t_l)\big)_{s=1,\dots,d-3} \in \mathbb{R}^{d-2}$. As for Theorem 3.16, these points allow us to reformulate Proposition 4.46 into a more handy criterion, that hinges on intersection of polytopes.

Theorem 4.48. *For $\boldsymbol{t} \in \mathsf{O}^\circ_{n+1}$, a triangulation T of $\mathsf{Cyc}_2(\boldsymbol{t})$ can be captured on $\boldsymbol{t}$ if and only if the following polytopes **do not** intersect:*

$$\mathsf{Q}^+_d(T,\boldsymbol{t}) = \operatorname{conv}\left\{\overline{\Omega}^d_\kappa(\boldsymbol{t}) \ ; \ \kappa \in Q^+(T)\right\} \quad \text{and} \quad \mathsf{Q}^-_d(T,\boldsymbol{t}) = \operatorname{conv}\left\{\overline{\Omega}^d_\kappa(\boldsymbol{t}) \ ; \ \kappa \in Q^-(T)\right\}$$

Proof. Fix $\boldsymbol{t} \in \mathsf{O}^\circ_{n+1}$. A triangulation T can be captured on $\boldsymbol{t}$ if and only if there exists $P(t) = w_d t^d + \cdots + w_1 t$ such that $\tau(\kappa) > 0$ for all $\kappa \in Q^+(T)$, and $\tau(\kappa) < 0$ for all $\kappa \in Q^-(T)$. One gets:

$$\tau(\kappa) = \sum_{s=1}^{d} w_s \det \begin{pmatrix} 1 & 1 & 1 & 1 \\ t_i & t_j & t_k & t_l \\ t_i^2 & t_j^2 & t_k^2 & t_l^2 \\ t_i^s & t_j^s & t_k^s & t_l^s \end{pmatrix} = \mathrm{VdM}_4(t_i,t_j,t_k,t_l) \sum_{s=1}^{d} w_s h_{s-3}(t_i,t_j,t_k,t_l)$$

The first equality comes from the linearity of the determinant. Besides, the above determinant appears in the definition of a Schur function (through the Jacobi's bialternant formula, see [SF99, Chapter 15]): it equals $s_{(s-3,0,\dots,0)}(\boldsymbol{t})\ \mathrm{VdM}_4(\boldsymbol{t})$ with the Vandermonde determinant $\mathrm{VdM}_4(t_i,t_j,t_k,t_l) = (t_l-t_k)(t_l-t_j)(t_l-t_i)(t_k-t_j)(t_k-t_i)(t_j-t_i)$. Thanks to the first Jacobi-Trudi formula, we obtain the second equality.

As $\mathrm{VdM}_4(t_i,t_j,t_k,t_l) > 0$ (as $i<j<k<l$ and $\boldsymbol{t} \in \mathsf{O}^\circ_{n+1}$), the existence of P amounts to the existence of a solution $\boldsymbol{w}$ to the system $\sum_s w_s h_{s-3}(\kappa) > 0$ if κ is positive, and negative respectively. By Gordan's lemma, this is equivalent to the existence of a $\lambda_\kappa \geq 0$, for all κ, non-identically zero, satisfying

$$\sum_{\kappa \in Q^+(T)} \lambda_\kappa \Omega^d_\kappa(\boldsymbol{t}) = \sum_{\kappa \in Q^-(T)} \lambda_\kappa \Omega^d_\kappa(\boldsymbol{t})$$

Since $\Omega^d_\kappa(\boldsymbol{t})_2 = 1$, it follows that $\Lambda = \sum_{\kappa \in Q^+(T)} \lambda_\kappa = \sum_{\kappa \in Q^-(T)} \lambda_\kappa > 0$. Dividing both sides of the previous equation by Λ yields a point in $\mathsf{Q}^+_d(T,\boldsymbol{t}) \cap \mathsf{Q}^-_d(T,\boldsymbol{t})$. □

Once defined the notion of capturing a triangulation, we can define the degree of a triangulation and its realization set, mirroring the ones of non-crossing arborescences. Even if it will be slightly confusing at first glance, we adopt the same notations for triangulations and non-crossing arborescences, as the ideas concerning them are too akin to be distinguished by new notations.

Definition 4.49. Let T be a triangulation of a $(n+1)$-gon.

For $\boldsymbol{t} \in \mathsf{O}^\circ_{n+1}$, the *degree* of T on $\boldsymbol{t}$ is $\mu(T,\boldsymbol{t}) = \min\{\deg P \ ; \ T \text{ is captured by } P \text{ on } \boldsymbol{t}\}$. The *intrinsic degree* of T is $\mu(T) = \min\{\mu(T,\boldsymbol{t}) \ ; \ \boldsymbol{t} \in \mathsf{O}^\circ_{n+1}\}$.

For $d \geq 2$, the *realization set* of T of degree d is $\mathcal{T}^\circ_d(T) = \{\boldsymbol{t} \in \mathsf{O}^\circ_{n+1} \ ; \ \mu(T,\boldsymbol{t}) \leq d\}$.

A triangulation T is *universal* when $\mathcal{T}^\circ_{\mu(T)} = \mathsf{O}^\circ_{n+1}$.

These notions respect the same straightforward properties as their counterparts for non-crossing arborescences. For all $\boldsymbol{t} \in \mathsf{O}^\circ_{n+1}$, one has $\mu(T, \boldsymbol{t}) \leq n+1$, and consequently $\mu(T) \leq n+1$. Indeed, if $d \geq n+1$, then $\mathsf{Cyc}_d(\boldsymbol{t})$ is a simplex and $\Sigma_2^d(\boldsymbol{t})$ is combinatorially isomorphic to the secondary polytope $\Sigma(\mathsf{Cyc}_2(\boldsymbol{t}))$: an associahedron.

For $d \geq 2$, the closure $\mathcal{T}_d(T)$ of $\mathcal{T}_d^\circ(T)$ is a (generally non-polyhedral and even non-convex) full-dimensional subcone of the order cone O_{n+1}, because if T can be captured on $\boldsymbol{t} \in \mathsf{O}^\circ_{n+1}$, then by translation, T can be captured on $(t_0 + c, \dots, t_n + c)$ for all $c \in \mathbb{R}$, and on $\lambda \boldsymbol{t}$ for $\lambda > 0$, by a polynomial of the same degree. Furthermore, the definition ensures that:

$$\mathcal{T}_3(T) \subseteq \mathcal{T}_4(T) \subseteq \cdots \subseteq \mathcal{T}_{n+1}(T) = \mathsf{O}_{n+1}$$

In addition, Theorem 4.48 gives the following powerful reformulation.

Proposition 4.50. *Let T be a triangulation of a $(n+1)$-gon. One has, for $\boldsymbol{t} \in \mathsf{O}^\circ_{n+1}$ and $d \geq 3$: $\mu(T, \boldsymbol{t}) = \min\{d \ ; \ \mathsf{Q}_d^+(T, \boldsymbol{t}) \cap \mathsf{Q}_d^-(T, \boldsymbol{t}) = \varnothing\}$, and $\mathcal{T}_d^\circ(T) = \{\boldsymbol{t} \ ; \ \mathsf{Q}_d^+(T, \boldsymbol{t}) \cap \mathsf{Q}_d^-(T, \boldsymbol{t}) = \varnothing\}$.*

Beside these properties, $\mu(T, \boldsymbol{t})$ and $\mu(T)$ are hard to describe: Theorem 4.48 gives a nice way to check whether a triangulation can be captured in some degree, but no mean to estimate the minimal degree after which it becomes possible. In particular, note that the coordinates of $\mathsf{Q}_d^+(T, \boldsymbol{t})$ and $\mathsf{Q}_d^-(T, \boldsymbol{t})$ are polynomials of degree up to $d-3$, thus it is simple to study the case $d = 4$, but when $d \geq 5$ deciding if their intersection is empty becomes as hard as deciding if there exists a solution to a certain polynomial system (of degree at least $d-3$). In the following part of this section, we focus on the case $d = 4$.

4.3.3 Realization sets and universal triangulations for $\mathsf{Cyc}_4(\boldsymbol{t}) \xrightarrow{\pi} \mathsf{Cyc}_2(\boldsymbol{t})$

In this section, we study the fiber polytope $\Sigma_2^4(\boldsymbol{t}) = \Sigma_\pi(\mathsf{Cyc}_4(\boldsymbol{t}), \mathsf{Cyc}_2(\boldsymbol{t}))$ for $\boldsymbol{t} \in \mathsf{O}^\circ_{n+1}$ where $\pi : \mathbb{R}^4 \to \mathbb{R}^2$ is the projection forgetting all but the two first coordinates. These results extend the last example of [ALRS00]. In particular, we give a complete characterization of which triangulations of a $(n+1)$-gon can be associated to a vertex of $\Sigma_2^d(\boldsymbol{t})$ for some $\boldsymbol{t} \in \mathsf{O}^\circ_{n+1}$, then we describe their realization sets, state which of them are universal, and conclude on the number of vertices of $\Sigma_2^d(\boldsymbol{t})$. Even though the computations of the present section are different from the ones of Section 3.2, the ideas behind them clearly look alike. Note however that there seems not to be a straightforward way to deduce the following results from the theorems of Section 3.2: we will see in Example 4.61 an example indicating that cyclic associahedra and fiber associahedra are indeed dissimilar.

Even though it will not be at the center of our proofs, the bijection $T \mapsto A_T$ between triangulations of a $(n+1)$-gon will help us get a better understanding of the notions at stake. Indeed, we will prove that this bijection induces a bijection between:

(i) Triangulations T with $\mu(T) = 3$ and non-crossing arborescences A with $\mu(A) = 2$ (Corollary 4.52(i)).
(ii) Triangulations T with $\mu(T) = 4$ and non-crossing arborescences A with $\mu(A) = 3$ (Theorem 4.55).
(iii) Universal triangulations T with $\mu(T) = 4$ and universal non-crossing arborescences A with $\mu(A) = 3$ (Corollary 4.54).

Nevertheless, this bijection is not a magic wand! Some powerful properties are not shared between cyclic associahedra and fiber associahedra, in particular:

(a) We don't have a theorem that characterizes $\mu(T)$ in terms of $\mathbb{L}(T)$ and $\mathbb{L}^\circ(T)$ (a twin to Corollary 3.13). In particular, we don't know if there exists a triangulation T such that $\mu(T) = 6$ but $\mu(A_T) = 4$.
(b) The vertices of $\Sigma_2^4(\boldsymbol{u})$ for $\boldsymbol{u} \in \mathsf{O}^\circ_{n+1}$ correspond to a family of triangulations, but the associated family of non-crossing arborescences does not necessarily correspond to the vertices of $\Pi_{\boldsymbol{t}}^3$ for any $\boldsymbol{t} \in \mathsf{O}^\circ_{n+1}$, see Example 4.61.

We first would like to show that triangulations T with $|\mathbb{L}(T)| + |\mathbb{L}^\circ(T)| \leq 2$ are exactly the ones satisfying $\mu(T) \leq 4$. We will prove this in two steps. We first state one inclusion, and postpone the reciprocal for later (see Theorem 4.55).

Proposition 4.51. *For a triangulation T of a $(n+1)$-gon: if $\mu(T) \leq 4$ then $|\mathbb{L}(T)| + |\mathbb{L}^\circ(T)| \leq 2$.*

Proof. Fix a triangulation T captured by $P(t) = w_1 t + w_2 t^2 + w_3 t^3 + w_4 t^4$ on $\boldsymbol{t} \in \mathsf{O}^\circ_{n+1}$. Suppose that $|\mathbb{L}(T)| + |\mathbb{L}^\circ(T)| > 2$, then either $|\mathbb{L}^\circ(T)| \geq 2$, or $\mathbb{L}(T) \cap \{1, n-1\} \neq \varnothing$ and $\mathbb{L}^\circ(T) \neq \varnothing$.

Suppose $|\mathbb{L}^\circ(T)| \geq 2$. Let $\ell \in \mathbb{L}^\circ(T)$. For $a < \ell - 1$ and $b > \ell + 1$, Lemma 4.47 ensures that:

$$\tau(\ell-1, \ell, \ell+1, a) > 0 \quad \text{and} \quad \tau(\ell-1, \ell, \ell+1, b) > 0$$

Giving:

$$\begin{cases} \mathrm{VdM}_4(t_{\ell-1}, t_\ell, t_{\ell+1}, t_a) \big(w_4(t_{\ell-1} + t_\ell + t_{\ell+1} + t_a) + w_3\big) & > & 0 \\ \mathrm{VdM}_4(t_{\ell-1}, t_\ell, t_{\ell+1}, t_b) \big(w_4(t_{\ell-1} + t_\ell + t_{\ell+1} + t_b) + w_3\big) & > & 0 \end{cases} \quad \text{and}$$

As $a < \ell - 1 < \ell < \ell + 1 < b$, the signs of the Vandermonde determinants give:

$$w_4(t_{\ell-1} + t_\ell + t_{\ell+1} + t_a) + w_3 < 0 \quad \text{and} \quad w_4(t_{\ell-1} + t_\ell + t_{\ell+1} + t_b) + w_3 > 0$$

But if $m \in \mathbb{L}^\circ(T)$ with $\ell < m$, then $w_4(t_{\ell-1} + t_\ell + t_{\ell+1} + t_m) + w_3 > 0$ as $\ell \in \mathbb{L}^\circ(T)$, and $w_4(t_{m-1} + t_m + t_{m+1} + t_\ell) + w_3 < 0$ as $m \in \mathbb{L}^\circ(T)$. But $t_{\ell-1} \leq t_{m-1}$ and $t_{\ell+1} \leq t_{m+1}$, so $w_4(t_{\ell-1} + t_\ell + t_{\ell+1} + t_m) + w_3 < w_4(t_{m-1} + t_m + t_{m+1} + t_\ell) + w_3$, which contradicts the signs of each side.

The same ideas apply when $\{1, n-1\} \cap \mathbb{L}(T) \neq \varnothing$ and $\mathbb{L}^\circ(T) \neq \varnothing$. □

The above theorem can be reformulated in saying that $T \mapsto A_T$ injects the family of triangulations T with $\mu(T) \leq 4$ into the family of non-crossing arborescences A with $\mu(A) \leq 3$. This allows us to give a description of the triangulations with $\mu(T) \leq 4$.

Corollary 4.52. *If T is a triangulation with $\mu(T) \leq 4$, then T falls in one of the following cases:*

(i) The triangulations T_m with interior edges $E^\circ(T_m) = \{(0,i)\ ;\ i \in [n-1]\}$, and T_M with interior edges $E^\circ(T_M) = \{(i,n)\ ;\ i \in [n-1]\}$. These are the only 2 triangulations with $\mu(T) = 3$. Note that $\mathbb{L}(T_m) = \{1\}$ and $\mathbb{L}(T_M) = \{n-1\}$.

(ii) For $1 < k < n-1$, triangulations with triangles $(0, i, i+1)$ for $i < k$, $(0, k, n)$, and $(i, i+1, n)$ for $i \geq k$. These are $n-1$ triangulations with $\mathbb{L}(T) = \{1, n-1\}$.

(iii) For $1 < \ell < n-2$, triangulations with $(\ell-1, \ell+1) \in E^\circ(T)$ and all $(x,y) \in E^\circ(T)$ satisfy $x < \ell < y$. These are $2^n - 2$ triangulations with $\mathbb{L}(T) = \{\ell\}$.

Proof. For (i), note that $Q^-(T_m) = \varnothing$ and $Q^+(T) = \big((0, i, i+1, i+2)\ ;\ i \in [n-2]\big)$, so Theorem 4.48 ensures that T_m can be captured on any $\boldsymbol{t}$ by a degree 3 polynomial, as $\mathsf{Q}_4^-(T_m, \boldsymbol{t}) = \varnothing$ (so the intersection is empty). The case of T_M is identical.

For (ii) and (iii), note that all triangulations (on a polygon of any number of vertices) have an immediate leave, by induction. If $\ell \in \mathbb{L}^\circ(T)$, and $(x,y) \in E^\circ(T)$ with $\ell \notin [x,y]$, then the sub-triangulation $T\big|_{[x,y]}$ is the triangulation of some polygon: there is an immediate leaf $m \in \mathbb{L}^\circ(T)$ with $x \leq m \leq y$, so $m \neq \ell$. Consequently, if $\mu(T) \leq 4$, then Proposition 4.51 implies that T is of the form (ii) or (iii). □

In the rest of this section, we give a description of the realization sets for triangulations T with $\mu(T) \leq 4$, and the characterization of universal triangulations.

Lemma 4.53. *Let T be a triangulation of a $(n+1)$-gon with $\mu(T) = 4$ and $\mathbb{L}(T) = \{\ell\}$, $1 < \ell < n-1$. Then $\mu(T, \boldsymbol{t}) = 4$ for all $\boldsymbol{t} \in \mathsf{O}^\circ_{n+1}$ satisfying:*

$$\max\{t_i + t_j + t_k + t_l\ ;\ (i,j,k,l) \in Q^-(T)\} \ < \ \min\{t_i + t_j + t_k + t_l\ ;\ (i,j,k,l) \in Q^+(T)\}$$

Proof. By Theorem 4.48, we know that T can be captured on $\boldsymbol{t} \in \mathsf{O}^\circ_{n+1}$ by a polynomial of degree 4 if and only if $\mathsf{Q}_4^+(T, \boldsymbol{t}) \cap \mathsf{Q}_4^-(T, \boldsymbol{t}) = \varnothing$. As they are 1-dimensional, we denote $\mathsf{Q}_4^+(T, \boldsymbol{t}) = [x_+, y_+]$ and $\mathsf{Q}_4^-(T, \boldsymbol{t}) = [x_-, y_-]$. Suppose proven that $x_- < y_+$, then $\mathsf{Q}_4^+(T, \boldsymbol{t}) \cap \mathsf{Q}_4^-(T, \boldsymbol{t}) = \varnothing$ if and only if $y_- < x_+$, which is what the lemma states.

For T non-universal with $\mu(T) = 4$, let ℓ be its immediate leaf. Corollary 4.52 ensures that negative quadrangles (i, j, k, l) satisfy either $i < j < \ell < k < l$ or $i < j < k < \ell < l$. There always exists a negative quadrangle of the first kind: if (i, j, k, l) is of the second kind, then the quadrangle which edge is $(\max\{x\ ;\ (x, l) \in E(T)\},\ l)$ is of the first kind.

For (i, j, k, l) of the first kind, if (j, k) is an interior edge, then there exists $a \in]j, k[$ such that $(j, a, k) \in T$: the quadrangle (j, a, k, l) is positive with $t_i + t_j + t_k + t_l < t_j + t_a + t_k + t_l$ (as $\boldsymbol{t} \in \mathsf{O}^\circ_{n+1}$). Else, $(j, k) = (\ell - 1, \ell)$, and taking $i' = \min\{x\ ;\ (x, \ell + 1) \in E(T)\}$ gives a negative quadrangle $(i', i' + 1, i' + 2, \ell)$ and a positive quadrangle $(i', i' + 1, \ell, \ell + 1)$ satisfying $t_{i'} + t_{i'+1} + t_{i'+2} + t_\ell < t_{i'} + t_{i'+1} + t_\ell + t_{\ell+1}$. In all cases, we have proven that $x_- < y_+$, yielding the lemma. □

Lemma 4.53 allows us to show that universal triangulations T for $\mu(T) \leq 4$ are in bijection with universal non-crossing arborescences A with $\mu(A) \leq 3$:

Corollary 4.54. *A triangulation T of a $(n + 1)$-gon is universal if and only if $\mu(T) = 3$, or if $\mu(T) = 4$ and one of the following holds:*

(i) $\mathbb{L}(T) = \{1, n - 1\}$;

(ii) $\mathbb{L}(T) = \{n - 2\}$ *and interior edges of T are either* $(1, 3)$ *and* $(0, i)$ *for* $i \in [3, n - 1]$, *or* $(1, 3)$, $(1, 4)$ *and* $(0, i)$ *for* $i \in [4, n - 1]$;

(iii) $\mathbb{L}(T) = \{2\}$ *and interior edges of T are either* $(n - 3, n - 1)$ *and* (i, n) *for* $i \in [1, n - 3]$, *or* $(n - 3, n - 1)$, $(n - 4, n - 1)$ *and* (i, n) *for* $i \in [1, n - 3]$.

Note that they are in bijection with universal non-crossing arborescences A with $\mu(A) = 3$, through the usual bijection $T \mapsto A_T$.

Proof. If $\mu(T) = 3$, then the universality of T follows directly from the proof of Corollary 4.52, as $\mathsf{Q}_4^-(T_m, \boldsymbol{t}) = \varnothing$, and $\mathsf{Q}_4^-(T_M, \boldsymbol{t}) = \varnothing$.

(i) In this case, by Corollary 4.52, there exists k such that $Q^+(T) = \big((0, i, i + 1, i + 2)\ ;\ i \in [k - 2]\big) \cup \big((0, k - 1, k, n)\big)$, and $Q^-(T) = \big((i, i + 1, i + 2, n)\ ;\ i \in [k, n - 3]\big) \cup \big((0, k, k + 1, , n)\big)$. Then $\mathsf{Q}_4^-(T, \boldsymbol{t}) \cap \mathsf{Q}_4^+(T, \boldsymbol{t}) = \varnothing$ for all $\boldsymbol{t} \in \mathsf{O}^\circ_{n+1}$, as $\sum_{i\in\kappa} t_i < \sum_{j\in\kappa'} t_j$ for all $\kappa \in Q^-(T)$ and $\kappa' \in Q^-(T)$. Thus by Theorem 4.48, T is universal.

(ii) Suppose $(1, 3) \in E(T)$ but $(1, 4) \notin E(T)$. In this case, $Q^-(T) = \big((0, 1, 2, 3)\big)$ and $Q^+(T) = \big((0, i, i + 1, i + 2)\ ;\ i \in [3, n - 2]\big)$. Thus $\mathsf{Q}_4^+(T, \boldsymbol{t}) \cap \mathsf{Q}_4^-(T, \boldsymbol{t}) = \varnothing$ for all $\boldsymbol{t} \in \mathsf{O}^\circ_{n+1}$.

(ii) Suppose $(1, 3) \in E(T)$ and $(1, 4) \in E(T)$. In this case, $Q^-(T) = \big((0, 1, 3, 4)\big)$ and $Q^+(T) = \big((0, i, i + 1, i + 2)\ ;\ i \in [4, n - 2]\big) \cup \big((1, 2, 3, 4)\big)$. Thus $\mathsf{Q}_4^+(T, \boldsymbol{t}) \cap \mathsf{Q}_4^-(T, \boldsymbol{t}) = \varnothing$ for all $\boldsymbol{t} \in \mathsf{O}^\circ_{n+1}$.

(iii) This case is symmetric to *(ii)*.

We finish by proving that if T does not belong to the above cases, then T is not universal, meaning there exists $\boldsymbol{t} \in \mathsf{O}^\circ_{n+1}$ with $\mathsf{Q}_4^+(T, \boldsymbol{t}) \cap \mathsf{Q}_4^-(T, \boldsymbol{t}) \neq \varnothing$. Fix T of the form of Corollary 4.52*(iii)*, and for $i < \ell$, denote j_i the index $j_i > \ell$ such that $(i - 1, i, j_i) \in T$. If $j_{\ell-1} \geq \ell + 2$, then $(\ell - 1, \ell, \ell + 1, \ell + 2) \in Q^+(T)$ and $(\ell - 2, \ell - 1, j_i, j_i - 1) \in Q^-(T)$. Taking an arbitrarily high value for t_{j_i} violates the inequality of Lemma 4.53. The case $j_i = \ell + 2$ is a mirror of the latter. □

With Corollary 4.52 and Lemma 4.53, we can also prove the reciprocal of Proposition 4.51:

Theorem 4.55. *For a triangulation T of a $(n+1)$-gon, $\mu(T) \leq 4$ if and only if $|\mathbb{L}(T)| + |\mathbb{L}^\circ(T)| \leq 2$.*

Proof. Proposition 4.51 states that if $\mu(T) \leq 4$ then $|\mathbb{L}(T)| + |\mathbb{L}^\circ(T)| \leq 2$. We prove the reciprocal by induction on n. The latter is clear for (the only) triangulation on $n + 1 = 3$ vertices.

Fix a triangulation T with $|\mathbb{L}(T)| + |\mathbb{L}^\circ(T)| \leq 2$. Corollary 4.54 ensures that $\mu(T) \leq 4$ if T is of the form of Corollary 4.52(i) or Corollary 4.52(ii). Suppose T is of the form Corollary 4.52(iii), then either $(0, 1, n) \in T$ or $(0, n - 1, n) \in T$. In the first case, set $T' = T\big|_{[1,n]}$ and construct, by induction, $\boldsymbol{t}' \in \mathsf{O}^\circ_n$ such that $\mu(T', \boldsymbol{t}') = 4$. Then, define $\boldsymbol{t} = (t_0, t'_1, \ldots, t'_n)$ by choosing t_0 arbitrarily small. Then, $Q^+(T) = Q^+(T')$, and $Q^-(T) = Q^-(T') \cup \big((0, 1, a, n)\big)$ with $a \in \{2, n-1\}$. As t_0 is small enough, we have $t_0 + t_1 + t_a + t_n < \min\{t_i + t_j + t_k + t_l\ ;\ (i, j, k, l) \in Q^+(T)\}$, so Lemma 4.53 ensures that $\mu(T, \boldsymbol{t}) = 4$.

The case of $(0, n - 1, n) \in T$ is solved similarly by setting t_n large enough. □

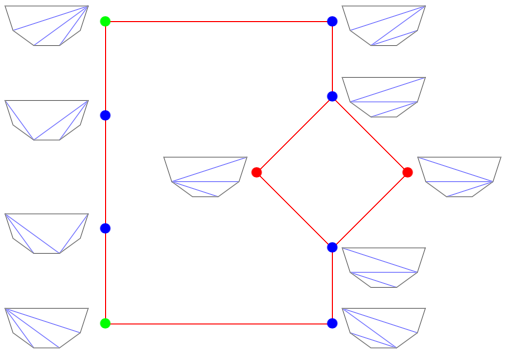

Figure 73: All triangulations T of a hexagon with $\mu(T) \leq 4$. Green and blue dots represent universal triangulations, red dots non-universal ones.

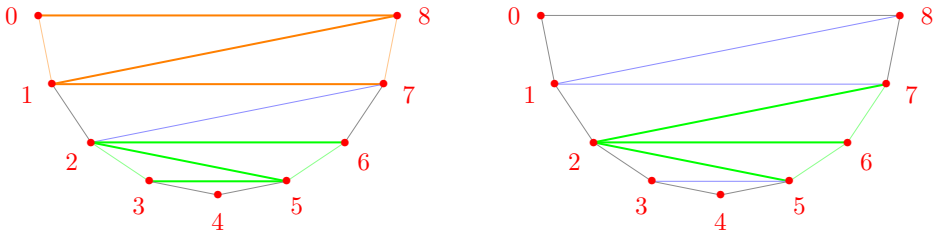

Figure 74: A non-universal triangulation T with $\mu(T) = 4$ and $\mathbb{L}(T) = \{4\}$. It has 2 minimal positive quadrangles among which $(2, 3, 5, 6)$, and 3 maximal negative quadrangles among which $(0, 1, 7, 8)$. It has 1 non-minimal positive quadrangle $(2, 5, 6, 7)$, and no non-maximal negative quadrangle.

As announced, we have proven that $T \mapsto A_T$ induces a bijection between:

(i) Triangulations T with $\mu(T) = 3$ and non-crossing arborescences A with $\mu(A) = 2$.

(ii) Triangulations T with $\mu(T) = 4$ and non-crossing arborescences A with $\mu(A) = 3$.

(iii) Universal triangulations T with $\mu(T) = 4$ and universal non-crossing arborescences A with $\mu(A) = 3$.

This allows us to construct in Figure 73 the graph of all triangulations T with $\mu(T) \leq 4$, similarly as in Figure 38 but with triangulations. This figure is closely related to Figure 1 of [ALRS00], and all its properties are the pendant as the one discussed in Example 3.23 about non-crossing arborescences A with $\mu(A) \leq A$.

It remains to study, for a fixed $\boldsymbol{t} \in \mathsf{O}^\circ_{n+1}$, the number of vertices of $\mathbf{\Sigma}^4_2(\boldsymbol{t})$, that is the number of triangulations T with $\mu(T, \boldsymbol{t}) \leq 4$.

Definition 4.56. In a non-universal triangulation T with $\mu(T) = 4$, a positive quadrangle $\kappa = (i, j, k, l)$ is *minimal* when $k = \min\{k' \ ; \ (i, k') \in E^\circ(T)\}$; a negative quadrangle $\kappa = (i, j, k, l)$ is *maximal* when $l = \max\{l' \ ; \ (j, l') \in E^\circ(T)\}$, see Figure 74.

Remark 4.57. Note that maximal negative quadrangles (i, j, k, l) are quadrangles that form a Z-shape, while minimal positive ones form a Σ-shape, see Figure 74. This illustrates the fact that flipping the edge of a minimal positive quadrangle turns it into a maximal negative quadrangle. Moreover, such flips send a triangulation T with $\mu(T) = 4$ either to another triangulation T' with $\mu(T') = 4$, or to one of the triangulations T_m or T_M of Corollary 4.52(i).

Theorem 4.58. *Let T be a non-universal triangulation with $\mu(T) = 4$, and $\boldsymbol{t} \in \mathsf{O}^\circ_{n+1}$, then $\boldsymbol{t} \in \mathcal{T}_4(T)$ if and only if $t_i + t_j + t_k + t_l < t_{i'} + t_{j'} + t_{k'} + t_{l'}$ for all $(i,j,k,l) \in Q^-(T)$ maximal and $(i',j',k',l') \in Q^+(T)$ minimal.*

Proof. Fix a non-universal triangulation T with $\mu(T) = 4$, and $\boldsymbol{t} \in \mathsf{O}^\circ_{n+1}$. By Lemma 4.53, this theorem amounts to proving that the minimum of $\{t_i + t_j + t_k + t_l \ ; \ (i,j,k,l) \in Q^+(T)\}$ is achieved when (i,j,k,l) is a minimal positive quadrangle, and conversely for negative quadrangles. Suppose that $(i,j,k,l) \in Q^+(T)$ is not minimal, and let $a = \max\{x \in]i,j[\ ; \ (i,x) \in E(T)\}$. Then $(i,a,j,k) \in Q^+(T)$ and $t_i + t_a + t_j + t_k < t_i + t_j + t_k + t_l$. A similar reasoning gives that a negative quadrangle achieves the maximum of $\{t_{i'} + t_{j'} + t_{k'} + t_{l'} \ ; \ (i',j',k',l') \in Q^-(T)\}$ only when it is maximal. □

For a triangulation T, if κ is a minimal positive quadrangle and ζ a maximal negative one, such that they do not share a triangle, then one can flip the edge e_κ and the edge e_ζ independently. We say that T and T' differ by a *diagonal switch with respect to these two quadrangles* when T' can be obtained by flipping two such edges.

The *switching arrangement* $\mathcal{G}_n$ is the collection of hyperplanes

$$G_{(\kappa,\zeta)} = \{\boldsymbol{t} \in \mathbb{R}^{n+1} \ ; \ t_i + t_j + t_k + t_l = t_{i'} + t_{j'} + t_{k'} + t_{l'}\}$$

for all couples of quadruples $\kappa = (i,j,k,l)$ and $\zeta = (i',j',k',l')$ such that $\kappa \in Q^+(T)$ is minimal and $\zeta \in Q^-(T)$ is maximal for some non-universal triangulation T with $\mu(T) = 4$.

Theorem 4.59. *For $\boldsymbol{t}_{lex} = (1, 2, \dots, 2^n) \in \mathsf{O}^\circ_{n+1}$ and $\boldsymbol{u}_{lex} = (2, \dots, 2^n) \in \mathsf{O}^\circ_n$, the triangulations T with $\mu(T, \boldsymbol{t}_{lex}) \leq 4$ are sent bijectively through $T \mapsto A_T$ to the non-crossing arborescences A with $\mu(A, \boldsymbol{u}_{lex}) \leq 3$. Informally, this amounts to say that $\Sigma^4_2(\boldsymbol{t}_{lex}) \simeq \Pi^3_{\boldsymbol{u}_{lex}}$.*

Proof. As universal triangulations and universal non-crossing arborescences are in bijection, we only focus on non-universal ones.

By Lemma 4.53, to know whether a non-universal triangulation T can be captured or not on $\boldsymbol{t}$, we need to compare the $t_i + t_j + t_k + t_l$ for different quadrangles (i,j,k,l). But comparing these values for $\boldsymbol{t}_{lex}$ amounts to comparing reverse-lexicographically the associated quadruplets (this is the principle of the binary numeral system). The lexicographic order is denoted $\leq_{lex}$.

Let T be a triangulation with $\mu(T) \leq 4$. On one side, $\boldsymbol{t}_{lex} \in \mathcal{T}^\circ_4(T)$ if and only if $(l,k,j,i) \leq_{lex} (l',k',j',i')$ for all $(i,j,k,l) \in Q^+(T)$ and $(i',j',k',l') \in Q^-(T)$. On the other side, Lemma 4.44 ensures that $(i,j,k,l) \in Q^+(T)$ if and only if $j \in \mathcal{I}^f_{A_T}$, and $(i',j',k',l') \in Q^-(T)$ if and only if $j' \in \mathcal{I}^b_{A_T}$; thus $\boldsymbol{u}_{lex} \in \mathcal{T}^\circ_3(A_T)$ if and only if $(l,k,j) \leq_{lex} (l',k',j')$ for all $(i,j,k,l) \in Q^+(T)$ and $(i',j',k',l') \in Q^-(T)$.

Moreover, if $(i,j,k,l) \in Q^+(T)$, then $(j,k,l) \notin T$, so there is no negative quadrangle in T of the form (a,j,k,l) for $a < j$. Therefore, i and i' are irrelevant in the comparison $(l,k,j,i) \leq_{lex} (l',k',j',i')$, meaning that: $(l,k,j,i) \leq_{lex} (l',k',j',i')$ if and only if $(l,k,j) \leq_{lex} (l',k',j')$.

Consequently, T can be captured on $\boldsymbol{t}_{lex}$ if and only if A_T can be captured on $\boldsymbol{u}_{lex}$. □

Theorem 4.60. *For all $\boldsymbol{t} \in \mathsf{O}^\circ_{n+1} \setminus \bigcap_{G \in \mathcal{G}_n} G$, the number of vertices of $\Sigma^d_2(\boldsymbol{t})$ is $\binom{n}{2} - 1$.*

Proof. By Theorem 4.58, if $\boldsymbol{t}$ and $\boldsymbol{t}'$ belong to the same maximal cone of $\mathsf{O}^\circ_{n+1} \setminus \bigcup_{G \in \mathcal{G}_n} G$, then the triangulations captured on $\boldsymbol{t}$ and $\boldsymbol{t}'$ are the same. Thus the number of vertices of $\Sigma^d_2(\boldsymbol{t})$ and $\Sigma^d_2(\boldsymbol{t}')$ are the same.

For a maximal cone C of the arrangement $\mathcal{G}_n$, we denote by $\mathcal{V}(\mathsf{C})$ the set of triangulations T such that $\mathsf{C} \subseteq \mathcal{T}^\circ_4(T)$. Take two adjacent maximal cones C and C'. Suppose that $T \in \mathcal{V}(\mathsf{C})$ but $T \notin \mathcal{V}(\mathsf{C}')$. Then the hyperplane separating C from C' is of the form $G = \{\boldsymbol{t} \ ; \ t_i + t_j + t_k + t_l = t_{i'} + t_{j'} + t_{k'} + t_{l'}\}$ for some $\kappa = (i,j,k,l) \in Q^+(T)$ minimal in T and $\zeta = (i',j',k',l') \in Q^-(T)$ maximal in T. As the two sums are equal for $\boldsymbol{t} \in G$, κ and ζ can not share a triangle. Let T' be obtained from T by first flipping (i,k) and then (j',l'). We know that $T' \notin \mathcal{V}(\mathsf{C})$ (because C is on the wrong side of G for T' to be captured), and we want to prove that $T' \in \mathcal{V}(\mathsf{C}')$, *i.e.* $\mathsf{C}' \subseteq \mathcal{T}^\circ_4(T')$.

Fix $\boldsymbol{t} \in G$.

Then, we know that $t_{i'} + t_{j'} + t_{k'} + t_{l'} < t_\alpha + t_\beta + t_\gamma + t_\eta$ for all $(\alpha, \beta, \gamma, \eta) \in Q^+(T)$ as these inequalities are respected in C because T can be captured there. Furthermore, $t_i + t_j + t_k + t_l = t_{i'} + t_{j'} + t_{k'} + t_{l'}$ as $\boldsymbol{t} \in G$. This proves that $t_i + t_j + t_k + t_l = \min\{t_\alpha + t_\beta + t_\gamma + t_\eta \ ; \ (\alpha, \beta, \gamma, \eta) \in Q^+(T) \text{ minimal}\}$.

Now take $(e, f, g, h) \in Q^+(T')$ minimal. If $(e, f, g, h) \in Q^+(T)$, then $t_e + t_f + t_g + t_h > t_i + t_j + t_k + t_l$. Otherwise, (e, f, g, h) comes from the diagonal switch. We detail this switch, see Figure 75. If it comes from the flip of (i, k), then its edge is either $(e, g) = (i, l)$ or $(e, g) = (j, k)$. But in the first case, $(e, f, g, h) = (i, j, l, h)$ with $h > l$ because $(e, f, g, h) \in Q^+(T')$. In the second case, $(e, f, g, h) = (j, f, k, l)$ because (e, f, g, h) is minimal in T'. In both cases $t_e + t_f + t_g + t_h > t_i + t_j + t_k + t_l$. No minimal positive quadrangle can appear when flipping (j', l') (apart (i', j', k', l') itself) because if $(e, g) = (i', l')$ then (e, f, g, h) is not minimal, and if $(e, g) = (j', k')$, then (e, f, g, h) can not be positive. This establishes that $t_i + t_j + t_k + t_l = \min\{t_\alpha + t_\beta + t_\gamma + t_\eta \ ; \ (\alpha, \beta, \gamma, \eta) \in Q^+(T') \text{ minimal}\}$.

The same holds for negative quadrangles: $t_{i'} + t_{j'} + t_{k'} + t_{l'} = \max\{t_\alpha + t_\beta + t_\gamma + t_\eta \ ; \ (\alpha, \beta, \gamma, \eta) \in Q^-(T') \text{ maximal}\}$.

Thus, $\boldsymbol{t}' \in \mathsf{C}'$ taken arbitrarily close to $\boldsymbol{t} \in G$ respects all inequalities of $\mathcal{T}_3^\circ(T')$. This ensures that $T' \in \mathcal{V}(\mathsf{C}')$ but $T' \notin \mathcal{V}(\mathsf{C})$, and consequently $|\mathcal{V}(\mathsf{C}')| \geq |\mathcal{V}(\mathsf{C})|$. As a result, the cardinal $|\mathcal{V}(\mathsf{C})|$ is the same for all maximal cones C of the hyperplane arrangement $\mathcal{G}_n$ (as the graph of adjacency of its maximal cones is connected).

Finally, Theorem 4.59 states that this cardinal is also the number of vertices of $\Pi_{\boldsymbol{t}}^3$: $\binom{n}{2} - 1$. □

Example 4.61. One can consider the graph on triangulations T of a $(n+1)$-gon with $\mu(T) \leq 4$ with an edge between T and T' if there exists $\boldsymbol{t} \in \mathsf{O}_{n+1}^\circ \backslash \bigcup_{G \in \mathcal{G}_n} G$ such that the vertices corresponding to T and T' are neighbors in $\Sigma_2^4(\boldsymbol{t})$. This is precisely the induced sub-graph of flips of triangulations, restricted to $\{T \ ; \ \mu(T) \leq 4\}$. By Theorem 4.55, this graph is isomorphic to the graph discussed in Example 3.23, through the bijection $T \mapsto A_T$. As previously, the polygons $\Sigma_2^4(\boldsymbol{t})$ correspond to great cycles in this graph, but not all great cycles do correspond to $\Sigma_2^4(\boldsymbol{t})$. Nevertheless, a given great cycle does not give rise to the same system of inequalities for triangulations as for non-crossing arborescences. In particular, one can compute the number of combinatorially different $\Sigma_2^4(\boldsymbol{t})$, *i.e.* the number of great cycle whose associated system of inequalities has a (full-dimension set of) solution:

- For $n = 5$, there are 2 possible $\Sigma_2^4(\boldsymbol{t})$, see Figure 1 of [ALRS00] and Figure 76.
- For $n = 6$, there are 12 possible $\Sigma_2^4(\boldsymbol{t})$.
- For $n = 7$, there are 216 possible $\Sigma_2^4(\boldsymbol{t})$.
- For $n = 8$, there are 8368 possible $\Sigma_2^4(\boldsymbol{t})$

For $n = 5$ and $n = 6$, the bijection $T \mapsto A_T$ extends to a bijection between possible $\Sigma_2^4(\boldsymbol{t})$ and possible $\Pi_{\boldsymbol{t}}^3$. But for $n = 7$, as there are 216 possible $\Sigma_2^4(\boldsymbol{t})$ and only 187 possible $\Pi_{\boldsymbol{t}}^3$, this is no longer plausible (and for $n = 8$, there are only 6179 possible $\Pi_{\boldsymbol{t}}^3$). Moreover, when applying $T \mapsto A_T$, one will conclude that 181 possible $\Sigma_2^4(\boldsymbol{t})$ map to $\Pi_{\boldsymbol{t}}^3$ while 35 do not, and 6 $\Pi_{\boldsymbol{t}}^3$ are not (images of) $\Sigma_2^4(\boldsymbol{t})$.

4.3.4 Perspectives and open questions

Computational remarks As usual, the objects of this section have been implemented with Sage. Especially, to compute the fiber polytopes at stake, we chose to first compute its secondary polytope and then project it. The secondary polytope can be computed by running through all triangulations of $\mathsf{Cyc}_2(\boldsymbol{t})$, and associating to each a vertex (whose coordinates have an explicit formula involving the area of its triangles). The projection is precisely the projection $\mathsf{Cyc}_4(\boldsymbol{t}) \to \mathsf{Cyc}_2(\boldsymbol{t})$. We could also have computed the fiber polytopes as a finite Minkowski sum, see Theorem 4.7, but

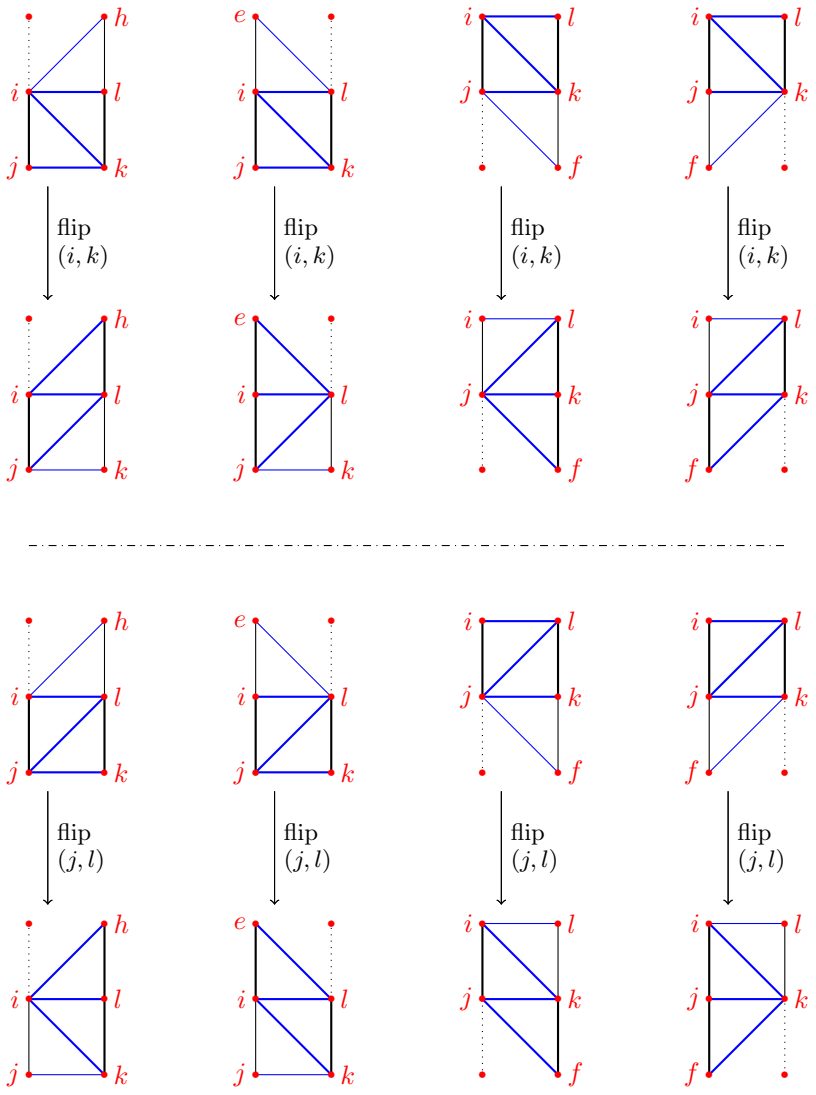

Figure 75: All possible quadrangles that can be created during a diagonal switch.

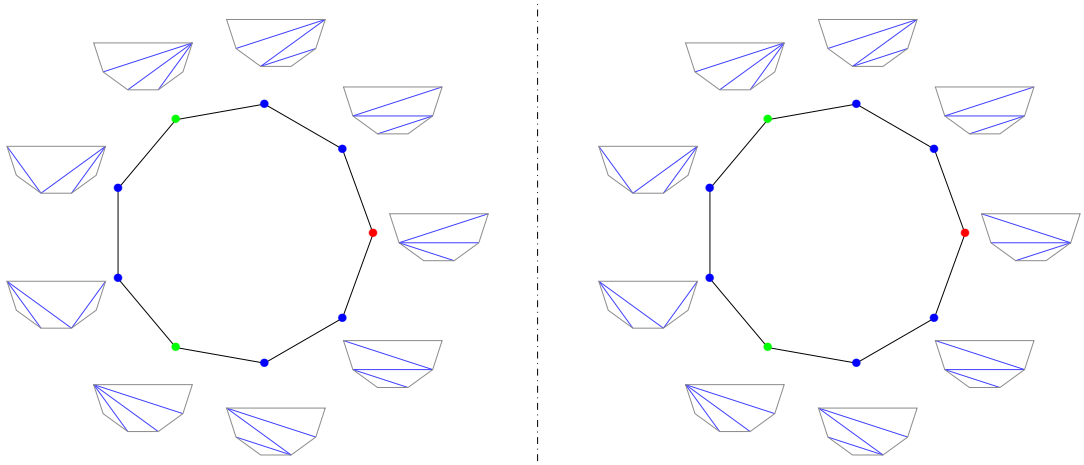

Figure 76: The 2 possible $\Sigma_2^4(\boldsymbol{t})$ for $n = 5$. Green vertices correspond to triangulations T with $\mu(T) = 3$, blue ones to universal T with $\mu(T) = 4$, and the red one to the non-universal triangulation (the only one that differs between Left and Right). Each $\Sigma_2^4(\boldsymbol{t})$ correspond to one of the two cones inside O_6 separated by the hyperplane $\{\boldsymbol{t}\ ;\ t_0 + t_1 + t_4 + t_5 = t_1 + t_2 + t_3 + t_4\}$. Contrarily to Figure 40, it is not possible to picture this subdivision of O_6 as, even when intersected with the hyperplanes $\{\boldsymbol{t}\ ;\ t_0 = 0\}$ and $\{\boldsymbol{t}\ ;\ t_5 = 1\}$, it is 4-dimensional.

the first method has the advantage to directly associate the vertices of $\Sigma_2^d(\boldsymbol{t})$ with triangulations of $\mathsf{Cyc}_2(\boldsymbol{t})$.

Besides, to calculate the values claimed in Example 4.61, one needs to construct the subdivision $\mathsf{O}_{n+1} \setminus \bigcup_{G \in \mathcal{G}_n} G$. The same issues as discussed in Section 3.2.4 occur, but note that most of the material developed for Section 3.2 can not be directly reused here, and need to be adapted.

Assets and limits of the current approach, open questions Lemma 4.44 is essential for proving Theorem 4.59, but to this end, we only use Lemma 4.44 on the triangulations with 1 interior immediate leaf or 2 exterior ones. As the lemma applies for all triangulations, we can hope for a generalization of Theorem 4.59, which would grant access to a theory of intrinsic degree for all triangulations. However, the way to do so remains unclear.

The fiber polytope we have studied in this section is very similar to the max-slope pivot rule polytope studied in Section 3.2, although they are not exactly the same. The mystery around the link between both is not totally unveiled. It would be interesting to determine whether this link is due to the combinatorics and geometry of the cyclic polytopes, or if this is but the tail of a more general phenomenon.

I was working on the proof of one of my poems all the morning, and took out a comma.
In the afternoon I put it back again.
– Oscar Wilde

References

[AA17] Marcelo Aguiar and Federico Ardila. Hopf monoids and generalized permutahedra, 2017. To appear in *Mem. Amer. Math. Soc.*

[ABD10] Federico Ardila, Carolina Benedetti, and Jeffrey Doker. Matroid polytopes and their volumes. *Discrete Comput. Geom.*, 43(4):841–854, 2010.

[ACEP20] Federico Ardila, Federico Castillo, Christopher Eur, and Alexander Postnikov. Coxeter submodular functions and deformations of Coxeter permutahedra. *Adv. Math.*, 365:107039, 36, 2020.

[AER00] Christos A Athanasiadis, Paul H Edelman, and Victor Reiner. Monotone paths on polytopes. *Mathematische Zeitschrift*, 235(2):315–334, 2000.

[AHBC+16] Nima Arkani-Hamed, Jacob Bourjaily, Freddy Cachazo, Alexander Goncharov, Alexander Postnikov, and Jaroslav Trnka. *Grassmannian geometry of scattering amplitudes*. Cambridge University Press, Cambridge, 2016.

[AHBHY18] Nima Arkani-Hamed, Yuntao Bai, Song He, and Gongwang Yan. Scattering forms and the positive geometry of kinematics, color and the worldsheet. *J. High Energy Phys.*, (5):096, front matter+75, 2018.

[AHBL17] Nima Arkani-Hamed, Yuntao Bai, and Thomas Lam. Positive geometries and canonical forms. *J. High Energy Phys.*, (11):039, front matter+121, 2017.

[AHHST22] Nima Arkani-Hamed, Song He, Giulio Salvatori, and Hugh Thomas. Causal diamonds, cluster polytopes and scattering amplitudes, 2022.

[AHT14] Nima Arkani-Hamed and Jaroslav Trnka. The amplituhedron. *J. High Energy Phys.*, (10):30, 2014.

[ALRS00] Christos A. Athanasiadis, Jesús A. De Loera, Victor Reiner, and Francisco Santos. Fiber polytopes for the projections between cyclic polytopes. *European Journal of Combinatorics*, 21(1):19–47, jan 2000.

[APR14] Ilan Adler, Christos Papadimitriou, and Aviad Rubinstein. On simplex pivoting rules and complexity theory, 2014.

[APR21] Doriann Albertin, Vincent Pilaud, and Julian Ritter. Removahedral congruences versus permutree congruences. *Electron. J. Combin.*, 28(4):Paper No. 4.8, 38, 2021.

[Ard21] Federico Ardila. The geometry of geometries: matroid theory, old and new, 2021.

[Ath99] Christos A Athanasiadis. Piles of cubes, monotone path polytopes, and hyperplane arrangements. *Discrete & Computational Geometry*, 21:117–130, 1999.

[BDLLS22] Alexander E. Black, Jesús A. De Loera, Niklas Lütjeharms, and Raman Sanyal. The polyhedral geometry of pivot rules and monotone paths, 2022.

[BDLLSon] Alexander E. Black, Jesús A. De Loera, Niklas Lütjeharms, and Raman Sanyal. On the geometric combinatorics of pivot rules. in preparation.

[Ber89] Claude Berge. *Hypergraphs*, volume 45 of *North-Holland Mathematical Library*. North-Holland Publishing Co., Amsterdam, 1989. Combinatorics of finite sets, Translated from the French.

[BFS90] Louis J. Billera, Paul Filliman, and Bernd Sturmfels. Constructions and complexity of secondary polytopes. *Adv. Math.*, 83(2):155–179, 1990.

[BKS94] Louis J. Billera, Mikhail M. Kapranov, and Bernd Sturmfels. Cellular strings on polytopes. *Proc. Amer. Math. Soc.*, 122(2):549–555, 1994.

[BL21] Alexander Black and Jesús De Loera. Monotone paths on cross-polytopes, 2021.

[BLL20] Moïse Blanchard, Jesùs A. De Loera, and Quentin Louveaux. On the length of monotone paths in polyhedra, 2020.

[BLS+99] Anders Björner, Michel Las Vergnas, Bernd Sturmfels, Neil White, and Günter M. Ziegler. *Oriented matroids*, volume 46 of *Encyclopedia of Mathematics and its Applications*. Cambridge University Press, Cambridge, second edition, 1999.

[BMDM+18] Véronique Bazier-Matte, Guillaume Douville, Kaveh Mousavand, Hugh Thomas, and Emine Yıldırım. ABHY Associahedra and Newton polytopes of F-polynomials for finite type cluster algebras.
arXiv:1808.09986, 2018.

[BML87] Roswitha Blind and Peter Mani-Levitska. Puzzles and polytope isomorphisms. *Aequationes Math.*, 34(2-3):287–297, 1987.

[Bot19] Nathaniel Bottman. 2–associahedra. *Algebraic & Geometric Topology*, 19(2):743–806, 2019.

[BPR06] Saugata Basu, Richard Pollack, and Marie-Françoise Roy. *Algorithms in Real Algebraic Geometry*, volume 2 of *Algorithms and Computation in Mathematics*. Springer Berlin, Heidelberg, 2006.

[BS92] Louis J. Billera and Bernd Sturmfels. Fiber polytopes. *Anals of Mathematics*, (135):527–549, 1992.

[CD06] Michael P. Carr and Satyan L. Devadoss. Coxeter complexes and graph-associahedra. *Topology Appl.*, 153(12):2155–2168, 2006.

[CDG+20] Federico Castillo, Joseph Doolittle, Bennet Goeckner, Michael S. Ross, and Li Ying. Minkowski summands of cubes. 2020.

[CFZ02] Frédéric Chapoton, Sergey Fomin, and Andrei Zelevinsky. Polytopal realizations of generalized associahedra. *Canad. Math. Bull.*, 45(4):537–566, 2002.

[CL20] Federico Castillo and Fu Liu. Deformation cones of nested braid fans. *Int. Math. Res. Not. IMRN*, 2020.

[CLS11] David A. Cox, John B. Little, and Henry K. Schenck. *Toric varieties*, volume 124 of *Graduate Studies in Mathematics*. American Mathematical Society, Providence, RI, 2011.

[CP22] Frédéric Chapoton and Vincent Pilaud. Shuffles of deformed permutahedra, multiplihedra, constrainahedra, and biassociahedra, 2022.

[Dan63] George B. Dantzig. *Linear programming and Extensions*. Princeton Landmarks in Mathematics and Physics. Princeton University Press, 1963.

[DCP95] Conrado De Concini and Claudio Procesi. Wonderful models of subspace arrangements. *Selecta Math. (N.S.)*, 1(3):459–494, 1995.

[Def21] Colin Defant. Fertilitopes. Preprint, arXiv:2102.11836, 2021.

[Dev09] Satyan L. Devadoss. A realization of graph associahedra. *Discrete Math.*, 309(1):271–276, 2009.

[DK00] Vladimir I. Danilov and Gleb A. Koshevoy. Cores of cooperative games, superdifferentials of functions, and the Minkowski difference of sets. *J. Math. Anal. Appl.*, 247(1):pp. 1–14, 2000.

[DLST95] Jesús A De Loera, Bernd Sturmfels, and Rekha R Thomas. Gröbner bases and triangulations of the second hypersimplex. *Combinatorica*, 15:409–424, 1995.

[DNT08] Antoine Deza, Eissa Nematollahi, and Tamás Terlaky. How good are interior point methods? klee–minty cubes tighten iteration-complexity bounds. *Mathematical Programming*, 113, 2008.

[DP11] Kosta Došen and Zoran Petrić. Hypergraph polytopes. *Topology Appl.*, 158(12):1405–1444, 2011.

[DRS10] Jesus A. De Loera, Jörg Rambau, and Francisco Santos. *Triangulations: Structures for Algorithms and Applications*, volume 25 of *Algorithms and Computation in Math.* Springer, 2010.

[DS14] Yann Disser and Martin Skutella. The simplex algorithm is np-mighty, 2014.

[Edm70] Jack Edmonds. Submodular functions, matroids, and certain polyhedra. In *Combinatorial Structures and their Applications (Proc. Calgary Internat. Conf., Calgary, Alta., 1969)*, pages 69–87. Gordon and Breach, New York, 1970.

[Est08] Alexander Esterov. On the existence of mixed fiber bodies. *Mosc. Math. J.*, 8(3):433–442, 615, 2008.

[For08] Stefan Forcey. Convex hull realizations of the multiplihedra. *Topology and its Applications*, 156(2):326–347, 2008.

[FS05] Eva Maria Feichtner and Bernd Sturmfels. Matroid polytopes, nested sets and Bergman fans. *Port. Math. (N.S.)*, 62(4):437–468, 2005.

[FS14] John Fearnley and Rahul Savani. The complexity of the simplex method, 2014.

[Fuj05] Satoru Fujishige. *Submodular functions and optimization*, volume 58 of *Annals of Discrete Mathematics*. Elsevier B. V., Amsterdam, second edition, 2005.

[FZ02] Sergey Fomin and Andrei Zelevinsky. Cluster algebras. I. Foundations. *J. Amer. Math. Soc.*, 15(2):497–529, 2002.

[GKZ90] Izrail Gelfand, Mikhail Kapranov, and Andrei Zelevinski. Newton polytopes of principal A-determinants. *Soviet Math Doklady*, 1990.

[GKZ91] Izrail Gelfand, Mikhail Kapranov, and Andrei Zelevinski. Discriminants of polynomials in several variables and triangulations of Newton polyhedra. *Leningrad Math. Journal*, 1991.

[GKZ08] Israel Gelfand, Mikhail Kapranov, and Andrei Zelevinsky. *Discriminants, resultants and multidimensional determinants*. Modern Birkhäuser Classics. Birkhäuser Boston Inc., Boston, MA, 2008. Reprint of the 1994 edition.

[GPW19] Pavel Galashin, Alexander Postnikov, and Lauren Williams. Higher secondary polytopes and regular plabic graphs, 2019.

[Grü03] Branko Grünbaum. *Convex polytopes*, volume 221 of *Graduate Texts in Mathematics*. Springer-Verlag, New York, second edition, 2003. Prepared and with a preface by Volker Kaibel, Victor Klee and Günter M. Ziegler.

[Hai84] Mark Haiman. Constructing the associahedron. Unpublished manuscript, 11 pages, available at http://www.math.berkeley.edu/~mhaiman/ftp/assoc/manuscript.pdf, 1984.

[Ham50] Richard W Hamming. Error detecting and error correcting codes. *The Bell system technical journal*, 29(2):147–160, 1950.

[Ham17] Simon Hampe. The intersection ring of matroids. *Journal of Combinatorial Theory, Series B*, 122:578–614, jan 2017.

[HL07] Christophe Hohlweg and Carsten Lange. Realizations of the associahedron and cyclohedron. *Discrete Comput. Geom.*, 37(4):517–543, 2007.

[Hoh12] Christophe Hohlweg. Permutahedra and associahedra: generalized associahedra from the geometry of finite reflection groups. In *Associahedra, Tamari lattices and related structures*, volume 299 of *Prog. Math. Phys.*, pages 129–159. Birkhäuser/Springer, 2012.

[JKS22] Michael Joswig, Max Klimm, and Sylvain Spitz. Generalized permutahedra and optimal auctions. *SIAM Journal on Applied Algebra and Geometry*, 6(4):711–739, 2022.

[Kel01] Bernhard Keller. Introduction to a-infinity algebras and modules. *Homology Homotopy Appl.*, 3(1):1–35., 2001.

[Kim08] Sangwook Kim. Shellable complexes and topology of diagonal arrangements. *Discrete Comput. Geom.*, 40(2):190–213, 2008.

[KM72] Victor Klee and George J. Minty. How good is the simplex algorithm?, 1972.

[Lee89] Carl Lee. The associahedron and triangulations of the n-gon. *European J. Combin.*, 10(6):551–560, 1989.

[Lod04] Jean-Louis Loday. Realization of the Stasheff polytope. *Arch. Math. (Basel)*, 83(3):267–278, 2004.

[LP07] Thomas Lam and Alexander Postnikov. Alcoved polytopes, i. *Discrete & Computational Geometry*, 38:453–478, 2007.

[LP20] Thomas Lam and Alexander Postnikov. Polypositroids, 2020.

[LRS10] Jesús A. De Loera, Jörg Rambau, and Francisco Santos. *Triangulations*. Algorithms and Computation in Mathematics. Springer Berlin, Heidelberg, 2010.

[McD95] John McDonald. Fiber polytopes and fractional power series. *Journal of Pure and Applied Algebra*, 104(2):213–233, 1995.

[McM70] Peter McMullen. The maximum numbers of faces of a convex polytope. *Mathematika*, 17:179–184, 1970.

[McM73] Peter McMullen. Representations of polytopes and polyhedral sets. *Geometriae Dedicata*, 2:83–99, 1973.

[McM93] Peter McMullen. On simple polytopes. *Inventiones mathematicae*, 113:419–444, 1993.

[McM96] Peter McMullen. Weights on polytopes. *Discrete Comput. Geom.*, 15(4):363–388, 1996.

[Mer22] Chiara Meroni. *Semialgebraic Convex Bodies*. PhD thesis, Fakultät für Mathematik und Informatik der Universität Leipzig, 2022.

[Mey74] Walter Meyer. Indecomposable polytopes. *Trans. Amer. Math. Soc.*, 190:77–86, 1974.

[MG07] Jiří Matoušek and Bernd Gärtner. *Understanding and Using Linear Programming*. Universitext. Springer Berlin, Heidelberg, 2007.

[MP17] Thibault Manneville and Vincent Pilaud. Compatibility fans for graphical nested complexes. *J. Combin. Theory Ser. A*, 150:36–107, 2017.

[MPS+09] Jason Morton, Lior Pachter, Anne Shiu, Bernd Sturmfels, and Oliver Wienand. Convex rank tests and semigraphoids. *SIAM J. Discrete Math.*, 23(3):1117–1134, 2009.

[MSS20] Sebastian Manecke, Raman Sanyal, and Jeonghoon So. S-hypersimplices, pulling triangulations, and monotone paths, 2020.

[MUWY18] Fatemeh Mohammadi, Caroline Uhler, Charles Wang, and Josephine Yu. Generalized permutohedra from probabilistic graphical models. *SIAM J. Discrete Math.*, 32(1):64–93, 2018.

[Pil17] Vincent Pilaud. Which nestohedra are removahedra? *Rev. Colombiana Mat.*, 51(1):21–42, 2017.

[Pil21] Vincent Pilaud. Acyclic reorientation lattices and their lattice quotients, 2021.

[PK92] Aleksandr Pukhlikov and Askold Khovanskiĭ. Finitely additive measures of virtual polyhedra. *Algebra i Analiz*, 4(2):161–185, 1992.

[Pol21] Daria Poliakova. *Homotopical algebra and combinatorics of polytopes*. PhD thesis, School of The Faculty of Science, University of Copenhagen, 2021.

[Pon18] Viviane Pons, 2018. https://www.lri.fr/~pons/static/spermutahedron/.

[Pos09] Alexander Postnikov. Permutohedra, associahedra, and beyond. *Int. Math. Res. Not. IMRN*, (6):1026–1106, 2009.

[PP22] Arnau Padrol and Eva Philippe. Sweeps, polytopes, oriented matroids, and allowable graphs of permutations, 2022.

[PPP22a] Arnau Padrol, Vincent Pilaud, and Germain Poullot. Deformation cones of hypergraphic polytopes. In *FPSAC 2022-34th International Conference on Formal Power Series and Algebraic Combinatorics*, volume 86, page 71, 2022.

[PPP22b] Arnau Padrol, Vincent Pilaud, and Germain Poullot. Deformed graphical zonotopes. *accepted for publication at Discrete and Computational Geometry*, 2022.

[PPP23] Arnau Padrol, Vincent Pilaud, and Germain Poullot. Deformation cones of graph associahedra and nestohedra. *European Journal of Combinatorics*, 107:103594, 2023.

[PPPP19] Arnau Padrol, Yann Palu, Vincent Pilaud, and Pierre-Guy Plamondon. Associahedra for finite type cluster algebras and minimal relations between **g**-vectors. arXiv:1906.06861, 2019.

[PRW08] Alexander Postnikov, Victor Reiner, and Lauren K. Williams. Faces of generalized permutohedra. *Doc. Math.*, 13:207–273, 2008.

[PS19] Vincent Pilaud and Francisco Santos. Quotientopes. *Bull. Lond. Math. Soc.*, 51(3):406–420, 2019.

[PSZ23] Vincent Pilaud, Francisco Santos, and Günter M. Ziegler. Celebrating loday's associahedron, 2023.

[Rei99] Victor Reiner. The generalized baues problem. *New perspectives in algebraic combinatorics*, 38:293–336, 1999.

[Rei02] Victor Reiner. Equivariant fiber polytopes. *Documenta Mathematica*, 7:113–132, 2002.

[RSS03] Günter Rote, Francisco Santos, and Ileana Streinu. Expansive motions and the polytope of pointed pseudo-triangulations. In *Discrete and computational geometry*, volume 25 of *Algorithms Combin.*, pages 699–736. Springer, Berlin, 2003.

[RTV05] Cornelis Roos, Tamás Terlaky, and Jean-Philipe Vial. *Interior Point Methods for Linear Optimization (2nd edition)*. Springer, 2005.

[San09] Samson Saneblidze. The bitwisted Cartesian model for the free loop fibration. *Topology Appl.*, 156(5):897–910, 2009.

[Sch11] Pieter Hendrik Schoute. *Analytical treatment of the polytopes regularly derived from the regular polytopes. Section I: The simplex.*, volume 11. 1911.

[Sch98] Alexander Schrijver. *Theory of linear and integer programming*. Wiley-Interscience, 1998.

[SF99] Richard P. Stanley and Sergey Fomin. *Enumerative Combinatorics*, volume 2 of *Cambridge Studies in Advanced Mathematics*. Cambridge University Press, 1999.

[She63] Geoffrey C. Shephard. Decomposable convex polyhedra. *Mathematika*, 10:89–95, 1963.

[Slo23] Neil Sloane. "a handbook of integer sequences" fifty years later, 2023.

[SP02] Richard P. Stanley and Jim Pitman. A polytope related to empirical distributions, plane trees, parking functions, and the associahedron. *Discrete Comput. Geom.*, 27(4):pp. 603–634, 2002.

[SS93] Steve Shnider and Shlomo Sternberg. *Quantum groups: From coalgebras to Drinfeld algebras*. Series in Mathematical Physics. International Press, Cambridge, MA, 1993.

[Sta63] Jim Stasheff. Homotopy associativity of H-spaces I & II. *Trans. Amer. Math. Soc.*, 108(2):275–312, 1963.

[Sta70] James Stasheff. *H-Spaces from a Homotopy Point of View*, volume 161 of *Lecture Notes in Mathematics*. Springer Berlin, Heidelberg, 1970.

[Sta80] Richard P Stanley. The number of faces of a simplicial convex polytope. *Advances in Mathematics*, 35(3):236–238, 1980.

[Sta07] Richard P. Stanley. An introduction to hyperplane arrangements. In *Geometric combinatorics*, volume 13 of *IAS/Park City Math. Ser.*, pages 389–496. Amer. Math. Soc., Providence, RI, 2007.

[Sta12] Richard P. Stanley. *Enumerative combinatorics. Volume 1*, volume 49 of *Cambridge Studies in Advanced Mathematics*. Cambridge University Press, second edition, 2012.

[Sta15] Richard P. Stanley. *Catalan Numbers*. Cambridge University Press, 2015.

[Tam51] Dov Tamari. *Monoides préordonnés et chaînes de Malcev*. PhD thesis, Université Paris Sorbonne, 1951.

[Zel06] Andrei Zelevinsky. Nested complexes and their polyhedral realizations. *Pure Appl. Math. Q.*, 2(3):655–671, 2006.

[Zie98] Günter M. Ziegler. *Lectures on Polytopes*, volume 152 of *Graduate texts in Mathematics*. Springer-Verlag, New York, 1998.